INFORMATION TO USERS

The most advanced technology has been used to photograph and reproduce this manuscript from the microfilm master. UMI films the text directly from the original or copy submitted. Thus, some thesis and dissertation copies are in typewriter face, while others may be from any type of computer printer.

The quality of this reproduction is dependent upon the quality of the copy submitted. Broken or indistinct print, colored or poor quality illustrations and photographs, print bleedthrough, substandard margins, and improper alignment can adversely affect reproduction.

In the unlikely event that the author did not send UMI a complete manuscript and there are missing pages, these will be noted. Also, if unauthorized copyright material had to be removed, a note will indicate the deletion.

Oversize materials (e.g., maps, drawings, charts) are reproduced by sectioning the original, beginning at the upper left-hand corner and continuing from left to right in equal sections with small overlaps. Each original is also photographed in one exposure and is included in reduced form at the back of the book. These are also available as one exposure on a standard 35mm slide or as a 17" x 23" black and white photographic print for an additional charge.

Photographs included in the original manuscript have been reproduced xerographically in this copy. Higher quality 6" x 9" black and white photographic prints are available for any photographs or illustrations appearing in this copy for an additional charge. Contact UMI directly to order.

U·M·I

University Microfilms International
A Bell & Howell Information Company
300 North Zeeb Road, Ann Arbor, MI 48106-1346 USA
313/761-4700 800/521-0600

Order Number 9009746

The electron spin echo studies of metalloproteins

Jin, Haiyong, Ph.D.

City University of New York, 1989

U·M·I
300 N. Zeeb Rd.
Ann Arbor, MI 48106

A

THE ELECTRON SPIN ECHO STUDIES OF METALLOPROTEINS

by

HAIYONG JIN

A dissertation submitted to the Graduate Faculty in Physics in partial fulfillment of the requirements for the degree of Doctor of Philosophy, The City University of New York.

1989

This manuscript has been read and accepted for the Graduate Faculty in Physics in satisfaction of the dissertation requirement for the degree of Doctor of Philosophy.

Sept. 27, 1989
Date

Frederick W. Smith
Chair of Examining Committee

Sept 27, 1989
Date

Executive Officer

Dr. Hans Thomann

Prof. William Sweeney

Prof. Robert Callender

Prof. Joel Gersten

Dr. Edward Stiefel

Supervisory Committee

The City University of New York

Abstract

THE ELECTRON SPIN ECHO STUDIES OF METALLOPROTEINS

by

Haiyong Jin

Adviser: Dr. Hans Thomann

A systematic method is developed to analyze Electron Spin Echo (ESE) spectra of frozen solution materials. The ESE signal of a frozen solution sample arises from molecules which orient differently with respect to the applied field. The "orientation selectivity" by EPR associates the ESE signal at a given field setting to a distinct subset of molecules. This, together with the dependence of ESE envelope modulation spectra on the field setting, makes it possible to obtain single crystal level information about the molecular structure from a frozen solution sample.

In the ESE spectra of both native and isotopically enriched nitrogenase molybdenum iron protein, nuclear modulation due to at least one nitrogen coordinated to the iron molybdenum cofactor, the protein active site, have been observed. Based on the nuclear quadrupole parameters (e^2qQ/h = 2.0 MHz, η = 0.65) obtained from numerical analysis, in comparison with existing ^{14}N Nuclear Quadrupole Resonance data and recent site–directed mutagenesis studies of the

protein, this nitrogen is most likely from the side chain of a histidine, or a glutamine. Furthermore, The significant change of the nitrogen modulation amplitude introduced by the difference in molybdenum isotope enrichment suggests that this nitrogen is likely connected to the FeMoco through coordination to the molybdenum.

In the ESE and EPR studies of the multicopper enzyme nitrous oxide reductase, two types of copper sites are identified: antiferromagnetically coupled ($J > 200\ cm^{-1}$) dimeric sites and unusual Cu(II) sites. The EPR susceptibility arises from these Cu(II) sites and from binuclear mixed valence Cu(I)/Cu(II) half – met sites which are derived from partially reduced dimers. On average, six of the eight copper ions per protein are in the form of the EPR silent binuclear type 3 dimers. The inverse proportionality of EPR activity and biological activity among various forms of the enzyme suggests that the reduction of N_2O may take place at the sites of EPR–silent binuclear dimers. Also, the ESE envelope modulation data of the enzyme provide a direct evidence that the Cu_A site, which exists in cytochrome c oxidase, is also present in this enzyme.

Dedicated to My Wife, Yueming

Acknowledgements

Many people contributed to this work, some directly and still more indirectly. I would like to give a special thanks to Dr. Hans Thomann for his constant support and encouragement. It would be difficult for me to complete this research, without his direction, patience and broad research interests, not to mention the opportunity he provided for me to complete the dissertation research at Exxon Corporate Research Lab. I am grateful to Dr. Bill Mims for his invaluable guidance. His scientific insights and intuitions are always inspirations to me. I also wish to acknowledge the help and encouragement from many friends at the Corporate Research Lab. Among them, the selfless friendship of Paul Tindall has made my work more pleasant, especially while I began my adventures in ESE experiments with little background. The computer expertise and helping hands of Marcelino Bernardo are constantly appreciated, no matter how trivial or complicated the problem is. Dr. Cathy Coyle has been of great help to me, and has answered many of my layman questions, since I stepped into the world of metalloproteins. Rick Bare has not only provided high quality nitrogenase samples, but also shared many of my joys and anxieties. The enthusiasm of Dr. Graham George has enlightened me during my research. I have also benefited a great deal from Dr. Ed Stiefel's remarkable insights and knowledge of nitrogenase. I wish to thank Drs. Bernie Silbernagel and Mike Melchior for encouraging and supporting the research, Layce Gebhard for technical assistances and permission for access to her office and EPR spectrometer, Dr. John Millar for many interesting discussions, and Manny Garcia for technical assistances. I wish to thank Eric Hustedt of University of Washington for many helpful discussions, especially on the LP

method. I also wish to thank Dr. Walter Zumft of Universität Karlsruhe for providing high quality N_2O reductase samples.

I would like to thank members of my dissertation committee for their time: every meetings have been scheduled on short notice. I also wish to thank Paul, Graham and Cathy for proofreading draft versions of this dissertation.

Most of all, I am indebted to my wife, Yueming for her support, encouragement, devotion, and sacrifice. My gratitude also goes to my parents for many years of encouragement and support.

The financial support of the City College, the City University of New York, and Exxon Research and Engineering Company is appreciated.

New York, New York
Annandale, New Jersey
September, 1989

CONTENTS

ABSTRACT iv

ACKNOWLEDGEMENTS vii

LIST OF TABLES xii

LIST OF FIGURES xiii

PART I. ELECTRON SPIN ECHO SPECTROSCOPY

CHAPTER 1. GENERAL INTRODUCTION 2

CHAPTER 2. INTRODUCTION TO ESE SPECTROSCOPY 8

2.1 Electron Spin Echo Envelope Modulation 12

2.2 Echo–induced EPR 15

CHAPTER 3. NUMERICAL SIMULATION METHODS 16

3.1 The Spin Hamiltonian 16

3.2 Expressions for the Echo Envelope Functions 24

3.3 "Orientation Selective" ESE 31

3.4 About the Simulation Software 36

3.5 The Spherical Average Method for ^{14}N ESEEM 38

CHAPTER 4. DATA ANALYSIS AND EXPERIMENTAL METHODS 42

4.1 The ESE Spectrometer 42

4.2 The "Dead Time" Problem 44

4.3 The Phase Correction Method 46

4.4 The Linear Prediction Back Extension Method 48

4.5 The Phase Cycling Method 55

4.6 The Waveform Division Method 58

References of Part I 61

PART II. ELECTRON SPIN ECHO STUDY OF THE NITROGENASE MOLYBDENUM IRON PROTEIN

CHAPTER 5. INTRODUCTION 68

CHAPTER 6. EXPERIMENTAL RESULTS 75

6.1 Experimental Results at 5 K 75

6.2 Experimental Results at 1.5 K 86

CHAPTER 7. DISCUSSION 115

7.1 Numerical Simulation 115

7.2 Identity of the Nitrogen Ligand 137

7.3 The Effect of Molybdenum Isotopes on the Nitrogen Modulation 146

7.4 Conclusions 149

References of Part II 151

PART III. COPPER COORDINATION IN NITROUS OXIDE REDUCTASE

CHAPTER 8. INTRODUCTION 157

CHAPTER 9. RESULTS 160

9.1 Experimental Conditions 160

9.2 EPR Studies 162

9.3 ESE Studies of Nitrogen Coordination 174

9.4 ESE Studies of the Base–Activated Enzyme 177

CHAPTER 10. DISCUSSION 183

10.1 Characterization of EPR Active Copper Sites 183

10.2 Numerical Simulation of ESE Frequency Spectra 186

10.3 Presence of Copper A Sites 192

10.4 The Spectroscopic Model 195

References of Part III 197

APPENDIX

1. The Transformation of Angular Momentum Eigenvectors Under Finite Rotations 200

2. Expressions of the NQI in Non–Principal Coordinate System 204

3. Preparation of the MoFe protein 206

4. Computer Program Listings 208

BIBLIOGRAPHY 239

LIST OF TABLES

Table		Page
6.2.1	Table of relative change of the normalized amplitudes of ^{14}N modulation frequencies due to molybdenum isotopic enrichments in the MoFe protein	114
7.2.1	The best–match simulation parameters for the ^{14}N modulation in ^{96}Mo isotopically enriched MoFe protein	125
9.1.1	Various forms of nitrous oxide reductase	161
9.2.1	List of percentage of Cu which is EPR active from the EPR susceptibility measurements on N_2O reductase	169

LIST OF FIGURES

Figure		Page
1.1	Biological Nitrogen Cycle (from Burgmayer *et al. J. Chem. Edu.* 1985, *62*, 943).	3
2.1	The Hahn echo (two–pulse) sequence and the echo forming process. Magnetization M of spin packets are shown in the rotating coordinates system: (a,b) before and after the $\pi/2$ pulse; (c,d) before and after the π pulse; (e) phase convergence of all spin packets at the time of the echo.	10
2.2.1	A four level spin system consisting of an electron and a spin 1/2 nucleus. The magnetic quantum numbers for the electronic and nuclear spin are denoted by M_S and M_I, respectively. The solid lines represent the "allowed" transitions $\Delta M_S = \pm 1$ and $\Delta M_I = 0$; the dashed lines represent the "partially forbidden" transitions $\Delta M_S = \pm 1$ and $\Delta M_I \pm 1$.	14
3.3.1	Correspondence between magnetic field values in an EPR spectrum and field orientations within the PAS of g–tensor. Left: EPR spectrum taken at 2K for the MoFe protein from *Azotobacter vinelandii*. Right: Unit sphere with curves of constant g value drawn and several correspondence indicated. (From Hoffman *et al. J. Magn. Reson.* 1984, *59*, 110)	32
4.1.1	Block digram of the Electron Spin Echo spectrometer used for the experiments. The probe shown is a slotted tube resonator. (Courtesy of M. Bernardo)	43
4.4.1	Comparison of of back–extension methods. Fourier transform spectra are from the same time–domain data as in (a) of Figure 6.1.1, but back extended with (a) a quarter sine function (b) LPBE method.	53
4.5.1	Echoes observed with the stimulated echo sequence. The experiment is performed to observe the stimulated echo denoted by SE. Echoes 1, 2, 3 and RE are two–pulse echoes resulted from various transmitter pulses and the refocused echo, respectively.	56
5.1	Schematic representation of an Mo–nitrogenase. (Courtesy of Dr. E. I. Stiefel.)	69
5.2	X–band EPR spectra taken at 5 K for (a) the nitrogenase MoFe protein from *Clostridium pasterianum*; and (b) the FeMoco extracted from the protein in NMF. Other experimental conditions: the microwave frequency 9.222 GHz, center field 2250 gauss, the field span = 4000 gauss, and the modulation field amplitude = 10 gauss.	71
6.1.1	The time–domain envelope waveform taken with the stimulated echo	

sequence is shown for the MoFe protein in (A) and its Fourier transform in (B) and for the FeMoco in (C) and its Fourier transform in (D). The experimental conditions were $\tau = 0.12$ μsec, $H = 1740$ gauss, microwave frequency 9.0595 GHz; temperature = 5 K; $\pi/2$ pulse width was 0.02 μsec. Fourier transformation was facilitated by using the LPBE method.
76

6.1.2. Comparison of (a) the experimental and (b) simulated spectra for the MoFe protein at $g = 3.70$. The experimental conditions have been described in Figure 6.1.1. The phase correction was performed following cosine Fourier transform, as discussed in Section 4.3. The simulation was performed with the spherical average method as discussed in Section 3.5 with $\nu_+ = 2.0$ MHz, $\nu_- = 1.4$ MHz, and $A_{iso} = 1.65$ MHz.
80

6.1.3. Comparison of (a) the experimental and (b) simulated spectra for the MoFe protein at $g = 2.50$. The experimental conditions are the same to those in Figure 6.1.1, except $H = 2577$ gauss, $\tau = 0.16$ μsec. The phase correction was performed following cosine Fourier transform, as discussed in Section 4.3. The simulation was performed in the same way as in Figure 6.1.2, except $\nu_+ = 2.2$ MHz, $\nu_- = 1.3$ MHz, and $A_{iso} = 1.50$ MHz.
82

6.2.1 ESE spectra at $g = 2.05$ for (a) FeMoco extracted in NMF; (b) FeMoco in ^{13}C, ^{15}N doubly labeled NMF. The experimental conditions were: a) microwave frequency $\nu_e = 9.154$ GHz, $H = 3186$ gauss and $\tau = 0.22$ μsec; b) $\nu_e = 9.170$ GHz, $H = 3196$ gauss, and $\tau = 0.22$ μsec, For both spectra, T = 1.5 K and $\pi/2$ pulse width was 0.03 μsec. The phase correction was performed following the cosine Fourier transform, as discussed in Section 4.3.
87

6.2.2 Comparison of CW–EPR and EI–EPR spectra of the MoFe protein isotopically enriched with ^{96}Mo. The experimental conditions were: $\nu_e = 9.056$ GHz; temperature, 1.5 K; $\pi/2$ pulse width 0.03 μsec; τ of the Hahn echo sequence is indicated for each EI–EPR spectrum in the Figure. Magnetic field values and corresponding g values are labeled as the absissa. The top spectrum was generated using the CW–EPR simulation parameters for the same protein at 4.2 K (George *et al. Biochem. J.* 1989, *262*, 349).
91

6.2.3 Comparison of CW–EPR and EI–EPR spectra of the MoFe protein isotopically enriched with ^{95}Mo. The top spectrum was generated using the CW–EPR simulation parameters for the same protein at 4.2K (George *et al. Biochem. J.* 1989, *262*, 349). The experimental conditions are identical to those in Figure 6.2.2.
93

6.2.4 ESEEM spectra at 1.5 K for the ^{96}Mo enriched MoFe protein. The experimental conditions were: $\nu_e = 9.056$ GHz; $\tau = 0.17$ μsec, and

$\pi/2$ pulse width was 0.03 μsec. Field settings and g values are (from the top): $g = 2.01$, $H = 3219$ gauss; $g = 2.54$, $H = 2548$ gauss; $g = 3.79$, $H = 1707$ gauss; and $g = 4.13$, $H = 1567$ gauss. Fourier transformation was facilitated by the application of LPBE method. 96

6.2.5 ESEEM spectra at 1.5 K for the ^{95}Mo enriched MoFe protein. The experimental conditions and data processing procedure are identical to those in Figure 6.2.4. 98

6.2.6 ESEEM spectra at 1.5 K for the ^{96}Mo enriched MoFe protein. Experimental conditions were: $\nu_e = 10.682$ GHz; $\tau = 0.25$ μsec, and $\pi/2$ pulse width, 0.03 μsec. Field settings and g values are (from the top): $g = 2.01$, $H = 3797$ gauss; $g = 2.54$, $H = 3005$ gauss; $g = 3.79$, $H = 2014$ gauss; and $g = 4.13$, $H = 1847$ gauss. The data processing procedure is the same as for Figure 6.2.4. 100

6.2.7 ESEEM spectra at 1.5 K for the ^{95}Mo enriched MoFe protein. The experimental conditions and data processing procedure are identical to those in Figure 6.2.6. 102

6.2.8 The time domain waveform at $g = 2.01$ for: (a) the ^{95}Mo enriched MoFe protein, and (b) the ^{96}Mo enriched MoFe protein. The quotient waveform of (a) over (b) is shown in (c). The experimental conditions are the same as in Figure 6.2.4 and 6.2.5. Data points from $\tau + T = 0.0$ to 0.34 μsec were back-extended using LPBE method. Baseline points are shown at the end of time domain data. 104

6.2.9 Fourier transform spectra for the time domain waveforms shown in Figure 6.2.8. 106

6.2.10 Fourier transform spectra for quotient waveforms obtained in the same way as in (c) in Figure 6.2.9. The experimental conditions are the same as in Figure 6.2.4 and 6.2.5, except in the middle spectrum $g = 2.23$, $H = 2901$ gauss. 107

6.2.11 ESEEM spectra at 1.5 K for the native MoFe protein. The experimental conditions are the same as in Figure 6.2.4, except that $g = 2.23$, $H = 2901$ gauss for the topmost spectrum (a). The Fourier transformation was facilitated by the application of the LPBE method. 110

7.1.1 Simulated spectra at $g = 2.01$ and $\nu_e = 9.056$ GHz using PSU_OS2. The principal g values are $g_1 = 4.28$, $g_2 = 3.79$, and $g_3 = 2.01$. The simulation parameters for the ^{14}N nucleus are: Q_{zz}/h $(e^2qQ/4) = 0.5$ MHz, $\eta = 0.5$, $\gamma = 0$; $A_{iso} = 0.7$ MHz (as defined in Eq. 3.1.10); $r_{eff} = 2.2$ Å, $\theta_n = 45°$, and $\varphi_n = 60$. α and β are: (a) 60°, 15°; (b) 60°, 165°; (c) 120°, 15°; (d) 120°, 165°; (e) 60°, 195°; (f) 60°, 345°; (g)

120°, 195°; and (h) 120°, 345°.

117

7.1.2 Simulated spectra at $g = 2.54$ and $\nu_e = 9.056$ GHz using PSU_OS2. The principal g values are listed in Figure 7.1.1. The simulation parameters for the ^{14}N nucleus are: $g_1 = 4.28$, $g_2 = 3.79$, $g_3 = 2.01$; $Q_{zz} = 0.5$ MHz, $\eta = 0.65$, $\gamma = 0$; $A_{iso} = -0.7$ MHz (as defined in Eq. 3.1.10); $r_{eff} = 2.2$ Å, $\theta_n = 35°$, and $\varphi_n = 50°$. α and β are: (a) 40°, 20°; (b) 40°, 160°; (c) 140°, 20°; (d) 140°, 160°; (e) 40°, 200°; (f) 40°, 340°; (g) 140°, 200°; and (h) 140°, 340°.

119

7.1.3 Simulated spectra at $g = 2.54$ and $\nu_e = 9.056$ GHz using PSU_OS2. The simulation parameters are the same as in Figure 7.1.2, except $\alpha = 40°$, $\beta = 20°$; and θ_n and φ_n values are: (a) 35°, 50°; (b) 35°, 130°; (c) 145°, 50°; (d) 145°, 130°; (e) 35°, 230°; (f) 35°, 310°; (g) 145°, 230°; and (h) 145°, 310°.

122

7.1.4 Comparison of (a) the experimental and (b) simulated spectra at $g = 2.01$ and $\nu_e = 9.056$ GHz. The experimental conditions are listed in Figure 6.2.4. The simulation input for the ^{14}N nucleus were: $Q_{zz}/h = 0.5$ MHz, $\eta = 0.7$, $\alpha = 0°$, $\beta = 10°$, $\gamma = 0°$; $A_{iso} = -0.4$ MHz (as defined in Eq. 3.1.10); $r_{eff} = 2.3$ Å, $\theta_n = 90°$, and $\varphi_n = 150°$. The principal g values are listed in Figure 7.1.2

126

7.1.5 Comparison of (a) the experimental and (b) simulated spectra at $g = 2.01$ and $\nu_e = 10.682$ GHz. The experimental conditions are listed in Figure 6.2.6. Other simulation input parameters are identical to those in Figure 7.1.4.

128

7.1.6 Comparison of (a) the experimental and (b) simulated spectra at $g = 2.54$ and $\nu_e = 10.682$ GHz. The experimental conditions are listed in Figure 6.2.6. The simulation input for ^{14}N nucleus were: $Q_{zz}/h = 0.51$ MHz, $\eta = 0.63$, $\alpha = 0°$, $\beta = 5°$, $\gamma = 0°$; $A_{iso} = -0.38$ MHz (as defined in Eq. 3.1.10); $r_{eff} = 2.3$ Å, $\theta_n = 105°$, and $\varphi_n = 142°$. The principal g values are listed in Figure 7.1.2

131

7.1.7 Comparison of (a) the experimental and (b) simulated spectra at $g = 2.54$ and $\nu_e = 10.682$ GHz. The experimental conditions are listed in Figure 6.2.6. The simulation input for the ^{95}Mo nucleus were: Q_{zz}/h

= 0.05 MHz, $\eta = 0.63$, $\alpha = 0^\circ$, $\beta = 10^\circ$, $\gamma = 0^\circ$; $A_{iso} = 2.5$ MHz (as defined in Eq. 3.1.10); $r_{eff} = 1.5$ Å, $\theta_n = 75^\circ$, and $\varphi_n = 45^\circ$. The principal g values are listed in Figure 7.1.2.

135

7.2.1 The structure of histidine at pH = 6.0.

139

7.2.2 Plot of h/e^2qQ *vs.* η for imidazole nitrogens. The linear relation was fitted without the data for the MoFe protein. (all data, except that for the MoFe protein, are Mims, *et al.* preprint, and references therein).

141

7.2.2 Plot of h/e^2qQ *vs.* η for the pyridine nitrogen in Zn(II)– or Cd(II)–pyridine complexes and the imino nitrogen in Zn(II)– or Cd(II)–imidazole complexes. Data were obtained from NQR experiments (Hsieh *et al. J. Am. Chem. Soc.* **1977**, *99*, 1394.; and Ashby *et al. J. Am. Chem. Soc.* **1978**, *100*, 6057.

142

9.2.1 X–band EPR spectra taken at 10 K for various oxidized forms of N_2O reductase: (A) pink form; (B) purple form; (C) cathodic form; (D) purple form at pH 9.8.

163

9.2.2 X–band EPR spectra taken at 10 K for various reduced forms of N_2O reductase: (A) pink; (B) purple; (C) cathodic.

164

9.2.3 Temperature dependence of inverse EPR susceptibility for various forms of N_2O reductase. (A) Total susceptibility for the oxidized enzymes; (B) normalized susceptibility obtained by subtracting the susceptibility for the reduced enzymes from (A).

167

9.2.4 X–band EPR spectra for (A) oxidized purple enzyme at pH 7.5 and (B) after the addition of a 400–fold excess of azide over copper.

171

9.2.5 X–band EPR spectra for (A) oxidized purple enzyme at pH 6.0; (B) after adding a 300–fold excess of azide over copper; and (C) following dialysis for 4 hours after the azide addition.

172

9.3.1 Time domain electron spin echo envelope waveforms for the oxidized N_2O reductase recorded at $T = 1.8$ K: (A) oxidized pink (aerobically isolated); (C) oxidized cathodic (anaerobically isolated); (B) and (D) are the Fourier transforms of (A) and (C) respectively. Other conditions: $\tau = 0.14$ μsec, $H = 3280$ gauss; $g = 2.03$. Inserts of the time domain waveforms show the baseline at the end of the data collection period.

175

9.4.1 Time domain spin echo envelope data for the oxidized (A) purple enzyme at pH 7.5 and (B) purple enzyme at pH 9.8, enzyme dialyzed against D_2O buffer. The intensities were normalized against the first peak in the modulation for easy comparison of the relative modulation depths. Spectra were recorded at $T = 5$ K, $\tau = 0.24$ μsec, other

conditions are the same as for Figure 9.3.1.
178

9.4.2 Ratio of spin echo envelope time domain waveforms for various oxidized enzymes dialyzed against TRIS buffer in D_2O: (A) purple at pH 9.8 over purple at pH 7.5; (B) purple at pH 7.5 over cathodic at pH 7.5.
181

10.2.1 Simulated spin echo envelope spectra for various nitrogenous ligands. The quadrupole coupling, e^2qQ/h (MHz); quadrupole asymmetry, η; and hyperfine contact couplings, A_{iso} (MHz), are: (A) 1.44, 0.7, 0.6; (B) 1.53, 0.87, 1.65; (C) 2.3, 0.76, 0.65. Other conditions: $g = 2.03$, $H = 3280$ gauss. The weighted intensities for spectrum D are: $1.0 \times A + 0.8 \times B + 0.2 \times C$.
189

A1 Euler angles and corresponding rotations. (From Edmonds, A. R. *Angular Momentum in Quantum Mechanics*; Princeton University Press, Princeton; 1974)
203

PART I

ELECTRON SPIN ECHO SPECTROSCOPY

ABSTRACT

The ESE signal of a frozen solution sample arises from molecules which orient differently with respect to the applied field. The "orientation selectivity" by EPR associates the ESE signal at a given field setting to a distinct subset of molecules. This, together with the dependence of ESE envelope modulation spectra on the field setting, makes it possible to obtain single crystal level information about the molecular structure from a frozen solution sample. A systematic method is developed to extract such information. Simulations, with the consideration of "orientation selection", are optimized by a least–square minimization to achieve the best–match to the experimental data. In addition, the uniqueness of the extracted parameters can be ensured by the constraint that they are independent of experimental conditions such as the resonant frequency, the field setting, or the choice of inter–pulse time intervals.

A finite instrument "dead time" due to the probe ringdown from high power transmitter pulses causes problems in cosine Fourier transform spectra of ESE data. They include distortions to the baseline and phases of modulation frequency lines. A number of methods, including phase correction and Linear Prediction back extension, will be discussed in order to minimize these distortions.

Chapter 1

GENERAL INTRODUCTION

Enzymes, the catalysts of biological systems, are remarkable for their catalytic power and specificity. Enzymes consist of proteins specifically folded in three–dimensional structures such that a catalytically active site is formed in a small region of the macromolecule. Important transition metals including iron, copper, molybdenum and vanadium are essential elements that often form the key parts of active sites of the enzymes which participate in many of the most relevant biological reactions. The enzymes studied in this dissertation, the nitrogenase and nitrous oxide reductase, are involved in one of the important metabolisms – the nitrogen cycle, as shown in Figure 1.1[1-2]. The process of nitrogen fixation ($N_2 \longrightarrow NH_3$) is an essential source for the availability of fixed nitrogen which is often the limiting factor in plant growth.[3] Most of the nitrogen fixation on earth is accomplished through the catalytic action of nitrogenase. On the other hand, nitrous oxide reductase is the terminal enzyme in the metabolic pathway for denitrification.[4] The catalytic mechanism for these enzymes is still unknown, as is the case for most metalloproteins. The correlation of biological function to microscopic structure has been a focal point of many intensive research efforts.[5-6] Knowledge of the structure of the active sites is needed to elucidate the catalytic mechanisms of these enzymes.

Biological systems often provide the motivation and testing ground for the development of spectroscopic probes. Electron Spin Echo (ESE) technique, a time domain extension of Electron Paramagnetic Resonance (EPR) spectroscopy, has

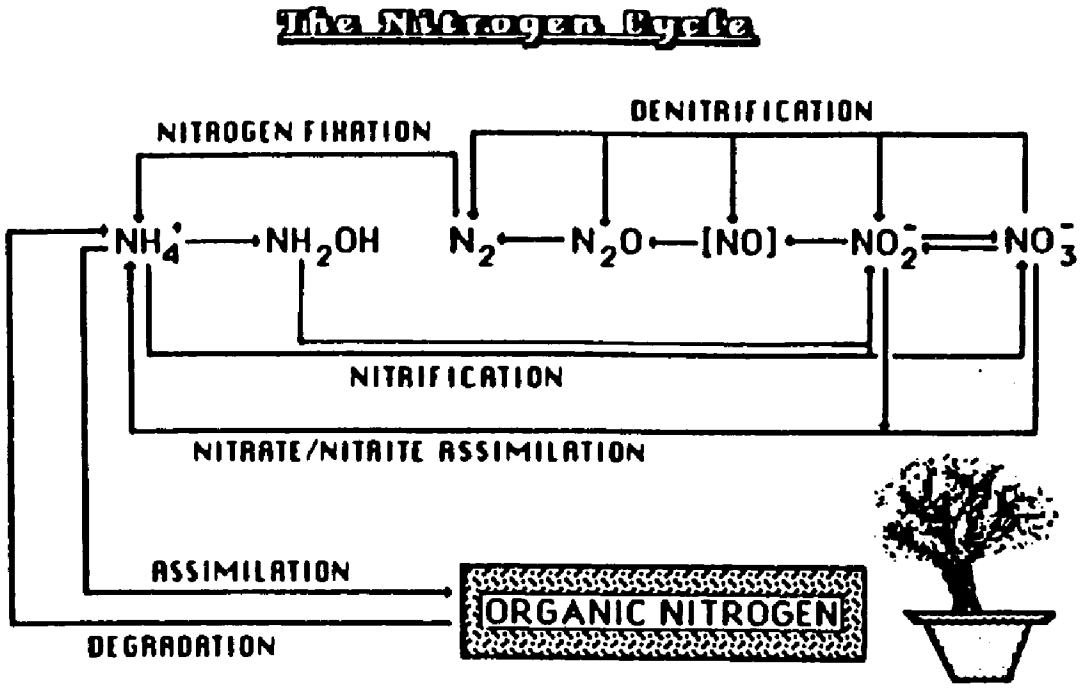

Figure 1.1 Biological Nitrogen Cycle (from Burgmayer *et al. J. Chem. Edu.* 1985, *62*, 943).

been applied extensively in metalloprotein studies.[7-9] By analyzing the envelope modulation of an ESE signal, which is associated with the electron–nuclear interaction, it is possible to obtain information such as ligand identity, coupling strength, and geometrical parameters of the molecular levels.

EPR probes the transitions among energy levels of paramagnetic electrons in the presence of an external magnetic field.[10,27-28] A paramagnetic complex contains ion(s) which have permanent magnetic moments. In the absence of an external field such moments are randomly oriented, but the application of a field results in a redistribution over the various orientations in such a way that the complex acquires a net magnetic moment. Permanent magnetic dipoles occur only when the ion(s) possess a resultant angular momentum. Many ions have closed electron shells which have no resultant angular momentum and hence no permanent electronic magnetic moment. Partly filled shells, with permanent magnetic moments due to the orbital motion of the electrons, or to their intrinsic spin, or both, occur in the transition groups. When a free ion has a resultant angular momentum J in its electron system, its magnetic moment μ is

$$\mu = -g\,\beta_e\,J, \tag{1.1}$$

where β_e is the Bohr magneton (9.2741×10^{-21} erg/gauss), and g is a pure number of the order of unity, whose value depends on the relative contributions of orbit and spin to the total angular momentum. If it contains a single unpaired electron characterized by an orbital angular momentum quantum number L and a spin quantum number S ($S = 1/2$). Spin and orbital moments are combined, via spin–orbit coupling, into a total angular momentum characterized by the quantum number J. The $2J+1$ states are degenerate in the absence of a magnetic field. But in a magnetic field H, the energy of each state is given by $g_L \beta\, H\, M_J$, where M_J is

the magnetic quantum number with integral or half integral values $-j$, $-j+1$, ..., $j-1$, j. The Landé g–factor g_L is given by

$$g_L = 1 + \frac{J(J+1) - L(L+1) + S(S+1)}{J(J+1)} \tag{1.2}$$

When a magnetic resonance experiment is performed, transitions may be induced among these levels if the excitation frequency is equal to the energy level splitting

$$h\nu = g_L \beta_e H \tag{1.3}$$

with the selection rule $\Delta M_J = \pm 1$. In Equation 1.3, h is the Planck constant (6.62×10^{-27} erg·s).

But, a paramagnetic ion in condensed media is by no means "free". It is surrounded by diamagnetic atoms or ions which are only a few angstroms away. These ligand ions produce a strong electrostatic field (the ligand field) which interacts with the paramagnetic ion. The energy associated with the interaction between the paramagnetic electrons and this ligand field varies roughly from 10^2 to 10^4 cm^{-1} which falls into the infra–red frequency region. Because of this interaction, the behavior of the ion in a magnetic field is profoundly changed. Quantum states which were degenerate in the free ion become widely separated in energy, and only those states which lie at the lowest among energy levels are thermally populated. EPR technique, which measures energy transitions of a few wave numbers or less, are only capable of observing those between low–lying levels. A convenient method is needed to represent the behavior of such a group of levels when a magnetic field is applied to the system. The concept of "effective spin", $\tilde{S}$, has been found useful.[10] It is a fictitious angular momentum such that the

degeneracy of the group of levels involved is set equal to $(2\tilde{S}+1)$. With the use of the "effective spin", it is possible to set up an "effective spin" Hamiltonian that gives a correct description of the behavior of the group of levels in terms as concise as those for a free atom or ion.

The "effective spin" Hamiltonian facilitates the analysis of experimental data. The experimental quantities measured are g values, hyperfine coupling constants, and areas under the absorption curve. For a paramagnetic complex, the g factor is usually not a number, but a tensor. The symmetry of the tensor reflects the symmetry of the electric field at the ion site.[10-13] For example, Cu(II) is normally found in an octahedral environment with tetragonal distortion, with four strongly bound equatorial ligands and one or two weakly bound axial ligands.[14] $g_{\|}$ is measured when the applied field is oriented along the axial ligand direction, and g_x or g_y is obtained when the field is in the equatorial plane. When g_x is found to be equal to g_y because of the symmetry of the site, Cu(II) complexes are described as having an axial g tensor. Hyperfine structure, found in many of the signals, not only enables the identification of the metal ion, but also reflects the immediate environment of the metal ion. For example, the copper nucleus with a nuclear spin I of 3/2 couples to the unpaired electron, producing a hyperfine splitting pattern of $2I + 1 = 4$ components. It has been observed in copper proteins that one can relate the hyperfine coupling values to the degree of tetrahedral distortion of the Cu(II) coordination geometry.[14] In fact, the magnitude of the hyperfine coupling is one of the distinguishing features between type 1 and type 2 copper sites, two distinct classes of Cu protein.

In short, an EPR spectrum of a metalloprotein is capable of yielding a diverse amount of information concerning the paramagnetic metal ion(s) and its environment: the symmetry of the metal binding site; the covalent character of the metal–ligand bonds; the oxidation–reduction state of the ion(s) and the total

amount of the paramagnetic spins. Usually, the EPR spectra of biological materials consist of a few broad lines rather than a well characterized hyperfine splitting pattern. Frozen solution samples containing transition metal ions generally have line widths on the order of several hundred gauss. This sets the limit as to how much information can be extracted from an EPR spectrum and provides one of motivations to perform Electron Spin Echo spectroscopy.

Chapter 2

INTRODUCTION TO ELECTRON SPIN ECHO SPECTROSCOPY

Electron Spin Echo spectroscopy is a time–domain technique. While a single pulse experiment can be performed in Fourier transform Nuclear Magnetic Resonance (FT–NMR) spectroscopy,[15] a time–domain EPR experiment usually can not be done with a single pulse. The NMR transitions can be uniformly excited by the applied pulse, while this is usually not the case for an EPR experiment. A typical pulse width for rotating electron spins by 90° is 20–30 nsec, corresponding to an excitation bandwidth of 30–50 MHz, or about 10 to 15 gauss. This is usually much smaller than typical transition–metal EPR line widths, for example, the EPR line width of the nitrogenase molybdenum–iron protein is about 2500 gauss, or about 6000 MHz. Furthermore, there are limitations due to fast relaxation rates. For example, lines of 1 gauss width (considered to be very narrow for most samples of transition metal ions) would yield free induction decay (FID) signals decaying on the order of 100 nsec. Because the resonator has a finite recovery time after the application of the high power microwave pulses, the FID can not be detected immediately. This missing information or "dead time" piece in the data prevents us from observing the fast decaying EPR FID. Therefore, the application of FID spectroscopy in EPR is limited to samples with very narrow line widths, hence longer relaxation times. To study broad EPR signals, ESE techniques involving the application of multiple pulses is needed.

The major advantage of ESE is that it can give much higher spectral resolution than EPR. Two line widths can be identified in an EPR spectrum.[16]

One is the line width corresponding to the intrinsic coherence lifetime of spectral components centered around certain frequencies or electron spin packets. That is the time during which the spin packets precess without serious disturbance from lattice relaxation, or from fluctuating magnetic fields due to other spins. This time is referred to as the phase memory time, T_m. The other is the line width observed in an EPR experiment, which is a superposition of a large number of narrow resonance lines accommodated within a smooth and slowly varying envelope which constitutes an "inhomogeneously broadened" line. Here the inhomogeneous broadening means that the precessions of individual spin packets are independent of one another. The inhomogeneous broadening can be due to the g–anisotropy in a polycrystalline sample, or to the presence of unresolved hyperfine lines. On the other hand, the spin packets have a coherence time determined by the macroscopic dynamics of the samples. The resolution obtainable in ESE studies is not limited by the inhomogeneous broadening, but by the intrinsic coherence lifetime of individual spin packets.

The spin echo forming process may be described quantum mechanically in terms of the density matrix formulation, or semi–classically in terms of precessing gyroscopic magnets. The semi–classical approach will be depicted here. Figure 2.1 shows the simplest ESE pulse sequence, the Hahn echo (two–pulse) sequence,[17] as well as the echo forming process for the sequence. The coordinate system shown in the figure represents a reference frame which rotates about the Zeeman field at an angular velocity $2\pi \nu_e$, where ν_e is the microwave frequency resonant with the EPR transitions. Since the EPR line is inhomogeneous, different spin packets precess about the Zeeman field at different rates. After the first pulse tilts the spin packets so that their average magnetization lies in the horizontal plane, the differences in precession rates among spin packets gives rise to a distribution of magnetization subsets. The second pulse, applied at time τ after the first pulse, reverses the

Figure 2.1 The Hahn echo (two–pulse) sequence and the echo forming process. Magnetization M of spin packets are shown in the rotating coordinates system: (a,b) before and after the $\pi/2$ pulse; (c,d) before and after the π pulse; (e) phase convergence of all spin packets at the time of the echo.

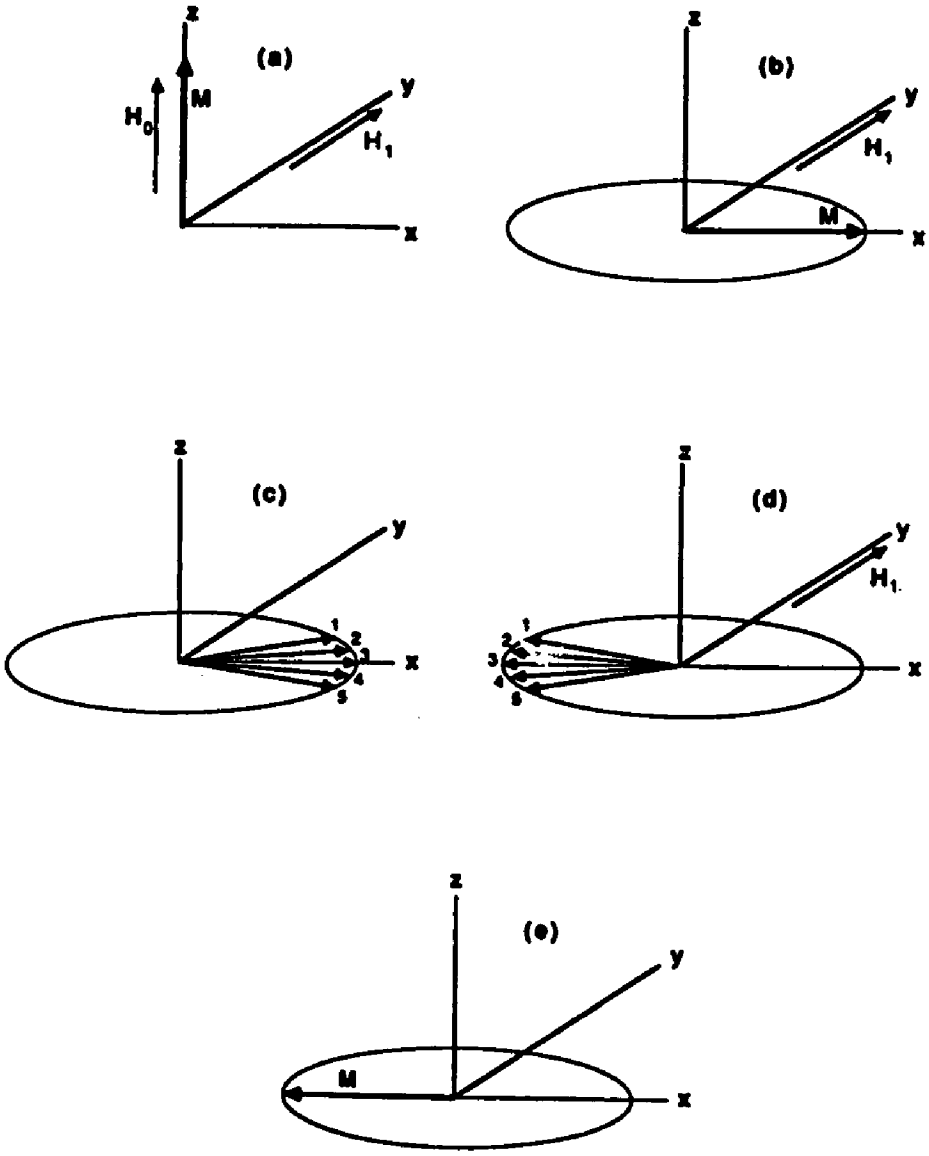
z
(a)
y
M
H_0
H_1
x
z
(b)
y
H_1
M
x
z
(c)
y
1
2
3
4
5
x
z
(d)
y
H_1
1
2
3
4
5
x
z
(e)
y
M
x

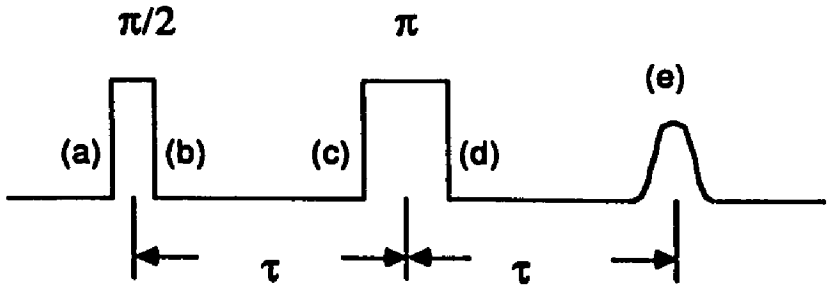
π/2
π
(e)
(a)
(b)
(c)
(d)
τ
τ

Figure 2.1

accumulated relative phases of the spin packets, but not their sense of precession. At time 2τ the magnetization of the spin packets interfere constructively, giving rise to the echo signal. In order for this constructive interference to occur, it is crucial that coherence be generated among the various "spin packets" by the first pulse. It is this coherence which makes cancellation of the accumulated relative phases possible, therefore, eliminating the effect of inhomogeneous broadening.

There are several types of ESE experiments, two of which are the nuclear modulation and echo–induced EPR (or echo detected EPR) experiments.

I. Electron Spin Echo Envelope Modulation (ESEEM)

In the nuclear modulation experiment, one sets the magnetic field to a value within the EPR line width, and with a sequence of microwave pulses generates a spin echo whose intensity is monitored as a function of the delay time between a pair of the pulses. The nuclear modulation effect, which changes the echo amplitude periodically, arises from the interaction of the electron spin with nearby nuclei. The local magnetic field at a nucleus is a sum of the applied magnetic field and the field produced by the electron. When the electron spins are rotated during the pulses in a time that is short compared to the precession frequency of the nuclear spin, the direction of the local field at the nuclear site is changed. The nucleus, aligned along the previous local field, begins to precess about the new local field, and a periodically varying local magnetic field will be seen by the electron. This changes the phase in the electron spin precession, therefore the echo amplitude. Thus, the analysis of the nuclear modulation effect affords a useful means of identifying the nuclei in a magnetic complex and investigating their interaction with an electron spin.

The nuclear modulation effect was experimentally demonstrated by Mims *et*

al.[18] and Cowen *et al.*[19] in their pioneering work. Rowan, Hahn and Mims[20] developed an expression describing the 2–pulse nuclear modulation effect, and confirmed it in their work on $CaWO_4$ single crystal doped with Ce^{+3}. Expressions for the echo envelope modulation functions for the 2–pulse and 3–pulse sequence, and their derivations and limitations are thoroughly discussed by Mims.[21-22] The nuclear modulation effect has been utilized extensively for studying biological samples, transition metal complexes, organic radicals, coal, conducting polymers, and catalysts. The subject of ESE envelope modulation (ESEEM) as well as its application have been reviewed by several authors, details of which can be consulted there.[7,16,23-25]

A qualitative understanding of ESEEM can be gained by analyzing a four level spin system where an electron spin $S = 1/2$ and a nuclear spin $I = 1/2$ interact. In Figure 2.2.1, the electron and nuclear spin quantum numbers M_S and M_I are shown as labels for each energy level. In the energy level diagram, solid lines represent "allowed" transitions, where $\Delta M_S = 1$, $\Delta M_I = 0$; while dashed lines represent "partially forbidden" transitions, where $\Delta M_S = 1$, $\Delta M_I \neq 0$. In an ESE experiment each pulse excites the transitions between the upper and lower manifolds. If the pulse excitation bandwidth is greater than the energy difference in either manifold, both the "allowed" and "partially forbidden" transitions can occur. For example, transitions from E_3 and E_4 to E_1 can be simultaneously pumped, emitting photons with time coherencies. These coherent photons will interfere with each other, giving rise to the periodic changes of the echo amplitude. The echo amplitude is therefore modulated by the frequency $(E_4-E_3)/h$. Likewise, the frequency component $(E_2-E_1)/h$ modulates the echo amplitude in the similar fashion. The nuclear modulation effect is the consequence of the interference between "allowed" and "partially forbidden" transitions. The amplitude of a modulation component, therefore, is expected to be proportional to the "partially

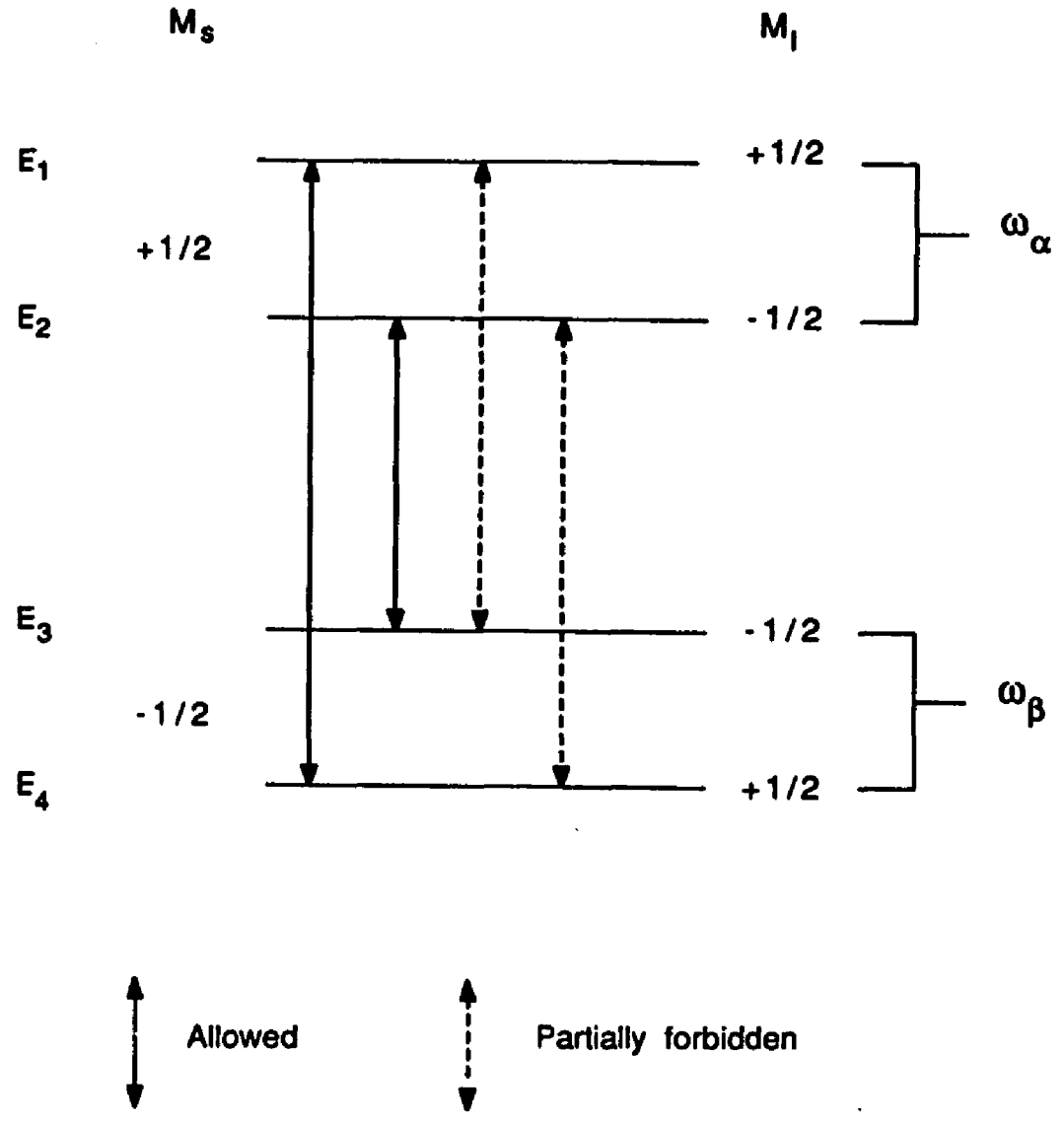

Figure 2.2.1 A four level spin system consisting of an electron and a spin 1/2 nucleus. The magnetic quantum numbers for the electronic and nuclear spin are denoted by M_S and M_I, respectively. The solid lines represent the "allowed" transitions $\Delta M_S = \pm 1$ and $\Delta M_I = 0$; the dashed lines represent the "partially forbidden" transitions $\Delta M_S = \pm 1$ and $\Delta M_I \pm 1$.

forbidden" transition probability.

II. Echo–Induced EPR

Another common experiment is the echo–induced EPR (EI–EPR). An EI–EPR spectrum is obtained when the inter–pulse time intervals are fixed and the echo signal is monitored while the applied magnetic field is varied. Usually, the Hahn–echo sequence with a fixed τ is used. Unlike CW–EPR where the "derivative" absorption spectrum is recorded, EI–EPR measures the absorption spectrum directly.

While CW–EPR is incapable of resolving the features caused by weak interactions, EI–EPR is susceptible to the the nuclear modulation effect.[16] This effect may depress or even remove signals from the EI–EPR spectrum for certain values of the pulse interval τ and for certain components of the spectrum. It has been observed that when a pronounced modulation effect is present, the EI–EPR spectrum can be quite distorted compared to the CW–EPR spectrum. Sometimes, EI–EPR can dramatically demonstrate the differences caused by the weak magnetic interactions which are unresolvable in CW–EPR. Caution should be exercised when extracting quantitative information. The straightforward approach of measuring directly from a spectrum the hyperfine coupling values or the relative amplitudes of different spectral components, as done in CW–EPR,[27] may not be appropriate for EI–EPR. Furthermore, the simulation of EI–EPR spectra may require knowledge of the coupling parameters obtained from a complete simulation of the ESEEM spectra.

Chapter 3

NUMERICAL SIMULATION METHODS

In this chapter, numerical simulation of the ESE envelope modulation will be discussed. Since an EI–EPR spectrum is taken with a fixed inter–pulse time duration τ while the magnetic field is varied, one can simulate the EI–EPR spectrum by calculating the echo amplitude at each field value for a particular τ value. That is, EI–EPR spectra can be simulated if the ESEEM simulation can be made. In this sense, the methods presented here are also applicable to the EI–EPR simulation.

I. The Hamiltonian for the Numerical Simulation

A spin Hamiltonian describes the interactions of a spin system mathematically. When properly written, its quantum mechanical solutions can be used to derive chemical and physical information about the sample.[10] Due to the complexities of a spin system, approximations need to be made. The limitation to how well the spin system is described by the numerical simulation will be determined by the approximations made. On one hand, a simple procedure is needed to extract information from the experiments; on the other hand, excessive approximations should be avoided so that extra errors are not introduced into the analysis.

1. Electron Zeeman Interaction

The interaction of paramagnetic electron spin $\tilde{S}$ with the applied magnetic field can be written as

$$\mathcal{H}_{Z_e} = \beta_e \, H \cdot g \cdot \tilde{S} \tag{3.1.1}$$

where g is the g–factor in the tensor form, β_e is the Bohr magneton, and H is the applied field. When $\tilde{S} \geq 1$, an electronic quadrupole term, $D\,[\tilde{S}_z^2 - \frac{1}{3}\,\tilde{S}(\tilde{S}+1)] + E\,(\tilde{S}_x^2 - \tilde{S}_y^2)$, can be added into the Hamiltonian to account for splittings at zero magnetic field, where D and E are axial and rhombic zero–field splitting parameters, respectively.

The g–factor is a second–rank tensor. When cross terms are present, it describes the anisotropy of the electron Zeeman interaction. Usually, it is symmetric, i.e. $g_{ij} = g_{ji}$ $(i,j = x, y, z)$. The cross terms can be eliminated by a suitable choice for the coordinate axes, yielding the simpler form

$$\mathcal{H}_{Z_e} = \beta_e \, (g_{xx} H_x \tilde{S}_x + g_{yy} H_y \tilde{S}_y + g_{zz} H_z \tilde{S}_z). \tag{3.1.2}$$

The coordinate system so chosen will be referred to as the principal axes system (PAS) of g–tensor. It is possible for g_{xx}, g_{yy}, and g_{zz} to have different signs. However, it is convenient to make them all be positive, because an EPR spectrum is not changed by reversing the direction of the applied field.[10] That is, the signs of g_{ii} do not change the EPR spectrum. By assuming all positive principal g values, as most researchers in the field, the author accepts the uncertainty of the direction of the axes.

The g–tensor reflects the symmetry of the paramagnetic ion site.[10]

Therefore, the PAS of the g–tensor can be used as a molecular reference frame. In a single crystal, there exists a fixed orientation of this coordinates system relative to the laboratory reference frame. Information gathered in one reference frame can be transformed into the other. But in a powder or a frozen solution sample, all orientations are present. As a consequence, the signal detected in the laboratory frame is a superposition of signals from many orientations. But relative to the PAS of the g–tensor, whether in a single crystal or a non–single crystal sample, the information obtained should be identical if it is recognized that a powder or a frozen solution sample consists of many randomly oriented molecules that have an identical molecular configuration. That is, information relative to the PAS of the g–tensor, if obtainable from a frozen solution sample, is equally informative as that from a single crystal. This point will be exploited further in Section 3.

Sometimes, it is possible to use a "fictitious spin" S', instead of $\tilde{S}$, to describe the lowest energy levels.[10] Without causing confusion, $\tilde{S}$ still represents the effective spin, and S, instead of S', will be used for the "fictitious spin". If S is different from $\tilde{S}$, an equation identical to Equation 3.1.2 can still be written, except that the g values are no longer the same. "Apparent" g values need to be used where principal "apparent" g values will be labeled as g_1, g_2 and g_3 with $g_1 \geq g_2 \geq g_3$. For example, the EPR signal from nitrogenase MoFe protein is from a paramagnetic center with spin 3/2.[29] A large zero field splitting ($D = 1.53 \times 10^5$ MHz, or 5.1 cm^{-1}) separates the $M_S = \pm \frac{1}{2}$ and $M_S = \pm \frac{3}{2}$ levels, with $M_S = \pm \frac{1}{2}$ lower than the other.[30-31] A fictitious spin S = 1/2 can be used to describe the $M_S = \pm \frac{1}{2}$ levels. According to Venters *et al.*[30] and Graham *et al.*[31], principal g values for nitrogenase MoFe protein from *Clostridium pasterianum* are 2.017, 2.017, and 2.025; while "apparent" ones are 4.27, 3.79, and 2.01. Similar to the PAS of the g–tensor, the PAS of the "apparent" g–tensor can be defined, with the x, y, and z axes being the principal axes of the "apparent" g tensor. The relation between a parameter

obtained in the PAS of the "effective spin" and that in the PAS of the "fictitious spin" can be derived by expressing the interaction in the two PAS, and comparing the tensor elements.

If the reference frame is defined, the orientation of the external field with respect to it can be defined by the spherical polar angles (θ, φ). H is then a function of these polar angles, H (sin θ cosφ, sin θ sin φ, cosθ). The electronic Zeeman interaction is now

$$\mathcal{H}_{Ze} = \beta_e (g_1 \sin\theta \cos\varphi + g_2 \sin\theta \sin\varphi + g_3 \cos\varphi) H S_z \qquad (3.1.3)$$

It can be rewritten as $\beta_e g H S_z$, which is similar to the expression for a free electron spin. Under a fixed microwave frequency, specifying a g value is equivalent to specifying the magnetic field setting H.

2. Hyperfine interaction

A hyperfine coupling term describes the interaction between spins of a paramagnetic electron and a nucleus. The expression for the hyperfine interaction is

$$\mathcal{H}_{HF} = \bar{S} \cdot A \cdot I \qquad (3.1.4)$$

where A is a hyperfine tensor, and I is the nuclear spin. This interaction can be separated into isotropic and anisotropic parts. The isotropic part A_{iso} ($S \cdot I$), is also called Fermi contact term. Fermi first introduced this term to account for hyperfine structure in atomic spectra.[32] It represents the interaction of the nuclear spin in the magnetic field produced at the nucleus by the electron. When an ion contains only one unpaired electron, A_{iso} has the form

$$(3.1.5) \qquad A_{iso} = \frac{8\pi}{3} g \beta_e g_N \beta_N |\psi(0)|^2$$

where β_N is 5.27×10^{-24} erg/gauss, g_N is the nuclear g value associated with the gyromagnetic ratio of the specific nucleus, and $|\psi(0)|^2$ is the spin density at the nucleus. In general, it is represented by the trace of the tensor A as

$$(3.1.6) \qquad A_{iso} = \frac{1}{3}(A_{xx} + A_{yy} + A_{zz}).$$

where A_{xx}, A_{yy}, and A_{zz} are the diagonal elements of the hyperfine tensor. It has the useful property that it is unchanged by the choice of the coordinate system. The anisotropic part of the interaction is sometimes referred to as the "pseudodipolar coupling". It is often approximated by the classical point–dipolar interaction, but they should be differentiated from each other. For a metal ion site with a low symmetry, which occurs in metalloproteins, it is unlikely that the interaction has the simple axial symmetry of the point–dipolar coupling. There is also no reason to suppose that the principal axes of A are collinear with the point–dipolar coupling vector. The approximation for the pseudodipolar interaction using the point–dipolar coupling has the form

$$(3.1.7) \qquad g \beta_e g_N \beta_N \frac{3\,(I\cdot r)(S\cdot r) - r^2(I\cdot S)}{r^5}.$$

In this expression, r should be properly denoted as r_{eff}, Since it is an approximation to the distance between the electron and the nucleus. This should not be confused with true distance, a structurally important quantity. In their ESEEM study of Cu(II)–imidazole complexes, Mims *et al.*[33] obtained $r_{eff} = 2.9$ Å for the distance

between the Cu and the observed remotely coordinated nitrogen, however the true distance is 4.1 Å. This difference can be attributed to covalency effects of the electrons.

Equation 3.1.4 can be written for the "fictitious" spin S, except that an "apparent" hyperfine tensor A' has to be defined in the place of A. The principal values of the hyperfine interaction tensor A'_j $(j = x, y, z)$ in the S′ coordinate system are related to the principal values of hyperfine interaction tensor A_j in the $\bar{S}$ coordinate system by the relation $A'_j = A_j g'_j / g_j$, when the g–tensor and hyperfine tensors are coaxial. A more complicated relation is expected if the two are not coaxial.

In the study of the nitrogenase MoFe protein, the g_j are all close to 2.0.[30-31] In order to simplify the conversion between A_j and A'_j so that one set of hyperfine values can be used across the resonant field, a modified form of hyperfine interaction has been written as

$$\mathcal{H}_{HF} = (\bar{S} \cdot g) \cdot A \cdot I \qquad (3.1.8)$$

in the $\bar{S}$ coordinate system, and as

$$\mathcal{H}_{HF} = (S \cdot g') \cdot A \cdot I \qquad (3.1.9)$$

in the S coordinate system. Now, no conversion is needed. The hyperfine tensor in the $\bar{S}$ coordinate system is $2.0 \cdot A$, and is $g' \cdot A$ in the S' coordinate system. If the hyperfine coupling in the S coordinate system is expressed in two parts, the isotropic and pseudodipolar parts, it can be written as

$$(3.1.10)\qquad \mathcal{H}_{HF} = A_{iso}\,(S \cdot g' \cdot I) + \beta_e\, g_N\, \beta_N \frac{3(I\cdot r_{eff})(S\cdot g'\cdot r_{eff}) - r_{eff}^2 (S\cdot g'\cdot I)}{r_{eff}^5}.$$

3. Nuclear Zeeman Interaction

The nuclear Zeeman interaction describes the interaction between a nuclear spin I and an external magnetic field. Usually, it is written as

$$(3.1.11)\qquad \mathcal{H}_{ZN} = g_N\, \beta_N\, (I \cdot H)\,,$$

and an isotropic nuclear Zeeman coupling factor is adopted. The electronic Zeeman interaction can mix excited states into the ground state, and change the magnetic hyperfine interaction by an amount proportional to the external magnetic field.[10] Since this term is linear in both the nuclear spin and the field, it seems that a term is added to the nuclear Zeeman coupling. This is called the "pseudo–nuclear Zeeman" interaction. Because the hyperfine coupling contains anisotropic components, the nuclear Zeeman coupling factor after the above correction becomes a tensor. For example, in the case of nitrogenase MoFe protein, it is

$$(3.1.12)\qquad (g_N)_{ij} = g_N \left[\, \delta_{ij} + \frac{3\; g_e\; \beta_e\; A_{ij}}{2\; g_N\; \beta_N\; \Delta} (\, 1 - \delta_{jB}\,)\right]$$

where $\delta_{ij} = 1$, if $i = j$, and 0 otherwise, and $\Delta = 2\sqrt{D^2 + 3\; E^2}$.[34]

4. Nuclear Electric Quadrupole Interaction

When a nucleus has a spin $I \geq 1$, and there is also an electric field gradient V_{ij} ($V_{ij} = \frac{dV}{dx_i dx_j}$, x_i , $x_j = x, y, z$) at the nucleus, an interaction of the nuclear electric quadrupole moment with the field gradient may arise.[35-37] If the principal values of a field gradient tensor are V_{xx} , V_{yy} , and V_{zz}, with $V_{xx} + V_{yy} + V_{zz} = 0$ and $|V_{xx}|$, $|V_{yy}| \leq |V_{zz}|$, the interaction can be described in the principal axes system (PAS) in an operator form

$$\mathcal{H}_Q = Q_{zz}[\,3\,I_z^2 - I(I+1) + \eta\,(I_x^2 - I_y^2)\,]\,. \tag{3.1.13}$$

Q_{zz} and η are defined as

$$\begin{cases} Q_{zz} = \dfrac{e^2 q Q}{4I\,(2I-1)} \\ \eta = \dfrac{V_{xx} - V_{yy}}{V_{zz}} \end{cases} \tag{3.1.14}$$

where Q is the scalar quadrupole moment, and $eq = V_{zz}$. In the case of I = 1 ($Q_{zz} = \frac{e^2 qQ}{4}$), NQR terminologies for the zero–field splitting ν_+, ν_-, and ν_0 ($\nu_+ - \nu_- = \nu_0$) have been defined as

$$\begin{cases} \nu_+ = (3 + \eta)\, Q_{zz} \\ \nu_- = (3 - \eta)\, Q_{zz} \\ \nu_0 = 2\,\eta\, Q_{zz}\,. \end{cases} \tag{3.1.15}$$

Since a full NQI tensor is symmetric, it has six different elements of which five are

independent (one of them is not independent, because of the requirement that the matrix is traceless). If (Q_{zz}, η) or (ν_+, ν_-) are two of the above parameters, the Euler angles (α, β, γ), relative to a known coordinate system (e.g., the PAS of the g–tensor), can be used as the other three parameters. The definitions of Euler angles are defined in Appendix 1. Therefore, the nuclear quadrupole interaction tensor is completely determined by these five parameters.

As will be discussed in Section 3.5, a large database exists for the quadrupole parameters of ^{14}N. A comparison of these parameters, between the existing ones and those obtained from an ESEEM experiment, makes the assignment of the nitrogen molecule possible.

II. Expressions for Echo Envelope Functions

There are two pulse sequences which are often used in ESE experiments. The first one is the Hahn echo (two–pulse) sequence, which has been introduced in Chapter 2. The sequence is $\pi/2 - \tau - \pi - \tau -$ echo, where $\pi/2$ and π denote the spin rotation angles produced by the microwave pulses. The other one is the stimulated echo (three–pulse) sequence, which is $\pi/2 - \tau - \pi/2 - T - \pi/2 - \tau -$ echo. The expressions for the envelope modulation function for these two sequences will be discussed below. The conventions for the symbols used by Mims[21-22] will be followed as closely as possible. The basic quantum mechanics can be found in many standard textbooks,[38-40] hence will not be repeated here.

If ρ stands for the density matrix of the spin system, then the equation of the motion is

$$\frac{d\rho}{dt} = \frac{2\pi i}{h}[\rho, \mathcal{H}] \qquad (3.2.1)$$

and,

$$(3.2.2) \qquad \mathcal{H} = \mathcal{H}_0 + \mathcal{H}_1$$

In the expression, $\mathcal{H}_0$ is a spin Hamiltonian without consideration of the applied resonant field and $\mathcal{H}_1$ describes the interaction of the spin system with the applied resonant field. During the pulses excitation, $\mathcal{H}_1$ is assumed much stronger than $\mathcal{H}_0$, so $\mathcal{H} = \mathcal{H}_1$; otherwise, $\mathcal{H}$ is equal to $\mathcal{H}_0$. The echo amplitude is given by

$$(3.2.3) \qquad E = \kappa \, Tr(\rho \, \mathcal{H}_1)$$

where κ is a constant of proportionality depending on experimental conditions. The solution to the differential equation in Equation 3.2.1 is

$$(3.2.4) \qquad \rho(t) = exp(-\frac{i \, \mathcal{H} \, t}{h/2\pi}) \, \rho(0) \, exp(\frac{i \, \mathcal{H} \, t}{h/2\pi}).$$

If $R_t = exp(\frac{i \, \mathcal{H} \, t}{h/2\pi})$, and $R_t^{-1} = exp(-\frac{i \, \mathcal{H} \, t}{h/2\pi})$ are used for individual evolution matrices, the time evolution of the density matrix in the Hahn echo sequence is

$$(3.2.5) \qquad \begin{cases} R = R_{t_{P1}} \, R_\tau R_{t_{PII}} \, R_\tau \\ \rho(2\tau + t_{P1} + t_{PII}) = R^{-1} \rho(0) R \, , \end{cases}$$

where t_{P1}, t_{PII}, and τ are time durations for the first, second pulses and the inter–pulse interval. Similar expressions can be obtained for the stimulated echo. These results are quite general, they are independent of the considered spin system.

In the system where S = 1/2 and the electron Zeeman is the dominant spin

interaction, there are two electron spin manifolds α and β. The spin Hamiltonian $\mathscr{H}_0$ can be written as a block matrix form

$$(3.2.6) \qquad \begin{matrix} & (\alpha \text{ states}) & (\beta \text{ states}) \\ (\alpha \text{ states}) & U & W \\ (\beta \text{ states}) & W^{\dagger} & V \end{matrix},$$

where U, V, and W are the block matrices containing nuclear spin Hamiltonians associated with $M_S = 1/2$, $M_S = -1/2$ and the creation operator S_+ (defined as $S_x + i S_y$), respectively. W may contain non–zero elements if there exists an anisotropy in the g–tensor. The energy levels diagram can be mapped out by diagonalizing $\mathscr{H}_0$. The diagonalization can be carried out in two steps. First, eigenstates of the electron Zeeman interaction are found. This can be achieved by the following matrix

$$(3.2.7) \qquad C\hat{I}\begin{pmatrix} -\sin\theta\,(g_1\cos\varphi - ig_2\sin\varphi) & g_3\cos\theta + g \\ g_3\cos\theta - g & \sin\theta(g_1\cos\varphi + ig_2\sin\varphi) \end{pmatrix}$$

where C is a normalization constant, and $\hat{I}$ is a unit matrix of dimension $2I+1$. In the new coordinate system, the magnitude of elements in the off–diagonal block matrices should be very small compared to the diagonal electron Zeeman terms. As an approximation, the off–diagonal block matrices can be set to zero. Therefore,

$$(3.2.8) \qquad \mathscr{H}_0 = \frac{h}{2\pi}\omega_e S_z + (\mathscr{H}_0)_N$$

where $\frac{h}{2\pi}\omega_e$ is the electronic Zeeman energy, and $(\mathscr{H}_0)_N$ is the rest of the Hamiltonian. The second transformation matrix

$$(3.2.9) \qquad \begin{pmatrix} M_\alpha & 0 \\ 0 & M_\beta \end{pmatrix}$$

can be applied to diagonalize the α and β manifolds respectively.

The resonant field interaction $\mathscr{H}_1$ induces EPR transitions between the two manifolds. In a laboratory reference frame, which may or may not be coaxial with the PAS of the g–tensor where $\mathscr{H}_0$ was first written, $\mathscr{H}_1$ can be written down in a block matrix form as

$$(3.2.10) \qquad \begin{array}{c} \\ (\alpha \text{ states}) \\ (\beta \text{ states}) \end{array} \begin{array}{c} \begin{array}{cc} (\alpha \text{ states}) & (\beta \text{ states}) \end{array} \\ \begin{pmatrix} 0 & H_N\, e^{i\omega t/2} \\ H_N^\dagger\, e^{-i\omega t/2} & 0 \end{pmatrix} \end{array}$$

where H_N is a time–independent Hermitian operator. If $\omega = \omega_e$, the resonant condition for absorption is met. Otherwise, no EPR transition will be induced, resulting in no ESE signal. If there is a resonance, $\mathscr{H}_0$ can be transformed into $(\mathscr{H}_0)_N$ in the resonance reference frame which is rotating at ω_e. The time dependence is removed simultaneously from $\mathscr{H}_1$ by the same transformation, leaving only the time–independent part. In the PAS of the g–tensor, $\mathscr{H}_1$ can also be written in the form of Expression 3.2.10, plus diagonal elements. The presence of the diagonal elements in $\mathscr{H}_1$ adds phase factors to individual spin states. But, if the pulse widths are negligible, the phase corrections due to the diagonal elements can be neglected. Therefore, these diagonal elements can be dropped from the expression for $\mathscr{H}_1$. The calculation of E is the simplest one if it is carried out in the coordinate system where $(\mathscr{H}_0)_N$ is diagonalized. If H_N is defined as $\frac{h}{4\pi}\,\omega_N\, I$, $\mathscr{H}_1$ can be transformed from the PAS of the g–tensor into the new coordinate system as

$$(3.2.11) \qquad \mathcal{H}_1 = \frac{h}{4\pi}\omega_N \begin{pmatrix} 0 & M \\ M^\dagger & 0 \end{pmatrix}$$

In Equation 3.2.11, $M = M_\alpha^\dagger M_\beta$ This is, exactly, Equation 34 in the publication by Mims.[21] The result for the normalized echo envelope modulation functions from his lengthy calculation can, therefore, be used. For the Hahn echo,

$$(3.2.12) \qquad E_{mod}(\tau) = \chi_0 + \sum_{i,j}^{i\neq j}{}' \chi_{ij}^{(a)} \cos \omega_{ij}^{(\alpha)}\tau + \sum_{k,n}^{k\neq n}{}' \chi_{kn}^{(\beta)} \cos \omega_{kn}^{(\beta)}\tau + \sum_{i,j}^{i\neq j}{}' \sum_{k,n}^{k\neq n}{}' \chi_{ij,kn}^{(a,\beta)}[\cos(\omega_{ij}^{(a)} + \omega_{kn}^{(\beta)})\tau + \cos(\omega_{ij}^{(a)} - \omega_{kn}^{(\beta)})\tau].$$

For the stimulated echo,

$$\begin{aligned}(3.2.13) \qquad E_{mod}(\tau, T) = \chi_0 \quad & + \tfrac{1}{2}\sum_{i,j}^{i\neq j}{}' \chi_{ij}^{(a)} [\cos \omega_{ij}^{(\alpha)}\tau + \cos \omega_{ij}^{(\alpha)}(T+\tau)] \\ & + \tfrac{1}{2}\sum_{k,n}^{k\neq n}{}' \chi_{kn}^{(\beta)} [\cos \omega_{kn}^{(\beta)}\tau + \cos \omega_{kn}^{(\beta)}(T+\tau)] \\ & + \sum_{i,j}^{i\neq j}{}' \sum_{k,n}^{k\neq n}{}' \chi_{ij,kn}^{(a,\beta)} [\cos\omega_{ij}^{(a)}(T+\tau) \cos\omega_{kn}^{(\beta)}\tau \\ & + \cos\omega_{ij}^{(a)}\tau \cos \omega_{kn}^{(\beta)}(T+\tau)]\end{aligned}$$

In Equations 3.2.12 and 3.2.13, $\{\chi\}$ are defined as

$$(3.2.14) \qquad \chi_0 = \left(\frac{1}{2I+1}\right) \sum_{i,k} |M_{ik}|^4;$$

(3.2.15) $$\chi_{ij}^{(\alpha)} = \left(\frac{2}{2I+1}\right) \sum_{k} |M_{ik}|^2 \, |M_{jk}|^2;$$

(3.2.16) $$\chi_{kn}^{(\beta)} = \left(\frac{2}{2I+1}\right) \sum_{i} |M_{ik}|^2 \, |M_{in}|^2;$$

(3.2.17) $$\chi_{ij,kn}^{(\alpha,\beta)} = \left(\frac{2}{2I+1}\right) Re\,(M_{ik}^{*} \, M_{in} \, M_{jn}^{*} \, M_{jk}).$$

There are several points to be made here:

First, when deriving the Equations 3.2.12 to 3.2.17 Mims specified that $\mathcal{H}_0$ is a matrix with zeroed off–diagonal block submatrices (see, e.g. Equation 22 in reference 21). This is equivalent to assuming that there is no g–anisotropy, hence, the EPR line is narrow. Or if an isotropic g–tensor is not required, a coaxiality is assumed between the eigenstate coordinate system of the electron Zeeman interaction and the laboratory coordinate system. In a single crystal experiment, it is possible to align the two. But usually, especially in experiments involving a powder or frozen solution sample where multiple orientations are present, this is not the case. What has been shown here is that these assumptions are not necessary.

Secondly, in the above derivations, diagonalization of the spin Hamiltonian was performed in two steps. A simultaneous diagonalization of both the electron and nuclear spins does not generate results differing significantly from the two–step diagonalization method. In fact, a comparison of the two has been performed by Cornelius,[41] and no significant difference was found. This is expected, since the electronic Zeeman is much more dominant than other terms.

Thirdly, although the collinearity is not required between the laboratory coordinate system and the PAS of the g–tensor, it is not strictly correct to write $\mathcal{H}_1$ in the form of Expression 3.2.10 in the PAS of the g–tensor. Other than non–zero diagonal components which can be neglected, ω_N depends on the projection cosines

between the two coordinate systems, therefore on the orientation of the PAS of the g–tensor. However, the echo amplitude is proportional to ω_N. This means that if the same pulsing conditions are used in the laboratory reference frame for the same single crystal sample, the proportionality constant for the echo amplitude is expected to change with the orientation of the sample with respect to the external field. The problem will be more serious in an experiment involving a powder or frozen solution sample, because the proportionality constant is different for different parts of the sample. However, the distribution of $\mathscr{H}_1$ in the resonator is determined by the details of the particular experiment. Therefore, it is difficult at this point to assess the errors due to this effect.

The fourth point to be made concerns the presence of multiple nuclei interacting with one paramagnetic center. When multiple nuclei are coupled to the same center, and the mutual interactions between them are negligible, individual Hamiltonians in $(\mathscr{H}_0)_N$ are independent of each other. In quantum mechanical terms, the independence of these individual Hamiltonians from one another means that they commute with each other. R in Equation 3.2.5 can be factored into a product, $\prod R_i$, in the rotating reference frame. Hence, E_{mod} is the product of individual envelope functions.

Lastly, it is noteworthy that the origin of the nuclear modulation effect is reflected in Equations 3.2.12 to 3.2.17. The modulation effect arises from the interference between the EPR transitions, as can be seen by the product of the probabilities corresponding to these transitions. If M_{ik} is rewritten as $\langle i|k\rangle$, $|M_{ik}|^2$ is the mixing between the pre–transition spin state $|i\rangle$ and the post–transition state $|k\rangle$, therefore, proportional to the probability of this transition. Similar comments can be applied to other transitions. One can see from Equation 3.2.15 that the amplitude of the interference frequency $\omega_{ij}^{(\alpha)}$ in the α manifold, $\chi_{ij}^{(\alpha)}$, is the summation of the product of the transition probabilities from

i to k and from j to k over all states k in the β manifold. It is also worth commenting that the form of $|M_{ik}|^2 \ |M_{jk}|^2$, or $|\langle i|k\rangle|^2 \ |\langle j|k\rangle|^2$ can not be changed to $|\langle i|k\rangle|^2 \ |\langle k|j\rangle|^2$ as suggested by Singel *et al.*.[42] The latter would mean that there is an interference between the transitions $i \longrightarrow k$ and $k \longrightarrow j$. These two transitions differ by a frequency of 2 ω_e, this difference can not be detected by the ESE experiment. Furthermore, it has been observed by the author of this dissertation that for the case of $I = 1$, when $\chi_{ij}^{(a)}$ is expressed as a summation of $|M_{ik}|^2 \ |M_{kj}|^2$ ($|\langle i|k\rangle|^2 \ |\langle k|j\rangle|^2$) it is not equivalent or equal to that of $|M_{ik}|^2 \ |M_{jk}|^2$, the correct one. No such difference is expected if $I < 1$.

III. "Orientation Selective" ESE

The EPR spectrum of a powder or frozen solution sample is a superposition of the resonances from the randomly oriented molecules. It is a summation of the signals for which the applied field assumes all possible (θ,φ) orientations with respect to the molecular reference frame. However, the ESE experiment is performed at a fixed magnetic field strength H with a finite pulse B_1, typically on the order of 5 – 10 gauss, which is usually much smaller than the inhomogeneous EPR line width. In metalloproteins, when the cross relaxation between the molecules is slow, so that spectral diffusion is negligible, the ESE signal arises only from the subset of molecules having orientations such that they contribute to the EPR intensity at H. This has been called the "orientation selectivity" of EPR. As an example, Figure 3.3.1 shows the frozen solution EPR absorption spectrum of the nitrogenase molybdenum–iron protein, and the correspondence between the magnetic field and the associated orientations of the fields with respect to the molecular reference frame.[34]

"Orientation selectivity" has been previously investigated in ENDOR

Figure 3.3.1 Correspondence between magnetic field values in an EPR spectrum and field orientations within the PAS of g–tensor. Left: EPR spectrum taken at 2K for the MoFe protein from *Azotobacter vinelandii*. Right: Unit sphere with curves of constant g value drawn and several correspondence indicated. (From Hoffman *et al. J. Magn. Reson.* **1984**, *59*, 110)

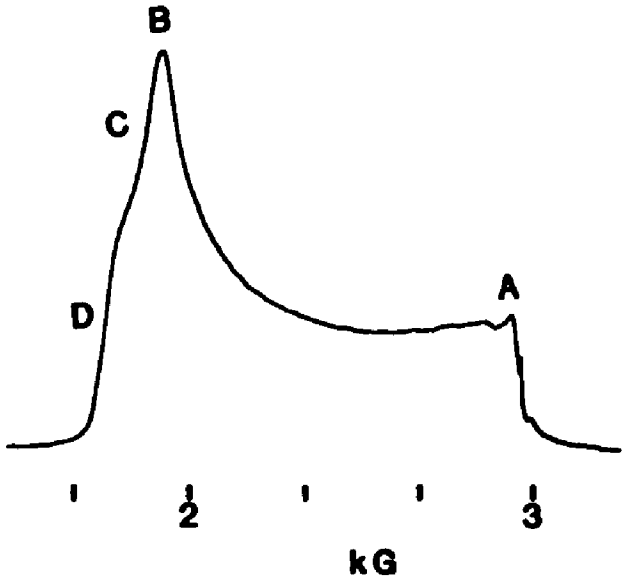

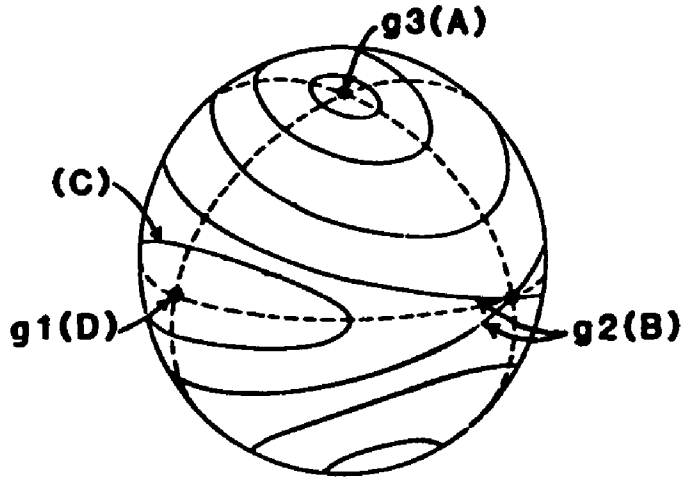

Figure 3.3.1

spectroscopy. As first noticed by Hyde *et al.*,[43-45] the orientation selectivity joins with other features of the ENDOR technique to permit the extraction of hyperfine parameters from the ENDOR spectra of powder samples. In particular, they noted that for magnetic field settings at the extreme edges of the EPR powder pattern, "single crystal like" spectra similar to those from an oriented single crystal will be observed from a frozen solution of paramagnetic centers with anisotropic magnetic interactions. Others (see for example, publications by Kreilick *et al.*[46-47] and Hoffman *et al.*[48-49]) have extended the work into other parts of the EPR spectra, and have developed methodologies to analyze such spectra. An ENDOR spectrum taken at H in the central region of the EPR powder pattern is itself a powder pattern, but not a complete one. It certainly differs from the case of an oriented single crystal where all the molecules presumably take only one known orientation and from the "single crystal like" case where a special orientation is involved. It is associated with a distinct subset of molecular orientations selected by H.

Because of the complementary nature of ESE and ENDOR, direct transfer of the concept to ESE should be feasible. Variations of ESEEM spectra with field settings within the EPR line have been reported.[50-54] For example, Dikanov *et al.*[50] recently observed a significant field dependence of the ESEEM spectra in VO^{+2} complexes in frozen solutions. Singel *et al.*[51] proposed a modulation amplitude fitting method and reexamined ^{14}N ESEEM in mercaptoethanol complexes of myoglobin. By fitting the amplitude extracted with the LP method, they inferred the orientation of NQI tensor with respect to the PAS of the g–tensor. Based on Kreilick's "orientation selective" CW–ENDOR software, Cornelius, McCracken *et al.*[52-54] developed a routine for analyzing "orientation selection" ESEEM data and have applied it to such systems as the Cu(II)–pyridine complexes,[52] amine oxidase,[53] and fumarate reductase[54].

A different method for the modulation analysis of the MoFe protein will be

presented next, although the method is not limited to the discussion of the MoFe protein alone. The spin Hamiltonian described in Section 3.1 will be used. The hyperfine couplings of the paramagnetic ions will not be considered here, in part because ^{96}Mo and ^{56}Fe do not have a nuclear spin in the MoFe protein isotopically enriched with ^{96}Mo. Inclusion of these terms in the analysis of other spin systems is quite straightforward, so long as a simulation of EPR can be made. The molecular reference frame is taken to be the PAS of g tensor. All interactions will be expressed in this coordinate system. Interactions expressed in other coordinate system are properly transformed as discussed in Appendix 2, with transformation matrices listed in Appendix 1. The external field is considered to rotate with respect to the molecular frame, for the convenience of discussion. If an ESEEM spectrum is taken at the field value H, it is known from Equation 3.1.3 that contributions to the signal come from a subset of molecules whose orientations $S(\theta,\varphi)$ satisfy

$$g^2 = g_1^2 \sin^2\theta \cos^2\varphi + g_2^2 \sin^2\theta \sin^2\varphi + g_3^2 \cos^2\theta \tag{3.3.1}$$

The modulation function $E_{mod}(g,t)$ ($t = \tau$ or $T + \tau$) is an average of E_{mod} over the orientations in $S(\theta,\varphi)$. In particular, when $g = g_{min}$ or $g = g_{max}$, the subset S consists of only one orientation. No average or summation is needed. An ESEEM experiment performed at g_{min} or g_{max} results in a "single crystal like" spectrum.

Variation of the field setting changes both the Zeeman energy and the subset of orientations over which the average is done. As a consequence, the interplay among various couplings will be different from one field setting to another. When both g and hyperfine tensor are anisotropic, contributions to the ESE signal will be different at different field settings, resulting in spectral variation across the EPR line. This provides clues for a complete determination of coupling parameters and

geometrical information.

One important requirement for the analysis is the consistency among the parameters extracted at different experimental conditions. This is based on the assumption that while molecules may be randomly oriented, they are identical with respect to the molecular reference frame. Therefore, only one set of parameters is needed to account for the spectral variations with the field settings , with the microwave frequencies, or with the inter–pulse time interval τ.

Experimentally, ESEEM spectra need to be taken across the EPR line, in particular at the extreme g values. The EPR intensity at the edges may not be large, but ESEEM spectra taken at the edges can be better resolved, because the signal arises from a very limited number of orientations. No exhaustive effort is needed to collect spectra with fine field value resolution, since a distinct yet known subset of orientations is associated with the g value chosen. However, it is helpful to collect spectra at different microwave frequencies, but at the same g values. Multiple frequency spectra allow observation of peak variations as a function of the excitation frequency, which can be useful in assigning frequencies, and also give an opportunity for verifying the extracted information. Similar remarks apply to the choice of the τ values in the stimulated echo sequence, since the stimulated echo sequence data is known to depend on the choice of τ.[55]

IV. About the Analysis Software

When analyzing ^{14}N modulation spectra, quite a number of input parameters are needed. To describe a hyperfine coupling term, six or four parameters (when using A_{iso} and point–dipolar model) are needed. To describe NQI, five are used. This is certainly a disadvantage, and skepticism has been raised about the feasibility of such simulations. One way to do the analysis, as proposed by McCracken *et al.*,[53]

is to start with an intelligent guess about the hyperfine coupling and NQI parameters, iterative efforts are made so that a fit of the desired degree of accuracy can be achieved. The huge parameter space makes this approach operator–dependent, experience and accidental success must be relied on.

A different approach has been taken. The method of least–square minimization is used in a simulation–fit program to achieve the best match of the simulation to the experimental data. Calculations based on equations given in Section 3.2, with the consideration of "orientation selectivity", are carried out in a specified parameter range. Each simulation is compared with the data using the measure of squared deviation. At the end of program, a list of the most probable parameter sets among all simulations is tabulated according to their least–square deviations. These parameters are compared with their counterparts at other field values, microwave frequencies, or τ values, in order to have a unique determination of these parameters.

A program PSU_OS2 in FORTRAN code has been written, the complete listing of the program can be found in Appendix 4. Before the subset average begins, all interactions, except the electron Zeeman term, are expressed in the PAS of the g–tensor. Each orientation is examined to see if it belongs to the "selected" subset at the field setting. For the elements of the "selected" subset, the incomplete Hamiltonian with the addition of the electron Zeeman term at this orientation (also expressed in the PAS of the g–tensor) is diagonalized with EISPACK subroutines,[56] energy levels and the M matrix in Equation 3.2.10 can be found. The echo amplitude at this orientation can be calculated with Equations 3.2.12 to 3.2.17. This process is repeated for the other orientations in the subset. The square deviation of the simulation from the experimental data is calculated after the completion of the subset average. The whole process is again repeated for the other parameter sets. After going through every parameters specified by the input range,

the program sorts out the most probable parameter sets and tabulates them according to the calculated squared deviation.

V. A Spherical Average Method for ^{14}N ESEEM

Of particular interest is the nuclear modulation effect due to ^{14}N nuclei in the vicinity of a paramagnetic electron. It is of interest to biological studies, because a great portion of the samples consist of amino acids which have nitrogen as a major constituent. Around the biologically active sites of metalloenzymes, amino acids act as ligands and affect the properties of the metal sites such as the symmetry, the oxidation states, etc.. Nitrogen couplings have been evaluated through ESEEM in a variety of situations.[7,53,57-61] Furthermore, ESEEM can provide information about the origin of the nitrogen modulation. Due to intensive studies of Nuclear Quadrupole Resonance (NQR) and ESEEM, there exists a large data base for nitrogen NQR parameters.[7,62-69] These parameters are observed to be a sensitive signature of nitrogen ligands. Upon being extracted from ESEEM experiments, nuclear quadrupole parameters can be compared with the data base. Thereby, the identity of the nitrogen ligand can be established.

It is of interest to spectroscopic studies, since ESEEM is very effective on detecting nitrogen modulation. Often, the nitrogen nuclear Zeeman splitting (0.92 MHz at 3,000 Gauss) is comparable to the hyperfine coupling between the nucleus and paramagnetic center, and to the nitrogen nuclear quadrupole splitting (e.g. nuclear quadrupole moments of the nitrogens in an imidazole ring are 1.43 and 3.23 MHz respectively). This will result in a favorable condition for the application of ESEEM, since the probability of "partially forbidden" transitions directly affect the modulation amplitudes. Furthermore, if the nuclear Zeeman and hyperfine interaction are comparable and cancel or nearly cancel each other in one of the

electronic spin manifolds, then the spin Hamiltonian of that manifold in the rotating reference frame is reduced to the nuclear quadrupole interaction. Effectively, the nuclear quadrupole interaction can be probed with EPR sensitivity. This is the so–called "cancellation effect". In their ESEEM study of Cu(II)–imidazole complexes, Mims and Peisach[33] observed the zero–field quadrupole frequencies for a protonated nitrogen of an imidazole given by Hunt *et al.*[67]. Numerous observations of this effect have been reported, notably in many metalloproteins involving Cu(II).[7,53,57-61]

But the extraction of the parameters is not straightforward, since the separation between the energy levels depends in a complex manner on the these interactions. This is significantly different from cases of $I = 1/2$ nuclei, where a simple relation exists between the magnetic couplings and the modulation frequencies observed in ESEEM. Analytical expressions for the envelope modulation function obtained through approximations are no longer applicable. Although a complete determination of coupling parameters from the ^{14}N modulation spectra can be performed, it does take a certain amount of computing time. Circumstances may arise when only qualitative information may be needed, instead of an elaborate analysis, a quick estimate of the parameter ranges can be made to reduce the amount of work needed for a detailed analysis. One can also ask if it is meaningful to have the pseudodipolar couplings determined, while there is little confidence in the extracted parameters.

The spherical average method, first developed by Mims and Peisack[33], is designed to simplify the analysis for ^{14}N modulation. The number of simulation parameters is greatly reduced if the anisotropic components of the hyperfine coupling are ignored. Neglect of the anisotropic components may result in artificially narrowed frequency lines and changes of the modulation depth, and the line widths and relative peak intensities in experimental spectra may not be

correctly represented. These limitations, however, do not prevent the determination of parameters for other more dominant couplings. A further simplification can be achieved if the spherical average approximation is adopted in which all orientations are equally probable.[70] That means, the relative orientation of the nuclear quadrupole moment to the molecular frame is no longer fixed, but allowed to rotate in order to encompass all possible orientations. The Hamiltonian after these approximations can be written down as

$$(3.5.1) \qquad (\mathscr{H}_0)_N = g_N \beta_N H I_z \pm \frac{1}{2} A_{iso} I_z + Q_{zz} [\, 3I_z'^2 - I(I+1) + \eta (I_x'^2 - I_y'^2) \,]$$

in a reference frame rotating at ω_e with the external field applied along the Z axis. Here, spin operators in the NQI term are primed to indicate that they are defined with respect their own principal axis system (PAS of the NQI), and to distinguish them from I_z in the nuclear Zeeman term. A convenient reference frame is the PAS of the NQI. The spin Hamiltonian becomes

$$(3.5.2) \qquad (\mathscr{H}_0)_N = (g_N \beta_N H \pm \frac{1}{2} A_{iso}) (I_x' \sin\theta \cos\varphi + I_y' \sin\theta \sin\varphi + I_z' \cos\theta) + Q_{zz} [\, 3I_z'^2 - I(I+1) + \eta (I_x'^2 - I_y'^2) \,]$$

If the first term almost cancels in one of electronic spin manifolds, the effective field experienced by the nuclear spin in the manifold is zero, and the effective Hamiltonian for the manifold looks like a zero filed NQR Hamiltonian. Using Equation 3.5.2, a frequency histogram can be calculated by sampling orientations uniformly over a hemisphere. In contrast to the full analysis, three parameters need to be determined, A_{iso}, Q_{zz} and η. At the near cancellation condition, often observed in nitrogen modulation spectra, A_{iso} can be estimated from the size of nuclear Zeeman coupling. The NQI parameters can be estimated from the

correlation of the peak positions with ν_+, ν_-, and ν_0. Sometimes, a peak at $2\sqrt{[(\nu_N + \frac{1}{2} A_{iso})^2 + Q_{zz}^2 (3 + \eta^2)]}$, associated with $\Delta m_I = 2$ "transitions" is also observed.

Discussions about the applicability of this method can be found in Chapter 10, where it has been applied to the nitrogen coordinations to the copper sites in Nitrous Oxide Reductase.

Chapter 4

DATA ANALYSIS AND EXPERIMENTAL METHODS

In this chapter, the ESE spectrometer will be briefly discussed. Then, problems in the cosine Fourier transform spectra of the ESE data due to the spectrometer "dead time" will be tackled. A few methods designed to minimize its effect will be presented. Also discussed is the phase cycling method for the transmitter pulses. Finally, a waveform division method utilized in the study of both nitrogenase MoFe protein and nitrous oxide reductase will be introduced.

I. The ESE Spectrometer

The home–built ESE spectrometer is operated at X–band over microwave frequency range of 8 – 11.5 GHz.[71] Currently, a slotted tube resonator mounted in a Janis variable temperature cryostat is used. The spectrometer can be operated from 1.4 K to room temperature, and the temperature is monitored by a doped germanium resistor placed just outside the resonator. Figure 4.1.1 shows a schematic drawing of the spectrometer transmitter and receiver arms, not drawn are the pulse control unit and the computer. All pulse timing intervals were derived from a home built pulse programmer[72] interfaced to a DEC LSI–11/73 minicomputer. The minicomputer is also used to store experimental data from the ADC.

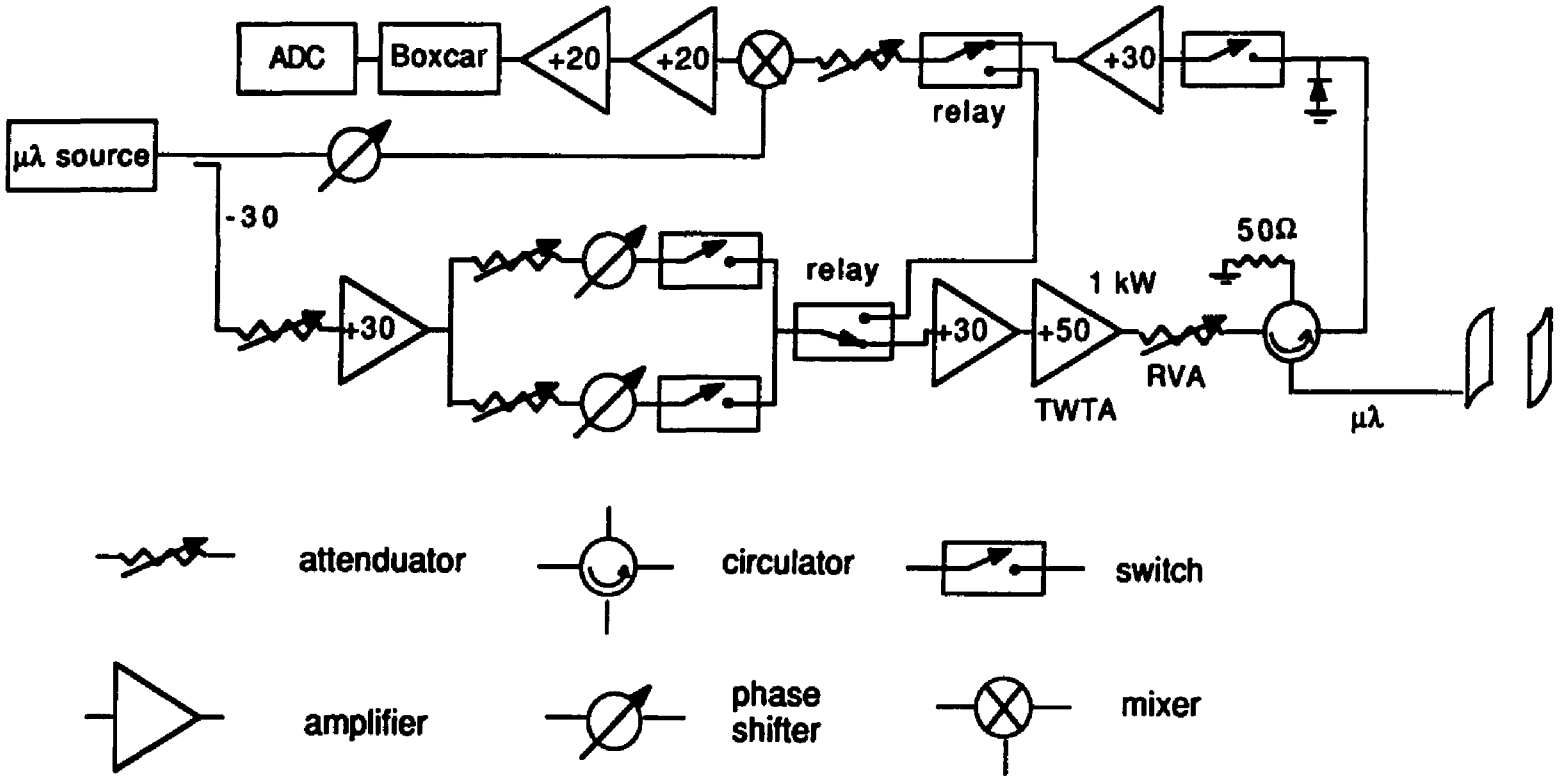

Figure 4.1.1 Block Digram of the Electron Spin Echo spectrometer used for the experiments. The probe shown is a slotted tube resonator. (courtesy of Marcelino Bernardo)

II. The Spectrometer "Dead Time"

The nuclear modulation pattern consists of a superposition of cosine waveforms, as discussed in Section 3.2. The argument of these cosines is either τ in the Hahn echo data or $T+\tau$ for the stimulated echo data. It would seem logical that the information contained in the time domain data could be presented in the most effective way in the frequency domain via a Fourier transform. Certain sets of frequency lines could then be assigned to nuclei associated with the paramagnetic center. The cosine transform would be the most effective, since the phase information of those cosine waveforms would be retained. Historically, it was not the case, either a magnitude Fourier transform was preferred[73] or no transform was performed.[25] The problems due to the spectrometer "dead time" arises when the cosine Fourier transform is applied to the modulation waveform.[74] Due to the ringdown time of the probe or the recovery time of the receiver (a microwave switch can be useful in preventing transmitter pulses and oscillations due to the probe ringdown from getting into the receiver arm) one has to start data collection a finite time after the application of the pulses, this finite time period is termed the "dead time" period. Another source of missing data is the time required to complete the stimulated echo sequence. In our laboratory, the typical "dead time" for the two–pulse sequence is about 0.12 μs for the ESE probe at 9 GHz. For the three–pulse sequence, it is about twice that of the two–pulse case. This missing piece of the modulation data introduces artifacts in a cosine Fourier transform spectrum. According to the Fourier transform theory, if the missing piece is ignored in the transform it is equivalent to zero filling the "dead time" piece or changing the origin of time to the initial recording time.[75] Mirroring the time domain data about the initial recording time results in phase changes in the frequency peaks, which changes the appearance of the spectrum. By zero filling we are convoluting the

transform of the waveform with that of a step function. The convolution can distort both the baseline and the peak intensities in the transform, weak peaks can be indistinguishable from the sidelobes of the sinc distortion resulting from the transform of the step function. On the other hand, the magnitude transform is not immune to these problems. It seems that it would not be affected by the incorrect phases of the frequency lines. In fact, any phase error present may introduce an off–phase (imaginary) component which is usually broader than the in–phase (real) component (this can be envisioned by examining the line shapes of both the real and imaginary parts of a Lorentzian line). Therefore, there is little advantage in doing the magnitude transform either. In the case of a powder or frozen solution sample the problem is even more pronounced, since in these materials the total duration of the modulation pattern is often shortened by a faster decaying time. The missing information due to the "dead time" may amount to a significant portion of the detectable modulation waveform. This will inevitably limit the amount of information one can extract from the experiment.

Two different approaches can be taken to overcome the "dead time" problem. One is to minimize the size of the "dead time" by: a) use of a two–mode microwave cavity. In this method, one mode is used for the application of the excitation pulses, the other mode, which is orthogonal to the first one, is used for detection.[76] b) Longitudinal detection.[77] This is a low frequency experiment, and is based on the observation of changes in the magnetization M_z along the static field direction. Detection coils oriented parallel to the static field permit the recording of the time–dependent M_z during the microwave pulses. c) The design of new pulse sequences. Five pulses, for example, are sequenced to produce waveforms which are equivalent to those from the Hahn–echo sequence with almost no "dead time".[78] Because more pulses means a longer time duration before the detection of the echo, this method may not be applicable to samples with short relaxation times, where

the problem of the "dead time" is the most severe. Furthermore, compared to the Hahn echo, the echo from this method loses intensity due to the presence of relaxation. The loss of signal intensity may result in longer experimental times if signal averaging is needed and therefore may not be applicable to samples with weak echoes.

The other approach is to "reconstruct" the missing portion of the waveform based on what can be detected, when the "dead time" portion is not a significant part of the observable modulation waveform. Since this is a "reconstruction" technique, caution must be exercised to prevent the introduction of extra artifacts.

Several methods will be discussed to minimize the distortions caused by the "dead time". The first one deals with the phase distortion only. The second method, Linear Prediction back extension (LPBE), can be used to calculate the missing portion. Therefore, it can restore the phases of the frequency peaks and remove the sinc function from the baseline of the spectrum.

III. Phase Correction in Fourier Transform Spectra

Phase correction has been used in NMR as a routine method in properly phasing the peaks in the spectrum. In ESEEM, as discussed above, there is a well–defined cosine function dependence and an easily identifiable starting time. The phase correction can therefore be calculated based on the duration of the "dead time" t_D and the time interval between consecutive data points, Δt.* If only the positive part of the transform is considered, the phase at frequency f is off by the amount

---

* Discussion of the subject initiated by M. Bernardo is gratefully acknowledged.

(4.1.1) $$\Delta\varphi = -(t_D / \Delta t) \cdot \pi \cdot (f \cdot \Delta t)$$

When both the positive and negative parts of the spectrum are considered,

(4.1.2) $$\Delta\varphi = -(t_D / \Delta t) \cdot 2\pi \cdot (f \cdot \Delta t).$$

The proof follows:

If the wave form can be described by (neglecting the decay function dependence)

(4.1.3) $$\sum_i A_i \cos \omega_i t,$$

and a new time is defined as $t' = t - t_D = n\,\Delta t - t_D$, then Equation 4.1.3 becomes

(4.1.4) $$\sum_i A_i \cos (\omega_i t' + \omega_i t_D),$$

or

(4.1.5) $$\sum_n A_i \cos (\omega_i n\,\Delta t + \omega_i t_D).$$

Now, $-\omega_i t_D$ is the phase correction term for the frequency component ω_i in the spectrum.

In a discrete form, ω_i is $2\pi\, n' / (N\,\Delta t)$, where $1/(N\,\Delta t)$ is the increment in the frequency domain, n' is the peak position, and N is the total number of data points of the waveform. The phase correction is

(4.1.6) $$-(t_D/\Delta t)\cdot\pi\cdot(n'/2N)$$

for the positive half of the transform spectrum, where $0 \leq n' < N/2$; and it is

(4.1.7) $$-(t_D/\Delta t)\cdot 2\pi\cdot(n'/N)$$

for both the positive and negative halves of the transform spectrum, where $-N/2 \leq n' < N/2$. In some NMR data processing software (e.g., FTNMR), this would correspond to the first order (not the frequency–independent zeroth order) phase correction, which scales the phase correction linearly with the frequency $(n'/\frac{N}{2}\Delta t)$ or $(n'/N\,\Delta t)$. The coefficient needs to be input into the phase correction is given by either $-(t_D/\Delta t)\cdot\pi$ or $-(t_D/\Delta t)\cdot 2\pi$.

The phase correction method is designed to remove the phase distortion only. Since it is equivalent to filling the "dead time" piece with the echo intensity at the initial recording time, it does not remove the distortion of the baseline caused by the step function. But, when the phases of the peaks are restored, it is sometimes possible to separate the real frequency peaks from the sinc function distortion. Also, when the missing piece due to the "dead time" constitutes a fairly small portion of the observed modulation pattern, data processing with the phase correction alone may be sufficient, as long as the part of interest in the spectrum are not affected by the baseline distortion.

IV. Reconstruction with Linear Prediction Back Extension (LPBE)

Various methods have been created for reconstructing the missing portion of the modulation pattern. One intuitive approach, as explained by Mims[79], is to start

with the estimation of the echo amplitude y_0 at the time t (τ or $\tau + T$) = 0, then connect y_0 to the first experimental data point y_i with a quarter sine function

$$(4.2.1) \qquad y = y_0 - (y_0 - y_i) \sin(\pi t / 2t_D).$$

The crudely reconstructed waveform is cosine transformed, and the prominent peaks in the transform spectrum are identified visually or with the aid of a subroutine. The peaks are then window–filtered one by one, mainly for the purpose of cosmetics. However, the window–filtering does have the potential of either unfaithfully represent the experimental results or unknowingly omitting hidden information. The corrected and filtered spectrum is then transformed back to the time domain in the range of $t = 0$ to $t = t_D$. The experimental waveform with the back transformed portion is transformed again. This process can be repeated over again, until the desired result is obtained.

Another method, the Linear Prediction (LP), is less operator–dependent than Mims' iterative approach, and has gained some popularity. It was introduced to the analysis of magnetic resonance spectra by Barkhuijsen *et al.*[80], based on the work of Kumaresan and Tufts[81]. Tang *et al.*[82-84] have developed similar analysis methods, and applied them to 1–D and 2–D NMR spectroscopy. The aim of the LP method is to estimate, without performing a Fast Fourier Transform (FFT), the parameters associated with damped cosine functions including frequency, amplitude, relaxation rate, and phase. The computationally efficient FFT is widely used in spectral analysis, including magnetic resonance. But the frequency resolution obtained is roughly the inverse of the duration of the signal, therefore it is poor when dealing with fast–relaxing or truncated data. And weak signals may be masked by sidelobes from nearby stronger signals. LP, when correctly applied, does yield higher resolution than FFT.

The LP method involves fitting a model of multiple exponentially damped sinusoids directly to the time–domain data, and generating a table of frequencies, relaxation rates, amplitudes, and phases. The mathematical model to be fitted to the data is set up in two steps. It is assumed that the signal, which is sampled at regular time intervals $n\Delta t$ ($0 \leq n \leq N-1$) consists of K exponentially damped sinusoids plus white noise w. In the frequency spectrum, an exponentially damped sinusoid corresponds to a frequency peak with a Lorentzian line shape. The data sequence y_n is given by

$$y_n = \sum_{j=1}^{I} A_j e^{-R_j n\Delta t} \cos(\omega_j n\Delta t + \varphi_j) + w \qquad (4.2.2)$$

It can be shown that without the presence of noise, each data point can be expressed as a linear combination of $2K$ previous data points,[85] i.e.,

$$y_n = \sum_{m=1}^{2I} a_m y_{n-m} \qquad (4.2.3)$$

The above linear prediction relation is mathematically less rigorous in the presence of noise. However, it is a good approximation to frequency peaks close to Lorentzian line shapes, except that the effective number of LP coefficients is increased to a larger value of M. The above equations are linear equation in M unknown coefficients a_m. On the right hand side is a data matrix of dimension $(N \times M) \times M$, while the data vector on the left hand side is of dimension $N - M$. Different linear least–square procedures, such as singular value decomposition (SVD)[81] or truncated Householder triangularization decomposition (QRD)[83], can be used to solve for these coefficients. The obtained LP coefficients contain

information about the frequencies and relaxation rates. It was shown that for a noiseless signal with K exponentially damped sinusoids, the roots of the polynomial equation

$$z^{2K} - \sum_{m=1}^{2K} a_m z^{2K-m} = 0 \qquad (4.2.3)$$

are given by $\exp[\,(R_j \pm i\omega_j)t\,]$, where $j = 1,2,\ldots,K$.[86] In practice, not all M roots are physical, only those with decay behavior are retained. The number can be further cut down to l coefficients with largest singular values among all roots retained. Calculation of the amplitudes and phases can be done by a second linear least–square fitting procedure for l sinusoids. The determination of l is straightforward, when the signal to noise ratio of the experimental data is good (> 30). It is accomplished by looking for the sharp step in the plot of singular values.[80] But when the signal to noise ratio is not so good, choice of l may become a problem. If l is too large, one might enhance the noise; if it is too small, one might suppress certain frequency components. Normally, the LP method is used in such a way that sinusoids are generated according to the table of parameters obtained. Therefore, LP gives an essentially noiseless spectrum.

As discussed above, the applicability of the LP method relies on the assumption that frequency lines involved in the experimental data are Lorentzian. In many cases, especially where lines are broad, the approximation is not good. As discussed by Astashkin *et al.*[87], the frequency lines are usually not Lorentzian. The example illustrated in that publication indicates that LP fails to give a faithful reconstruction of the simulated data, when an artificial "dead time" is present. In all, caution must be exercised when generating spectrum solely based on parameters obtained from LP.

On the other hand, using the LP method to reconstruct the "dead time" portion only, namely, extending the LP–calculated data points from the last missed point toward the zero time, may not cause as significant a problem as in the above case. After all, the experimentally recorded values constitute the major portion of the data to be Fourier transformed. As observed from practice, prominent features of the spectrum are not changed drastically by variations in the "dead time" piece. Fig. 4.4.1 shows the transform spectra from data filled with a quarter sine function in (a) and with LPBE in (b) in the "dead time" portion. The positions of prominent frequency peaks are barely altered. The application of LPBE makes it possible to minimize disadvantages from the application of LP alone and from Mims' intuitive approach. On one hand, the small "made up" piece is not likely to distort the transform seriously (caution should be excised for a very fast decaying echo signal, for which a major portion of the information may have already been lost); on the other hand, operator–dependence inherent in Mims' intuitive approach can be avoided.

It is worth mentioning that when reconstructing the "dead time" portion with LPBE method the number of LP coefficients l is usually kept significantly larger than the number of prominent frequency lines. This helps to obtain a better fit of the experimental data than with a smaller l. This has been also observed by others in their researches.[83] Another practical measure to avoid possible distortion by LPBE is to check how well the LP method can fit the experimental data before utilizing it for reconstruction.

As for the study of the nitrogenase MoFe protein, ESEEM signal tends to be abnormally long for frozen solution samples, lines are quite well resolved, therefore, problems caused by the "dead time" are not pronounced. This is partly because the subset of molecular orientations associated with a field setting is a small one resulted from the unusually large g anisotropy. But when two waveforms are

Figure 4.4.1 Comparison of of back–extension methods. Fourier transform spectra are from the same time–domain data as in (a) of Figure 6.1.1, but back extended with (a) a quarter sine function (b) LPBE method.

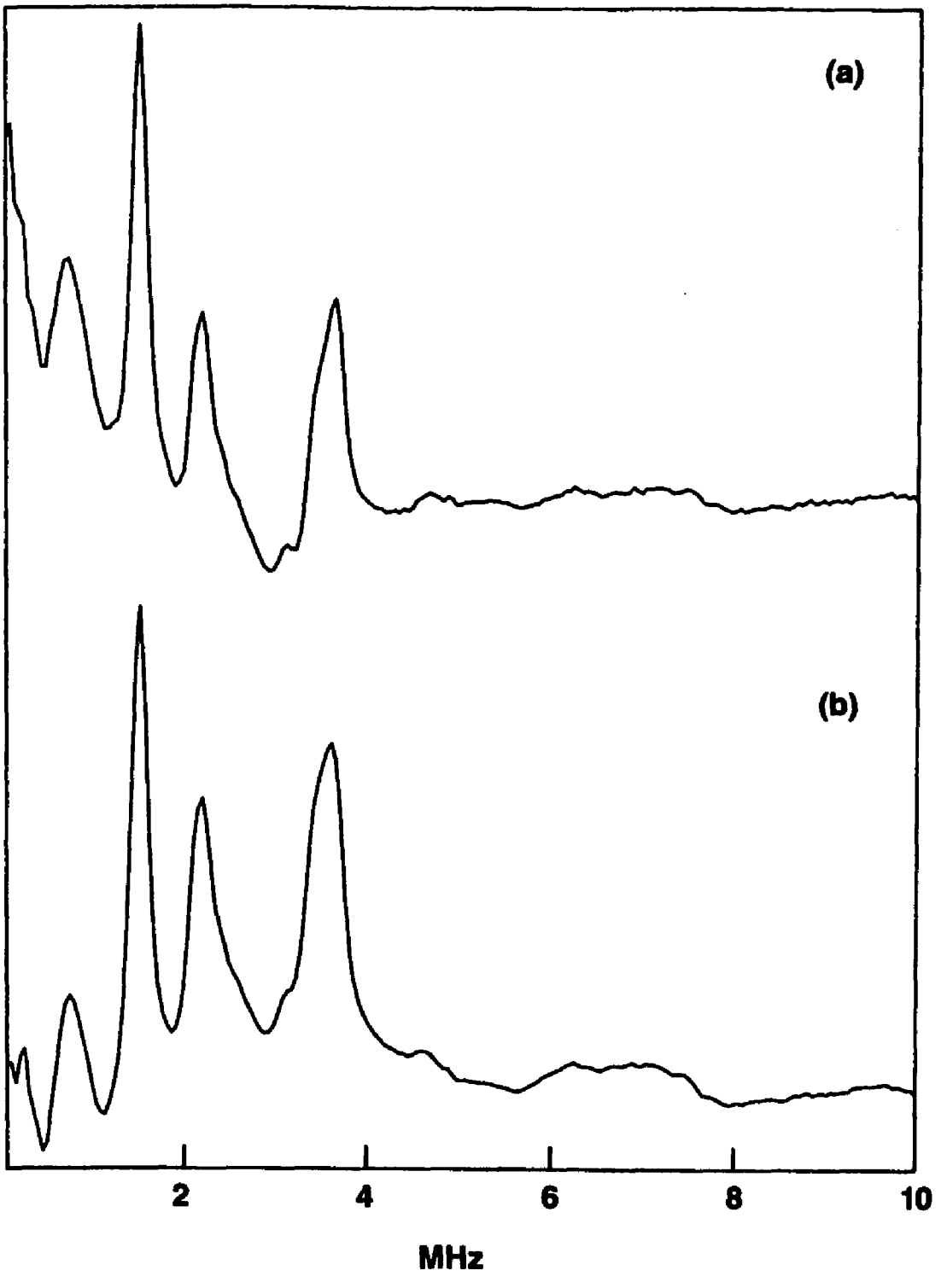

Figure 4.4.1

divided, it becomes necessary to minimize distortions to the baseline in the transform spectrum, so that weak frequency lines in the quotient waveform can be identified. That is the reason for the application of LPBE in the study of the nitrogenase MoFe protein.

V. Phase Cycling of Microwave Pulses

When more than two pulses are applied, other than the echo monitored, there exists unwanted echoes.[88-89] For example, in the stimulated echo sequence as illustrated in Figure 4.5.1, unwanted echoes are present at 2τ, $2T$, $2T + \tau$, and $2T + 2\tau$. Echoes 1, 2, and 3 result from the application of the first and second pulse, the second and third pulses, and the first and the third pulses. And the echo at $2T$ is the consequence of phase reversal of the focused magnetization at 2τ. When T is varied, these echoes vary accordingly. It is possible that some of echoes may move in such a way that they coincide with the stimulated echo at certain value of T, therefore causing spurious peaks or "glitches" in the recorded echo envelope.[89] When $\tau = T$, one of the unwanted echoes at $2T + \tau$ will coincide with the stimulated echo at $2\tau + T$. Another unwanted echo at $2T$ will coincide with the stimulated echo at $T = 2\tau$. Though these spurious peaks are easy to identify and only occur at specified times, it causes inconveniences in the data analysis. If not removed from the time domain data, they will introduce artifacts or distortions to the transform spectrum. If removed, they have to be replaced by values which are not obtained from experiments, rather, from intelligent guesses. When both τ and T are small, the glitch have be observed to be quite significant as to overwhelm the interested echo, hence may prevent the effort to shorten the "dead time".

To overcome the problem, Bowman[90] has proposed the method of phase cycling. By alternating the microwave phases of the first and the second

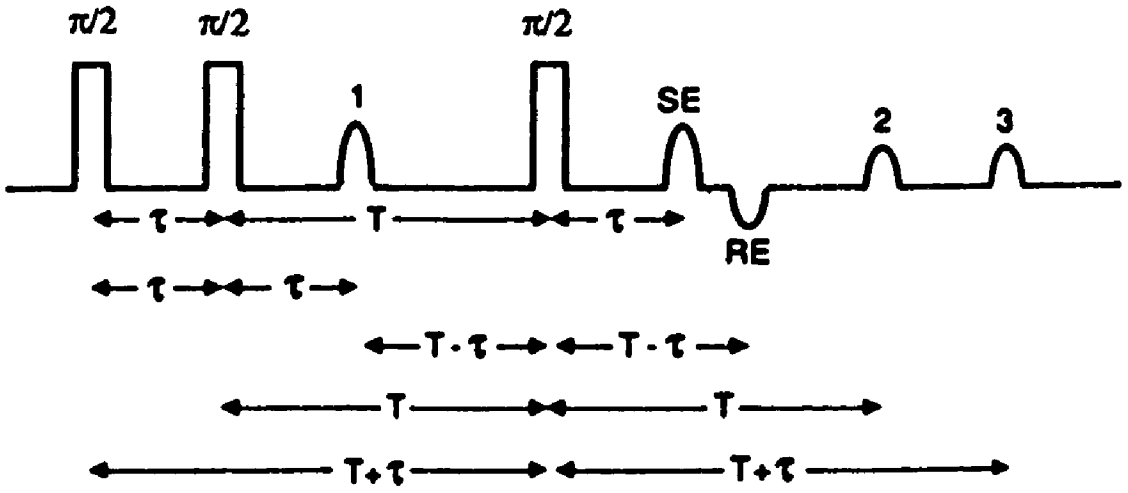

Figure 4.5.1 Echoes observed with the stimulated echo sequence. The experiment is performed to observe the stimulated echo denoted by SE. Echoes 1,2,3 and RE are two–pulse echoes resulted from various transmitter pulses and the refocused echo, respectively.

transmitter pulses of the stimulated echo sequence, therefore alternating the phases of unwanted echoes resulted from two pulses, the glitches can be canceled. But the stimulated echo, which is the consequence of three pulses, is kept the same sign and added together.

The method of the phase cycling can be further developed.** Phases of all pulses can be alternated, as long as the addition and subtraction of the interested echo are carried out properly. This will be referred to as the complete phase cycling. If n pulses are present, the variations of the pulse sequence based on complete phase cycling will total 2^n. In the stimulated echo sequence, for example, the phase of the third pulse is also alternated. Then there are eight non--identical pulse sequences altogether. The recorded echo amplitude is now subtracted from, instead added to, the signal from the other phase. If the phase cycling is carried out in this fashion, the benefit is not only getting rid of glitches, but also obtaining a true baseline. Of course, the baseline can be obtained by collecting a separate data set at identical experimental conditions except that the paramagnetic species are not on resonance; it can also be obtained by measuring the signal at the time when no echo occurs. The baseline obtained is then subtracted from the echo data obtained separately. If a signal average is performed and the noise is taken into account, the signal to noise ratio is enhanced by the application of phase cycling by a factor of $\sqrt{2}$, compared to the other approaches. This is because the averaged signal is proportional to the number of repetition, yet the noise is proportional to the square root of that number. Twice the number of repetitions would be needed with other methods to achieve the same signal to noise ratio as with the phase cycling method.

One may wonder whether a complete phase cycling is necessary, if the

---

** Helpful discussions with P. Tindall and M. Bernardo are gratefully acknowledged.

purpose is to get rid of glitches and obtaining a true baseline. Usually it is not. But there are cases where a complete phase cycling does help to eliminate problems due to differences in transmitter pulses. It has been observed that when a microwave phase modulator is used to change the transmitter pulses its insertion loss is different when it is on or off. The small difference between pulses generated at low power is magnified by the preamplifier and high power amplifier in the transmitter arm. This causes an incomplete cancellation of glitches and other deviations from baseline, when the phase cycling is incomplete. The complete phase cycling overcomes this problem. It has also been observed that even though on the oscilloscope the echo is still masked partially by the pulse ringdown, the data collected with the complete phase cycling are free from effects of pulse ringdown and glitches. The tail of pulse ringdown has been canceled. Of course, this can not extend too far into the pulse ringdown regime. But it does help minimizing the effects due to the "dead time".

VI. Method of Waveform Division

Waveform division technique is the most effective when small differences exist between two otherwise identical samples. The small differences can be enhanced by the quotient waveform which does not contain the common features between the numerator and denominator waveform. The usefulness of the method has been illustrated in several studies where different isotopes were enriched separately to the otherwise identical samples.[9,53,91] For example, Zweier *et al.*[91] reported the experimental results on the metalloprotein complex Cu(II) conalbumin. When the two–pulse echo data were taken on Cu(II) conalbumin bound by ^{12}C oxalate or bound by ^{13}C oxalate, certain minor differences between these two were detected. But both patterns were dominated by modulation due to protons and due

to ^{14}N nuclei. To enhance the detected minor differences, the two waveforms were divided, and ESEEM component due to ^{13}C was thus revealed. It was then established that oxalate was closely bonded to the metal ion in Cu(II) conalbumin.

As noted by Rowan *et al.*[20] and Mims[21], when several nuclei are coupled to the paramagnetic center, the resulting modulation pattern is given by the product of the modulation patterns due to each individual nucleus. But strictly speaking, this will be true only for a single crystal and when mutual interactions between these nuclei are negligible. As far as a powder or frozen sample is concerned, it is at best a good approximation, since the average of the multiple nuclei modulation pattern over different molecular orientations may be different from the product of the individually averaged pattern. Mathematically, it is equivalent to interchanging the multiplication of individual modulation patterns at a single orientation with the average over the orientations, which may or may not be valid. Given the success of past applications, it is fair to say that the approximation is reasonable. So, the division of two time domain modulation waveforms taken at identical experimental conditions and with an identical EPR spectrum will reveal any difference between the two samples, but not their common features. Any peaks with a phase of zero (or pointing upward) in the cosine Fourier transform of the quotient waveform are associated with the numerator waveform; those with a phase of π are associated with the denominator waveform.

It is worth commenting that when the difference is small between two spectra, a flat baseline is much needed. Otherwise, one may not be able to distinguish small frequency peaks from distortions to the baseline. For this reason, the LPBE method serves the purpose: By removing baseline distortions from Fourier transforms of both numerator and denominator waveform, the distortions to the Fourier transform of the quotient waveform will be minimized.

Another related point to be noted is that the multiplication of individual

modulation patterns may result in the so–called "combination frequency" peaks.[21,61,92-93] Due to the fact that more than one nuclei magnetically couple to the same paramagnetic center, the sum or difference of involved nuclear modulation frequencies may show up in the observed spectrum. McCracken *et al.*[61] have combined the observation of "combination frequency" lines, the model compound comparison, and numerical simulations to show two nitrogens coordinations (from two imidazoles) to the Cu(II) center in the phenylalanine hydroxylase from *Chromobacterium violaceum*. The waveform division method may provide an extra help when "combination frequencies" are present: these peaks will be removed simultaneously with those which cause these peaks. That is, if peak C is the combination of peak A and B, removal of peak A or B will affect C. In a complex spectrum where many peaks are present, this will simplify the task of assigning frequency peaks.

REFERENCES FOR PART I:

1. Blackburn, T. H. in *Microbial Geochemistry*; Krumbein, W. E. ed.; Blackwell Scientific, Oxford, 1983.

2. Dagley, S.; Nicholson, D. E. *Metabolic Pathways*; Wiley, New York; 1970.

3. Postage, J. R. *Fundamentals* of *Nitrogen Fixation*; Cambridge University Press, Cambridge, New York, 1982.

4. Zumft, G. W.; Matsubara, T. *FEBS Lett.* 1982, *148*, 107–112.

5. Deisenhofer, J.; Epp., O.; Miki, K.; Huber, R.; Michel, H. *Nature* 1985, *918*, 618.

6. L. Que ed. *Metal Clusters in Proteins*; ACS Symposium Series 372, Washington, D. C., 1988.

7. Mims, W. B.; Peisach, J. Preprint.

8. Thomann, H.; Morgan, T. V.; Jin, H.; Bergmayer, S. J. N.; Bare, R. E.; Stiefel, E. I. *J. Am. Chem. Soc.* 1987, *109*, 7913.

9. Jin, H.; Thomann, H.; Coyle, C. L.; Zumft, W. G. *J. Am. Chem. Soc.* 1989, *111*, 4262.

10. Abragam, A.; Bleaney, B. *Electron Paramagnetic Resonance of Transition Ions*, Clarendon, Oxford, 1970.

11. Griffith, J. S. *The Theory of Transition–Metal Ions*, Cambridge University Press, 1961.

12. McGarvey, B., R. in "*Transition Metal Chemistry*"; Carlin, R. L. ed.; Marcel Dekker, New York, 1966; Vol. 3, 89–201.

13. Orton, J. W. *Electron Paramagnetic Resonance*; Iliffe, London, 1968.

14. Solomon, E. I.; Penfield, K. W.; Wilcox, D. E. *Structure and Bonding* 1983, *53*, 1–57, and references therein.

15. Slichter, C. P. *Principle of Magnetic Resonance*; Springer–Verlag, New York, 1980.

16. Mims, W. B. *Electron Paramagnetic Resonance*, S. Geschwind ed.; Plenum, New York, 1972.

17. Hahn, E. L. *Phys. Rev.* 1950, *80*, 580.

18. Mims, W. B.; Nassau, K.; McGee, J. D. *Phys. Rev.* 1961, *123*, 2059.

19. Cowen, J. A.; Kaplan, D. A. *ibid.* 1961, *124*, 1098.

20. Rowan, L. G.; Hahn, E. L.; Mims, W. B. *Phys. Rev.* 1965, *137*, A61.

21. Mims, W. B. *Phys. Rev.* 1972, *B5* 2409 (1972).

22. Mims, W. B. *ibid* 1972, *B6*, 3543.

23. Mims, W. B.; Peisach, J. *Biological Application of Magnetic Resonance*, Shulman, R. G. ed.; Academic Press, New York; 1979, 221.

24 W. B. Mims, W. B.; Peisach, J. *Biological Magnetic Resonance*, Berliner L. J. ; Reuben, J. eds.; Plenum, New York, 1981; Vol.3, 213.

25. Kevan, L. in *Time Domain Electron Spin Resonance*, Kevan, L.; Schwartz, R. N. eds.; Wiley, New York, 1979, 279.

26. For example, Part II of this thesis.

27. For example, Wertz, J. E.; Bolton, J. R. *Electron Spin Resonance*; Chapman and Hall, New York, 1986.

28. Zaviosky, E. *J. Phys. U. S. S. R.* 1945, *9*, 211.

29. Palmer, G.; Multani, J. S.; Zumft, W. G.; Mortenson, L. E. *Arch Biochem. Biophys.* 1972, *153*, 325.

30. Venter, R. A.; Nelson, M.; McLean, P. A.; True, A. E.; Levy, M. A.; Hoffman, B. M.; Orme–Johnson, W. H. *J. Am. Chem. Soc.* 1986, *108*, 3487.

31. George, G. N.; Bare, R. E.; Jin, H.; Stiefel, E. I.; Prince, R. C. *Biochem. J.* 1989, *262*, 349–352.

32. Fermi, E. *Z. Physik* 1930, *60*, 320.

33. Mims, W. B.; Peisach, J. *J. Chem. Phys.* 1978, *69*, 4921.

34. True., A. E.; Nelson, M. J.; Venters, R. A.; Orme–Johnson, W. H.; Hoffman, B. M. *J. Am. Chem. Soc.* 1988, *110*, 1935–1943.

35. Lucken, E. A. C. *Nuclear Quadrupole Coupling Constants*; Academic, New York, 1969.

36. Cohen, M. H.; Reif, F. *Solid State Physics*; Academic, New York, 1957; Vol. 5, 321.

37. Das, T. P.; Hahn, E. L. *Solid State Physics*; Academic, New York, 1958; Suppl. 1.

38. Schiff, L. E. *Quantum Mechanics*; McGraw–Hill, New York, 1968.

39. Merzbacher, E. *Quantum Mechanics*; John Wiley, New York, 1970.

40. Messiah, A. *Quantum Mechanics*; Interscience, John Wiley, New York, 1972.

41. Cornelius, J. Personal Comminication.

42. Flanagan, H. L.; Singel, D. J. *J. Chem. Phys.* 1987, *88*, 5606.

43. Rist, G. H.; Hyde, J. S. *J. Chem. Phys.* 1968, *49*, 2449.

44. Rist, G. H.; Hyde, J. S. *J. Chem. Phys.* 1970, *52*, 4532.

45. Rist, G. H.; Hyde, J. S. *J. Chem. Phys.* 1970, *52*, 4633.

46. Hurst, G. C.;Henderson, T. A.; Kreilick, R. W. *J. Am. Chem. Soc.* 1985, *107*, 7294.

47. Hurst, G. C.; Henderson, T. A.; Kreilick, R. W. *ibid*, 1985, *107*, 7299.

48. Hoffman, B. M.; Martisen, J.; Venters, R. A. *J. Magn. Reson.* 1984, *59*, 110.

49. Hoffman, B. M.; Venters, R. A.; Martisen, J. *ibid*, 1985, *62*, 537.

50. Dikanov, S. A.; Evelo, R. G.; Hoff, A. J.; Tyryshkin, A. M. *Chem. Phys. Lett.* 1989, *154*, 34.

51. Flanagan, H. L.; Gerfen, G. L.; Lai, A.; Singel, D. J. *J. Chem. Phys.* 1988, *88*, 2162.

52. Cornelius, J.; Peisach, J. to be published.

53. McCracken, J.; Peisach, J.; Dooley, D. M. *J. Am. Chem. Soc.* 1987, *109*, 4064–4072.

54. Cammack, R.; Chapman, A.; McCracken, J.; Cornelius, J. B.; Peisach, J.; Weiner, J. H. *Biochim. Biophys. Acta.* 1988, *956*, 307–312.

55. Peisach, J.; Mims, W. B.; Davis, J. L. *J. Biol. Chem.* 1979, *254*, 12379–12389.

56. (a) Wilkinson, J. H.; Reinsch, C. *Linear Algebra*, Vol. 11 of *Automatic Computations*; Springer–Verlag, New York, 1971.

(b)Smith, B. T. *et al. Matrix Eigensystem Routines – EISPACK Guide*, 2nd ed.; Lecture Notes in Computer Science, Springer–Verlag, New York; 1981.

57. Mims, W. B.; Peisach, J.; Shaw, R. W.; Beinert, H. *J. Biol. Chem.* 1980, *255*, 6843–6846.

58. Fee, J. A.;Peisach, J.; Mims, W. B. *J. Biol. Phys.* 1981, *256*, 1910–1914.

59. Zweier, J. J.; Peisach, J.; Mims, W. B. *J. Biol. Phys.* 1982, *257*, 10314–10316.

60. Mims, W. B.; Peisach, J. *J. Biol. Phys.* 1979, *254*, 4321–4323.

61. McCracken, J.; Pember, S.; Benkovic, S.; Villafrance, J. J.; Miller, R. J.; Peisach, J. *J. Am. Chem. Soc.* 1988, *110*, 1069–1074.

62. Ashby, C. I. H.; Cheng, C. P.; Brown, T. L. *J. Am. Chem. Soc.* 1978, *100*,

6057–6063.

63. Ashby, C. I. H.; Cheng, C. P.; Duesler, E. N.; Brown, T. L. *J. Am. Chem. Soc.* **1978**, *100*, 6063.

64. Edmonds, D. T. *Physics Reports* **1977**, *29*, 233–290.

65. Edmonds, D. T.; Summers, C. P. *J. Magn. Reson.* **1973**, *12*, 134–142.

66. Hsieh, Y. –N.; Rubebacker, G. V.; Cheng, C. P.; Brown, T. L. *J. Am. Chem. Soc.* **1977**, *99*, 1394–1389.

67. Hunt, M. J.; Mackay, A. L.; Edmonds, D. T. *Chem. Phys. Lett.* **1975**, *34*, 473–475.

68. Hunt, M. J.; Mackay, A. L. *J. Magn. Reson.* **1974**, *15*, 402–414.

69. Hunt, M. J.; Mackay, A. L. *J. Magn. Reson.* **1976**, *22*, 295–301.

70. Mims, W. B.; Davis, J. L. *J. Chem. Phys.* **1976**, *64*, 4836–4846.

71. Thomann, H.; Tindall, P.; Bernardo, M. *Anal. Instrum.*, To be submitted.

72. Thomann, H.; Dalton, L. R.; Pancake, C. *Rev. Sci. Instrum.* **1984**, *55*, 389–398.

73. Blumberg, W. E.; Mims, W. B.; Zuckerman, D. *Rev. Sci. Instrum.* **1973**, *44*, 546.

74. Shimizu, T.; Mims, W. B.; Peisach, J.; Davis, J. L. *J. Chem. Phys.* **1979**, *70*, 2249.

75. Marshall, A. G. ed. *Fourier, Hadamad, and Hilbert Transforms in Chemistry*, Plunum, New York, **1982**.

76. (a) Biehl, R.; Schmalbein, D. *United States Patent* **1982**, 4312204.

(b) Barendswaard, W.; Disselhorst, J. A. J. M.; Schmidt, J. *J. Magn. Reson.* **1984**, *58*, 477.

(c) Huisjen, M.; Hyde, J. S. *Rev. Sci. Instrum.* **1974**, *45*, 669.

77. Schweiger, A.; Ernst, R. R. *J. Magn. Reson.* **1988**, *77*, 512–523.

78. Cho, H.; Pfenninger, S.; Gemperle, C.; Schweiger, A.; Ernst, R. R. *Chem. Phys. Lett.* **1989**, *160*, 391.

79. Mims, W. B. *J. Magn. Reson.* **1984**, *59*, 291–306.

80. Barkhuijsen, H.; de Beer, J.; Bovee, W. M. M. J.; Van Ormondt, D. *J. Magn. Reson.* **1985**, *61*, 465.

81. Kamaresan, R.; Tufts, D. W. *IEEE Trans.* **1982**, *ASSP–30*, 833,

82. Tang, J.; Lin, C. P.; Bowman, M. K.; Norris, J. R. *J. Magn. Reson.* **1985**, *62*, 167–171.

83. Tang, J.; Norris, J. R. *J. Magn. Reson.* **1988**, *78*, 23–30.

84. Tang, J.; Norris, J. R. *J. Magn. Reson.* **1988**, *79*, 190–196.

85. Makhoul, J. In *Modern Spectral Analysis*, Childers, D. G. ed.; IEEE Press, Wiley, New York, **1978**, 99–118.

86. Kay, S. M.; Marple, S. L. *Proc. IEEE* **1981**, *69*, 1380.

87. Astashkin, A. V.; Dikanov, S. A.; Tsvetkov, Y. D. *Chem. Phys. Lett.* **1987**, *136*, 204.

88. Mims, W. B. in Reference 75.

89. Fauth, J. –M.; Schweiger, A.; Braunschwieler, L.; Forrer, J.; Ernst, R. R. *J. Magn. Reson.* **1986**, *66*, 74–85.

90. Bowman, M. K. Quoted in the footnote in Reference 79.

91. Zweier, J. J.; Peisach, J.; Mims, W. B. *J. Biol. Chem.* **1982**, *257*, 10314–10316.

92. Kosman, D. J.; Peisach, J.; Mims, W. B. *Biochemistry.* **1980**, *19*, 1304–1308.

93. Dikanov, S. A.; Shubin, A. A.; Parmon, V. N. *J. Magn. Reson.* **1981**, *42*, 474–487.

PART II ELECTRON SPIN ECHO STUDY

OF THE NITROGENASE

MOLYBDENUM IRON PROTEIN

ABSTRACT

An ESEEM spectroscopic study has been performed on the nitrogenase molybdenum–iron protein from *Clostridium pasteurianum*. The analysis of the data and conclusions concerning the coordination structure of the molybdenum–iron cofactor (FeMoco) will be discussed.

Although the EPR spectrum of the ± 1/2 Kramers doublet of the $\tilde{S} = 3/2$ system from the protein enriched with ^{95}Mo (I = 5/2) was observed to be essentially indistinguishable from the EPR spectrum of the protein enriched with ^{96}Mo (I = 0), differences were observed in ESEEM and EI–EPR spectra at resonance frequencies of both 10.7 GHz and 9 GHz. To isolate any difference between the two, the time domain ESEEM data of the ^{95}Mo enriched MoFe protein were divided by the ^{96}Mo enriched protein time domain ESEEM data taken at identical experimental conditions. The cosine Fourier transform from the division quotient clearly indicated the presence of multiple sharp peaks associated with transitions among quantum states of the molybdenum spin. The hyperfine coupling and nuclear quadrupolar coupling of the molybdenum obtained from the preliminary analysis are lower than the values obtained from the CW–ENDOR analysis.[22]

In all spectra, whether from the native protein or the proteins that were

isotopically enriched, the nuclear modulation due to at least one nitrogen has been observed. The interplay of the nuclear Zeeman, hyperfine, and nuclear electric quadrupolar interactions, together with the effect of "orientational selectivity", results in a pronounced dependence of the ESEEM spectra on the resonance magnetic field. This enables the extraction of a unique set of coupling parameters. Based on this analysis, in comparison with existing Nuclear Quadrupole Resonance data and recent site–directed mutagenesis studies, it is likely that the modulation is due to a nitrogen in the side chain of a histidine or a glutamine residue which is coordinated to the FeMoco. However, the possibility that the modulation is due to a nitrogen in the side chain of a lysine can not be ruled out.

While the nitrogen modulation frequencies do not depend on whether the protein is enriched with ^{95}Mo or ^{98}Mo, the modulation amplitudes are quite different. The significant change of the nitrogen modulation amplitudes introduced by the difference in molybdenum isotope enrichment suggests that this nitrogen is likely connected to the FeMoco through coordination to the molybdenum.

Chapter 5

INTRODUCTION TO NITROGENASE

Nitrogen fixation, either as the biological process or the industrial Haber–Bosch process, is often a limiting factor in supplying a reduced form of nitrogen to bacteria and plants, thus directly affecting growth.[1] Most of the nitrogen fixation on earth is accomplished through the catalytic action of the enzyme nitrogenase. Nitrogenase is the enzyme in bacteria capable of reducing N_2 at ambient temperature and pressure, in contrast to the industrial process where high temperatures and pressures are needed.[2] Studies of this enzyme are directed toward the understanding of how this enzyme utilizes the metal clusters which have unusual composition and novel physical properties to achieve its catalytic efficiency.

When isolated from various bacteria, nitrogenase is found to be an iron–sulphur protein containing molybdenum.[3-5] It was believed for quite a long time that molybdenum was the essential element for biological nitrogen fixation. Recently, evidence for Mo–independent nitrogenases, namely, V–nitrogenase systems and possibly an Fe only nitrogenase, has been presented.[6-8] This dissertation will, however, focus on the Mo–nitrogenase. In the following, unless otherwise specified, Mo–nitrogenase will be implicitly assumed.

Nitrogenase consists of two separate and distinct proteins, the MoFe protein (or component 1) and the Fe protein (or component 2), as shown schematically in Figure 5.1. They must act concertedly for catalysis in any of the biological reactions.[9,10] The exact details of the catalysis of N_2 reduction are still unknown,

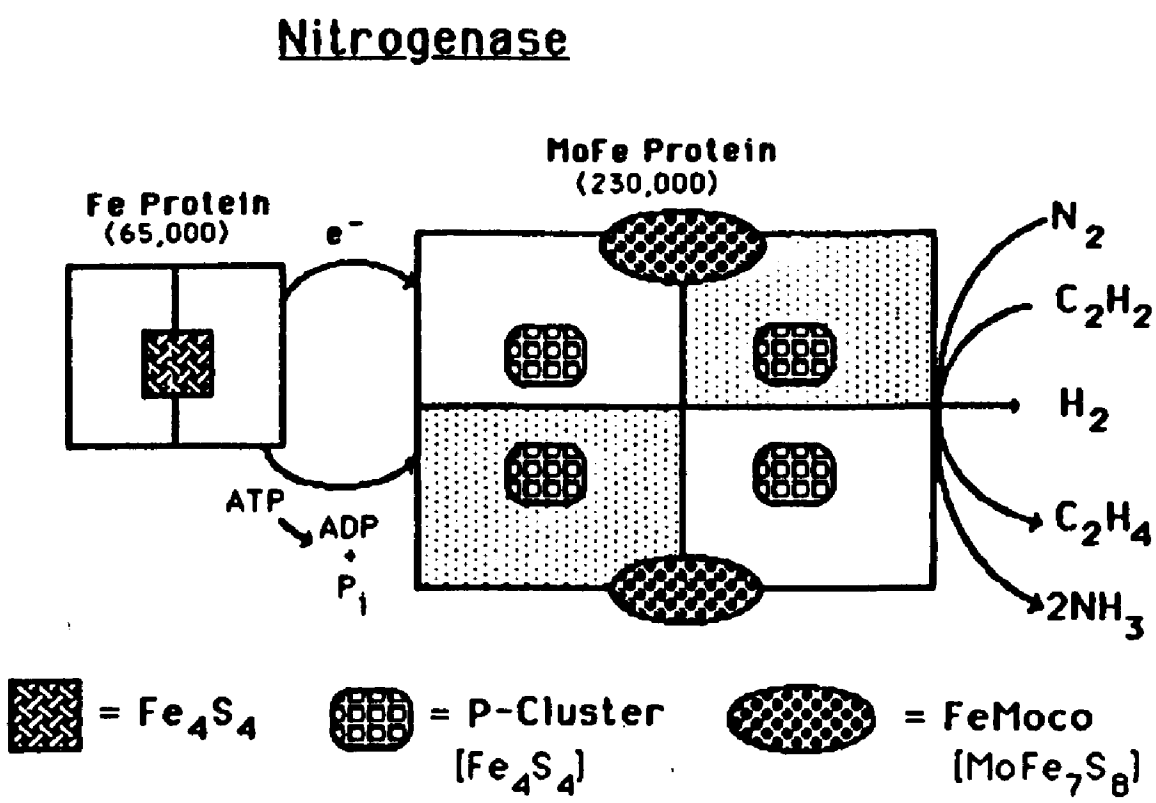

Figure 5.1 Schematic representation of Mo–nitrogenase (Courtesy of Dr. E. I. Stiefel).

though a considerable amount of structural, kinetic, and biochemical data on the system is available. The Fe protein contains two identical subunits of molecular weight 30,000.[11] A single Fe_4S_4 center is present in the protein and appears to be bound between the two subunits.[12] During enzyme turnover this protein transfers electrons to the MoFe protein.[13,14] The MoFe protein has a molecular weight around 220,000, and is isolated as a $\alpha_2\beta_2$ tetramer with subunit molecular weight of 50,000 and 60,000 respectively. It contains 2 Mo, and approximately 30 Fe and 30 S^{2-} per molecule.[9,10] There are at least six metal–containing prosthetic groups, two of which constitute the so–called M center. The other four, called "P clusters", are thought to be involved in electron transfer and storage, presumably providing a reservoir of low potential electrons to be used by the M centers in substrate reduction.[10,15]

The Iron–Molybdenum cofactor (FeMoco) has been extracted from the protein into N–methyl formamide (NMF) and other solvents. The similarity of FeMoco to the M center can be shown by the fact that FeMoco activates the MoFe protein from a mutant organism that produces protein which lacks the M center.[16] FeMoco consists of Mo, Fe and S with the ratio estimated to be 1 : 6–7 : 9–10.[17] Also, it contains homocitrate, recently proven as an intrinsic organic component.[18] Recent genetic evidence strongly implicates the FeMoco as the active site of N_2 binding and reduction.[19] The resemblance of the extracted cofactor to that of the M center in the protein has been shown spectroscopically and structurally.[20-26] EPR spectra of FeMoco and the MoFe protein in its resting state are shown in Figure 5.2. In the case of the protein, the EPR signal is attributed to the M center, since all P clusters are reduced to a spin state of $S = 0$. Both spectra are characteristic of an $\tilde{S} = 3/2$ center in which the $M_{\tilde{S}} = \pm 1/2$ Kramers doublet lies lowest in energy. The spectrum of the cofactor is considerably broader and has somewhat greater rhombicity compared to that of the M center in the protein. Nevertheless, the $\tilde{S} =$

Figure 5.2 X–band EPR spectra taken at 5 K for the (a) the nitrogenase MoFe protein from *Clostridium pasterianum*; and (b) the FeMoco extracted from the protein in NMF. Other experimental conditions: microwave frequency at 9.222 GHz, H = 2250 gauss, field span = 4000 gauss, and modulation field amplitude = 10 gauss.

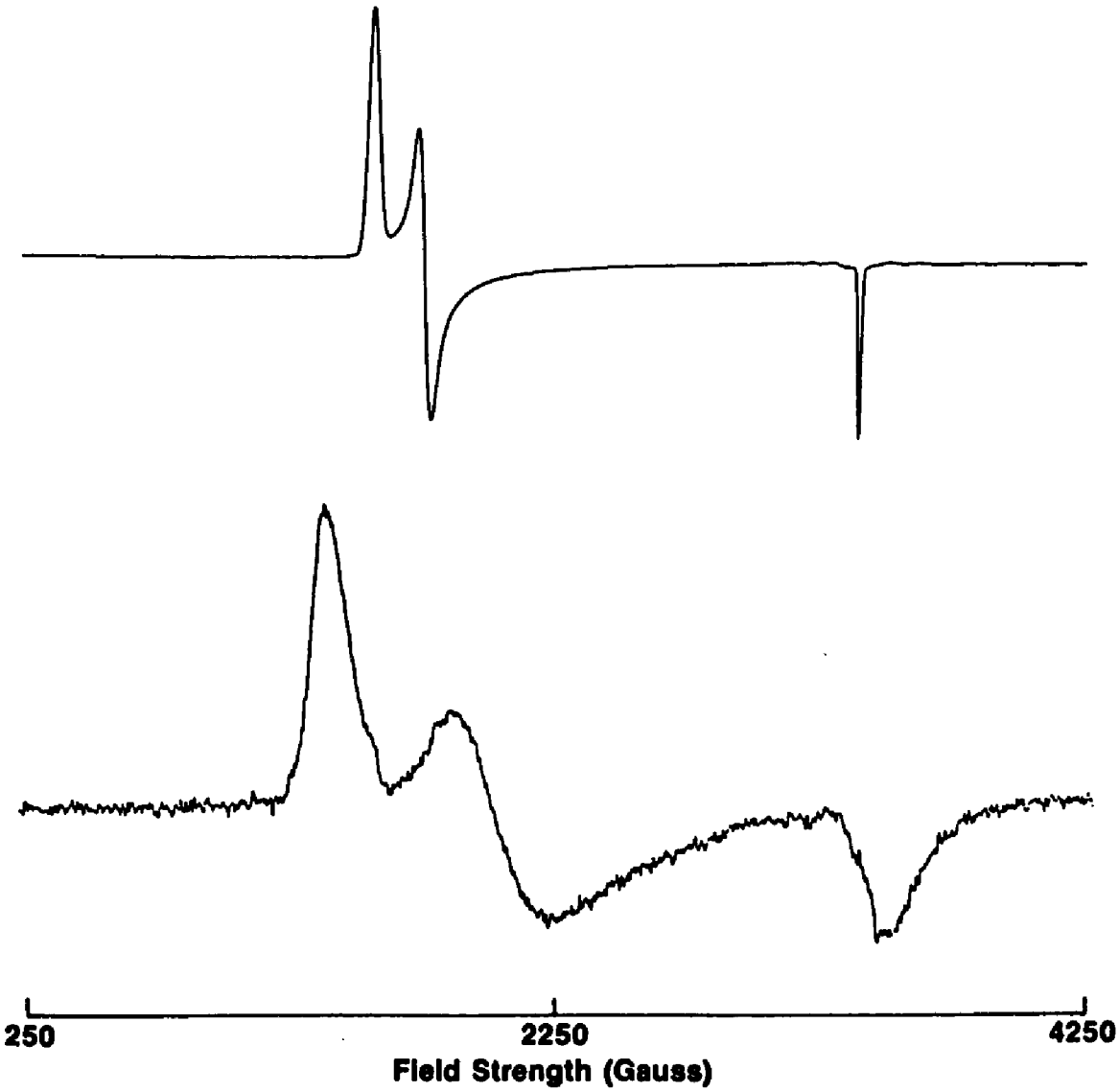

Figure 5.2

3/2 signature is unique for this protein system, and its presence in FeMoco and the M center spectra is indicative of the structural similarity. X–ray absorption spectroscopy (XAS) has given further support of the structural similarities.[23-25] The Mo XAS on MoFe proteins from both *Clostridium pasterianum* and *Azotobacter vinelandii*, as well as on FeMoco extracted in NMF indicates that the FeMoco extraction procedure leaves the metal coordination surroundings unchanged from the protein. The extended X–ray absorption fine structure (EXAFS) also reveals similarity between the Mo in FeMoco and in MoFe protein. In both the protein and FeMoco, $3-4$ Sulphur at 2.4 Å from the Mo, plus $2-4$ Iron at 2.7 Å, and $1-2$ low Z atoms (N or O) at 2.2 Å are found.

Additional support for the $\bar{S} = 3/2$ formulation comes from Mössbauer and Electron Nuclear Double Resonance (ENDOR) spectroscopy.[26,22] Mössbauer spectra of the $\bar{S} = 3/2$ center have been decomposed into six components. They are spin–coupled as evident by the fact that the spin is shared by these iron atoms and by the observation of positive and negative hyperfine coupling constants. These conclusions have been supported by recent CW–ENDOR experiment. From their ENDOR analysis on ^{57}Fe enriched protein, True *et al.*[27] concluded that at least five inequivalent iron sites could be identified. In a separate report by Venters *et al.*[22], ^{95}Mo ENDOR measurements also confirms that a single molybdenum is an integral part of the cluster.

Since the EPR signal of MoFe protein arises from the M center (or FeMoco), numerous EPR studies, including those on MoFe protein enriched with individual isotopes, have been performed in order to gather more information about this center. Among them, Palmer *et al.*[28] examined the EPR of the $\pm \frac{1}{2}$ signal from the protein enriched with ^{95}Mo, and observed that the spectra from the molybdenum enriched protein and from the native protein were essentially indistinguishable from each other. Similar results were also obtained from the protein isolated from

different organisms by Smith *et al.*.[29] In addition, they observed a subtle broadening in the signal from $\pm \frac{1}{2}$ Kramers doublet for the protein isotopically enriched with ^{57}Fe, suggesting the participation of Fe in the center. Recently, George *et al.*[30] have performed EPR experiments on proteins enriched with various isotopes including ^{57}Fe, ^{95}Mo, and ^{96}Mo, and on proteins exchanged with isotopically labeled water. The sharpness of the signal from the excited states enabled the observation and quantitation of incompletely resolved hyperfine splittings from the magnetic nuclei ^{95}Mo and ^{57}Fe. Also, ^{95}Mo hyperfine coupling deduced from that experiment were found to be different than that obtained from previous CW–ENDOR.

As discussed previously, the inhomogeneous broadening of the EPR spectra precludes more detailed analysis of the FeMoco structure. CW–ENDOR has been utilized to gather more information about this cluster. In a series of studies, Hoffman *et al.*[22,27] examined native and isotopically enriched MoFe proteins. The major conclusions have been stated above. It is worth commenting that the ^{95}Mo ENDOR frequency peaks reported are rather broad with only a doublet present. Some peaks are assigned, but not clearly present. In addition, no observation of the cluster ligation was reported.

Because of its complementary nature to ENDOR spectroscopy, ESEEM should be an effective tool for exploring the environment of the cluster. Indeed, in the unpublished 2–pulse ESEEM data, Mims and Orme–Johnson observed[31] differences between the ^{95}Mo–enriched and ^{96}Mo–enriched proteins. without further analysis, it was assumed as an indication of the participation of molybdenum in the paramagnetic cluster. The purpose of this study is to investigate spectroscopic properties of FeMoco, and to provide information about the structure and coordination of the cluster.

Chapter 6

RESULTS

In this chapter, the ESE study on the nitrogenase MoFe protein and FeMoco extracted in NMF, both of natural isotopic abundance, will be first discussed. Initial experiments were performed at the temperature T ≈ 5 K. From this study, protein nitrogen coordination to FeMoco was identified. Then the study, performed at T ≈ 1.5 K, on the protein enriched with molybdenum isotopes will be described. Discussions will be focused on identifying the origin of this nitrogen coordination and the mode of coordination to FeMoco. The preparation method of the protein sample is included as Appendix 3. The extraction procedure of FeMoco can be found in, for example, reference 17.

I. Experimental Results at 5 K

The experiments were performed on the nitrogenase MoFe protein and FeMoco which was extracted from the protein with NMF. Both samples were from *Clostridium pasteurianum*. ESEEM data were recorded on the spectrometer described, though with an overcoupled TE102 microwave cavity as the resonator, which is mounted on an Oxford Instruments E9 helium flow cryostat. The time domain waveform and its Fourier transform on the MoFe protein are shown in (A) and (B) of Figure 6.1.1. The time domain data were taken at $g = 3.70$ using the stimulated echo sequence with $\tau = 0.12$ μsec. The time duration for all pulses was 20 nsec, and the time increment between consecutive data points was 10 nsec.

Figure 6.1.1 The time–domain envelope waveform taken with the stimulated echo sequence is shown for the MoFe protein in (A) and its Fourier transform in (B) and for the FeMoco in (C) and its Fourier transform in (D). The experimental conditions were $\tau = 0.12$ μsec, $H = 1740$ gauss, microwave frequency 9.0595 GHz; temperature T = 5 K; and $\pi/2$ pulse width was 0.02 μsec. Fourier transformation was facilitated by using the LPBE method.

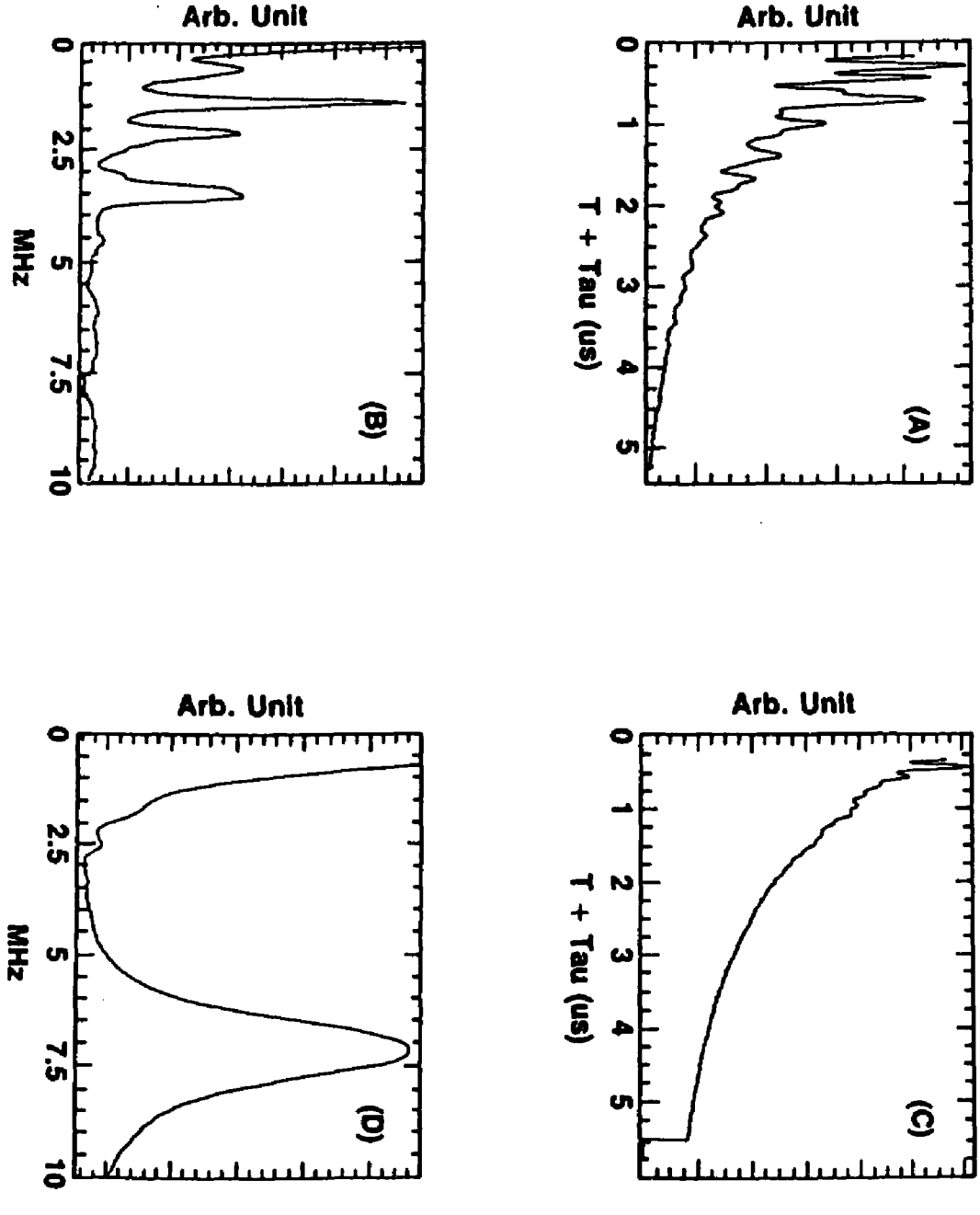
Arb. Unit
0
1
2
3
4
5
T + Tau (us)
(A)
Arb. Unit
0
2.5
5
7.5
10
MHz
(B)
Arb. Unit
0
1
2
3
4
5
T + Tau (us)
(C)
Arb. Unit
0
2.5
5
7.5
10
MHz
(D)

Figure 6.1.1

The Fourier transforms were obtained after reconstructing the "dead time" piece with LP method. Neither baseline correction before the transform nor phase correction after the transform were taken. The appreciable periodical amplitude change and sustained signal are transformed to well resolved sharp lines. There are four distinct modulation frequency lines located at 0.66, 1.45, 2.09, and 3.48 MHz. These well resolved lines are characteristic of nuclear quadrupole transitions for nitrogen coordinated to the paramagnetic metal center. Proton modulations are suppressed in the spectrum, due to proper choice of τ such that the stimulated echo sequence suppresses the proton Larmor frequency.[32]

ESEEM time domain data and its transform shown in (C) and (D) of Figure 6.1.1 are from the experiment on FeMoco. At the end of time domain data, 20 baseline points were collected in addition to 512 data points. The data were taken at the same experimental conditions as for the MoFe protein. No other data processing technique was applied except a cosine Fourier transform following the reconstruction of the "dead time" portion. The broad peak centered at 7.2 MHz, which is the Larmor frequency of a proton at that field, can be assigned to proton(s). The broad linewidth may indicate presence of very fast decaying protons or numerous coordinated protons. Given that the number of protons present in the sample is very large, and that no other information about distribution of protons surrounding the paramagnetic center, no attempt has been made to characterize these protons.

There are visible differences in both the time domain and frequency domain spectra between the MoFe protein and FeMoco. The most obvious difference is the absence of the four sharp modulation peaks discussed above in the FeMoco spectrum. The extra nitrogen modulation in the protein may have several possible origins. It may come from the substrate (N_2) molecules which remain associated with the protein, or from the TRIS buffer when the protein is prepared (FeMoco is

extracted from the protein in NMF, therefore, should be independent of which buffer is used), or from the protein structure surrounding FeMoco. When phosphate buffer was used to prepare the protein, no difference in the nitrogen modulation of the protein was found, indicating that the nitrogen does not come from buffer. Furthermore, allowing nitrogenase turn over with $^{15}N_2$ (^{15}N possesses a spin I = 1/2, while ^{14}N, I = 1) as substrate did not change ESEEM modulation spectrum. If the modulation observed is due to remnant substrate nitrogen in the protein, it would be expected to be replaced by ^{15}N in this experiment. The fact that no spectral change were observed eliminates this hypothesis. Therefore the modulation comes from a part of the protein adjacent to the FeMoco.

In principle, nitrogen modulation can be observed if a nitrogen is directly coordinated to, indirectly coordinated to (coordination through other bonds), or located nearby but without any bonds with the paramagnetic center. To confirm the assignment of nitrogen, as well as to determine how the nitrogen connects to the FeMoco, a numerical simulation was performed based on the method described in Section 3.5.

Shown in Figure 6.1.2 and 6.1.3 are the comparisons of simulated spectra and experimental data for the MoFe protein at $g = 3.70$ and 2.50. The parameters used to generate the simulated spectrum in Figure 6.1.2 are: $\nu_+ = 2.00$ MHz, $\nu_- = 1.40$ MHz, $A_{iso} = 1.65$ MHz. ν_+ and ν_- can be converted to $e^2qQ/h = 2.27$ MHz and $\eta = 0.53$. The frequency peaks in the simulated spectrum are 0.66, 1.45, 2.11 and 3.48 MHz, which compare favorably with the experimental ones of 0.66, 1.45, 2.09, and 3.45 MHz. The nuclear quadrupole parameters used to generate the simulated spectrum at $g = 2.50$ in Figure 6.1.3 are: $\nu_+ = 2.19$ MHz, $\nu_- = 1.33$ MHz, $A_{iso} = 1.50$ MHz. ν_+ and ν_- can be converted to $e^2qQ/h = 2.35$ MHz and $\eta = 0.73$. The simulated frequency peaks are 0.86, 1.34, 2.19, and 3.75 MHz, which compare favorably with experimental ones at 0.86, 1.34, 2.19, and 3.78 MHz. Although

Figure 6.1.2. Comparison of (a) the experimental and (b) simulated spectra for the MoFe protein at $g = 3.70$. The experimental conditions have been described in Figure 6.1.1. The phase correction, as discussed in Section 4.3, was performed following cosine Fourier transform. The simulation was performed with the spherical average method, as discussed in Section 3.5, with $\nu_+ = 2.00$ MHz, $\nu_- = 1.40$ MHz, and $A_{iso} = 1.65$ MHz.

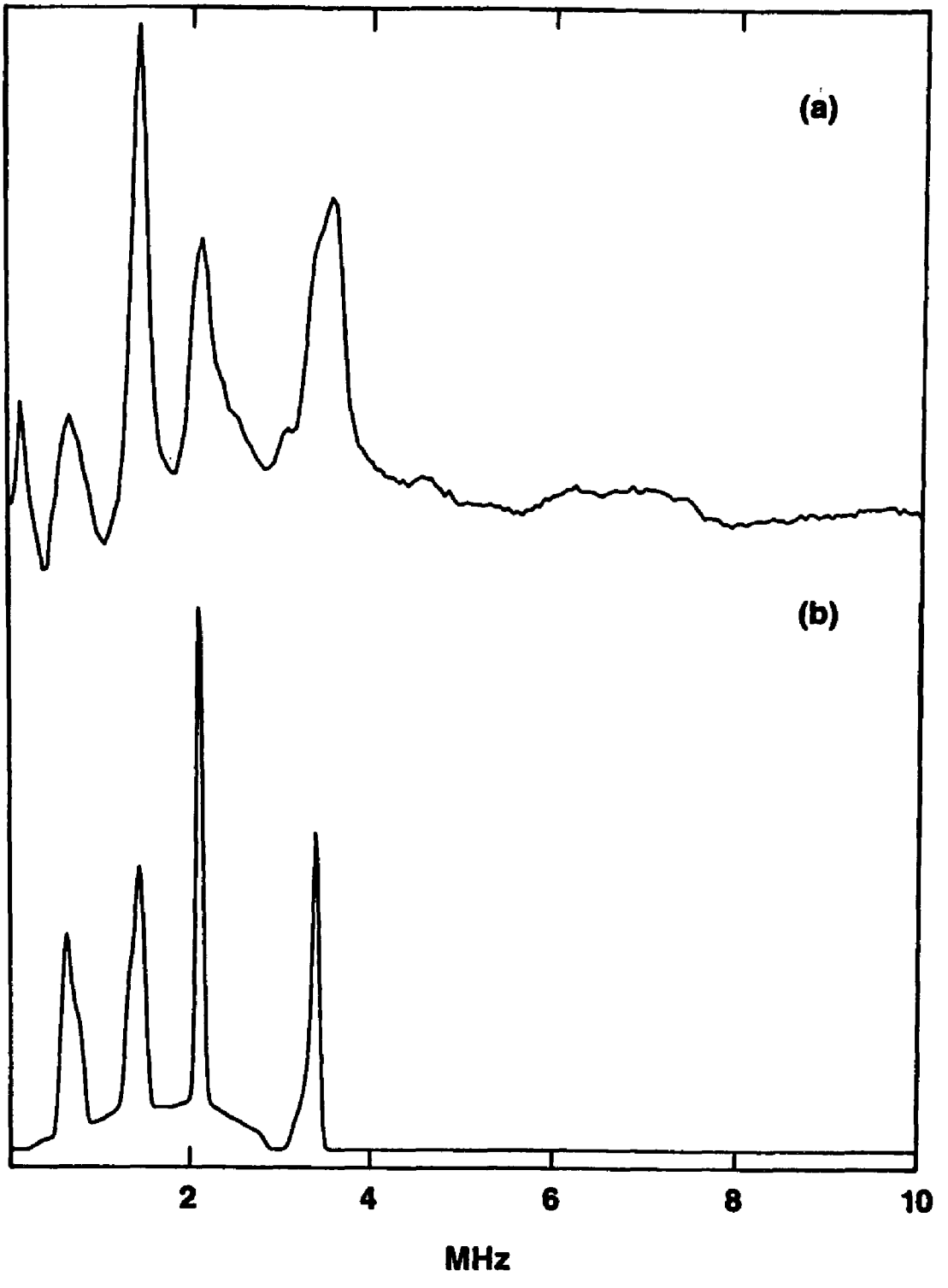

Figure 6.1.2

Figure 6.1.3. Comparison of (a) the experimental and (b) simulated spectra for the MoFe protein at $g = 2.50$. The experimental conditions are the same to those in Figure 6.1.1, except $H = 2577$ gauss, $\tau = 0.16$ μsec. The phase correction, as discussed in Section 4.3, was performed following cosine Fourier transform. The simulation was performed in the same way as in Figure 6.1.2, except the simulation conditions: $\nu_+ = 2.19$ MHz, $\nu_- = 1.33$ MHz; $A_{iso} = 1.50$ MHz.

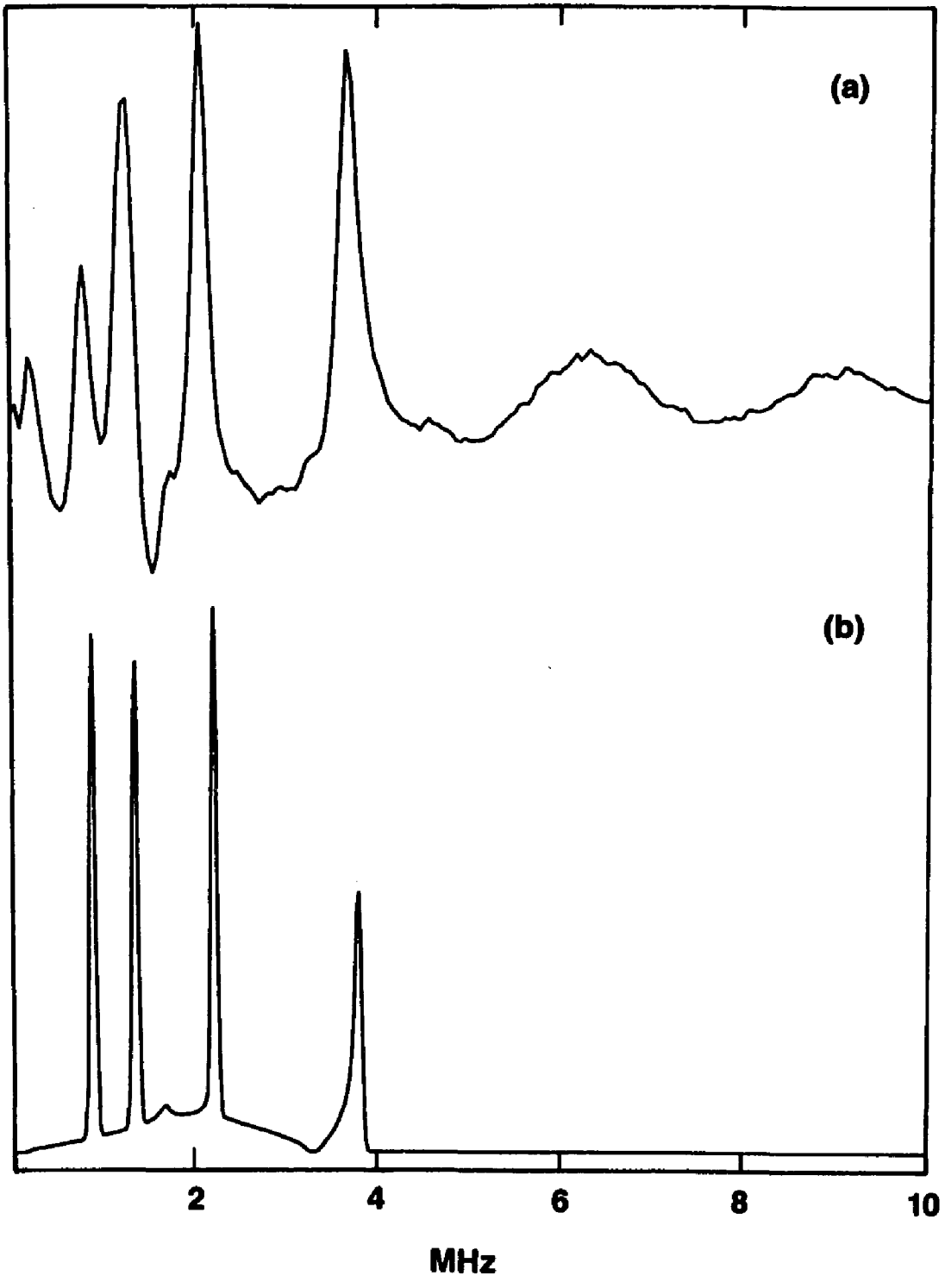

Figure 6.1.3

modulation amplitudes are not well represented, but the frequencies are correctly reproduced.

It is interesting to note that the nuclear quadrupole parameters inferred are very similar to those involving the imidazole nitrogen directly bound to low–spin heme where $e^2qQ/h = 2.53$ MHz and $\eta = 0.32$.[33] It is also interesting that there exists a non–zero isotropic hyperfine coupling constant from the current analysis. The hyperfine coupling here is, sometimes, called "superhyperfine" coupling to distinguish the hyperfine coupling due to a ligand from that due to the metallic ion. Fermi has shown that for systems with one electron the metallic isotropic hyperfine interaction is given by

$$(6.1.1) \qquad -\frac{8\pi}{3} |\psi(0)|^2 \mu_e \mu_N$$

where μ_e and μ_N are magnetic moments of electron and nucleus respectively, $\psi(0)$ represents the wave function evaluated at the nucleus.[34] Expressed in operator form, the Fermi contact interaction is

$$(6.1.2) \qquad \frac{8\pi}{3} g \beta_e g_N \beta_N |\psi(0)|^2 (\mathbf{I}\cdot\mathbf{S}).$$

From the quantum mechanical model for the hydrogen atom, only electrons in s orbital have a non–zero probability of being at the nucleus. In general, the contact interaction is due to the presence of unpaired s–electron spins, which arises from polarization of the filled electron shells.[35] By analogy, a non–zero isotropic superhyperfine coupling would mean the presence of paramagnetic electrons at the ligand nucleus, resulting from ligand coordination. The similarity of nitrogen quadrupole parameters in the MoFe protein to those in metal–imidazole complexes suggests that the observed frequencies most likely come from a directly coordinated

nitrogen on an imidazole ring.

In summary, the ESEEM spectrum of the protein taken at T ~ 5 K contains lines characteristic of nuclear quadrupolar transitions for nitrogen coordination to the M center. These frequencies are absent from the spectrum of FeMoco isolated in NMF, suggesting that the FeMoco is coordinated to the protein through at least one nitrogen ligand. This conclusion is reinforced by the determination of a non–zero isotropic hyperfine term which shows direct interaction of the ^{14}N nuclear and electron spins.

However, these results were obtained at T ~ 5 K, where the electronic phase–memory time is shorter than that at T ~ 1.5 K. Also, spectra were taken at only a few g values, and the effect of "orientation selection" was not adequately considered. Due to differences of the EPR spectra between the MoFe protein and FeMoco, the comparison of the ESEEM spectra may be based on different sets of molecules whose molecular reference frames have different orientations to the external magnetic field. In addition, in the FeMoco spectrum, some low frequency lines are visible, though with small amplitude. It is arguable that the nitrogen observed in the MoFe protein could be present in FeMoco with a change of the magnetic coupling.

There are several questions concerning the nitrogen modulation need to be answered:

1) How many nitrogens does the modulation represent?

2) What is the identity of the nitrogen?

3) To which part of the FeMoco does the nitrogen bind?

These are the motivations of the study presented in the next section.

II. Experimental Results at 1.5 K

The data were taken on the spectrometer described. When taking EI–EPR spectra, the Hahn echo sequence was used, and typical field strength increment were 5 or 10 gauss. The ESEEM data were taken typically at the time interval of 20 or 30 nsec, which corresponds to Nyquist frequency of 25 or 16.67 MHz. The pulse repetition rate at which the pulse sequence is repeated is typically 400 Hz, or one pulse sequence per 2.5 msec. Unless specified, the stimulated echo (3–pulse) sequence were used. Five baseline points were collected at the end of scans. In order to prevent baseline artifacts in the Fourier transform spectra, Linear Prediction was used to back–extend the time–domain data to zero time, filling in the small missing piece due to the spectrometer "dead time". The decay backgrounds were removed by subtraction of suitably fitted polynomials. If LPBE was not applied, cosine Fourier transformed spectra taken were phase corrected according to the points missing at the beginning of the time data file, as described in Section 4.3. Data involved in the waveform division were taken under identical experimental conditions, i.e., the resonant frequency, magnetic field setting, temperature, and time intervals, etc..

1. ESEEM of FeMoco at 1.5 K

EPR spectra of FeMoco in unenriched NMF and $^{13}C^{15}N$ doubly labeled NMF at 5 K are observed to be indistinguishable (not shown). The identical spectra makes the comparison of ESEEM spectra between the two a fair one, in the sense that the "orientation selectivity" by EPR will be identical for both.

The comparison of ESEEM spectra of the two samples is shown in Figure 6.2.1. Because the modulation is shallow and the echo envelope decays fast, it is

Figure 6.2.1 ESE spectra at $g = 2.05$ for (a) FeMoco extracted in NMF; (b) FeMoco in ^{13}C, ^{15}N doubly labeled NMF. The experimental conditions were: (a) microwave frequency $\nu_e = 9.154$ GHz, $H =$ 3186 gauss and $\tau = 0.22$ μsec; (b) $\nu_e = 9.170$ GHz, $H = 3196$ gauss; $\tau = 0.22$ μsec; T = 1.5 K, and $\pi/2$ pulse width was 0.03 μsec. The phase correction was performed following the cosine Fourier transformation, as discussed in Section 4.3.

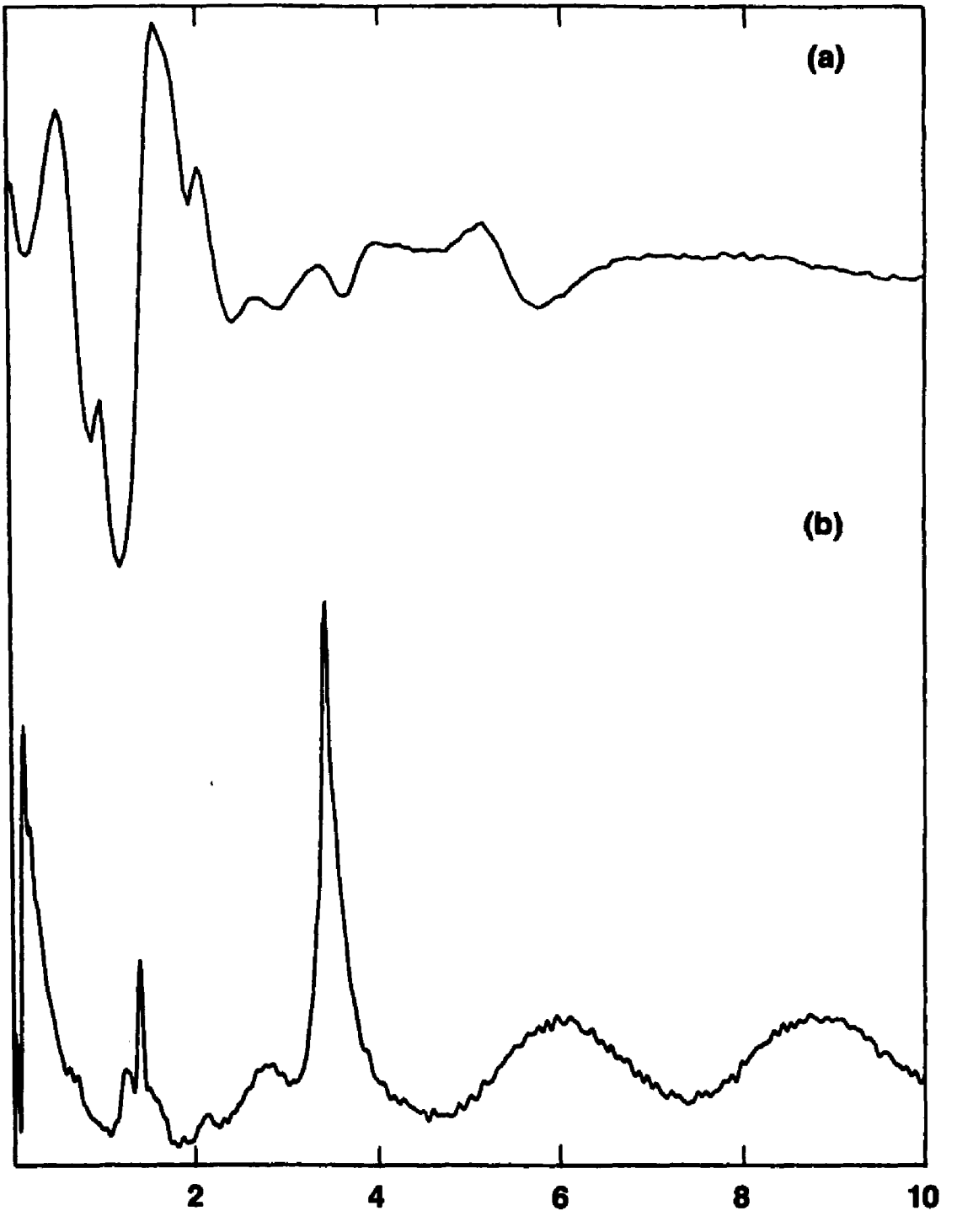

Figure 6.2.1

difficult to remove the decay background from the time domain data properly, therefore distortions to the transform spectra are pronounced. But it is quite obvious that there are significant differences between the two spectra. Spectrum (a) contains a number of broad frequency peaks, which can possibly be assigned to ^{14}N or Mo (^{95}Mo and ^{97}Mo) nuclei. In spectrum (b), the sharp frequency peaks centered at 1.40 MHz and 3.45 MHz are very close to the Larmor frequencies of ^{15}N (1.38 MHz) and ^{13}C (3.42 MHz) at that field setting. Therefore, they can be assigned to ^{15}N and ^{13}C nuclei in labeled NMF, respectively. The significant differences in the two spectra indicate that the observed frequencies in spectrum (a) are most likely due to NMF, not to the FeMoco. If a part of the observed frequencies in spectrum (a) are hypothesized to be due to the same nitrogen(s) responsible for the observed modulation in the MoFe protein, it would be inconsistent with the observation that these frequencies were replaced by the ^{15}N frequency in spectrum (b). Therefore, it is firmly established that the non–cofactor part of the MoFe protein is responsible for the nitrogen modulation.

The above result is not only significant in confirming protein coordination, but also informative about the role of NMF. FeMoco was first isolated by Shah and Brill[35] by extraction from acid–denatured MoFe protein into NMF. Efforts have been made to investigate why NMF remains a more successful and reliable extracting agent than other solvents. Yang *et al.*[36] developed several modifications of the original extracting procedure; and concluded that NMF is not essential for the effective isolation or structural stability of FeMoco. There have been speculations about the connection between the protein coordination structure and the role of NMF. Walters *et al.*[37] inferred from their FT–IR analysis that NMF is ligated to FeMoco via deprotonated nitrogen, and further hypothesized that in the MoFe protein, the primary coordination of the cofactor is via deprotonated backbone amide ligands. ESEEM study on FeMoco in individually labeled NMF, aimed at

elucidating how many NMF molecules are bound, thus mode of binding to FeMoco, has been planned. The data and analysis will be presented on a later date.

2 EI–EPR Studies

The EI–EPR spectra at 9 GHz with different inter–pulse time intervals on MoFe protein enriched with ^{95}Mo and with ^{96}Mo are shown in Figures 6.2.2 and 6.2.3. Those at 10.7 GHz (not shown) are very similar to these figures. The pronounced differences in the spectra of different molybdenum isotopic enrichments clearly indicate the effect of the molybdenum, especially at the higher magnetic field region of the spectra.

The stable isotopes ^{95}Mo and ^{96}Mo possess nuclear spins I = 5/2 and I = 0, respectively. So while the presence of the ^{96}Mo nucleus should not cause any hyperfine splitting of the EPR signal, the presence of the ^{95}Mo nucleus would be expected to do so. The EPR signal of the ± 1/2 Kramers doublet of the 3/2 system from the MoFe protein enriched with ^{95}Mo were observed to be essentially indistinguishable from that enriched with ^{96}Mo, or that with natural abundance of isotopes, indicating a very small hyperfine coupling for the molybdenum.[28,29] While EPR is not sensitive to small hyperfine couplings, EI–EPR can be susceptible to the nuclear modulation effect caused by weak magnetic interactions. As discussed in Chapter 2, EI–EPR spectra would be identical to EPR spectra if the time interval between pulses were zero. Otherwise, the nuclear modulation effect needs to be considered. Because the nuclear modulation effect modifies the echo amplitude, the EI–EPR data depend both on the interplay of various magnetic interactions and on the time interval between pulses. The differences in EI–EPR spectra, notably in the higher field region, of the proteins enriched with ^{95}Mo and with ^{96}Mo clearly indicate the presence of magnetic interactions of the molybdenum. On the other

Figure 6.2.2 Comparison of CW–EPR and EI–EPR spectra of the MoFe protein isotopically enriched with ^{96}Mo. The experimental conditions: ν_e = 9.056 GHz; temperature, 1.5 K; $\pi/2$ pulse width 0.03 μsec; τ of the Hahn echo sequence is indicated for each EI–EPR spectrum in the Figure. Magnetic field strength and corresponding g values are labeled as the abscissa. The top spectrum was generated using the CW–EPR simulation parameters for the same protein at 4.2 K (George *et al. Biochem. J.* 1989, *262*, 349).

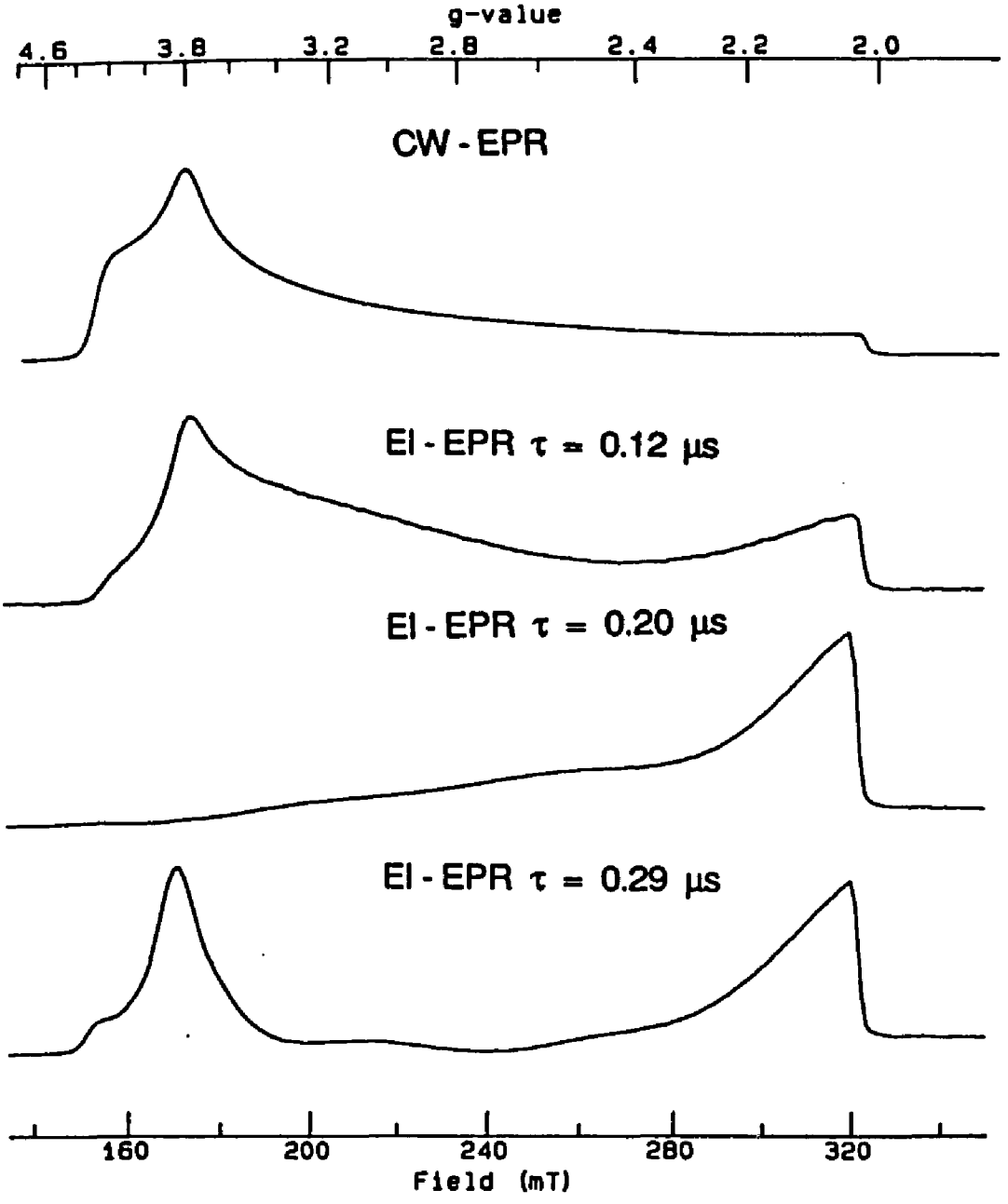
g-value
4.6
3.8
3.2
2.8
2.4
2.2
2.0
CW - EPR
EI - EPR τ = 0.12 μs
EI - EPR τ = 0.20 μs
EI - EPR τ = 0.29 μs
160
200
240
280
320
Field (mT)

Figure 6.2.2

Figure 6.2.3 Comparison of CW–EPR and EI–EPR spectra of the MoFe protein isotopically enriched with ^{95}Mo. The top spectrum was generated using the CW–EPR simulation parameters for the same protein at 4.2 K (George *et al. Biochem. J.* 1989, *262*, 349). The experimental conditions are identical to those in Figure 6.2.2.

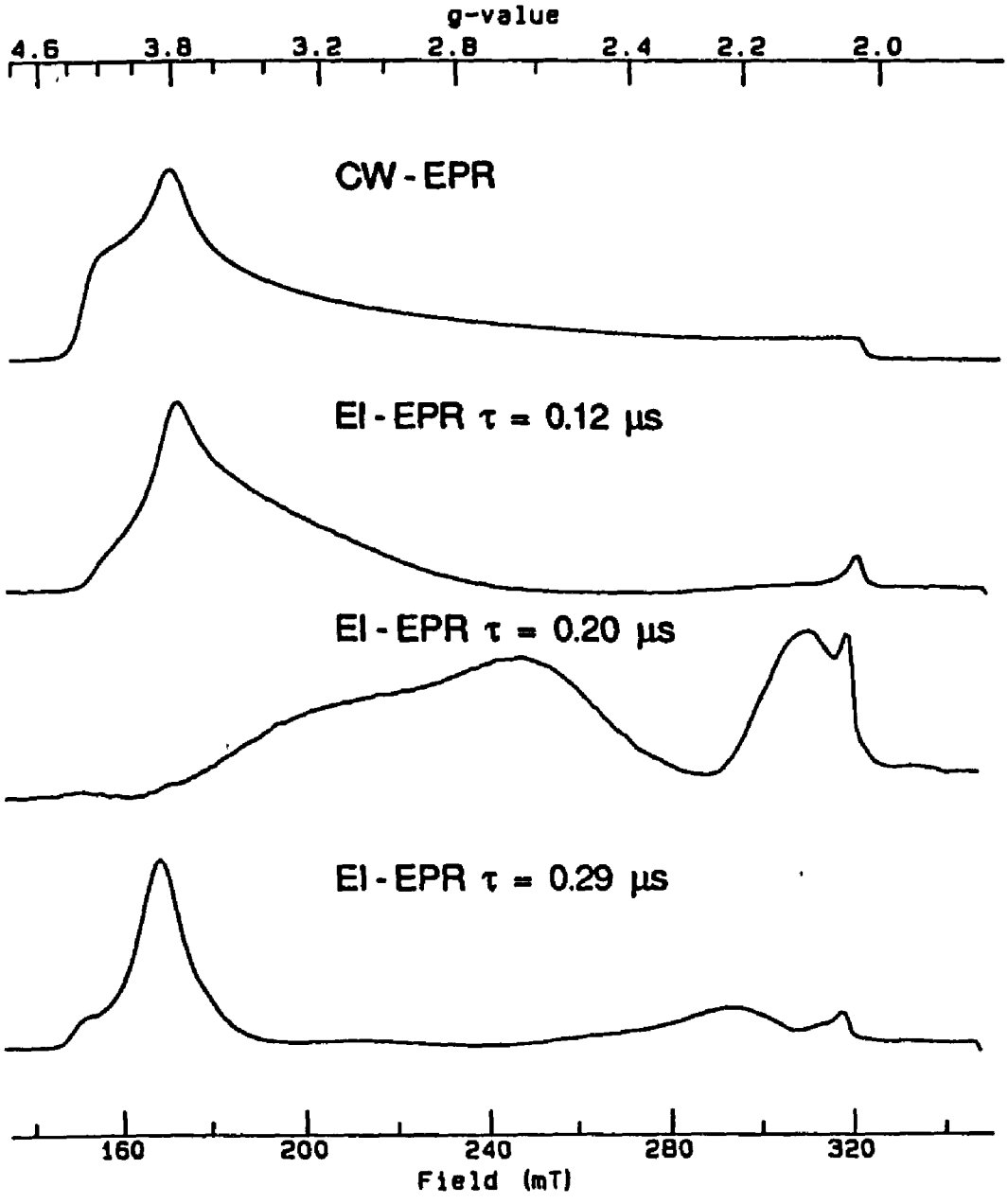
g-value
4.6
3.8
3.2
2.8
2.4
2.2
2.0
CW - EPR
EI - EPR τ = 0.12 μs
EI - EPR τ = 0.20 μs
EI - EPR τ = 0.29 μs
160
200
240
280
320
Field (mT)

Figure 6.2.3

hand, the technique does not allow the extraction of the hyperfine coupling and other interaction in a fashion similar to EPR. To extract these interactions, one needs to analyze the more informative ESEEM data.

3 ESEEM Studies

The ESEEM spectra of the MoFe protein with ^{96}Mo and ^{95}Mo enrichment at excitation frequencies of both 9 GHz and 10.7 GHz are shown in Figures 6.2.4 to 6.2.7. The g values at which these spectra were taken are 2.01, 2.54, 3.79, and 4.13. Except $g = 2.54$, they are very close to the principal apparent g values. The first thing to be noticed is the difference between the two sets of spectra. Additional peaks exist in the spectrum for ^{95}Mo spectrum. These peaks can be associated with the nuclear modulation effect due to ^{95}Mo. In order to isolate the differences, the method of waveform division was used. As discussed in Chapter 4, if the nuclear modulation effect is due to multiple nuclei magnetically coupled to the same paramagnetic center with negligible mutual interactions, then the time domain modulation is the product of those individual modulation functions. Because of this, the division of two sets of time domain modulation data taken at identical experimental conditions and with identical EPR spectra will reveal any difference between the two samples, but not their common features. Any peaks in the cosine Fourier transform of the division data with a phase of zero are associated with the numerator spectrum, ones with a phase of π, associated with the denominator spectrum Shown in Figure 6.2.8 are the time domain waveforms taken at 9 GHz and $g = 2.01$ for the ^{95}Mo enriched and ^{96}Mo enriched protein and the quotient from the division of the two waveforms. The corresponding cosine Fourier transform spectra are shown in Figure 6.2.9. The spectra from the quotient waveforms at other g values are shown in Figure 6.2.10. The presence of molybdenum is clearly

Figure 6.2.4 ESEEM spectra at 1.5 K for the ^{96}Mo enriched MoFe protein. The experimental conditions were: ν_e = 9.056 GHz; τ = 0.17 μsec, and $\pi/2$ pulse width, 0.03 μsec. Field settings and g values are (from the top): $g = 2.01$, $H = 3219$ gauss; $g = 2.54$, $H = 2548$ gauss; $g = 3.79$, $H = 1707$ gauss; and $g = 4.13$, $H = 1567$ gauss. Fourier transformation was facilitated by using the LPBE method.

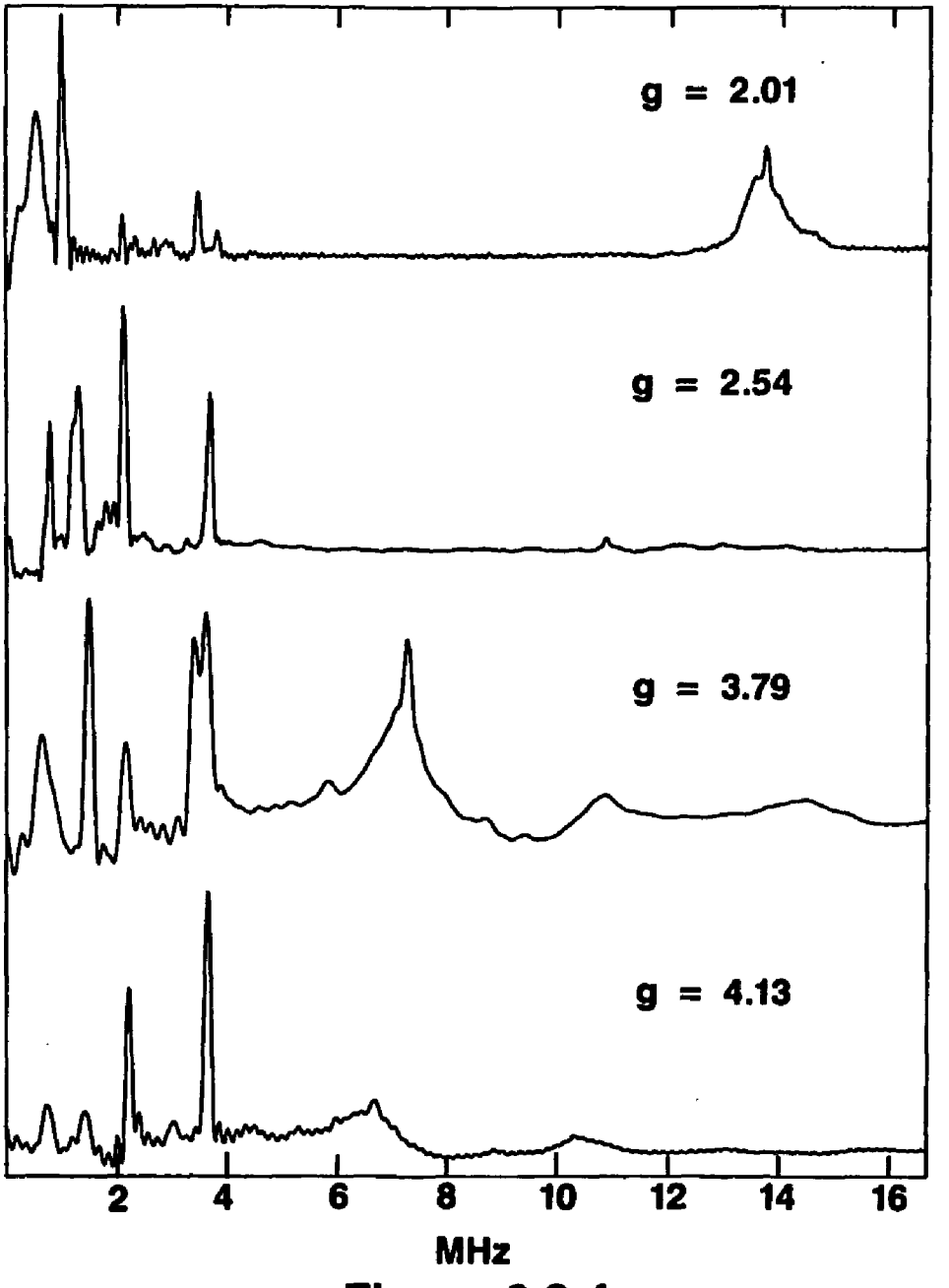

Figure 6.2.4

Figure 6.2.5 ESEEM spectra at 1.5 K for the ^{95}Mo enriched MoFe protein. The experimental conditions and data processing procedure are identical to those in Figure 6.2.4.

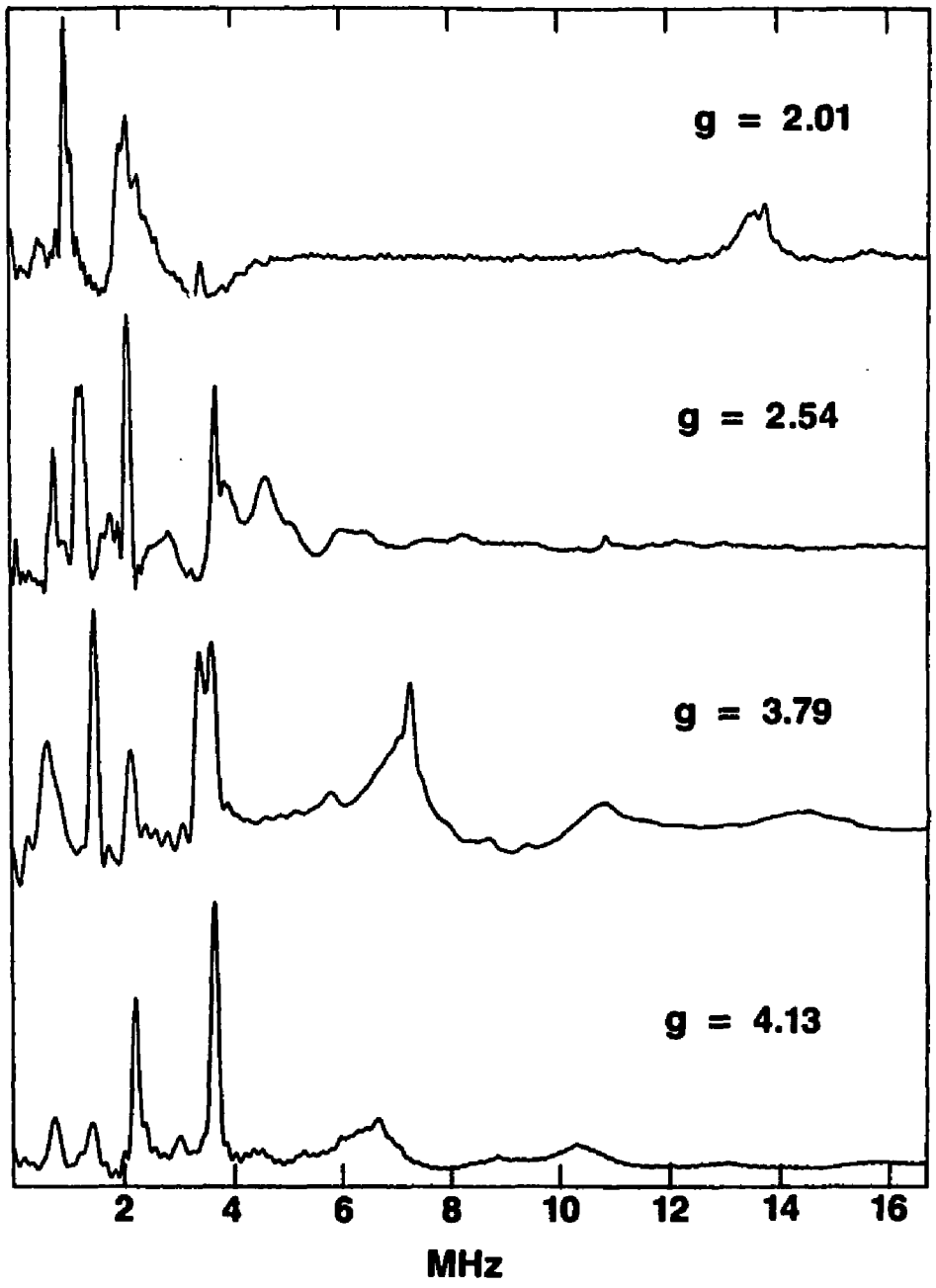

Figure 6.2.5

Figure 6.2.6 ESEEM spectra at 1.5 K for the ^{96}Mo enriched MoFe protein. Experimental conditions were: ν_e = 10.682 GHz; τ = 0.25 μsec, and $\pi/2$ pulse width, 0.03 μsec. Field settings and g values are (from the top): g = 2.01, H = 3797 gauss; g = 2.54, H = 3005 gauss; g = 3.79, H = 2014 gauss; and g = 4.13, H = 1847 gauss. The data processing procedure is the same as for Figure 6.2.4.

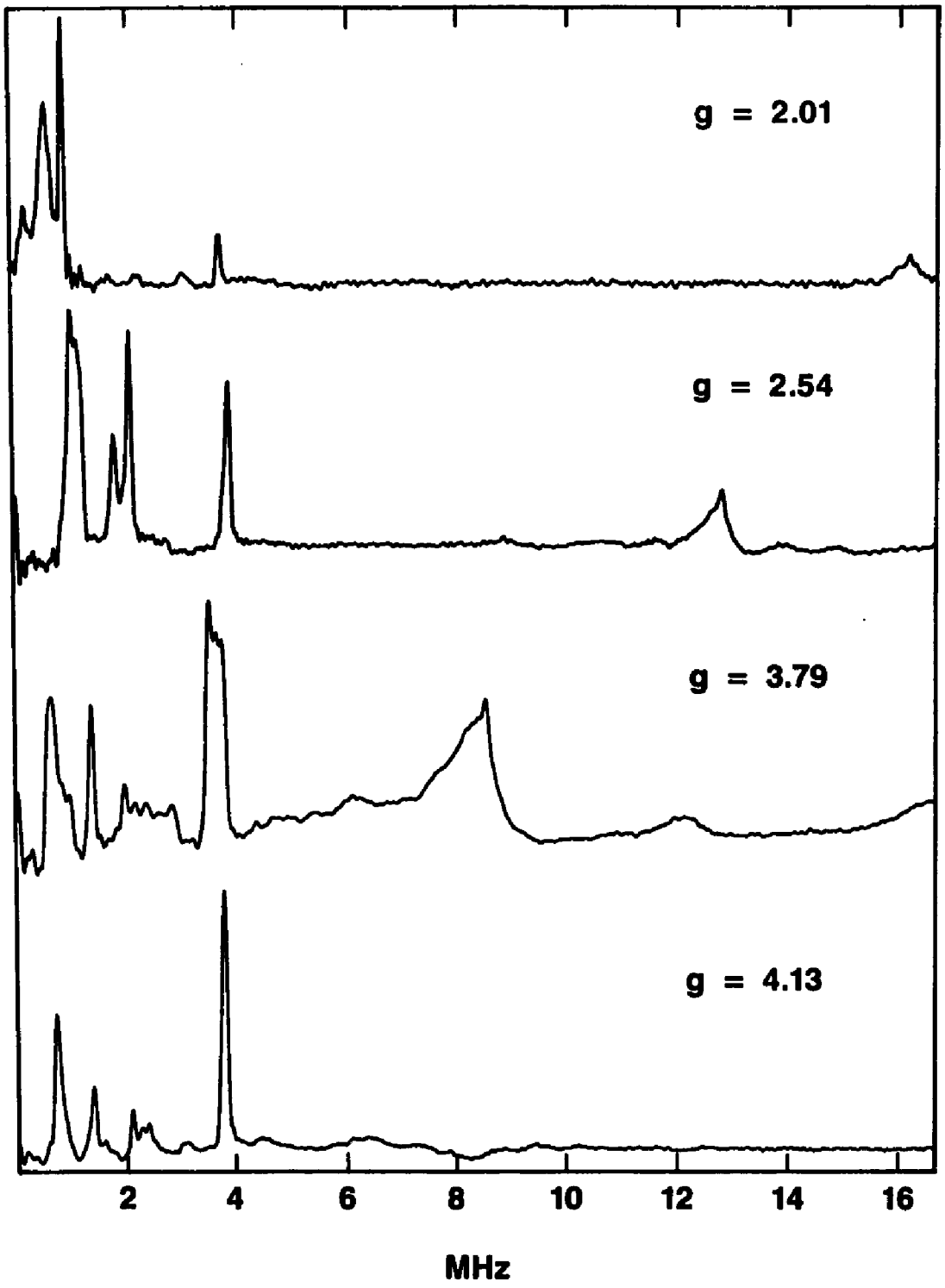

Figure 6.2.6

Figure 6.2.7 ESEEM spectra at 1.5 K for the ^{95}Mo enriched MoFe protein. The experimental conditions and data processing procedure are identical to those in Figure 6.2.6.

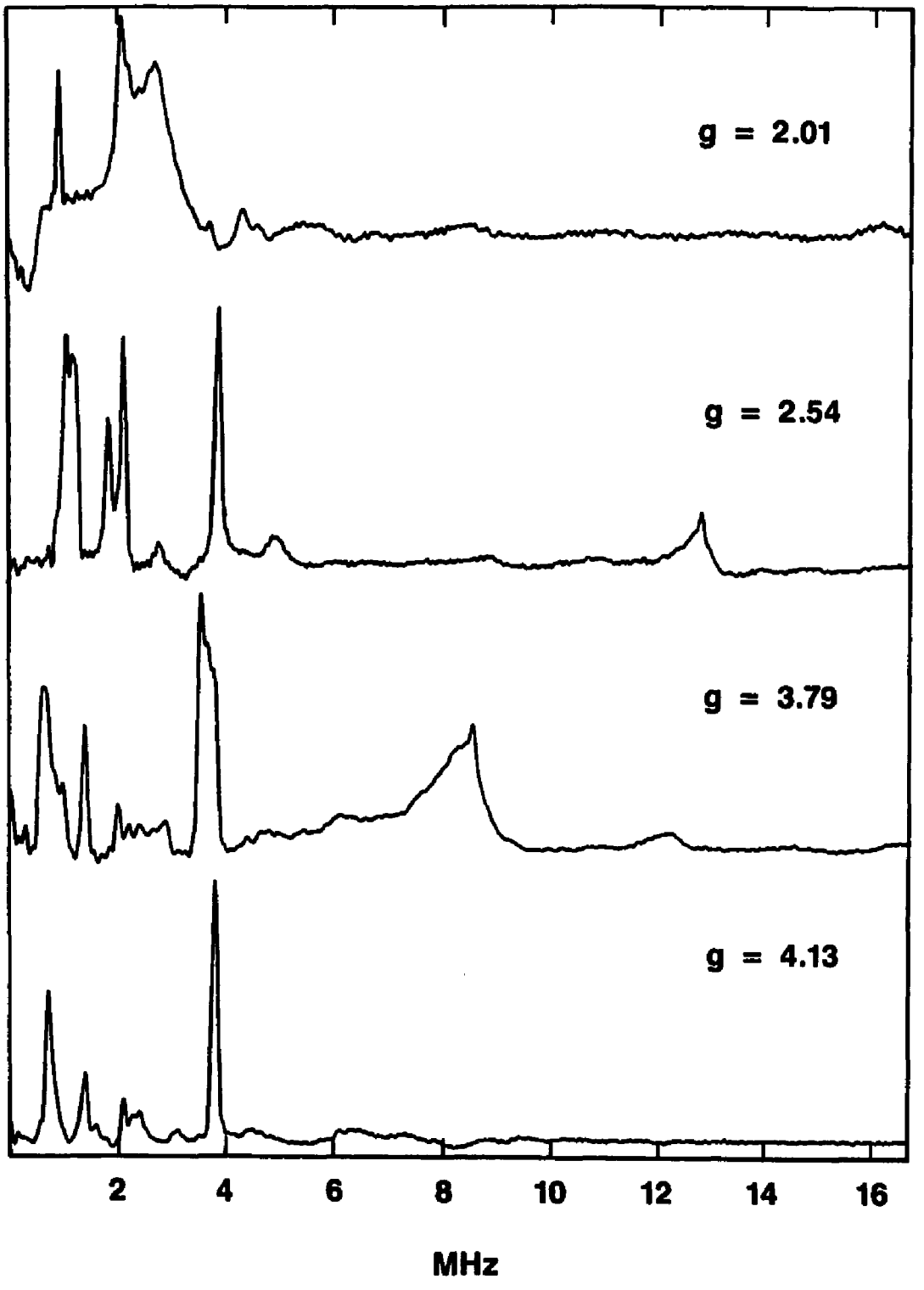

Figure 6.2.7

Figure 6.2.8 The time domain waveform at $g = 2.01$ for: (a) the ^{95}Mo enriched MoFe protein, and (b) the ^{96}Mo enriched MoFe protein. The quotient waveform of (a) over (b) is shown in (c). The experimental conditions are the same as in Figure 6.2.4 and 6.2.5. Data points from $\tau + T = 0.0$ to 0.34 μsec were back–extended using LPBE method. Baseline points are shown at the end of time–domain data.

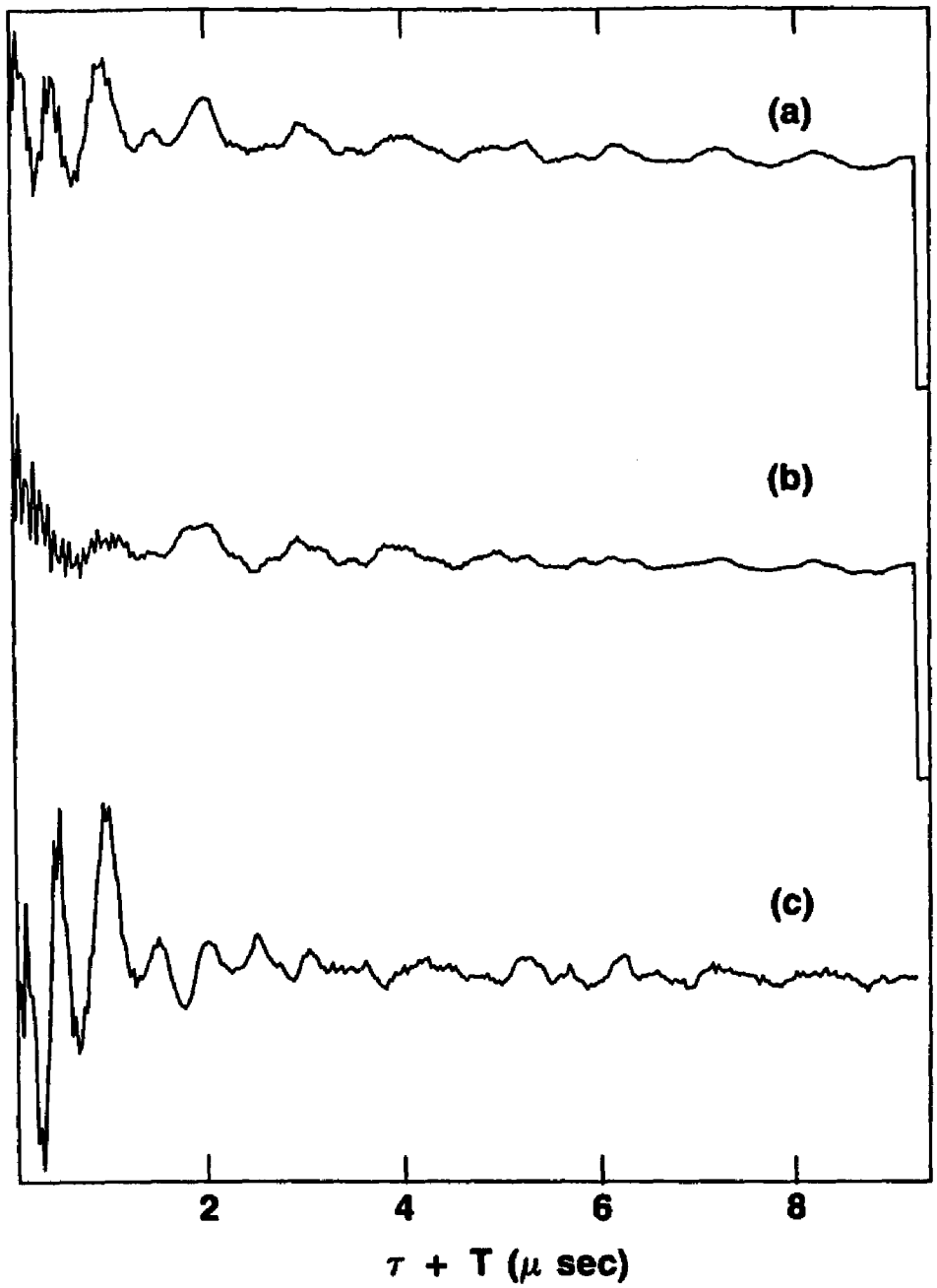

Figure 6.2.8

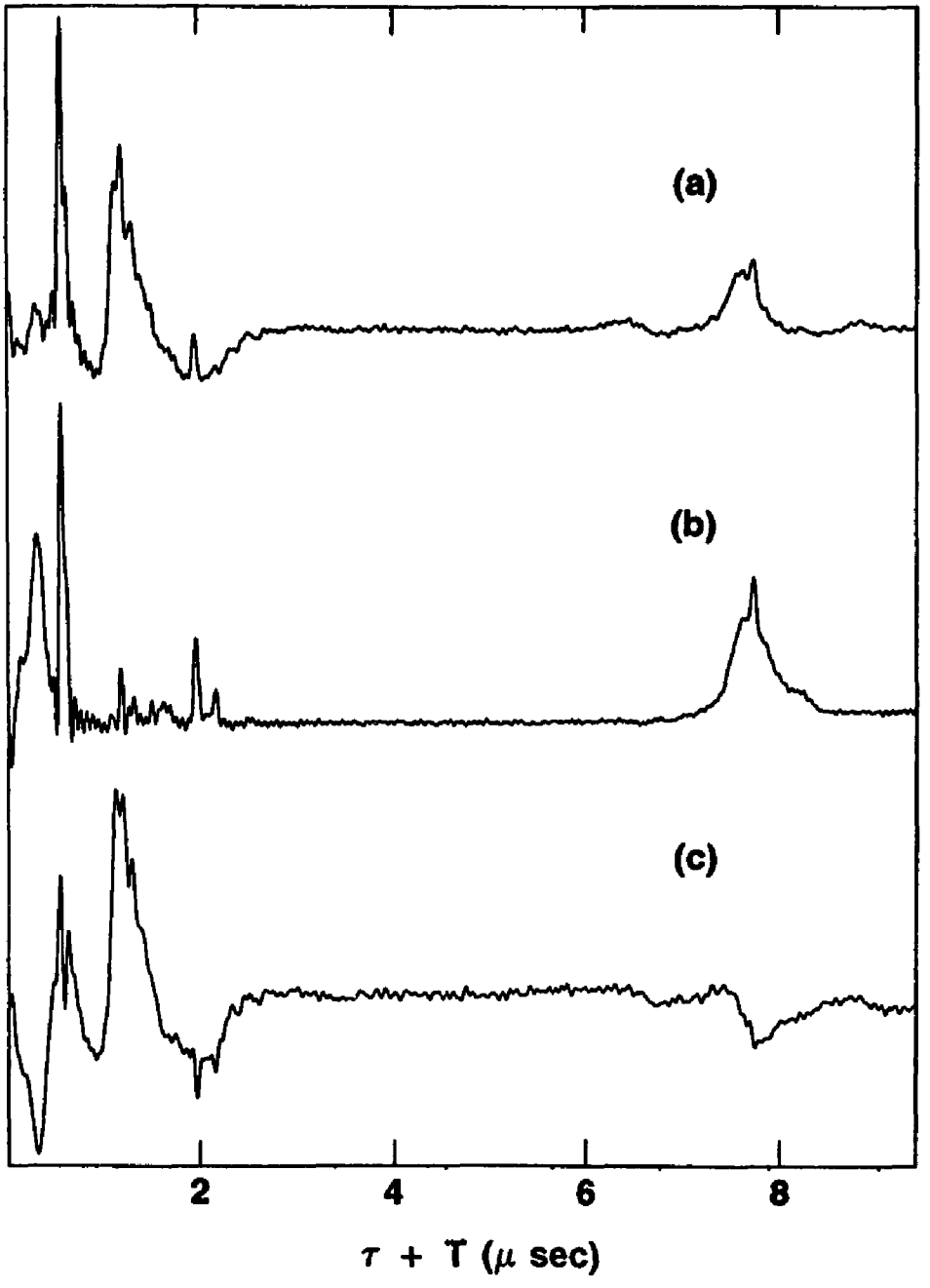

Figure 6.2.9 Fourier transform spectra for the time domain waveforms shown in Figure 6.2.8.

Figure 6.2.10 Fourier transform spectra for quotient waveforms obtained in the same way as in (c) in Figure 6.2.9. The experimental conditions are the same as in Figure 6.2.4 and 6.2.5, except in the middle spectrum: $g = 2.23$, and $H = 2901$ gauss.

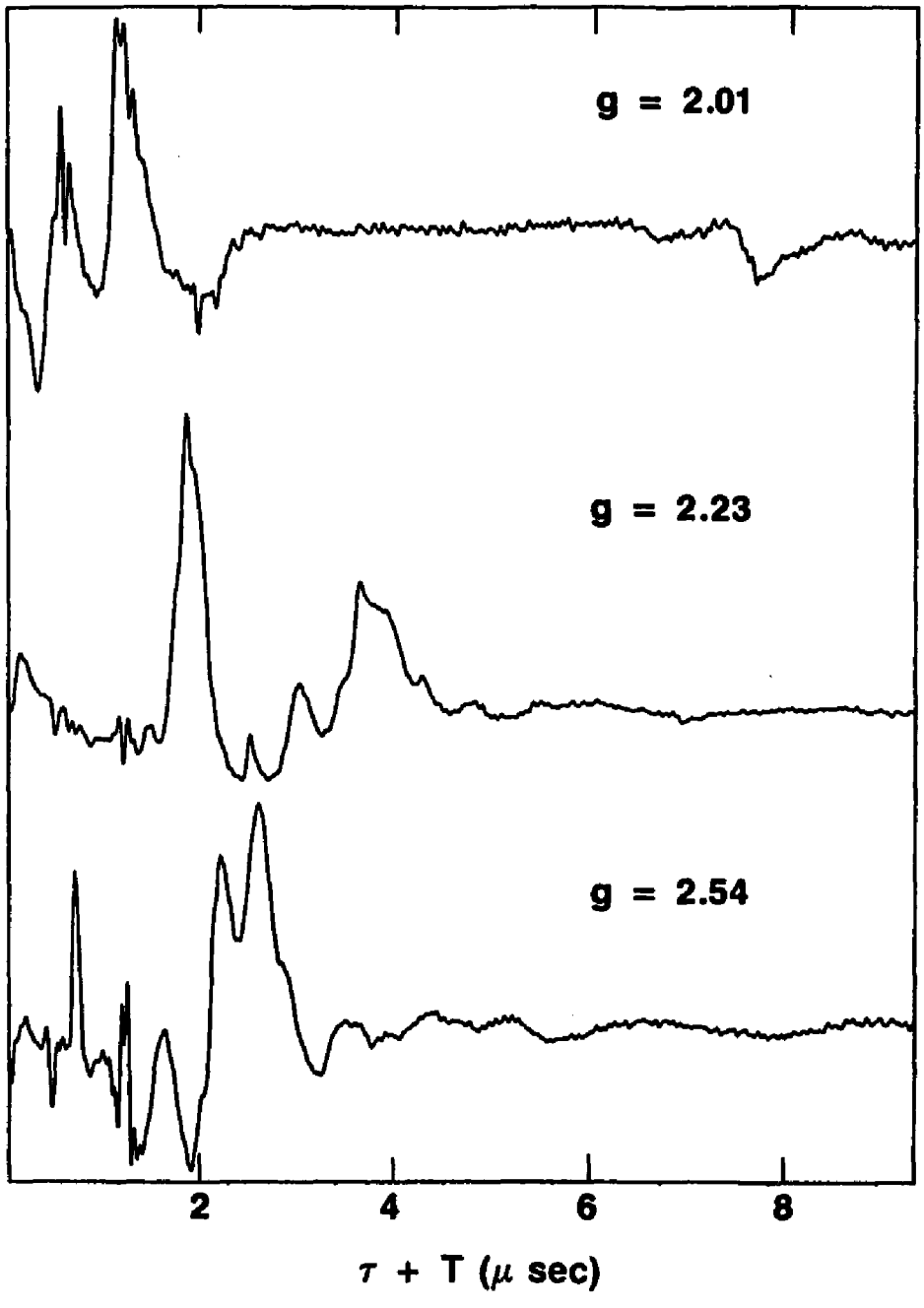

Figure 6.2.10

indicated by the multiple sharp peaks pointing upward. Efforts were made to simulate numerically the experimental spectra with the consideration of "orientational selective averaging". The preliminary simulation results indicated that the spectra can be assigned to a molybdenum with hyperfine coupling of about 5 MHz in the $S = 3/2$ spin coordinate system, and nuclear quadrupolar coupling e^2qQ/h of about 2.5 MHz.

Both spectra contain sharp modulation peaks ranging from about 0.5 MHz to about 4 MHz whose amplitudes are strongly field dependent. These frequencies were also observed in the spectra of the protein with natural isotopic abundance, which are closer to those with ^{96}Mo enrichment than with ^{95}Mo enrichment, as shown in Figure 6.2.11. Comparisons to ESEEM data taken at 5 K were also made in order to assign these frequencies. Inspection of the 5 K spectrum at $g = 3.70$ and 1.5 K spectrum at $g = 3.79$ has revealed that modulation frequencies are comparable to each other. Based on the previous discussion, these frequencies present in all forms of the protein have been attributed to nitrogen modulation. One interesting feature is that these modulation frequencies do not change significantly with g values changing from 2.01 to 4.13, while the modulation amplitudes change appreciably. The strong field dependence of these modulation amplitudes is the consequence of the "orientational selection" and the interplay of the nuclear Zeeman interaction, hyperfine interaction and the nuclear quadrupole interaction. Thorough analysis of these modulation patterns, with the consideration of "orientation selectivity", will provide information on the molecular level. From the analysis, which will be discussed in detail in Section 7.1, it is concluded the modulations can be assigned to at least one nitrogen atom.

Not only have these nitrogen modulations been observed for spectra for both ^{96}Mo and ^{95}Mo, but part of these modulations peaks have been observed in the transform spectra of quotient waveform from the division of ^{95}Mo over ^{96}Mo.

Figure 6.2.11 ESEEM spectra at 1.5 K for the native MoFe protein. The experimental conditions are the same as in Figure 6.2.4, except that $g = 2.23$, $H = 2901$ gauss for spectrum (a). The Fourier transformation was facilitated by the application of the LPBE method.

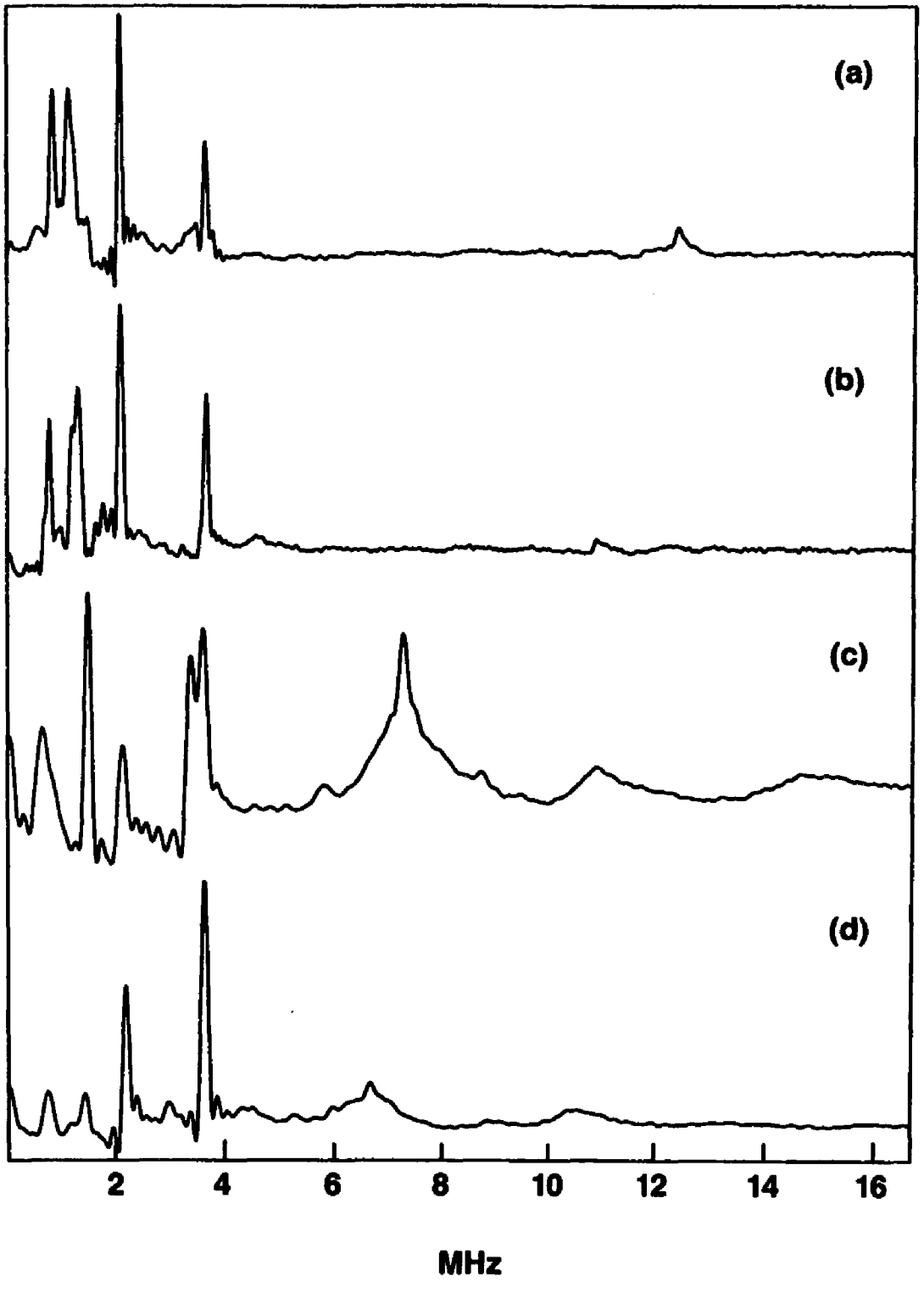

Figure 6.2.11

Because no frequency shifts, the presence of these modulations is the consequence of differences in the nitrogen modulation amplitude between the numerator and denominator spectra. To quantitate the differences, the time domain data of both ^{95}Mo and ^{96}Mo enriched proteins have been normalized against the echo amplitude at zero time prior to being Fourier transformed. If we measure the difference in modulation frequency amplitudes between the two Mo enriched proteins by the percentage deviation (defined as $|(A-B)/(A+B)|$) it can be as large as 100%. Table 6.2.1 lists nitrogen modulation amplitudes measured from transform spectra of normalized time–domain data for both proteins and the corresponding percentage deviations.

In Figures 6.2.4 and 6.2.5, some frequencies are peaked at twice of the proton Larmor frequency, and some around the proton Larmor frequency. And these peaks were observed to shift with the proton Larmor frequency. These are the so–called "combination frequencies" arising from the couplings of the nitrogen and proton(s) to the same paramagnetic ion, or from the couplings of multiple protons to the same paramagnetic ion. Given that no knowledge about the distribution of protons surrounding the FeMoco is present, no attempt has been made to characterize these protons. However, it is conceivable that the "combination frequencies" could be due to protons on the nitrogen ligand.

On the other hand, no combination between the nitrogen modulation frequencies were found other than those assignable to the nitrogen or molybdenum. If multiple nitrogens exist and couple to the same paramagnetic center, "combination frequencies" are expected to arise due to the deep modulation depth observed. The absence suggests that only one nitrogen is needed to account for those frequencies with pronounced amplitudes. Also, no combination between ^{95}Mo modulation or between ^{95}Mo and ^{14}N modulation frequencies was detected. The first part is expected since there is only one molybdenum present in the FeMoco,

and the second part is compatible with the explanation that the nitrogen is ligated to the molybdenum, rather than to the rest of the FeMoco.

TABLE 6.2.1 Table of Relative Change of the Normalised Amplitudes of ^{14}N Modulation Frequencies Due to Molybdenum Isotopic Enrichments in the MoFe Protein

	9 GHz			10.7 GHz		
		$g = 2.01$			$g = 2.01$	
f(MHz)	0.57	1.07	3.46	0.65	0.95	3.75
Amp. (^{95}Mo)	2.51	4.43	0.93	1.27	3.56	0.56
Amp. (^{96}Mo)	5.15	6.15	1.75	4.72	7.21	1.07
Δ (%)	−69	−33	−61	−100	−68	−63
		$g = 2.54$			$g = 2.54$	
f(MHz)	0.78	1.30	2.10	1.06	1.21	2.11
Amp. (^{95}Mo)	6.56	9.64	12.30	3.88	4.51	4.38
Amp. (^{96}Mo)	6.32	7.49	9.85	9.45	9.09	8.27
Δ (%)	−4	25	22	−84	−67	−62

1. Δ is defined as $\frac{\text{Amp.}(^{95}\text{Mo}) - \text{Amp.}(^{96}\text{Mo})}{\text{Amp.}(^{95}\text{Mo}) + \text{Amp.}(^{96}\text{Mo})}$, where Amp.(^{96}Mo) or Amp. (^{95}Mo) is the normalized amplitude at the indicated ^{14}N frequency in the ESEEM spectrum of the MoFe protein isotopically enriched with ^{96}Mo or ^{95}Mo.

2. Prior to being Fourier transformed, time–domain data were normalized against the echo amplitude at $\tau + T = 0$, which was obtained by LPBE.

3. Experimental conditions: T = 1.5 K; at the indicated microwave frequencies and g values; obtained with the stimulated echo sequence: τ =0.17 μsec for the 9 GHz data; τ = 0.25 μsec for the 10.7 GHz data.

4. Only those frequencies which are present in the quotient spectra are listed in the table.

Chapter 7

DISCUSSION

The numerical simulations of nitrogen modulation spectra at 1.5 K will be described in Section 1. Based on the simulations and on recent genetic studies on the MoFe protein, an origin for the nitrogen modulation is postulated. The implication of the dependence of nitrogen modulation amplitudes on molybdenum isotopes will be discussed.

I. Numerical Simulation

Numerical simulations, based on the method described in Chapter 3, were carried out on CRAY XMP/14se, DEC VAX 8350, and VAX 750 computers, and were optimized by least–square minimization performed on the calculated envelope functions in order to find the best fit to the experimental spectra.

To reduce computing time, a multi–step approach has been taken. First, the input range is set to cover all possible parameter variations which can fit the input spectrum. This may not be necessary, if clues can be found about the best–fit parameters, using the spherical average method as discussed in Section 3.5. Ranges of variation for orientation parameters will be discussed later in this section. Then, calculations are made within the specified range, though usually without pseudodipolar coupling terms. In analyzing ^{14}N modulations, the pseudodipolar coupling is usually the smallest of all, and only small errors are expected when it is neglected (compared to other coupling terms), also parameters describing other

couplings can be better defined. The output, from the first minimization, is examined to give a reduced parameter range. The second minimization can be performed within the newer parameter range plus that for the pseudodipolar couplings. If input parameter ranges are properly set, this calculation should yield the best–fit parameters for the input spectrum. Refinements to the obtained parameters can be achieved by choices of finer parameter resolutions. The obtained parameter set are compared with their similarly extracted counterparts for other spectra. Often, further simulations are needed for visual examinations, or to verify the uniqueness of the parameter set, so that fits for all spectra of the same sample, at different field values, microwave frequencies or τ values, can be simulated with the same set of parameters.

The ranges over which orientational parameters may vary will be first considered. There are two sets: α, β and γ for the NQI, and θ_N,and φ_N for the pseudodipolar coupling, all with respect to the PAS of g–tensor. From Appendix 1, it is known that $0 \leq \alpha \leq 360^\circ$, $0 \leq \beta \leq 180^\circ$, and $0 \leq \gamma \leq 360^\circ$. But there is no one to one correspondence for all three parameters. For example, if $\beta = 0$, $\alpha + \gamma = \alpha' + \gamma'$. If α and β are viewed as the polar and azimuthal angles in a spherical coordinates, the range specified for these two parameters should cover all possible orientations. To reduce the number of parameters, γ has been set to 0 (although it is not difficult to include it as a simulation parameter). Therefore, the number of variable parameters used for simulations is eight: Q_{zz}, η, α, β, A_{iso}, r_{eff}, θ_N and φ_N.

Since the spin operators in NQI are all in squared forms, one might wonder if the ranges for α and β can be reduced. To answer this, tests have been performed with the simulation software, results are shown in Figure 7.1.1 to 7.1.2. In Figure 7.1.1, principal g values were those of the MoFe protein; microwave frequency ν_e= 9.056 GHz; $g = 2.01$; Q_{zz}/h and η were set to 0.5 MHz, 0.8 respectively; $A_{iso} = 0.7$ MHz as defined in Equation 3.1.10; r_{eff}, θ_N, and φ_N were 2.2 Å, 45°, and 60°,

Figure 7.1.1 Simulated spectra at $g = 2.01$ and $\nu_e = 9.056$ GHz using PSU_OS2. The principal g values are $g_1 = 4.28$, $g_2 = 3.79$, and $g_3 = 2.01$. The simulation parameters for the ^{14}N nucleus are: Q_{zz}/h ($e^2qQ/4h$) = 0.5 MHz, $\eta = 0.5$, $\gamma = 0$; $A_{iso} = 0.7$ MHz (as defined in Eq. 3.1.10); $r_{eff} = 2.2$ Å, $\theta_n = 45^\circ$, and $\varphi_n = 60$. α and β are: (a) 60°, 15°; (b) 60°, 165°; (c) 120°, 15°; (d) 120°, 165°; (e) 60°, 195°; (f) 60°, 345°; (g) 120°, 195°; and (h) 120°, 345°.

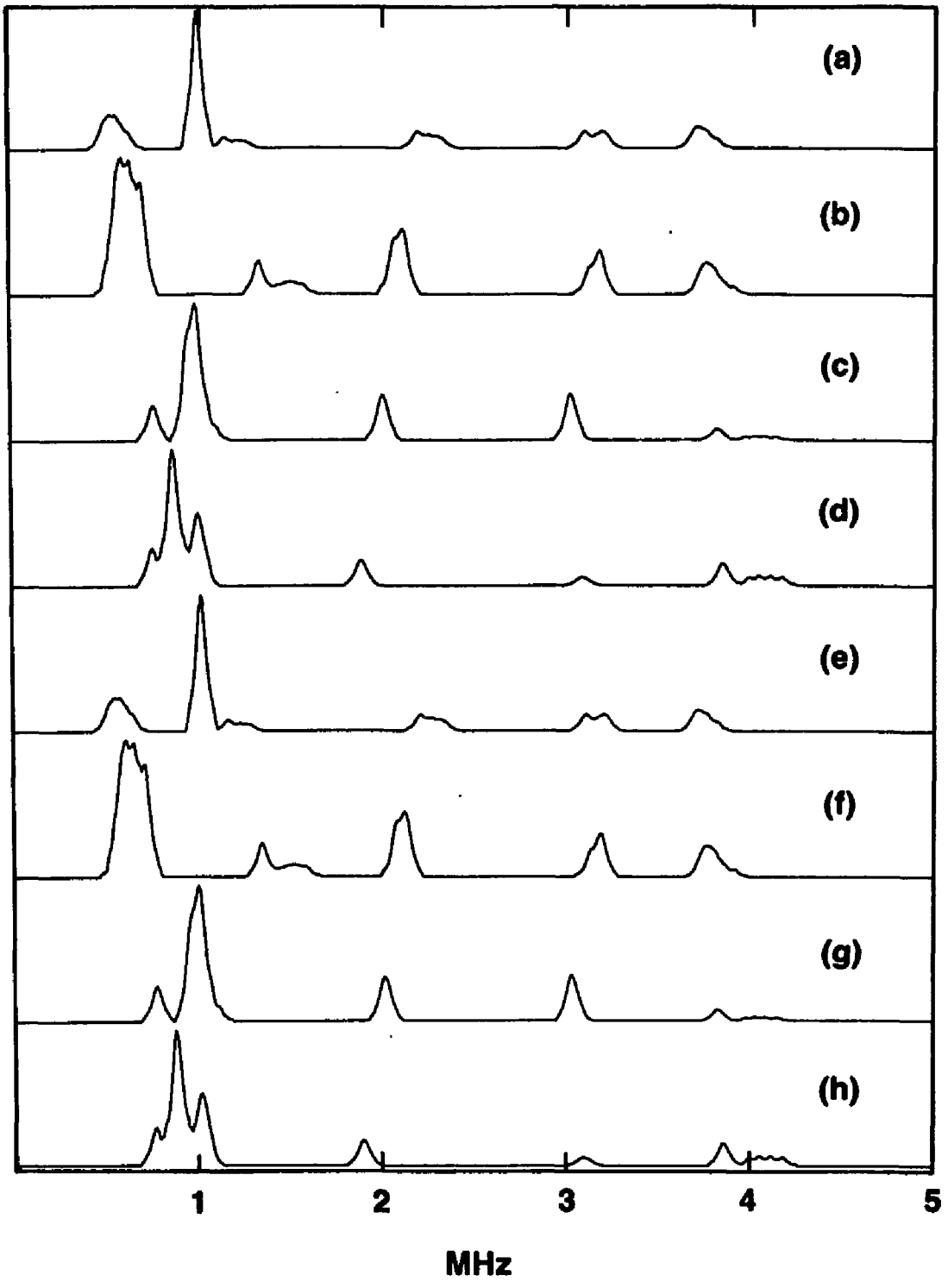

Figure 7.1.1

Figure 7.1.2 Simulated spectra at $g = 2.54$ and $\nu_e = 9.056$ GHz using PSU_OS2. The principal g values are listed in Figure 7.1.1. The simulation parameters for the ^{14}N nucleus are: $g_1 = 4.28$, $g_2 = 3.79$, $g_3 = 2.01$; $Q_{zz}/h = 0.5$ MHz, $\eta = 0.65$, $\gamma = 0$; $A_{iso} = -0.7$ MHz (as defined in Eq. 3.1.10); $r_{eff} = 2.2$ Å, $\theta_n = 35°$, and $\varphi_n = 50°$. α and β are: (a) 40°, 20°; (b) 40°, 160°; (c) 140°, 20°; (d) 140°, 160°; (e) 40°, 200°; (f) 40°, 340°; (g) 140°, 200°; and (h) 140°, 340°.

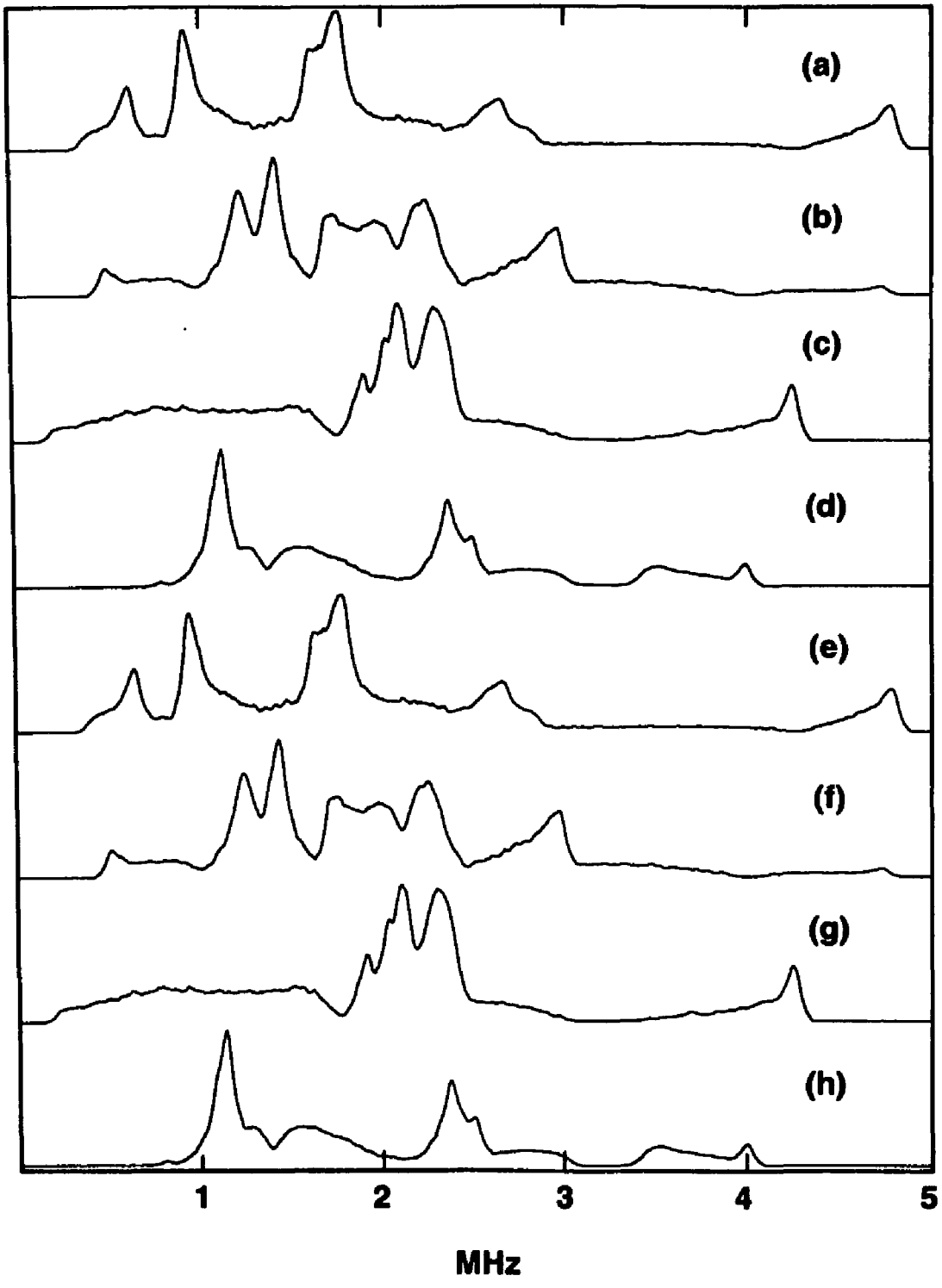

Figure 7.1.2

respectively. α and β were set to 60° and 15°, as well as their variations in all other quadrants (i.e. $180^\circ - \alpha$, $180^\circ + \alpha$ and $360^\circ - \alpha$; and $180^\circ - \beta$). It is clear that the spectra in the second half of the figure are identical to those in the first half. In other words, without introducing errors, the variation range of α is from 0 to 180° (or from -90° to 90°), that of β, from 0 to 180°. The same conclusions can be reached by examining Figure 7.1.2. There, the inputs are: $g = 2.54$; (Q_{zz}/h, η) are (0.50 MHz, 0.65); $A_{iso} = -0.6$ MHz; r_{eff}, θ_N and φ_N are 2.2 Å, 35° and 50°. $\alpha = 40^\circ$, $\beta = 20^\circ$ and their variations similar to those in Figure 7.1.1 was used. As for θ_N and φ_N, the orientation parameters for the pseudodipolar coupling, similar tests have been performed. A typical comparison is shown in Figure 7.1.3. The conditions for Figure 7.1.2 were used, except that α and β were fixed at 60° and 15°. θ_N and φ_N were varied in a similar fashion as described for Figure 7.1.1, with $\theta_N = 45^\circ$ and $\varphi_N = 60^\circ$ in the first quadrant. The conclusion is: $0 \leq \theta_N < 180^\circ$ and $0 \leq \varphi_N < 180^\circ$. From these tests, the ranges of parameter variations have been cut by a factor of 4.

As discussed in the last chapter, modulations due to nitrogen have been observed for the M–center. An important feature of the results is that the modulation frequencies change very little when the g value is varied from 2.01 to 4.13, (i.e., the nuclear Zeeman coupling is decreased by a factor of 2). Obviously, this result is difficult to explain in terms of the "cancellation effect". Furthermore, the other responsible party of the "cancellation effect", isotropic hyperfine coupling, is changing in the opposite direction. From Equations 3.1.9 and 3.1.10, the "apparent" hyperfine coupling in the effective spin coordinates ($S = 1/2$) is proportional to the effective g value, which is increasing. The fact that the observed frequencies change little suggests that the nuclear quadrupole interaction is the dominant coupling, being larger than any other individual terms.

Simulation–fitting was performed in frequency domain for data obtained at

Figure 7.1.3 Simulated spectra at $g = 2.54$ and $\nu_e = 9.056$ GHz using PSU_OS2. The simulation parameters are the same as in Figure 7.1.2, except following: $\alpha = 40^\circ$, $\beta = 20^\circ$; and θ_n and φ_n values are: (a) 35°, 50°; (b) 35°, 130°; (c) 145°, 50°; (d) 145°, 130°; (e) 35°, 230°; (f) 35°, 310°; (g) 145°, 230°; and (h) 145°, 310°.

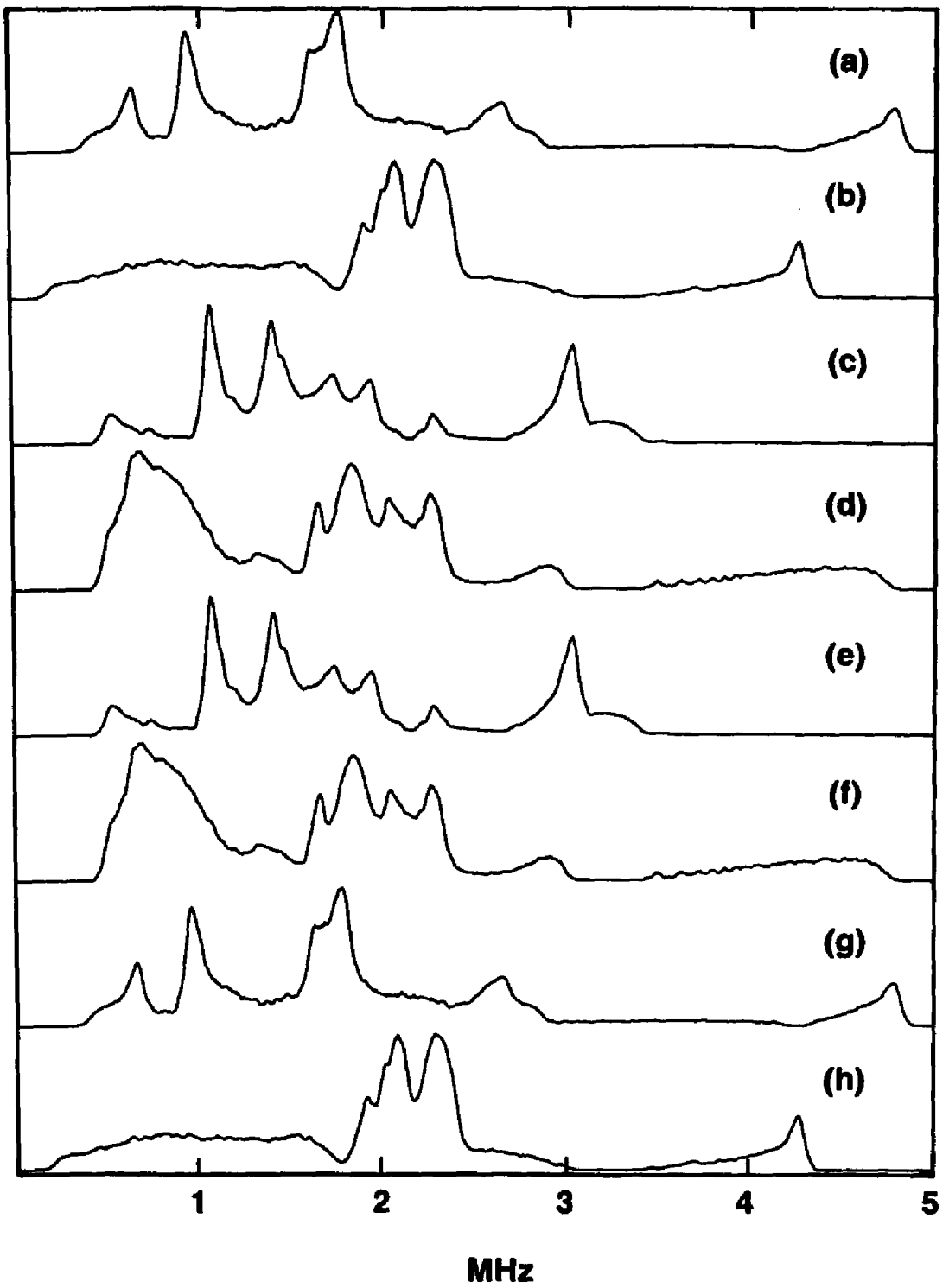

Figure 7.1.3

both 9 GHz and 10.7 GHz. The results from simulations are tabulated in Table 7.1.1. A typical comparison of the fit and data are shown in Figure 7.1.4. The spectrum represents Fourier transform of the data at 9 GHz, $g = 2.01$ and $\tau = 0.17$ μsec. The comparison at 10.7 GHz, $\tau = 0.25$ μsec and at the same g value is shown in Figure 7.1.5. The simulation was generated with the same input parameters as that of Figure 7.1.4. Inspection of Table 7.1.1 has revealed that although different values may be determined for a given parameter at different experimental conditions, there is a very limited range within which the determined values fluctuate. For example, Q_{zz}/h varies from 0.5 to 0.52 MHz; η varies from 0.55 to 0.7, though 0.65 is the most frequent. If the variations are considered fluctuations around a mean value, the accuracy of the fit can be defined. The mean values, defined this way, for the simulation parameters are: $Q_{zz}/h = 0.51 \pm 0.01$ MHz ($e^2qQ/h = 2.04 \pm 0.04$ MHz); $\eta = 0.63 \pm 0.8$; $\alpha = 0$; $\beta = 5^\circ \pm 5^\circ$; $\gamma = 0$ (not examined); $A_{iso} = -0.375 \pm 0.025$ MHz (as defined in Equation 3.1.10, i.e. the isotropic hyperfine coupling constant in the $\tilde{S} = 3/2$ coordinate system is -0.75 MHz); $r_{eff} = 2.3 \pm 0.1$ Å; $\theta_N = 105^\circ \pm 15^\circ$; and $\varphi_N = 142^\circ \pm 8^\circ$. The accuracy of α is no larger than 5°, which is the smallest division in α used.

The negative sign of A_{iso} is difficult to explain in terms of Equation 3.1.5, this would mean an existence of negative spin densities. A negative isotropic hyperfine coupling has been observed for the proton of a C–H fragment in the malonic acid radical,[38] and confirmed both by molecular orbital calculations and proton NMR experiments.[39,40] When multiple electrons are present, Equation 3.1.5 can be written as $Q\,\rho$, where Q is a proportionality constant, ρ is the net spin density at the nucleus. The negative isotropic hyperfine term has been interpreted as the presence of electron spin at the nucleus opposite to that of the system. They originate from the slight unpairing of bonding electrons affected by the spin (a good discussion can be found in Chapter 6 of reference 41). If the concept is applied to

TABLE 7.1.1 The Best–Match Simulation Parameters
for the ^{14}N Modulation in ^{96}Mo Isotopically Enriched MoFe Protein

ν_e	9 GHz				10.7 GHz		
g	2.01	2.54	3.79	4.13	2.01	3.79	4.13
Q_{zz}/h (MHz)	0.52	0.5	0.5	0.5	0.52	0.5	0.5
η	0.7	0.55	0.65	0.65	0.7	0.65	0.65
α (degree)	0.	0.	0.	0.	0.	0.	0.
β (degree)	10.	0.	0.	0.	10.	0.	0.
A_{iso} (MHz)	–0.4	–0.4	–0.375	–0.4	–0.4	–0.35	–0.4
r_{eff} (Å)	2.3	2.2	2.4	2.4	2.3	2.4	2.4
θ_n (degree)	90.	100.	120.	125.	90.	125.	125.
φ_n (degree)	150.	135.	150.	150.	150.	150.	150.

1. These parameters are the outputs of the program PSU_OS2. γ has been set to 0.
2. Experimental conditions: T = 1.5 K; τ of the stimulated echo sequence: 0.17 μsec for the 9 GHz data, 0.25 μsec for the 10.7 GHz data. Other conditions can be found in Figures 6.2.4 and 6.2.6.
3. No satisfactory fit was obtained for the data taken at $\nu_e = 10.7$ GHz and $g = 2.54$.
4. A_{iso} is defined in Equation 3.1.10.

Figure 7.1.4 Comparison of (a) the experimental and (b) simulated spectra at $g = 2.01$ and $\nu_e = 9.056$ GHz. The experimental conditions are listed in Figure 6.2.4. The simulation input for the ^{14}N nucleus are: $Q_{zz}/h = 0.5$ MHz, $\eta = 0.7$, $\alpha = 0^\circ$, $\beta = 10^\circ$, $\gamma = 0^\circ$; $A_{iso} = -0.4$ MHz (as defined in Eq. 3.1.10); $r_{eff} = 2.3$ Å, $\theta_n = 90^\circ$, and $\varphi_n = 150^\circ$. The principal g values are listed in Figure 7.1.2

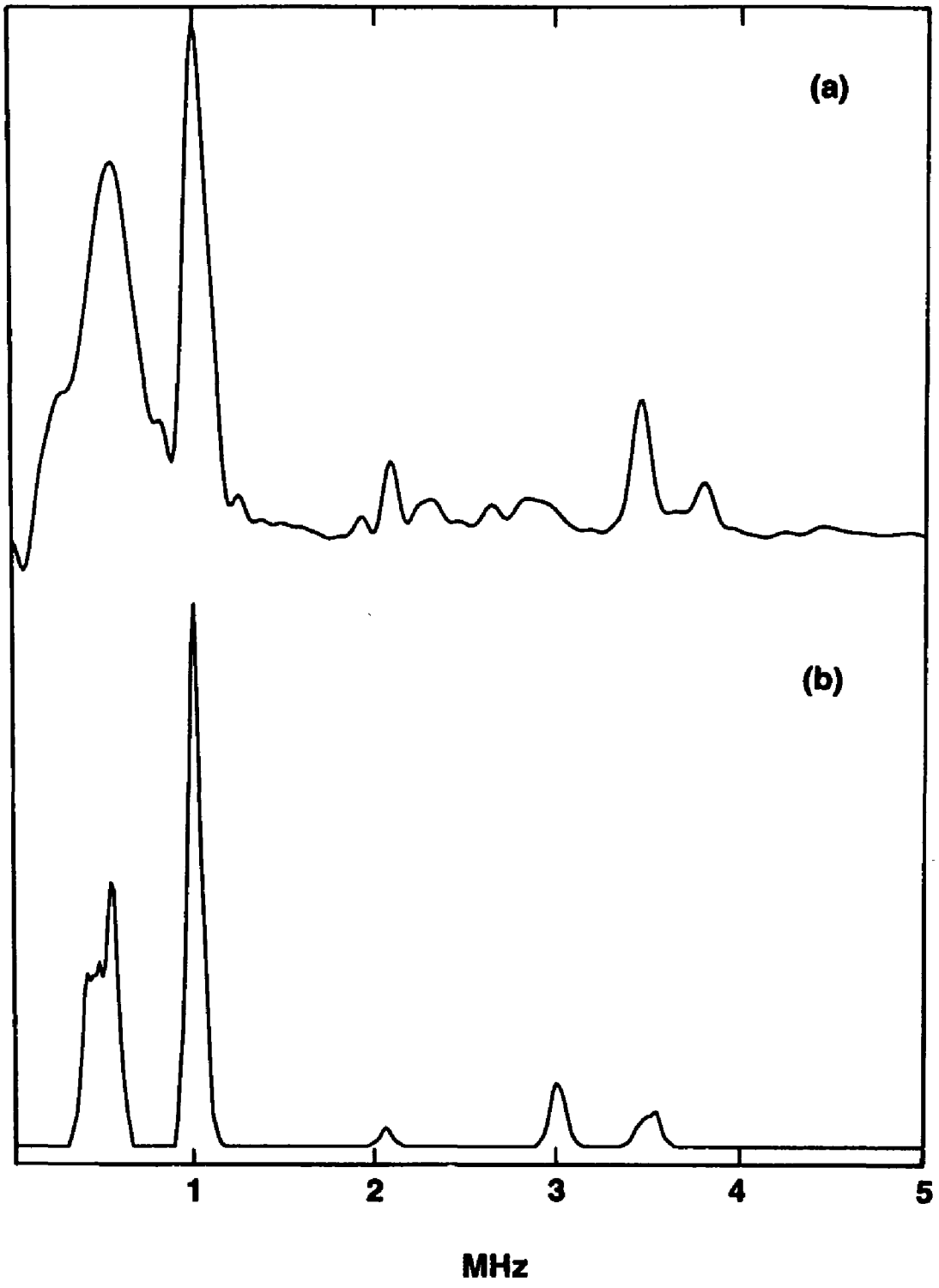

Figure 7.1.4

Figure 7.1.5 Comparison of (a) the experimental and (b) simulated spectra at $g = 2.01$ and $\nu_e = 10.682$ GHz. The experimental conditions are listed in Figure 6.2.6. Other simulation input parameters are identical to those in Figure 7.1.4.

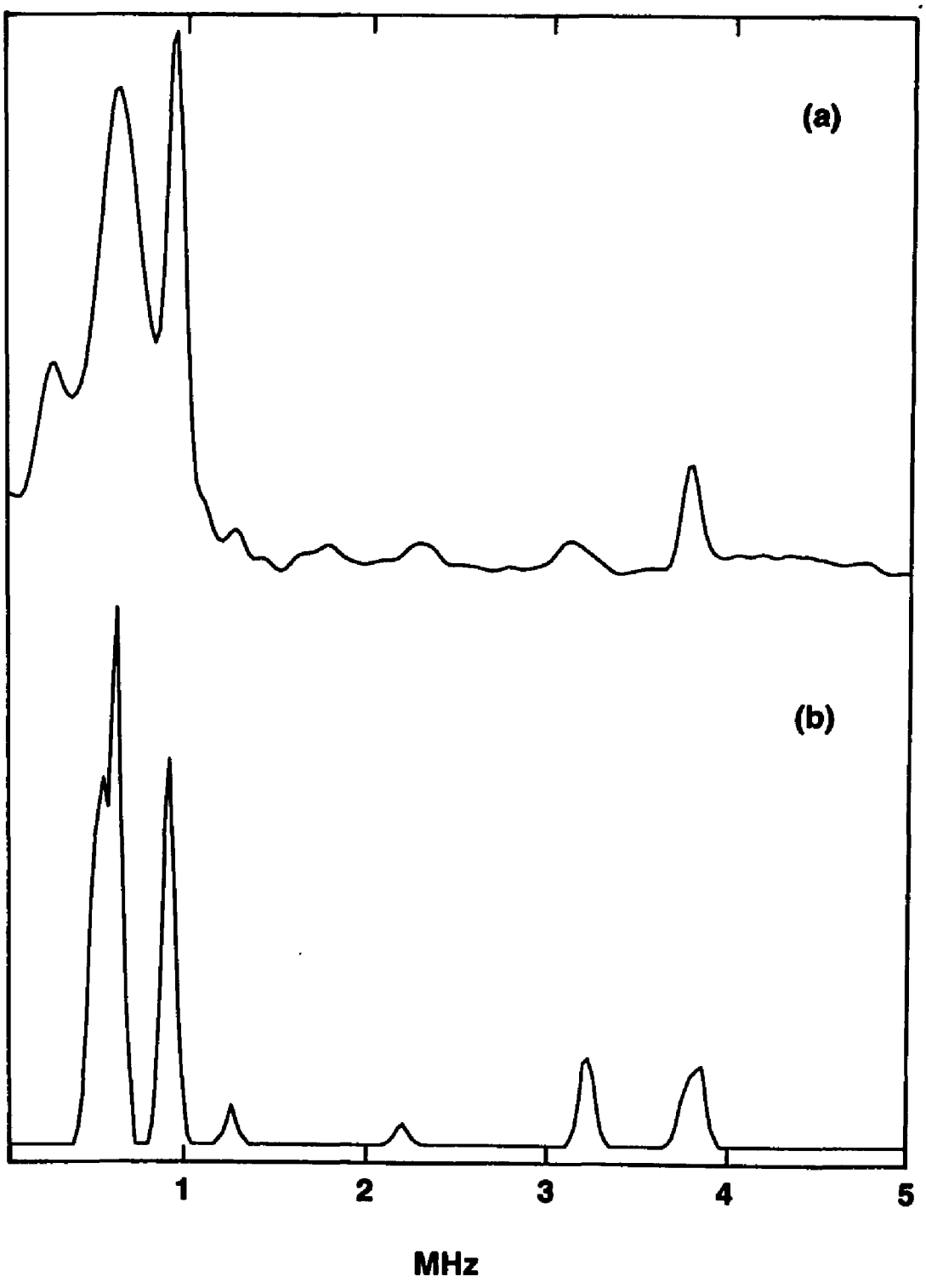

Figure 7.1.5

the present case, the negative isotropic hyperfine term can be interpreted as evidence for a nitrogen ligation to the FeMoco. And because of the ligation, electrons with spin directions opposite to those of paramagnetic electrons are present at the nitrogen nucleus. But Equation 3.1.10 contains the g–tensor. It can not be ruled out that the negative A_{iso} is attributable to the sign of the g–tensor elements, therefore the direction of axes in the PAS of the the g–tensor. It is worth noting that because of the inherent ambiguity about the axes direction in the PAS of the g–tensor, caution should be exercised when interpreting orientational parameters.

As remarked in Table 7.1.1, no satisfactory fit was obtained for the spectrum taken at g = 2.54 and at 10.5 GHz. The peaks at 2.0 and 2.2 MHz were not properly represented in the simulation, as shown in Figure 7.1.6. An exhaustive effort has been made in the parameter range of 0.4 to 0.6 MHz for Q_{zz}/h, 0.05 to 0.95 for η, 1.8 to 2.8 Å for r_{eff}, and – 1.0 to 1.0 MHz for A_{iso} (as defined in Equation 3.1.10), as well as finer resolutions around the mean values listed above. No better fit than that presented in Figure 7.1.6 was obtained. In addition, frequencies in other spectra were generally well simulated, but relative amplitudes and linewidths, were not always correctly represented. It is true that ESEEM spectra may be modified by the presence of the "dead time",[42] but sharp frequency peaks in a transform spectrum (as observed for all protein data) correspond to a sustained time–domain signal with little decay, and the much smaller "dead time" will not be a serious problem. A better explanation for the difference may be the limitations of the current model: a full hyperfine tensor may be needed, instead of an approximation by A_{iso} and a point–dipolar coupling.

As remarked in Chapter 3, the analysis is not limited to systems containing an $I = 1$ nuclear spin. The least–square minimization is not necessary the best way to achieve fits. An overall match of modulation peaks is not guaranteed, since the

Figure 7.1.6 Comparison of (a) the experimental and (b) simulated spectra at $g = 2.54$ and $\nu_e = 10.682$ GHz. The experimental conditions are listed in Figure 6.2.6. The simulation input for ^{14}N nucleus were: $Q_{zz}/h = 0.51$ MHz, $\eta = 0.63$, $\alpha = 0^\circ$, $\beta = 5^\circ$, $\gamma = 0^\circ$; $A_{iso} = -0.38$ MHz (as defined in Eq. 3.1.10); $r_{eff} = 2.3$ Å, $\theta_n = 105^\circ$, and $\varphi_n = 142^\circ$. The principal g values are listed in Figure 7.1.2.

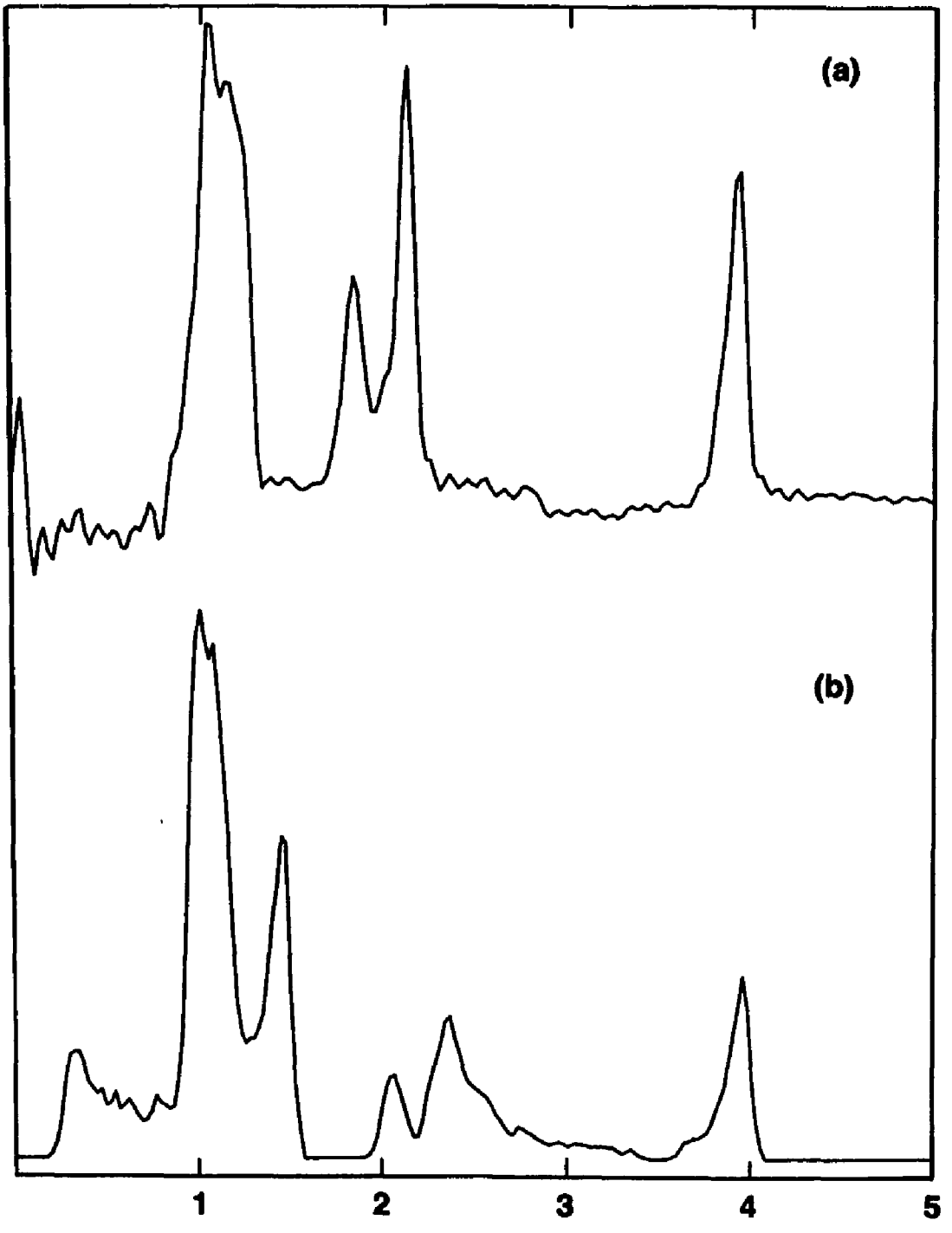

Figure 7.1.6

least–square minimization is not effective on fitting less pronounced features in spectra. In fact, some of the fits were obtained in the vicinity of the output parameters from the least–square minimization, after adjustments with visual examinations were made. However, it is fair to say that the output from the least–square minimization is close to the best–fit parameter set obtained. Therefore, only a refinement to the output, but not a major correction, is needed.

Less effort has been made, compared to the case of ^{14}N, to analyze modulations due to ^{95}Mo, partly because no similar NQR database to that of ^{14}N exists for ^{95}Mo. Furthermore, there has only been one report of observation of ^{95}Mo modulations: Doi *et al.*[43] observed ^{95}Mo frequencies in both ESEEM and CW–ENDOR experiments on complexes of molybdate with uteroferrin, a protein which probably contains a redox–active binuclear iron center.[43] These workers observed a doublet around the ^{95}Mo Larmor frequency with a hyperfine coupling of 1.2 MHz at g = 1.52 by both ESEEM and CW–ENDOR. Since the molybdate is not a suitable model compound for the FeMoco, the differences of ESEEM spectra between Doi's study and the current one is not surprising. In addition, measurements on ^{97}Mo enriched MoFe protein are planned, but have not yet been made. The Larmor frequency of ^{97}Mo differs from that of ^{95}Mo only by 2 %, but ^{97}Mo possesses a nuclear quadrupole moment about ten times as large as that of ^{95}Mo. The measurement will not only provide further evidences for the effect of Mo NQI, but might also assist in understanding the effect of molybdenum isotopes on nitrogen modulations.

Unlike ENDOR spectra, where a doublet assignable to $m_I = \pm 1/2$ and other broad features has been observed, the modulation patterns are quite complicated. There is, however, a trend that modulation peaks with stronger intensities move toward the upper bound of the spectra as the field value is decreased. If these frequencies all arise from the same "transitions", then this suggests that interactions

are dominated by the isotropic hyperfine term. As discussed at the beginning of the section, the apparent isotropic hyperfine coupling is expected to increase as the field value is decreased, and this is consistent with the experimental observations. On the other hand, this may also contribute to the disappearance of ^{95}Mo signal at the lower field region. The nuclear modulation effect is dependent on the presence of "partially forbidden" EPR transitions. The more dominating the hyperfine coupling, the better quantized the spin energy levels, and the smaller the "partially forbidden" transitions. In which case, it is expected to be difficult to observe the nuclear modulations due to the molybdenum. Furthermore, the nuclear Zeeman coupling, which may partially cancel the apparent hyperfine coupling in one of the electron spin manifolds, is expected to decrease as the field value decreases. The result is an even more unfavorable condition for detecting the molybdenum modulation at the low field region, which may account for the observations that in ESE spectra no difference was found between proteins enriched with different isotopes at lower field value region.

A comparison of the experimental spectrum with the fit from a preliminary simulation is shown in Figure 7.1.7. The Fourier transform spectrum is from the quotient waveform of the ^{95}Mo enriched protein data over the ^{96}Mo enriched protein data. Both the numerator and denominator data were taken at 10.5 GHz and at g = 2.54. The sharp frequency peaks pointing downward in the experimental spectrum are associated with nitrogen modulations. The simulation was done using the same method as that for the nitrogen modulations, except that all Euler angles were artificially set to zero. While this is not strictly correct, but it is justified by the consistency of the extracted parameters. The parameters are: A_{iso} = 2.5 MHz (the isotropic hyperfine coupling in the $\tilde{S}$ = 3/2 coordinate system is 5.0 MHz); Q_{zz}/h = 0.05 MHz (or e^2qQ/h = 2.0 MHz); η = 0.5; r_{eff} = 1.5 Å; θ_N = 75°; and φ_N = 45°. The fact that Q_{zz}/h is very small and that the simulated spectra are

Figure 7.1.7 Comparison of (a) the experimental and (b) simulated spectra at $g = 2.54$ and $\nu_e = 10.682$ GHz. The experimental conditions are listed in Figure 6.2.6. The simulation input for the ^{95}Mo nucleus were: $Q_{zz}/h = 0.05$ MHz, $\eta = 0.63$, $\alpha = 0^\circ$, $\beta = 10^\circ$, $\gamma = 0^\circ$; $A_{iso} = 2.5$ MHz (as defined in Eq. 3.1.10); $r_{eff} = 1.5$ Å, $\theta_n = 75^\circ$, and $\varphi_n = 45^\circ$. The principal g values are listed in Figure 7.1.2.

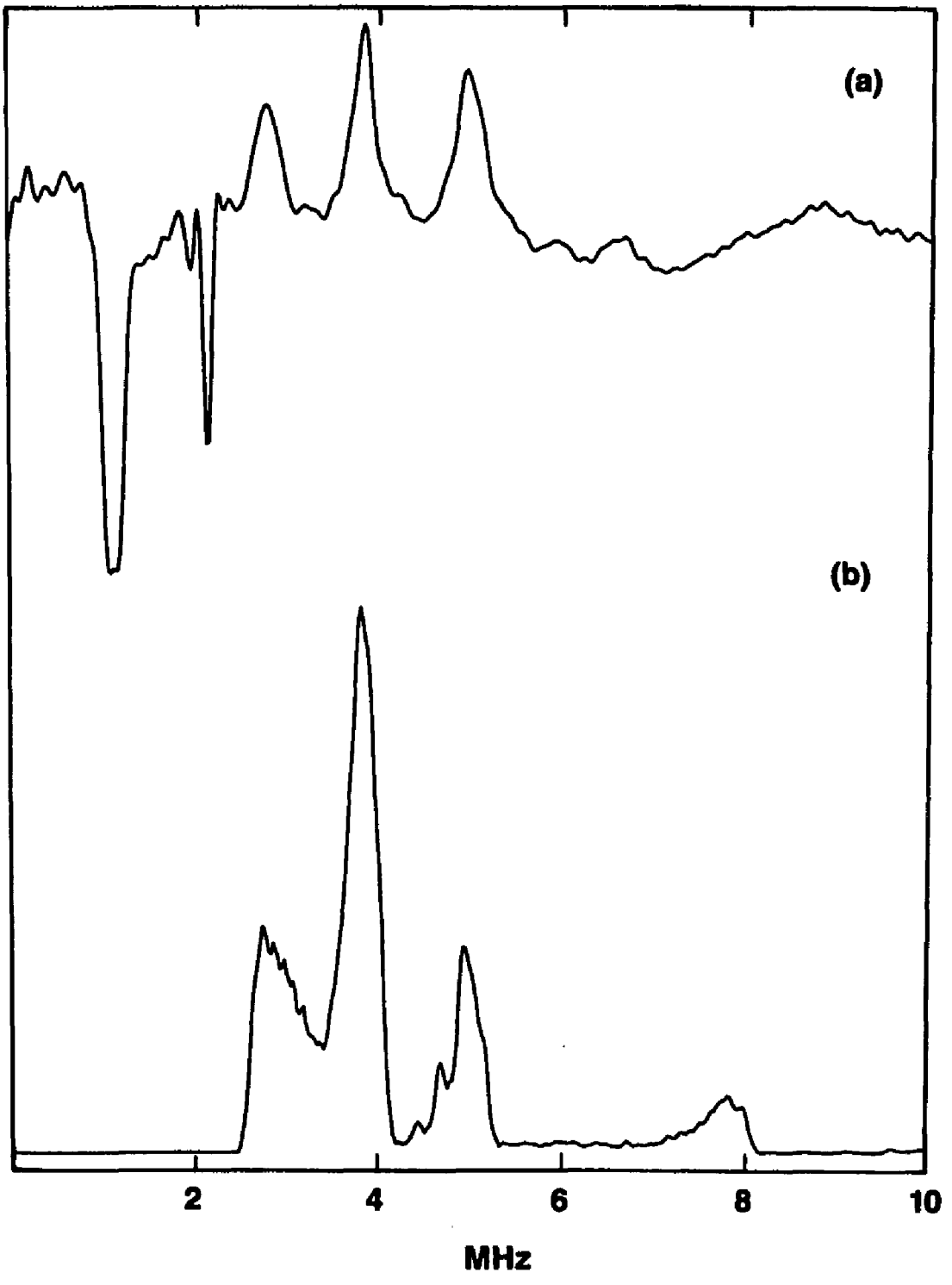

Figure 7.1.7

insensitive to η both suggest an insignificant role for the NQI. With further works, a better fit might be obtained, but for the moment, the current simulation may be worth some discussion. A small isotropic hyperfine coupling indicates that the paramagnetic spin density at the molybdenum nucleus is small. It could mean that electrons reside mainly on Fe sites, and/or that electrons are quite delocalized at the molybdenum site. The observation of a small A_{iso} is qualitatively consistent with the conclusions from EPR and CW–ENDOR studies. Venters *et al.*[22] estimated the quadrupole moment e^2qQ/h and hyperfine coupling from their CW–ENDOR study as 32.0 MHz and 8.1 MHz, respectively. Their e^2qQ/h value is significantly larger than that obtained in the present study. A very different simulation from the experimental data would be obtained if their e^2qQ/h and hyperfine value are used (not shown). Utilizing the sharpness of the excited states EPR transition, George *et al.*[30] gave an estimation of ^{95}Mo hyperfine couplings as 2.9 MHz. This is certainly very different from that given by the CW–ENDOR study, and the resolution to this discrepancy may depend on a more complete ESEEM analysis. In ESEEM spectra, more spectral features are present than the CW–ENDOR spectra which contain only a single doublet; and a much better spectral resolution than that of EPR can be obtained. Because a further effort is needed to improve the present simulation, and the uniqueness of the parameters needs to be fully established, the ^{95}Mo ESEEM simulation should be considered preliminary.

II. Identity of the Nitrogen Ligand

From the systematic analysis presented in the last section, experimental spectra across the resonance field range can be simulated using a unique set of coupling parameters. Among them, the quadrupole coupling constant e^2qQ/h and asymmetry factor η are 2.04 MHz and 0.63, respectively. This information,

combined with the database of nuclear quadrupole parameters for nitrogen compounds, and with recent genetic studies on the MoFe protein enable the possible identification of this nitrogen ligand.

As was discussed in Chapter 6, the nitrogen modulation does not arise from a nitrogen in the buffer (as different buffers do not alter the ESEEM spectra), or from substrate or product nitrogen (as turnover with ^{15}N does not affect the spectrum). Furthermore, the ESEEM experiments on the FeMoco extracted in spin–labeled NMF and regular NMF revealed only the ligation of NMF to FeMoco, but no nitrogen modulation from the FeMoco itself. Therefore, the existence of protein nitrogen coordination has been unequivocally established. Based on indirect evidence from FT–IR study on FeMoco in NMF, Walters *et al.*[37] have hypothesized that in the MoFe protein, the primary coordination of the cofactor is via deprotonated backbone amide ligands. According to NQR data, and an ESEEM study of *Escherichia coli* fumarate reductase, e^2qQ/h and η for the backbone amide nitrogen are 3.3 MHz and 0.5, respectively.[44] These values are very different form those observed for the MoFe protein, so the nitrogen ligation is unlikely to be from the polypeptide backbone of the protein. This possibility should not be completely excluded as it may be possible for amide nitrogens to coordinate differently than in fumarate reductase. Nevertheless, given that no significant difference is expected between polypeptide amides, substantially different nuclear quadrupole parameters would be unexpected.

The most likely source of the nitrogen modulation is a polypeptide side chain. Among all the amino acids, arginine, asparagine, glutamine, histidine, lysine, and tryptophan contain at least one nitrogen in their side chains. According to the available NQR data on amino acids in their unbound form (no data has been reported for arginine or lysine), none of the above side chains contains a nitrogen which matches the observed one.[45,46,47] Given that the modulation comes from a

nitrogen ligand, this is not surprising as coordination of the nitrogen to metal ions are likely to change quadrupole parameters of nitrogen. The observed nuclear quadrupole parameters are, however, close to that of an imidazole nitrogen coordinated to low spin heme Fe in heme–imidazole complexes.[33] There, the imidazole nitrogen observed was assigned as directly coordinated to the Fe. The observed nuclear quadrupole parameters are also close to those for the imino nitrogen in Zn(II)–imidazole and Cd(II)–imidazole complexes measured by NQR.[48] For example, the directly coordinated imidazole nitrogen was found to have e^2qQ/h = 2.0 MHz and $\eta = 0.68$ in Zn(II) $(imid)_4$ $(NO_3)_2$, and to have $e^2qQ/h = 2.09$ MHz and $\eta = 0.58$ in Zn(II) $(imid)_2$ Br_2. Therefore, it is likely that the modulations in nitrogenase observed in the present work originate from histidine nitrogen.

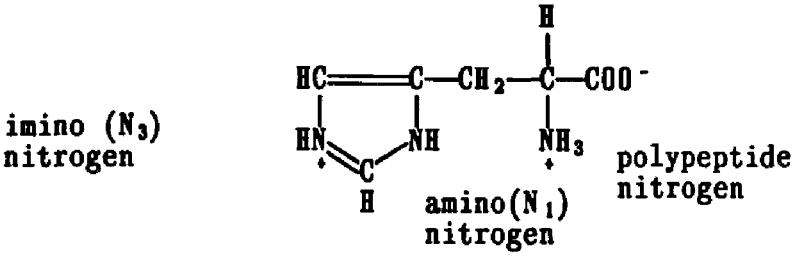

Figure 7.2.1 The structure of histidine at pH = 6.0.

Recently, Mims *et al.*[49] has collected ^{14}N quadrupole parameters from NQR and ESEEM for imidazole, metal imidazole complexes and metalloproteins, and plotted them as e^2qQ/h *vs.* η. It is interesting to note that they fall in three regions, which are labeled as A, B and C. Region A is for the deprotonated ^{14}N in histidine and imidazole. Region C contains the parameters for protonated ^{14}N in histidine, in imidazole, and in copper proteins. Region B between the two contains

the parameters for metal imidazole models in which the observed ^{14}N is directly coordinated by a metal ion, and for similar metalloproteins centers. The ^{14}N quadrupole parameters in this study would be plotted at the edge of region B close to the region C. This further supports the hypothesis that the observed nitrogen ligand is from a histidine.

Another way to aid the assignment is to use a different plot. Instead of plotting e^2qQ/h *vs.* η, h/e^2qQ *vs.* η is plotted, as shown in Figure 7.2.2. If these data points are fitted to a linear relation between h/e^2qQ and η, almost all the points representing imidazole complexes fall on or close to the line. On the other hand, the point representing the polypeptide amide nitrogen from fumarate reductase would be way off the line. In contrast, the parameters from the MoFe protein give a point very close to the line, again implicating histidine nitrogen.

Inverse relation between e^2qQ/h and η has been found to exist in coordinated pyridine complexes.[50] Hsieh *et al.*[50] used a modified Townes–Dailey model to study metal ion–pyridine NQR data. The theory of Townes and Dailey relates NQR parameters to atomic orbital electron densities.[51] While relating the electric field gradient at the nitrogen in pyridine complexes to the extent of charge transfer from nitrogen, Hsieh *et al.* derived a linear relationship between e^2qQ/h and η. Such a linear relationship was, indeed, observed for a number of Zn(II)–pyridine and Cd(II)–pyridine complexes.[50] A similar conclusion has been obtained by Ashby *et al.*[48] in the NQR study of Zn(II)–imidazole and Cd(II)–imidazole complexes. But the linear relation between e^2qQ/h and η is not identical for the two nitrogens, as shown in Figure 7.2.3. Again, if the data for the MoFe nitrogen modulation is plotted the point would lie close to the line for the imino nitrogen. Therefore, the assignment of an imino nitrogen for the protein nitrogen coordinated to FeMoco is favored. Although similar work on other nitrogen–containing complexes needs to be done, it would be straightforward to assign ESEEM frequencies according to which

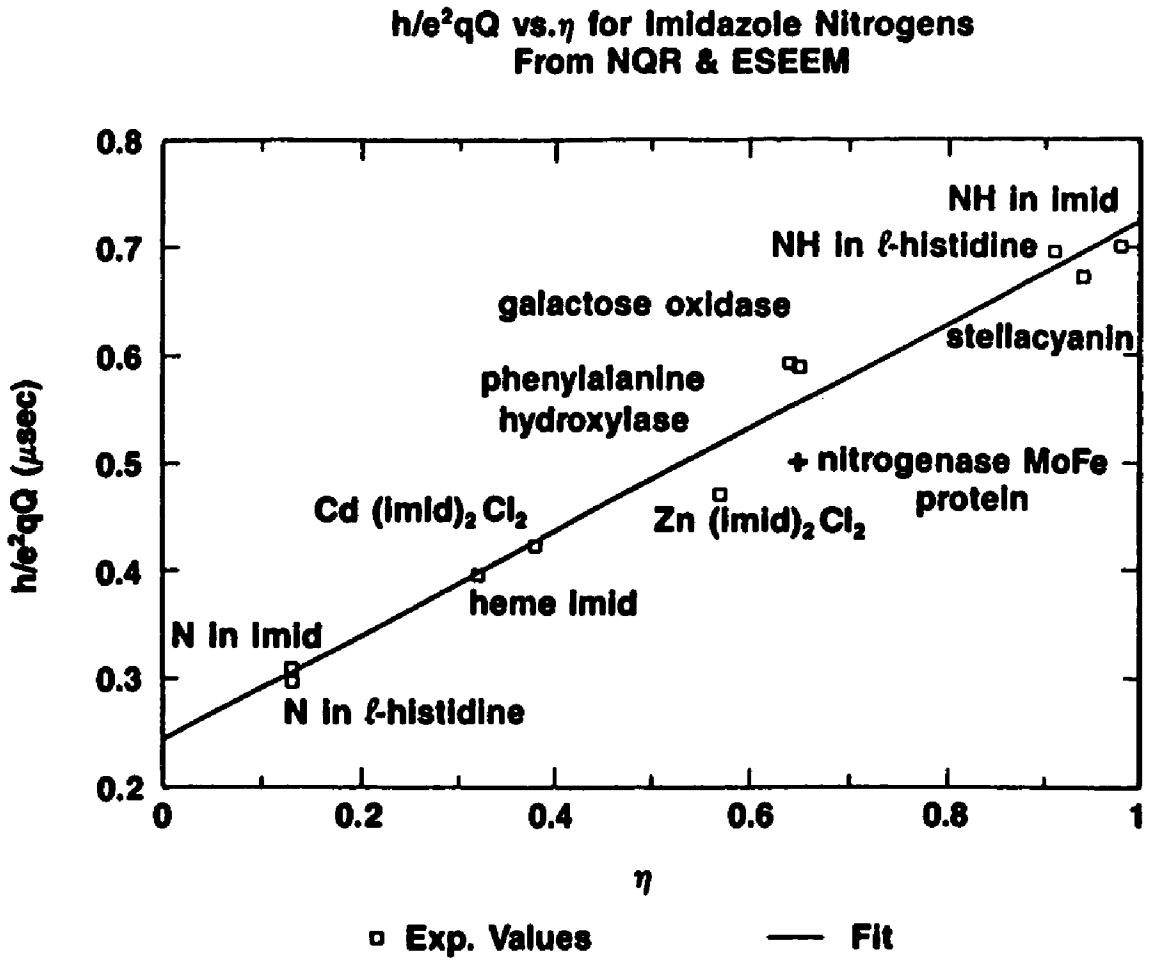

Figure 7.2.2 Plot of h/e^2qQ *vs.* η for imidazole nitrogens. The linear relation was fitted without the data for the MoFe protein. (All data, except that for the MoFe protein, are from Mims *et al.* preprint, and references therein.)

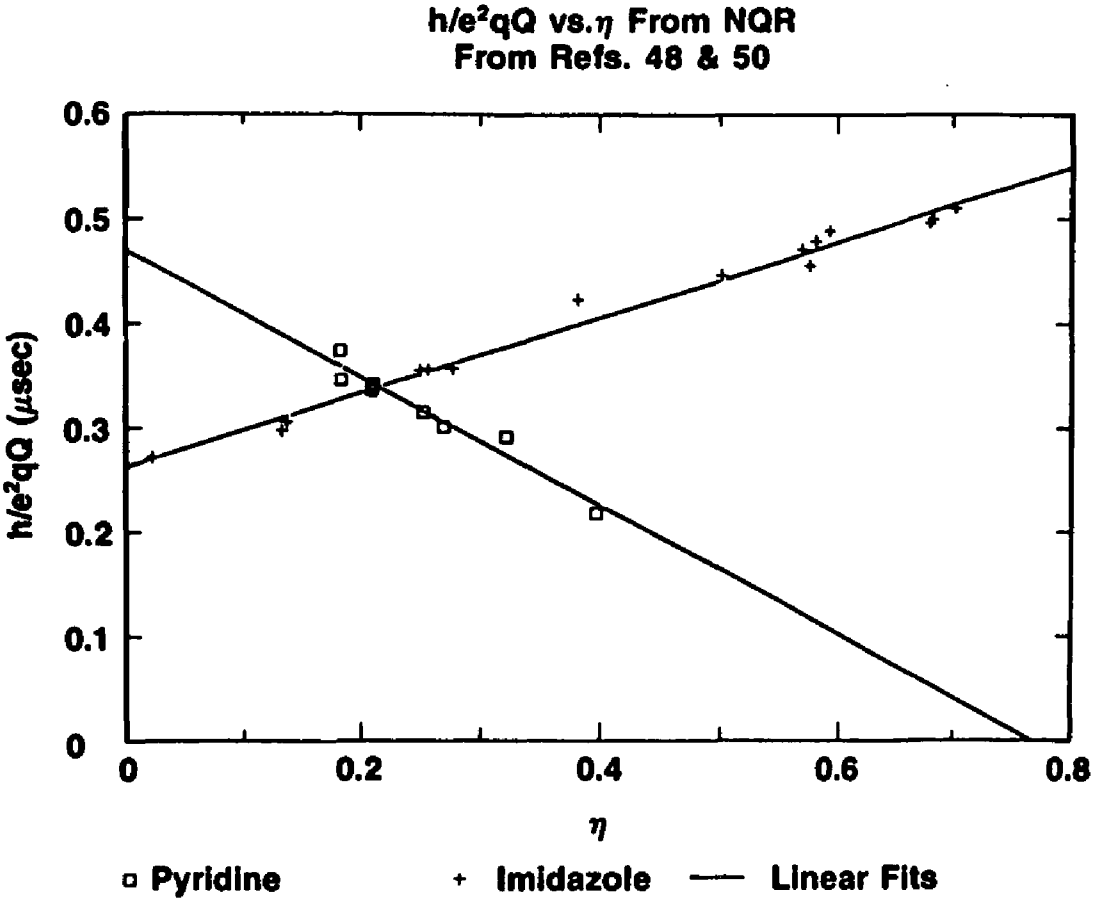

Figure 7.2.3 Plot of h/e^2qQ *vs.* η for the pyridine nitrogen in Zn(II)– or Cd(II)–pyridine complexes and the imino nitrogen in Zn(II)– or Cd(II)–imidazole complexes. Data were obtained from NQR experiments (Hsieh *et al. J. Am. Chem. Soc.* **1977**, *99*, 1394.; and Ashby *et al. J. Am. Chem. Soc.* **1978**, *100*, 6057).

lines of h/e^2qQ *vs.* η the observed quadrupole parameters fall on. This proposal can be tested for other observed ^{14}N quadrupole parameters.

There are two nitrogens on the imidazole ring of a histidine. If the observed nitrogen is remotely coordinated to the paramagnetic center, the directly coordinated one would possess appreciable hyperfine coupling, as in the case of Cu–imidazole complexes. This would be detected easily by ENDOR techniques, even possibly by EPR. So far, there is no report of large hyperfine coupling due to nitrogen in either EPR or CW–ENDOR. Preliminary pulsed–ENDOR data on ^{95}Mo enriched protein showed no sign of such coupling in the range of 0. to 40 MHz. Hence the possibility that the observed nitrogen is a remotely coordinated one is unlikely. It is not unreasonable that this nitrogen is a directly coordinated nitrogen, and that the remote nitrogen is unobservable in ESEEM due to unfavorable conditions.

It is known that the binding of nitrogen at a metal site decreases the quadrupole coupling constant e^2qQ/h. For example, the study by Hsieh *et al.*[50] established that e^2qQ/h decreases as $1/\eta$ in pyridine complexes, and the above–mentioned plot for imidazole complexes showed a linear relationship of h/e^2qQ with η. If a Townes–Dailey model can be applied to the present case, an inverse relation of e^2qQ/h and η is expected to exist for the side chain nitrogen of amino acids in metal–bound form and in unbound form. In unbound form, (e^2qQ/h (MHz), η) are observed to be (2.83, 0.29) for glutamine, (2.72, 0.38) for asparagine, and (3.01, 0.18) for tryptophan. Each of them has a qualitative inverse relation with the quadrupole parameters observed for the MoFe protein. No data on arginine or lysine has been reported. But the side chain of an arginine contains three nitrogens near to each other. It is less likely that the observed nitrogen is that of arginine, since it is difficult to account for the other two missing nitrogens. The side chain nitrogen in lysine is of the amine type. Nuclear quadrupole values from

CH_3NH_2 and $C_2H_8N_2$ (or $H_2N\ CH_2\ CH_2\ NH_2$) are (4.0, 0.37) and (4.0, 0.31) respectively.[57] Though they are significantly different from the observed (2.0, 0.65), an inverse relationship does exist between them. By analogy, it is possible that lysine is a candidate for providing nitrogen coordination to the FeMoco.

According to the nucleotide sequence study on *Azotobacter vinelandii* nitrogenase structural gene cluster[52] and the latest mutagenetic results[53,61], the regions encompassing amino acids 183 – 196 and 264 – 289 in α subunit (or nitrogen fixation gene D) of the protein are the most favorable candidates for providing ligands to FeMoco. In the following discussions the numbering of residue sequences will follow the convention for the MoFe protein of *Azotobacter vinelandii* (Av1) sequence, instead of *Clostridium pasterianum* (Cp1), for convenience of comparison with the genetic work in the literature. Scott *et al.*[61] have shown that a mutant strain resulted from the substitution either at histidine 195 (His 195) or at glutamine 191 (Gln 191) exhibited an EPR spectrum which was changed in both lineshape and g value when compared with that of the wild–type. The change for the mutant strain with His 195 substitution was more pronounced and the intensity of EPR signal was also considerably diminished. Furthermore, the catalytic activity of nitrogenase containing these mutant strains was changed from the isogenic wild–type. It is very likely that the nitrogen modulation, which is responsible for the coordination to the FeMoco, comes from either His 195 or Gln 191. On the other hand, the mutation at asparagine 271 or 280 (Asn 271 and Asn 280) had no effect on the diazotrophic growth capabilities of the respective mutant strain, indicating that these residues are unlikely to provide essential N–ligands to FeMoco.

Other than Asn 271 and Asn 280, the region encompassing residue 264 to 289 contains one asparagine (Asn 265), two glutamines (Gln 264 and Gln 274), one histidine (His 276), and two lysines (Lys 267 and Lys 289). None of them is conserved, except Lys 267 and Lys 289, in the nucleotide sequence among various

organisms such as *Clostridium pasterianum*, *Azotobacter vinelandii*, etc..[54,55] Differences in nitrogen modulation from the Cp1 and other MoFe proteins could be expected if there is a difference in the amino acid type or the position on the polypeptide chain between different organisms. In particular, the comparison of the nitrogen modulation from Cp1 and Av1 would be especially informative, since in Av1 there is no glutamine, and a histidine is at different position in Cp1 in this region of amino acids. There is an extra lysine in Av1 (Lys 269), and a nonconserved lysine (Lys 187) in Cp1 in the region of 183 – 196. These can be distinguished by the comparison between Av1 and Cp1 using ESEEM. But the other two lysines (Lys 267 and Lys 289) are conserved in both Av1 and Cp1. Further genetic work on these lysines is needed.

Based on the ESEEM and genetic study, His 195 and Gln 191 are leading candidates to provide nitrogen ligand to FeMoco. It is also possible that this nitrogen comes from His 196. There is no tryptophan in the two regions, and therefore, this amino acid is not considered a candidate for the nitrogen ligand. Asparagines may not provide the nitrogen ligand either, except Asn 265. But it is not present in other organisms. The comparison of nitrogen modulation from the Av1 with the Cp1 can not only clarify whether the nitrogen comes from Asn 265, but also provide answers to the role of other residues, such as that of Lys 187, Gln 264, Gln 274 or His 276. No report of site–directed mutation at lysines has been reported. It can not be ruled out that the nitrogen ligation to the FeMoco is provided by a lysine.

Potentials of ESEEM as a ligand–identifying spectroscopic tool need to be exploited further. If the spectroscopy is applied to the site–directed substituted protein, unequivocal identification of the origin of the nitrogen ligated to the FeMoco should be accomplished. It is expected that when the residue which provides the nitrogen ligation is mutated, both EPR and biological activity would

be changed; and ESEEM would give a null result as far as nitrogen ligation is concerned. The EPR properties concerning molybdenum are expected to change sharply, since the nitrogen binds at molybdenum first, then to the rest of the cofactor, as will be discussed next.

III. The Effect of Molybdenum Isotopes on the Nitrogen Modulation

The effect of molybdenum isotopes on the nitrogen modulation is an interesting one. With no frequency shift, or only a small shift within the frequency resolution of the Fourier transform (typically 0.04 MHz), the nitrogen modulation amplitude changes significantly when ^{95}Mo is present instead of ^{96}Mo. To account for this observation, it is proposed that the nitrogen is connected to the paramagnetic cluster through coordination to the molybdenum, and that the competition between ^{95}Mo and ^{14}N for polarization of the spin magnetization may be responsible for the ^{14}N modulation amplitude change.

According to ESEEM theory, the modulation amplitude due to a nucleus is directly affected by the anisotropic part of the hyperfine interaction. If the anisotropic hyperfine interaction is modeled to be due to the pseudodipolar interaction or due to the bonding between the paramagnetic ion and the nucleus, the dependence of nitrogen modulation amplitudes on the molybdenum isotopic enrichments would mean the dependence of nitrogen hyperfine interactions on the presence of Mo. However, in the present case, the pseudodipolar distance or the bond length are not expected to be altered by the presence of such small magnetic interaction of ^{95}Mo hyperfine coupling.

In order to account for the effect of the molybdenum on the nitrogen modulation amplitudes, an interaction between the molybdenum and the nitrogen must be considered. The interaction can result from the situations: 1) that the

nitrogen acts as a bridging ligand between the molybdenum and the rest of the FeMoco; 2) that the nitrogen is coordinated to other parts of the FeMoco, but not to the molybdenum; 3) that the nitrogen binds both the molybdenum and other parts of the FeMoco, but not as bridging ligand; and 4) that the nitrogen connects to the FeMoco through direct coordination to the molybdenum.

Situation 1) is directly opposed to the assignment of the nitrogen being from the polypeptide side chain. Since no nitrogen modulation from FeMoco is observed, and an indistinguishable environment around the molybdenum exists both in the MoFe protein and FeMoco,[23-25] the possibility of a nitrogen bridging ligand is unlikely.

The effect of the molybdenum on the nitrogen modulation amplitudes must be due to nuclear–nuclear interactions between the molybdenum and the nitrogen. If there is no coordination between them, two types of interaction can be imagined: the interaction through paramagnetic bonds and nuclear dipolar coupling. Bloembergen *et al.*[56] gave an estimate of size of the nuclear–nuclear interaction through paramagnetic bonds as $\gamma_{Mo}\ \gamma_{N}\ A_{Mo}\ A_{N}\ /\ \Delta E$, where γ represents the gyromagnetic ratio, A, the hyperfine coupling in gauss, and ΔE is the energy difference between the ground state and the excited state. With both hyperfine couplings being very small ($|A| < 2$ gauss), the interaction through paramagnetic bonds is exceedingly small, therefore can not account for the observation. The nuclear dipolar interaction is of the order of $g_N^{Mo}\ g_N^{N}\ \beta_N^2\ /r^3$. For $r = 1.0$ Å, the dipolar coupling is about 0.5 kHz, which is too small to cause a significant change of nitrogen modulation amplitude. For this interaction to contribute to the variation of modulation amplitudes, very long τ value, about 1/ (0.5 KHz) or 2 μsec, for the stimulated echo sequence would be needed.[58] Yet, this is not at all the case for this study. Therefore, situation 2) is not likely.

Situation 3) is not unlikely, but is consistent with 4) in that the molybdenum

and the nitrogen are directly coordinated. However, the coordination of the nitrogen to the molybdenum should be stronger than other bond(s). Otherwise, the effect of molybdenum isotopes on the nitrogen would be minor one, since major portions of paramagnetic spin density reside in the other part of the FeMoco.

From the above discussions, the effect of the molybdenum on the nitrogen modulation amplitudes arises most likely from the situation 4) where the nitrogen is directly coordinated to the molybdenum, rather than to the rest of the FeMoco. The dependence of nitrogen modulation amplitudes on molybdenum isotopes may be plausibly explained by the competition for polarization of spin magnetization between the ^{14}N and ^{95}Mo. The effect of the competition for polarization is an enhancement or suppression of certain transitions among energy levels, therefore affecting the nuclear modulation amplitudes without changing modulation frequencies. It is conceivable that the effect is the strongest when energy level splittings associated with the two individual nuclei are comparable to each other. This is consistent with the experimental observation in the higher field region that the modulation frequencies for ^{14}N and ^{95}Mo overlapped, and that the change of nitrogen modulation amplitudes due to molybdenum isotopes was also more pronounced. Similar observations of spectral changes due to difference in isotopic enrichments have been reported by Thomann *et al.*[59] in a CW–ENDOR experiment, and Robinson *et al.*[60] in a saturation recovery experiment, both on polyacetylene. They have also hypothesized the competition for polarization between considered nuclei in order to explain their observations.

In short, the dependence of nitrogen modulation amplitudes on molybdenum isotopes may be plausibly explained by the competition for polarization of magnetization between the ^{14}N and ^{95}Mo nuclei. This can occur when the connection between the nitrogen to FeMoco is mostly, if not entirely, through coordination to the molybdenum.

IV. Conclusions about Coordination Structure of FeMoco

The spectroscopic findings from the ESEEM studies have been analyzed. The pronounced field dependence of ESEEM spectra can be accounted for by the "orientation selectivity" by EPR and the interplay of various interactions involved. The application of the systematic analysis method has benefited from the narrow excitation bandwidth of microwave pulses, in comparison with the very broad EPR line, and the absence of metallic hyperfine coupling in the ^{96}Mo enriched protein.

Differences, some significant, have been observed in ESEEM and EI–EPR spectra at X–band microwave frequencies for the ^{95}Mo enriched and for the ^{96}Mo enriched MoFe proteins. The waveform division method has been used to isolate these differences effectively. The cosine Fourier transform from the division quotient clearly indicates the presence of multiple sharp peaks associated with transitions among quantum states of molybdenum spin. The hyperfine coupling and nuclear quadrupolar coupling of the molybdenum obtained from the preliminary analysis are lower than that obtained from the CW–ENDOR analysis.

In all spectra, whether from native proteins or from proteins with molybdenum isotopic enrichment, nuclear modulations due to one nitrogen have been observed. The systematic analysis has resulted in a unique set of coupling parameters from the data. The nuclear quadrupole parameters obtained, in comparison with NQR data and genetic study, suggest that the nitrogen modulations observed are most plausibly assigned to the imino nitrogen of a histidine, or the amide nitrogen of a glutamine. The possibility that the modulations are due to the amine nitrogen of a lysine can not be ruled out.

Although the nitrogen modulation frequencies do not depend on whether the protein is enriched with ^{95}Mo or with ^{96}Mo, the modulation amplitudes are quite

different. The significant change of the modulation amplitude of the nitrogen introduced by the difference in molybdenum isotope enrichment suggests that this nitrogen is most likely connected to the FeMoco through coordination to the molybdenum.

REFERENCES FOR PART II:

1. Postage, J. R. *Fundamentals* of *Nitrogen Fixation*; Cambridge University Press, Cambridge, New York, 1982.

2. Hardy, R. W. F. *Treatise on Dinitrogen fixation*, Wiley and Sons, New York, 1979.

3. Shah, V. K.; Davis, L. C.; Brill, W. J. *Biochim. Biophys. Acta.* 1971, *256*, 498–511.

4. Nakos, G.; Mortenson, L. E. *Biochim. Biophys. Acta.* 1971, *229*, 431–436.

5. Zumft, W. G.; Hase, T.; Matsubara, H. in *Molybdenum Chemistry of Biological Significance*; Newtow, W. E.; Otsuka, S., Eds.; Plunum, New York, 1980; 59–72.

6. Bishop, P. E.; Jarlenski, D. M. L.; Hetherington, D. R. *Proc. Natl. Acad. Sci. USA*, 1980, *77*, 7342.

7. Bishop, P. E. *Trends Biochem. Sci.* 1986, *11*, 225–227.

8. Pau, R. N. *Trends Biochem. Sci.* 1989, *14*, 5.

9. Mortensen, L. E.; Thorneley, R. N. F. *Ann. Rev. Biochem.* 1979, *48*, 387–418.

10 Stiefel, E. I.; Thomann, H.; Jin, H.; Bare, R. E.; Morgan, T. V.; Burgmayer, S. J. N.; Coyle, C. L. *Metal Clusters in Proteins*; Que, L. ed., ACS Symposium Series 372, Washington, D. C., 1988.

11. Sundaresan, V.; Ausubel, F. M. *J. Biol. Chem.* 1981, *256*, 2808.

12. Hausinger, R. P.; Howard, J. B. *J. Biol. Chem.* 1983, *258*, 13486.

13. Smith, B. E.; Lowe, D. J.; Bray, R. C. *Biochem. J.* 1972, *130*, 641–643.

14. Orme–Johnson, W. H.; Hamilton, W. D.; Ljones, T.; Tso, M.– Y.; Burris, R. H.; Shah, V. K.; Brill, W. J. *Proc. Natl. Acad. Sci. USA* 1972, *69*, 3142–3145.

15. Dixon, R. A. *J. Gen. Micro.* 1984, *130*, 2745.

16. Shah, V. K.; Brill, W. J. *Proc. Natl. Acad. Sci. USA* 1977, *74*, 3249.

17. Stiefel, E. I.; Cramer, S. P. in *Molybdenum Enzymes*; Spiro, T. G. ed.; Wiley and Sons, New York, 1985, 88.

18. Hoover, T. R.; Imperial, J.; Ludden, P. W.; Shah, V. K. *Biochemistry* 1989, *28*, 2768–2771.

19. Hawkes, T. R.; McLean, P. A.; Smith, B. E. *Biochem. J.* 1984 *217*, 317.

20. Stephens, P. J. in *Molybdenum Enzymes*; Spiro, T. G. ed.; Wiley and Sons, New York, 1985, 117.

21. Orme–Johnson, W. H.; Davis, L. C.; Henzl, M. T.; Averill, B. A.; Orme–Hohnson, N. R.; Münck, E.; Zimmerman, R. *Recent Developments in Nitrogen Fixation*; Newton, W. E.; Postage, J. R.; Barrueco, C. R. eds.; Academic press, New York, 1977, 131.

22. Venters, R. A.; Nelson, M.; McLean, P. A.; True, A. E.; Levy, M. A.; Hoffman, B. M.; Orme–Johnson, W. H. *J. Am. Chem. Soc.* 1986, *108*, 3487.

23. Cramer, S. P.; Hodgson, K. O.; Gillum, W. O.; Mortensen, L. E. *J. Am. Chem. Soc.* 1978, *100*, 3398.

24 Conradson, S. D.; Burgess, B. K.; Newton, W. E.; Mortenson, L. E.; Hodgson, K. O. *J. Am. Chem. Soc.* 1987, *109*, 7507.

25. Antonio, M. R.; Teo, B. –K.; Orme–Johnson, W. H.; Nelson, M. J.; Groh, S. E.; Lundahl, P. A.; Kauzlarich, S. M.; Averill, B. A. *J. Am. Chem. Soc.* 1982, *104*, 4703.

26. Münck, E.; Rhodes, H.; Orme–Johnson, W. H.; Davis, L. C.; Brill, W. J.; Shah, V. K. *Biochim. Biophys. Acta.* 1975, *400*, 32.

27. True., A. E.; Nelson, M. J.; Venters, R. A.; Orme–Johnson, W. H.; Hoffman, B. M. *J. Am. Chem. Soc.* 1988, *110*, 1935–1943.

28. Palmer, G.; Multani, J. S.; Zumft, W. G.; Mortenson, L. E. *Arch Biochem. Biophys.* 1972, *153*, 325.

29. Smith, B. E.; Lowe, D. J.; Bray, R. C. *Biochem. J.* 1973, *135*, 331–341.

30. George, G. N.; Bare, R. E.; Jin, H.; Stiefel, E. I.; Prince, R. C. *Biochem. J.* 1989, *262*, 349–352.

31. Cramer, S. P. *Adv. in Inorg. & Bioinorg. Meth.* , 1983, *2*, 259–316.

32. Peisach, J.; Mims, W. B.; Davis, J. L. *J. Biol. Chem.* 1979, *254*, 12379–12389.

33. (a) Ashby, C. I. H.; Cheng, C. P.; Brown, T. L. *J. Am. Chem. Soc.* 1978, *100*, 6057–6063.

(b) Ashby, C. I. H.; Cheng, C. P.; Duesler, E. N.; Brown, T. L. *J. Am. Chem. Soc.* 1978, *100*, 6063.

34. Fermi, E. *Z. Physik* 1930, *60*, 320.

35. Abragam, A.; Bleaney, B. *Electron Paramagnetic Resonance of Transition Ions*, Clarendon, Oxford, 1970.

36. Yang, S. S.; Pan, W. H.; Friesen, G. D.; Burgess, B. K.; Corbin, J. L.; Stiefel, E. I.; Newton, W. E. *J. Biol. Chem.* 1982, *257*, 8042.

37. Walters, M. A.; Chapman, S. K.; Orme–Johnson, W. H. *Polyhedron* 1986, *5*, 561.

38. Cole, T.; Heller, C.; McCornell, H. M. *Proc. Natl. Acad. Sci. USA* 1959, *45*, 525.

39. McCornell, H. M.; Chestnut, D. B. *J. Chem. Phys.* 1958, *28*, 107.

40. Canters, G. W.; de Boer, E. *Mol. Phys.* 1967, *13*, 395.

41. Wertz, J. E.; Bolton, J. R. *Electron Spin Resonance*, Chapman and Hall, New York, 1986.

42. Astashkin, A. V.; Dikanov, S. A.; Tsvetkov, Y. D. *Chem. Phys. Lett.* 1987, *136*, 204.

43. Doi, K.; McCracken, J.; Peisach, J.; Aisen, P. *J. Biol. Chem.* 1988, *263*, 5757–5763.

44. Cammack, R.; Chapman, A.; McCracken, J.; Cornelius, J. B.; Peisach, J.; Weiner, J. H. *Biochim. Biophys. Acta.* 1988, *956*, 307–312.

45. Edmonds, D. T. *Physics Report* 1977, *29*, 233–290.

46. Hunt, M. J.; Mackay, A. L. *J. Magn. Reson.* 1974, *15*, 402–414.

47. Hunt, M. J.; Mackay, A. L. *J. Magn. Reson.* 1976, *22*, 295–301.

48. (a) Ashby, C. I. H.; Cheng, C. P.; Brown, T. L. *J. Am. Chem. Soc.* 1978, *100*, 6057–6063.

49. Mims, W. B.; Peisach, J. submitted.

50. Hsieh, Y. –N.; Rubebacker, G. V.; Cheng, C. P.; Brown, T. L. *J. Am. Chem. Soc.* 1977, *99*, 1394–1389.

51. Townes, C. H.; Dailey, B. P. *J. Chem. Phys.* 1949, *17*, 782–796.

52. Brigle, K. E.; Newton, W. E.; Dean, D. R. *Gene* 1985, *37*, 37–44.

53. Dean, D. R. Personal communication.

54. Hase, T.; Wakabayashi, S.; Nakano, T.; Zumft, W. G.; Matsubara, H. *FEBS* 1984, *166*, 39–43

55. Wang, S. –Z.; Chen, J. –S.; Johnson, J. L. *Biochemistry* 1988, *27*, 2800–2810.

56. Bloembergen, N.; Rowland, T. J. *Phys. Rev.* 1955, *97*, 1679.

57. Semin, G. K.; Babnshkina, T. A.; Yakobson, G. G. *Nuclear Quadrupole Resonance in Chemistry*; Isreal Program for Scientific Translation, John Wiley, New York; 1972.

58. Jin, H.; Thomann, H. Unpublished result.

59. Thomann, H. *et al.* in *Electron Magnetic Resonance in Solid States*, Weil, J. ed.; Canadian Chemical Society, Ottowa; 1988.

60. Robinson, B. *et al.* in *Electron Magnetic Resonance in Solid States*, Weil, J. ed.; Canadian Chemical Society, Ottowa; 1988.

61. Scott, D. J.; May, H. D.; Newton, W. E.; Brigle, K. E.; Dean, D. R. Submitted to *Nature*.

PART III

COPPER COORDINATION

IN NITROUS OXIDE REDUCTASE

ABSTRACT

The structure of the copper sites in the multicopper enzyme nitrous oxide (N_2O) reductase from *Pseudomonas stutzeri* have been studied by EPR and ESE spectroscopies. Correlations between the enzyme activity and paramagnetic susceptibility, the pH dependence of the EPR spectra, and exogenous ligand binding were investigated.

Two types of copper sites are identified; antiferromagnetically coupled ($J >$ 200 cm^{-1}) dimeric sites and unusual Cu(II) sites. The EPR susceptibility arises from these Cu(II) sites and from binuclear mixed valence Cu(I)/Cu(II) half–met sites which are derived from partially reduced dimers. On average, six of the eight copper ions per protein, are in the form of the EPR silent binuclear type 3 dimers.

At $g = 2.03$ in the EPR spectrum, the Fourier transform of the stimulated echo envelope reveals a complex spectrum with narrow lines at 1.5, 1.9, 2.5, 2.9, 3.4 MHz and broad lines centered at 0.8 and 3.8 MHz. This spectrum is not typical of either blue (type 1) or square planar (type 2) sites in copper proteins. However, with the exception of the lines at 2.5 and 3.4 MHz, the spectrum for N_2O reductase is very similar to that observed for the Cu_A site in cytochrome c oxidase. This is

the first time that the Cu_A site has been observed in an enzyme other than cytochrome c oxidase.

The ESE envelope spectrum can be simulated using three sets of ^{14}N quadrupole coupling parameters. Two of these are characteristic of the distal nitrogen on imidazole ligands bound to Cu(II). By analogy to the ESE envelope spectra for the Cu_A site in cytochrome c oxidase, these two imidazole ligands are coordinated to the Cu_A site in N_2O reductase. The third ^{14}N, which is most likely coordinated to the half-met site, has a quadrupole coupling that is close to that observed by NQR for amide nitrogen and to that deduced from ESE measurements for the distal nitrogen of substituted imidazoles in copper-imidazole complexes. However, in both cases the quadrupole asymmetry is much smaller than that deduced from the present data.

Water accessibility of the copper sites was investigated by ESE envelope spectroscopy. The deuteron modulation frequency observed for all forms of the enzyme dialyzed against D_2O at different pH values indicates that the EPR active copper sites are accessible to water. A ten-fold increase in catalytic activity was observed after dialysis of the enzyme at pH 9.8. No concomitant change in the nitrogen ESE envelope spectrum was observed; but a significantly deeper deuteron modulation was observed for the enzyme dialyzed against D_2O. The envelope waveform is characteristic of a directly coordinated deuterated ligand, most likely a water or hydroxide. The increase in EPR line width and paramagnetic susceptibility, also observed at high pH, suggests that a new EPR active copper site which has more exchangeable protons is generated at high pH. However, a pH-induced protein conformation change or base-catalyzed proton exchange allowing enhanced solvent accessibility to the copper sites can not be ruled out.

CHAPTER 8

INTRODUCTION

Denitrification is the reduction of nitrate to dinitrogen, as shown schematically:

$$2NO_3^- \longrightarrow 2NO_2^- \longrightarrow 2NO \longrightarrow N_2O \longrightarrow N_2.$$

Nitrous oxide (N_2O) is reduced to dinitrogen by denitrifying bacteria as part of the denitrification process. Nitrous oxide reductase is the enzyme that catalyzes the reduction of N_2O to N_2 and H_2O. The multicopper enzyme from *Pseudomonas stutzeri* (formally *Pseudomonas perfectomarina*) has been isolated and purified to homogeneity. The enzyme contains about eight copper atoms per molecular weight 140,000 and is composed of two identical subunits[1]. No other metal ions have been detected by plasma emission studies. Several different forms of the enzyme have been prepared. The more active purple form is obtained by purifying the enzyme under anaerobic conditions.[2] Aerobic purification of N_2O reductase produces a pink form which contains less copper and is two to five fold less active. Preparative isoelectric focusing of the purple form results in the resolution of two protein bands with slightly different isoelectric points (an anodic band at pI= 4.97 and a cathodic band at pI= 5.06). A blue inactive form is obtained by reduction with excess dithionite or ascorbate. A high pH form of the enzyme, prepared by dialysis against buffer at pH 9.8, has an activity approximately ten fold higher than that of the same enzyme at pH 7.5.[3]

Most copper centers in proteins have been classified into three types: "blue" (type 1), "normal" (type 2), and dimeric (type 3) that are distinguished by their

characteristic EPR and UV–visible spectroscopic properties[4].

Of the three types, type 1 copper centers are the best characterized, and detailed discussions of type 1 copper centers are found in several reviews.[5] Stellacyanin, the plastocyanins, and the azurins are the most widely studied metalloproteins which contain type 1 coppers. They are thought to take part in electron–transfer process. The most striking spectral feature of the these proteins, and the source of their name, is their intense optical absorption band in the region of 600 nm. For type 1 proteins, extinction coefficients at this wavelength are on the order of 5000 $M^{-1}cm^{-1}$, while for "normal" cupric complexes, values are typically two orders of magnitude smaller. Another distinguishing spectroscopic feature is the narrowness of the cupric hyperfine splitting in EPR spectra (There is no EPR signal for cuprous, Cu(I) ion, since no unpaired electron is present.). $g_{\|} > g_{\perp} > 2$ is a common feature for paramagnetic Cu(II), this is also found for type 1 copper. However, the hyperfine splitting is always less than 100 Gauss, while inorganic copper complexes and type 2 sites usually exhibit hyperfine splitting greater than 100 G. The coordination of the Cu sites, including type of ligands and symmetry associated with ligation, determines these spectral features. X – ray crystallographic studies on the plastocyanins have shown that two sulfur (from a cysteine and a methionine) and nitrogen (from two histidines) are the Cu ligands.[6]

Complexes containing type 2 copper centers have optical and EPR properties similar to those containing inorganic copper. Superoxide dismutase, galactose oxidase, and the amine oxidase are examples such proteins. The EPR spectra consist of four hyperfine lines, with typical couplings ranging from 130 to 200 Gauss. Peisach and Blumberg[7] compared the EPR characteristics of copper complexes with known structure to those of well–characterized type 2 proteins, and found that the latter closely resemble model compounds having 4 nitrogen or 2 nitrogen and 2 oxygen ligands to Cu. The X–ray crystal structure of superoxide dismutase has

been solved, and indicates that four nitrogen ligands (from three imidazoles and an imidazolate) coordinate to the type 2 center in a square plane with a limited tetrahedral distortion.

Type 3 copper proteins contain two copper atoms and are generally referred to as "binuclear copper". These include hemocyanin, tyrosinase, and laccase. Laccase also contains a type 1 and a type 2 copper center. In contrast to the other types of copper centers, type 3 sites are EPR silent. Adequately resolved X–ray crystallographic structural information does not yet exist; however, fairly detailed structural information has been inferred from other spectroscopic means. Extensive studies by Solomon *et al.*[8] on a series of derivatives of type 3 copper complexes, especially with exogenous ligands, have shown that there is probably a bridging endogenous ligand (most likely the oxygen of tyrosine) which allows for antiferromagnetic coupling of the two cupric atoms.

Previous EPR and optical absorption data on N_2O reductase could not be readily described in terms of these three categories. N_2O reductase displays an unusual EPR spectrum consisting of four to seven equidistant lines with hyperfine values $A_{\|} = 38$ Gauss. The lack of additional signals at low magnetic field, as would be expected for larger hyperfine splittings, indicates that type 2 copper is absent. Furthermore, $g = 4$ signal, which would come from weakly coupled copper dimer, is not observed. Both the magnitude of $A_{\|}$ and optical parameters differ from those reported for type 1 copper proteins. It is concluded that N_2O reductase contains a novel copper center.[3] In this study, a further investigation of the copper sites has been performed by detailed EPR and ESE studies on the different forms of the enzyme as a function of temperature and pH. The copper sites have also been probed by exogenous ligand binding studies. From this study, a spectroscopic model for the copper coordination in N_2O reductase is constructed.

CHAPTER 9

EXPERIMENTAL RESULTS

I. Experimental Conditions

N_2O reductase from *Pseudomonas stutzeri* (formerly *Pseudomonas perfectomarina*) was purified as previously described in the literature.[1,2,3] All manipulations were performed at 4° C, and 25mM TRIS–HCl, pH 7.5 was used throughout unless otherwise stated. The different forms of the enzyme used in this study are described in Table 9.1.1. N_2O reductase activity was monitored spectrophotometrically as reported previously.[2,3] Copper was detected using inductively coupled plasma/atomic absorption spectroscopy. The protein concentration was determined by the method of Lowry et al.[9]

The EPR spectra were recorded on an X–band Varian E109 spectrometer equipped with an Oxford Instruments E9 helium flow–through cryostat and interfaced to a Digital Equipment Corporation (DEC) MINC–11 microcomputer. The spectra were digitized at 2048 points over the full sweep width using a 12–bit analog–to–digital converter and integrated directly on the MINC–11. The spin susceptibility was determined using a $MoS_2(S_2CNEt_2)_3$ standard whose susceptibility was independently calibrated using both a dc vibrating magnetometer and an National Bureau of Standard ruby standard. Parameters for recording EPR spectra were typically: 100 Gauss/min. sweep rate, 10 Gauss peak to peak modulation amplitude, 100 kHz modulation frequency, and 0.1 mW incident microwave power, depending on the temperature.

Table 9.1.1 **Various Forms of Nitrous Oxide Reductase**

Form	Observations or Characteristics
A ('purple')	High–activity form; ca. 8 Cu per Mr 140 Da; isolated anaerobically (except IEF); 7 line EPR hyperfine splitting (ref. 2,3).
B ('cathodic')	Part of form A that focuses in IEF towards the cathode at pI 5.06; integrity closest to native enzyme (ref. 3).
C ('anodic')	Part of form A that focuses in IEF towards the anode at pI 4.97; integrity closest to native enzyme (ref. 3).
D ('pink')	Low–activity form; ca. 7 Cu per Mr; isolated aerobically; 4–5 line EPR hyperfine splitting (ref.1).
E ('blue')	Catalytically inactive; obtained from A, B, C or D upon addition of reductant; largely featureless EPR; indications for presence of type I Cu (ref. 1–3).
F ('pH 9.8')	Form A after 24 hr. dialysis against 50 mM CHES buffer at pH = 9.8. Specific activity increases 10 fold (ref.1).

ESE data were recorded on the home built spectrometer operating at several resonance frequencies in X–band, as discussed in Chapter 3. Above 4.2 K, either an overcoupled TE102 microwave cavity or a slotted tube resonator mounted directly on the quartz insert dewar of an Oxford Instruments E9 helium flow cryostat was used.[10] Below 4.2 K, a slotted tube resonator mounted in a Janis variable temperature cryostat was used. Typically, 400 data points were recorded in the time domain with 20 or 30 nsec increments between data points and at a 100 Hz repetition rate. Cosine Fourier transformation was performed after subtracting the spin relaxation decay function using a polynomial fit and zero filling to 2048 data points. No back extension method is used to reconstruct the "dead time" missing piece.

II. EPR Studies

EPR spectra were recorded for the oxidized and reduced pink, purple, and cathodic forms of the enzyme as well as the purple enzyme at pH9.8, over the temperature range 5 K to 50 K. Representative spectra, recorded at 10 K, for the oxidized (active) and reduced (inactive) forms of the enzyme are shown in Figures 9.2.1 and 9.2.2, respectively. Spectra were recorded under a variety of operating conditions to check for possible lineshape distortion effects, particularly microwave power saturation and rapid passage effects. The onset of power saturation was established by determining the microwave power at which the signal intensity no longer doubled for a 6 dB change in incident power. At a given temperature, the onset of power saturation varied slightly ($\sim$ 20 %) among the different forms of the enzyme. A more significant difference between saturation powers was observed between each of the oxidized and their respective reduced forms. In this case, power differences of a factor of two were typically observed at T $\sim$ 10 K.

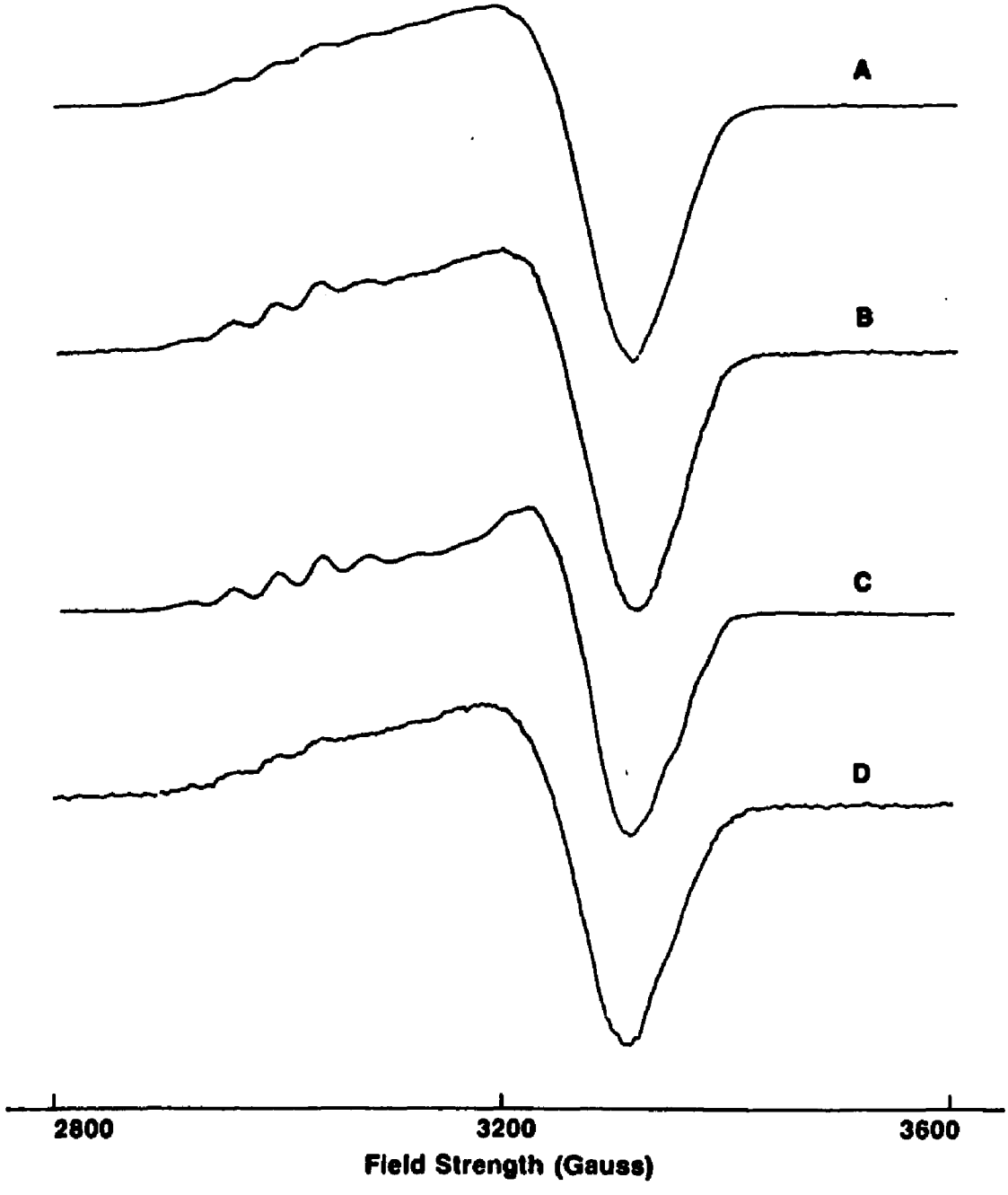

Figure 9.2.1 X–band EPR spectra taken at 10 K for various oxidized forms of N_2O reductase: (A) pink form; (B) purple form; (C) cathodic form; (D) purple form at pH 9.8.

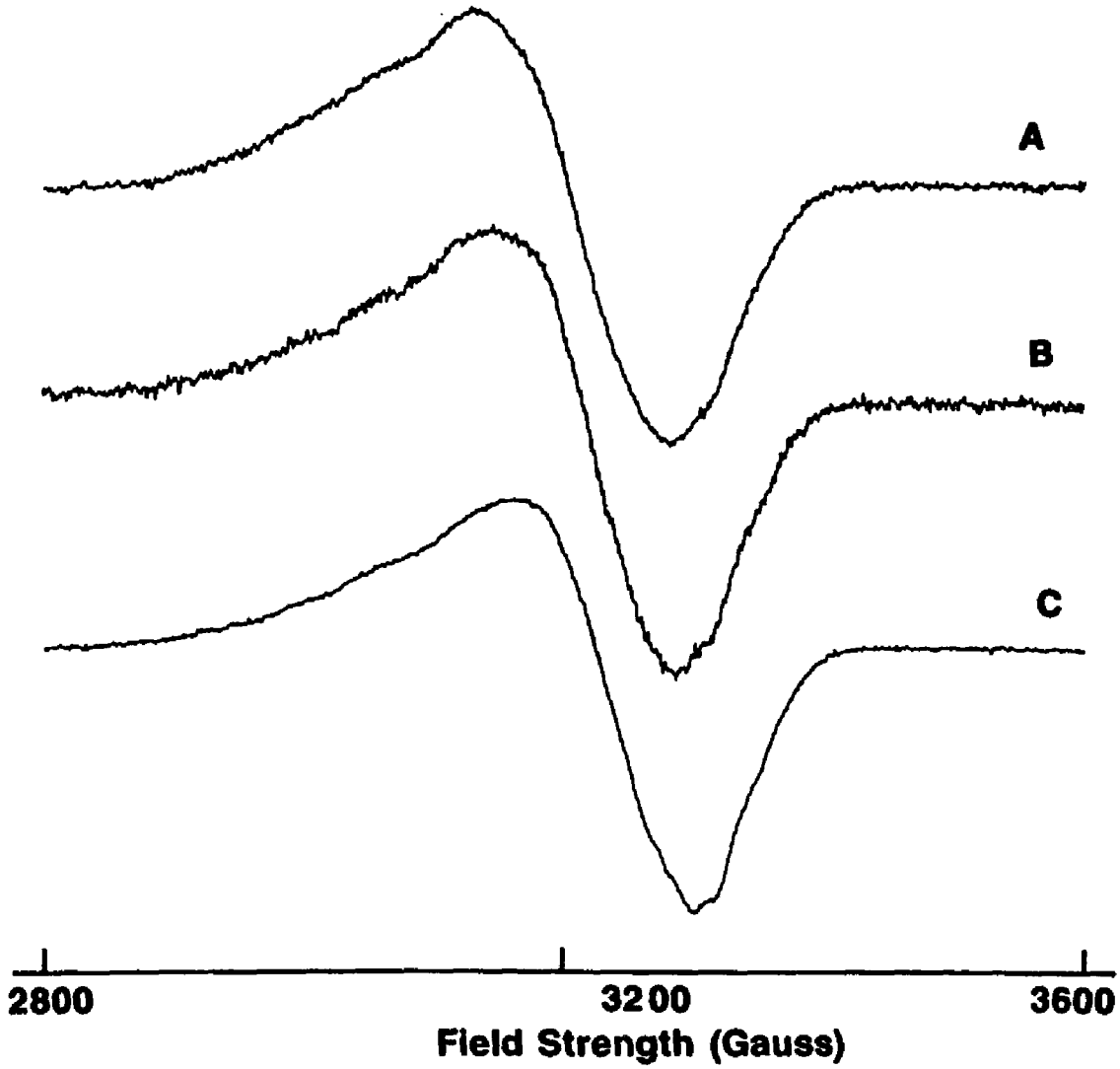

Figure 9.2.2 X–band EPR spectra taken at 10 K for various reduced forms of N_2O reductase: (A) pink; (B) purple; (C) cathodic.

In previous EPR studies of this enzyme, four to seven copper hyperfine splitting was observed. An exception to this trend was the pH 9.8 form (D of Figure 9.2.1), which had the highest activity but the poorest resolution of the hyperfine splitting pattern. At 10 K, the EPR linewidth decreased in the order: pink, purple, and cathodic, with the purple sample at pH 9.8 again exhibiting an anomalously broad line, comparable to the linewidth for the pink form. The resolution of the hyperfine splitting also depended on the temperature and the optimum temperature varied for each form of the enzyme.

An unusual feature of N_2O reductase is that an EPR signal is still observed after the enzyme is reduced with an excess of dithionite. Although it is possible that N_2O reductase has some copper sites with an anomoulously low reduction potential, a more reasonable explanation is that the EPR is due to the inaccessibility of some of the copper sites to the reductant. The spectra for each of the reduced enzymes are shown in Figure 9.2.2. Weak hyperfine splittings characteristic of type 1 (blue) copper are observed for the reduced enzymes. Recent resonance Raman results on the reduced enzyme also suggested that the copper sites were typical type 1, blue copper sites.[12] Additional hyperfine structure is observed for the reduced purple enzyme at pH 9.8; however, this enzyme became partially denatured upon addition of excess dithionite as evident by the formation of a precipitate.

The broadening of the linewidth, and the poorer resolution of the hyperfine splittings may indicate that subtle differences exist in the copper coordination among the different forms of the enzyme. Alternately, it may indicate that there are different EPR active copper sites and the relative concentration of these sites depends on the form of the enzyme. In this case, copper sites with slightly different g–values but similar hyperfine splittings may be present in different amounts for the different forms of the enzyme. This is consistent with the observation that the

hyperfine splittings for each of the two individual components (cathodic and anodic) of the purple form are better resolved than that observed for the purple form itself. The resolution is better for the cathodic form than for the anodic form, consistent with the higher enzyme activity of the cathodic form. In addition, the apparent $g_{\|}$ value for the cathodic form is shifted slightly with respect to the anodic form. This can account for the lower resolution observed for the purple form, which is actually a mixture of the cathodic and anodic forms. It is likely that at pH 9.8, some of the sites that were EPR silent at pH 7.5 become EPR active. If these new sites have slightly different EPR properties than those present at pH 7.5, the superposition of the EPR signals would result in an increase in the EPR susceptibility, broader EPR linewidth, and decreased resolution of hyperfine splittings.

The temperature dependence of the EPR susceptibility for the pink, purple, and cathodic forms of the enzyme are shown in Figure 9.2.3. The inverse of the molar susceptibilities of the oxidized enzyme are shown in A of Figure 9.2.3, and the inverse of the "normalized" susceptibilities, where $\chi_{\text{normalized}} = \chi_{\text{oxidized}} - \chi_{\text{reduced}}$, are plotted in B of Figure 9.2.3. EPR susceptibilities for all forms of the enzyme (χ_{oxidized}, χ_{reduced}, and $\chi_{\text{normalized}}$) follow the Curie's law, $1/\chi = A(T-T_c)$ with $T_c < 2$ K (the experimental precision on the Curie temperature). The percentage of the copper that is EPR active can be calculated from the slope of the inverse susceptibility curves in Figure 9.2.3. These results are summarized in Table 9.2.1. Both χ_{oxidized} values (A of Figure 9.2.3) and $\chi_{\text{normalized}}$ (B of Figure 9.2.3) decrease monotonically with enzyme activity for the pink, purple, and cathodic enzymes. Differences in EPR susceptibility observed between the enzyme from different preparations correlate with corresponding differences in enzyme activity. A notable exception is observed for purple enzyme at pH 9.8 which had the highest activity and the highest susceptibility. This is consistent with the formation of new EPR active sites at high pH.

Figure 9.2.3 Temperature dependence of inverse EPR susceptibility for various forms of N_2O reductase. (A) Total susceptibility for the oxidized enzymes; (B) normalized susceptibility obtained by subtracting the susceptibility for the reduced enzymes from (A).

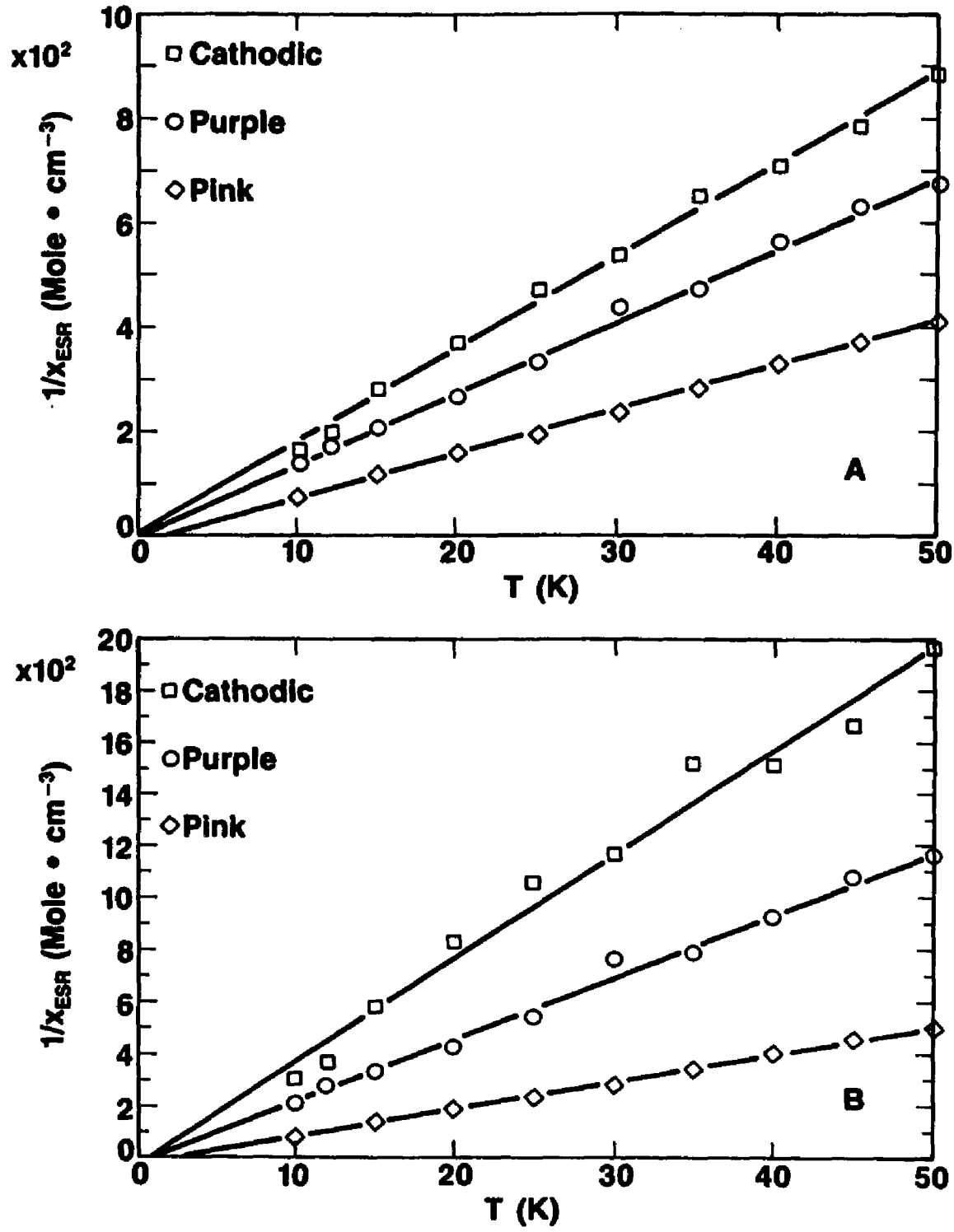
x10²
1/χESR (Mole • cm⁻³)
Cathodic
Purple
Pink
A
T (K)
x10²
1/χESR (Mole • cm⁻³)
Cathodic
Purple
Pink
B
T (K)

Figure 9.2.3

Table 9.2.1 List of Percentage of Cu Which is EPR Active from the EPR Susceptibility Measurements on N_2O Reductase

Form of Enzyme	Oxidized	"Normalized"
PINK	31.2	5.7
PURPLE	19.3	11.2
CATHODIC	15.0	6.7
pH 9.8 (from purple)	28.9	–

1. Measurement made within temperature range of 10 K – 50 K.

2. Curie–Weiss formula was used with Curie temperature of all forms less than 2.0 K, which is the experimental precision on Curie temperature.

Between 15 and 30 % of the copper sites are EPR active depending on the form of the enzyme, the pH, and the particular enzyme preparation. The magnetic coupling between these EPR active sites is very small, as indicated by the very small values of T_c. No EPR signal was observed near g = 4 as would be expected for weakly coupled copper dimers. The remaining copper is EPR inactive, and most likely associated with strongly coupled Cu(II) dimers with an antiferromagnetic exchange coupling greater than 200 cm^{-1}. The EPR silent sites are not likely to be Cu(I) sites because the EPR is not affected by ferricyanide oxidation.

The enzyme activity decreases and the number of copper sites that are EPR active increases upon lowering the pH from 7.5 to 6.0. Furthermore, the seven line hyperfine pattern sharpens significantly on lowering the pH from 7.5 to 6.0 (compare A of Figures 9.2.4 (purple, pH 7.5) and 9.2.5 (purple, pH 6.0)). These results are similar to the trends observed for hemocyanin and tyrosinase where the concentration of the mixed valence Cu(I)/Cu(II) half–met sites increases upon lowering the pH.[8] These observations motivated exogenous azide binding studies as a spectroscopic probe of the copper sites. The addition of azide inhibits N_2O reductase activity and reduces the EPR susceptibility. The relative change in susceptibility is sensitive to the pH and to the amount of azide used. At pH 6.0, a 25 % decrease in the number of copper sites observed by EPR is obtained with a 2500–fold excess of azide. At pH 7.5, a 25 % decrease was also observed using only a 400–fold excess of azide. Addition of azide also resulted in the complete loss of the seven line hyperfine structure in the EPR spectrum (B of Figure 9.2.4). In addition, new weak hyperfine splittings characteristic of square planar, type 2 copper, were observed (B of Figure 9.2.5) for the sample at pH 6.0. Dialysis to remove excess azide and any type 2 Cu not bound to the protein did not restore the original EPR spectrum (C of Figure 9.2.5) and resulted in the loss of the type 2 Cu and a 20 % decrease in EPR susceptibility compared to the original value. The

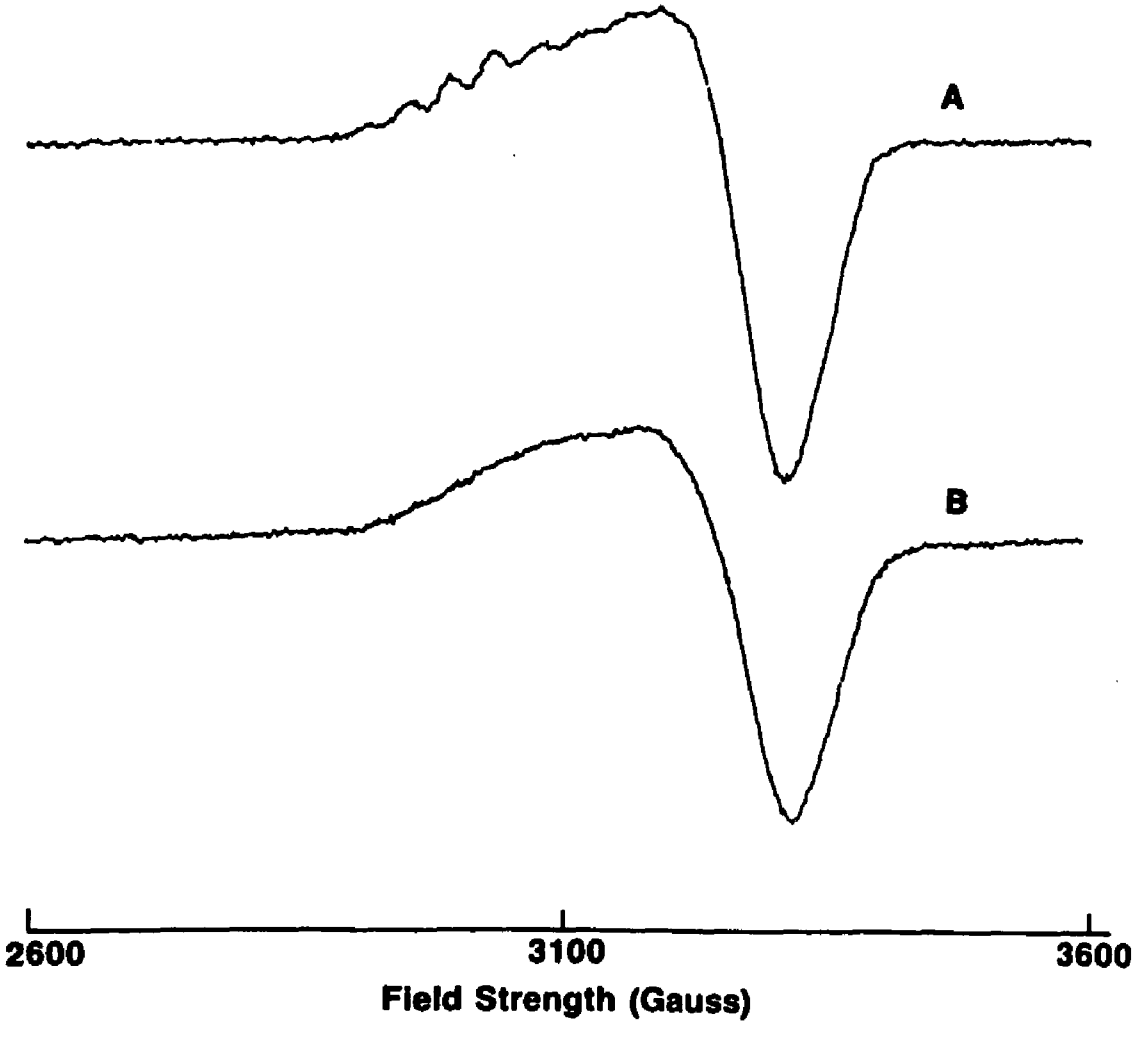

Figure 9.2.4 X–band EPR spectra for (A) oxidized purple enzyme at pH 7.5 and (B) after the addition of a 400–fold excess of azide over copper.

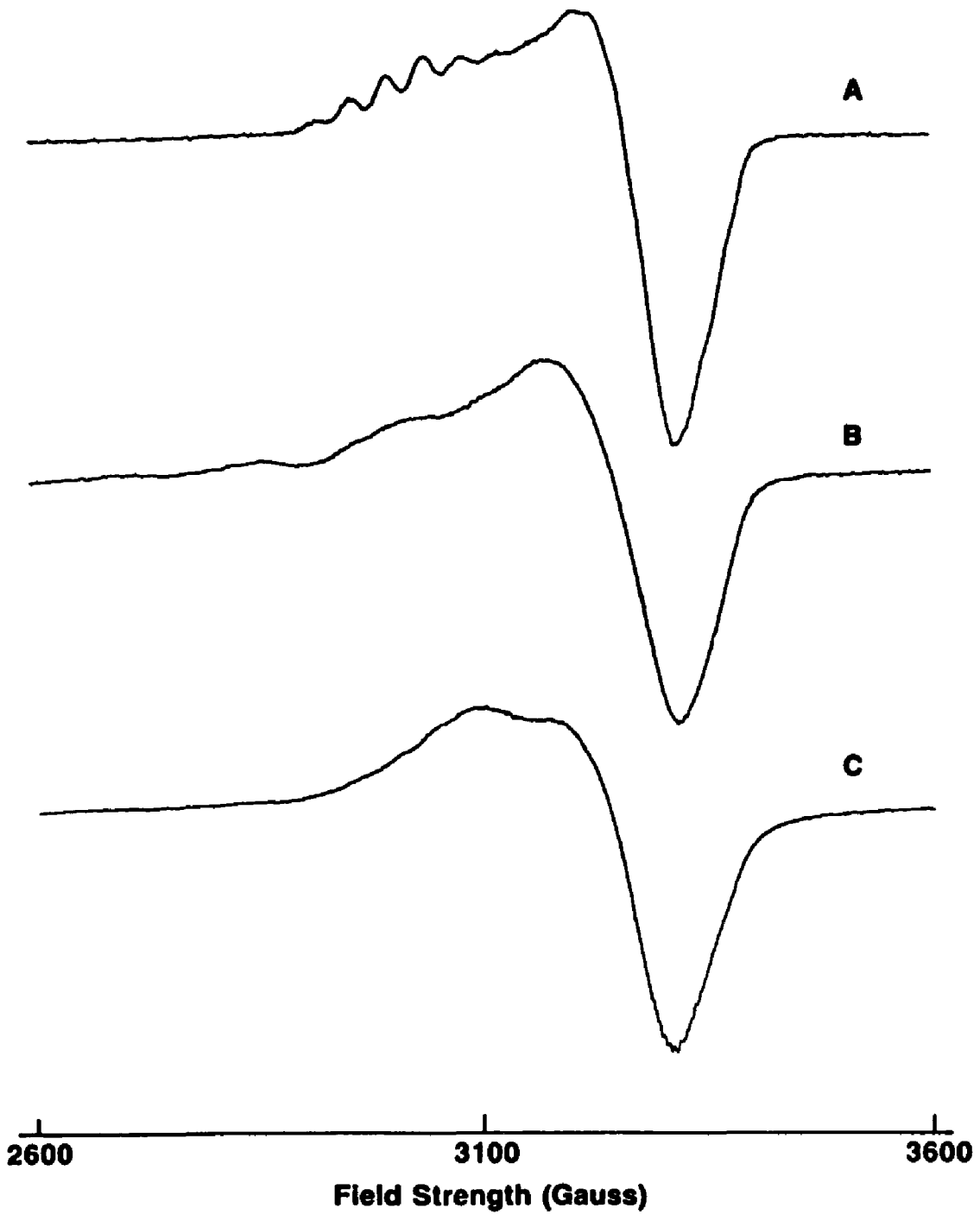

Figure 9.2.5 X–band EPR spectra for (A) oxidized purple enzyme at pH 6.0; (B) after adding a 300–fold excess of azide over copper; and (C) following dialysis for 4 hours after the azide addition.

resulting EPR spectrum (C of Figure 9.2.5) recorded at 10 K suggests a more isotropic magnetic interaction, consistent with a rapid electron exchange between the two copper atoms of a half–met site.[8] These results suggest that azide binds irreversibly to the EPR active sites.

Mechanisms by which azide binding can reduce the number of paramagnetically active sites are by oxidation of the cuprous ion in a half–met site, by bridging two uncoupled cupric ions to form a diamagnetic dimer, or by bridging a half–met (or dimer) site with a cupric ion to form a trimer. In hemocyanin and tryosinase, azide bridges the binuclear coupled copper site and reduces the strong antiferromagnetic exchange coupling between the coppers.[8] For this type of binding, azide addition would be expected to increase, not decrease, the EPR susceptibility. On the other hand, azide also binds to the binuclear copper site in laccase, but not as a bridging ligand.[8] In this case, the EPR susceptibility would not be expected to change with addition of azide. Neither of these two binding mechanisms appear to be operative in N_2O reductase since the EPR susceptibility decreases after azide addition. Two binding mechanisms consistent with the decrease in EPR susceptibility are for azide to bridge two closely lying Cu (II) ions or for the azide to bridge a cupric ion with a half–met site, forming effectively a copper trinuclear site. In either case, the azide bridging can increase the dipolar and exchange coupling between the EPR active copper ions to render them EPR silent. The Cu sites that remain EPR active after azide addition can be attributed to half–met sites where azide is bound, but not as a bridging ligand, or to the azide bridging of Cu(II) ions with EPR silent dimers, again forming an (EPR silent) trinuclear site. In either case, the non–bridged binding of azide can modify the copper hyperfine splittings (as observed) without modifying the EPR susceptibility.

II. ESE Studies of Nitrogen Coordination

The ESE envelope time domain waveforms observed at T = 1.8 K for the oxidized pink, and cathodic enzyme at pH 7.5 are shown in A and C of Figure 9.3.1. The most striking feature of the data is the extremely shallow modulation depth, roughly only 5% of the total signal intensity. The shallowness of the modulation depth is clearly evident by noting the modulation depth compared to the true baseline at longer time values, shown as inserts in Figure 9.3.1. The shallow modulation depth observed on the waveforms for N_2O reductase is in sharp contrast to that observed for most other copper proteins where intense modulation, typically 25% or more of the echo intensity, is observed for data recorded under similar experimental conditions.[13]

Low frequency oscillations are observed on the waveforms for the oxidized, but not on those for the reduced enzyme. The identification of these modulation frequencies is facilitated by Fourier transformation to obtain the ESE envelope spectra, shown in B and D of Figures 9.3.1, for the oxidized pink and cathodic enzymes. In addition to the proton peak at 13.6 MHz (not shown), complex spectra comprised of narrow lines at 1.5, 1.9, 2.5, 2.9, 3.4 MHz and broad lines between 0.7 – 0.9 and 3.6 – 4.0 MHz are observed for the oxidized pink and cathodic enzyme. The modulation frequencies are characteristic of nuclear quadrupole transitions observed for nitrogen atoms coordinated to Cu(II).[13] When the echo envelope modulation depth is extremely shallow, as in the present case, the assignment of peaks below 0.5 MHz becomes unreliable because low frequency peaks can be introduced by subtraction of the echo decay function. Although the paramagnetic susceptibility depends on the form of the enzyme, very little difference is observed in the low temperature echo envelope spectra, as evident in B and D of Figure 9.3.1.

Figure 9.3.1 Time domain electron spin echo envelope waveforms for oxidized N_2O reductase recorded at $T = 1.8$ K: (A) oxidized pink (aerobically isolated); (C) oxidized cathodic (anaerobically isolated); (B) and (D) are the Fourier transforms of (A) and (C) respectively. Other conditions: $\tau = 0.14$ μsec, $H = 3280$ gauss; $g = 2.03$. Inserts of the time domain waveforms show the baseline at the end of the data collection period.

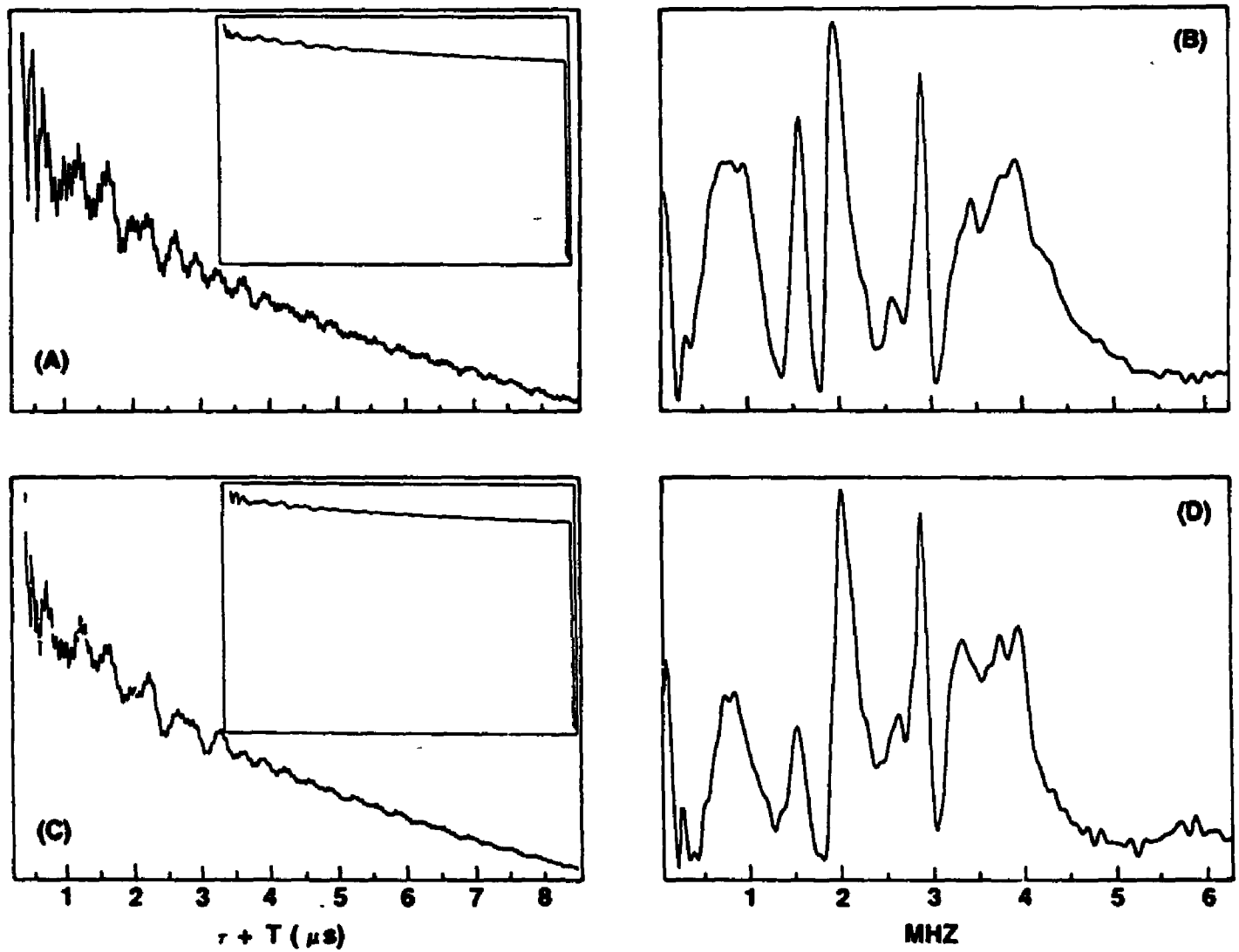

Figure 9.3.1

IV. ESE Studies of the Base–Activated Enzyme

A ten fold increase in catalytic activity has been observed after dialysis of the enzyme in buffer at pH 9.8.[3] As noted above, a 50% increase in EPR susceptibility was observed for the enzyme at pH 9.8 but no significant change was observed in the ESE modulation spectrum. Differences were observed in the deuteron modulation pattern for all forms of the enzyme dialyzed against D_2O. The waveforms for the purple oxidized enzyme at pH 7.5 and at pH 9.8 are shown in A and B of Figures 9.4.1, respectively. In order to facilitate comparison of the modulation depths, the echo amplitudes in A and B of Figure 9.4.1 have been normalized to the same vertical scale. It is apparent that the deuteron modulation depth for the enzyme at pH 9.8 is substantially deeper than that observed for the same enzyme at pH 7.5. The modulation depth of the purple enzyme at pH 9.8 is also substantially deeper than observed for the cathodic form at pH 7.5 (not shown).

A more direct demonstration of the deeper deuteron modulation on the purple enzyme at pH 9.8 is obtained by dividing the time domain waveform for the pH 9.8 sample by the time domain waveform for the purple sample that was used to prepare it, as shown in A of Figure 9.4.2. As discussed in Chapter 4, when more than one nucleus is coupled to the paramagnetic center, the total modulation depth depends on the product of the modulation depth due to each nucleus per copper center. For data collected under identical experimental conditions, the ratio of two time domain waveforms isolates any differences in modulation depth between the waveforms. The deuteron modulation period is clearly visible in the quotient time domain waveforms as shown in A of Figure 9.4.2. The waveform division method was also performed by dividing the time domain waveforms of the purple by cathodic samples, both at pH 7.5, as shown in B of Figure 9.4.2. In this case, only a smooth decay and no deuteron modulation is observed in the ratio of the two

Figure 9.4.1 Time domain spin echo envelope data for oxidized (A) purple enzyme at pH 7.5 and (B) purple enzyme at pH 9.8, enzyme dialyzed against D_2O buffer. The intensities were normalized against the first peak in the modulation for easy comparison of the relative modulation depths. Spectra were recorded at $T =$ 5 K, $\tau = 0.24$ μsec, other conditions are the same as for Figure 9.3.1.

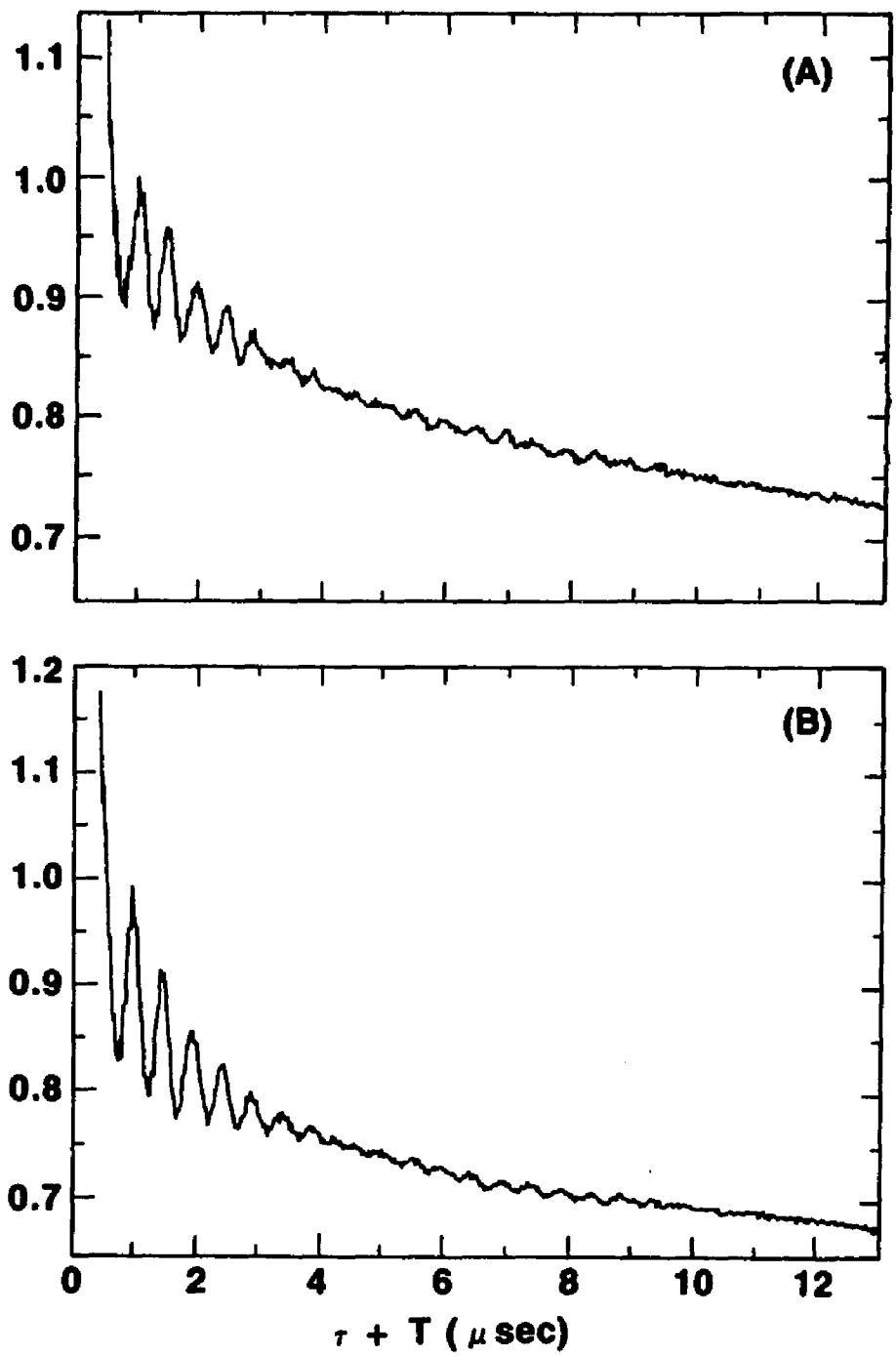

Figure 9.4.1

waveforms.

The deuteron modulation may arise from water or hydroxide in the inner or outer copper coordination sphere or from labile protons associated with the copper site. Based on comparison to the deuteron modulation data observed for amine oxidase[14] and several other Cu(II) complexes,[15] the modulation pattern observed is consistent with the presence of a directly coordinated protonated ligand.

The deeper deuteron modulation associated with the oxidized purple enzyme at pH 9.8 indicates that there are more deuterons associated with the EPR active sites at high pH. The increased susceptibility observed at pH 9.8 suggests that these additional deuterons result from a new EPR active site generated at higher pH that has more deuterons associated with it than the EPR active sites present at pH 7.5. Dissociation of the EPR silent dimeric copper sites at high pH has previously been invoked by Solomon *et al.* to account for similar changes in the EPR spectra of binuclear copper sites.[8]

An alternate interpretation is that the deeper modulation at high pH arises from additional water or hydroxide in the inner or outer coordination sphere of the copper that is EPR active at pH 7.5. This increased proton accessibility would be consistent with either a pH–induced protein conformational change or base–catalyzed proton exchange allowing enhanced access to the copper sites.

Figure 9.4.2 Ratio of spin echo envelope time domain waveforms for various oxidized enzymes dialyzed against TRIS buffer in D_2O: (A) purple at pH 9.8 over purple at pH 7.5; (B) purple at pH 7.5 over cathodic at pH 7.5.

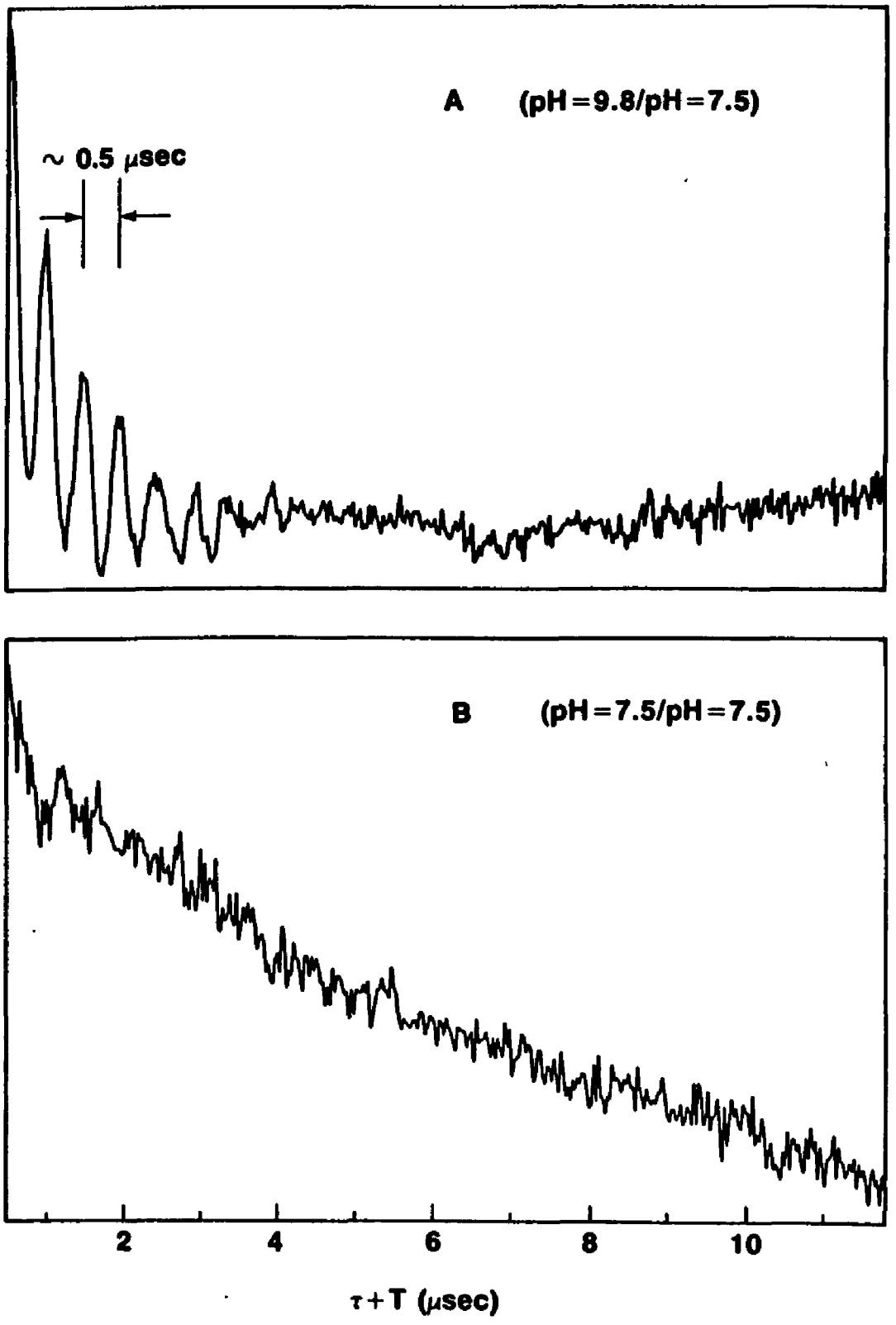

Figure 9.4.2

CHAPTER 10

DISCUSSION

According to the EPR susceptibility data, an apparent inverse correlation exists between the activity of the enzyme and the number of copper sites observed by EPR. In other words, EPR active Cu sites may not represent the catalytically active sites. Nevertheless, EPR and ESE studies provide important information about the catalytically active copper sites. EPR and ESE experiments are used to systematically follow changes in the structure of the EPR active sites between the different enzyme forms. Furthermore, the number of EPR active sites can be reversibly increased by changing the pH, in effect "turning on" the EPR silent copper sites for spectroscopic study. Additionally, exogenous ligands can be used as spectroscopic probes of EPR silent sites. Such experiments have been of considerable value in elucidating the structure of the EPR silent sites in other binuclear copper enzymes such as hemocyanin and tyrosinase.[8] Finally, the results of the EPR and ESE experiments are correlated with other experiments including CW–ENDOR, [26] extended X–ray absorption fine structure (EXAFS),[16] resonance Raman,[10] and chemical analysis[1-3] to develop a consistent spectroscopic model of the catalytically active copper sites.

I. Characterization of EPR Active Copper Sites

The hyperfine pattern in the EPR spectrum of N_2O reductase is not

characteristic of either type 1 or type 2 centers in copper proteins.[17] One possibility is that the spectrum arises from the overlap of two type 1 copper spectra with $A_{\|} \sim$ 80 G and a relative shift in $g_{\|} \approx A_{\|}/2$. This would result in an eight line hyperfine pattern (the eighth line is not resolved) with equal line intensities, in rather poor agreement with the approximately 1:2:3:4:3:2:1 intensity ratio observed in the experimental spectra. Two other possibilities are that the unusual hyperfine pattern arises from the superposition of two spectra from type 1 copper sites or from a mixed valence Cu(I)/Cu(II) half–met site. A seven line copper hyperfine pattern can be obtained from the partial overlap of the spectra for two type 1 copper centers. An intensity ratio of 1:1:1:2:1:1:1 can be obtained if the $A_{\|}$ hyperfine coupling is ~ 38.5 G (which is unusually small) and if the shift in $g_{\|}$ between the two sites is also approximately equal to $A_{\|}$ so that only one line of the two four line hyperfine patterns overlap. On the other hand, a seven line hyperfine pattern with an intensity ratio 1:2:3:4:3:2:1 and a hyperfine splitting one half the value of the usual blue copper value is expected for a mixed valence half–met site in which the unpaired electron spin density is shared equally between the two copper ions. The binuclear structure of the half–met site provides a natural mechanism for more extensive delocalization of the paramagnetic electron, compared to the usual blue copper center. This delocalization provides a mechanism for reducing the unpaired electron spin density on a particular ligand, consistent with the shallow modulation depth and unusually small contact hyperfine coupling observed in the ESE experiments. While it would be highly fortuitous to obtain the relationship between the two unusual type 1 coppers, where $A_{\|}$ is exactly one half the value typically observed for type 1 copper, it is not possible, based on the EPR results alone, to unambiguously distinguish between a mixed valence half–met site and these unusual type 1 sites. However, EPR experiments at other microwave frequencies[17] and the ESE results discussed below indicate that the EPR spectrum is comprised of

contributions from both the half–met and the unusual Cu(II) type 1 sites.

The electron spin echo modulation data for N_2O reductase differs markedly from that observed for most other copper proteins.[12] Intense (typically 25% or more of the echo intensity) low frequency modulation on the echo envelope waveforms is generally observed for all copper proteins containing type 1 or type 2 Cu(II) centers. This arises from the interaction of the paramagnetic electron on the Cu(II) ion with a nitrogenous ligand; usually the distal (N1) nitrogen on a coordinated imidazole ligand. The labelling of nitrogen on an imidazole ring is shown in Figure 7.2.1. Nuclear quadrupole transitions on this nitrogen can give rise to up to three peaks for each of the electron spin manifolds. The actual number of peaks observed depends on the relative magnitudes of the quadrupole and hyperfine couplings and on the hyperfine anisotropy and quadrupole asymmetry.[13] When the applied magnetic field is chosen so that the nuclear Larmor frequency will be canceled by the hyperfine coupling in one of the electron manifolds, three narrow pure nuclear quadrupole transitions are observed below 1.7 MHz in the echo envelope spectrum. In addition, a broader line near 4.0 – 4.5 MHz, corresponding to the double quantum transition in the other electron manifold, is usually observed. In contrast, an extremely shallow modulation depth (approximately 5 % of the echo intensity) and uncharacteristic peaks in the modulation spectrum are observed for N_2O reductase. The spectra for N_2O reductase also contain many more peaks than are usually observed for type 1 or type 2 Cu(II) proteins. It is not likely that these additional peaks are due to combination frequencies arising from the coupling to more than one magnetically equivalent nitrogen (from more than one magnetically equivalent imidazole ligand on the same Cu(II) complex)[18] because the coefficients of the product frequencies will be extremely small due to the extremely shallow modulation depth.

One possible interpretation of these results is that the paramagnetic center in

N_2O reductase is not a paramagnetic Cu(II) site. However, the EPR spectrum clearly exhibits resolved Cu nuclear hyperfine splittings (albeit with an unusual hyperfine coupling pattern) which are not observed in the spectrum of the reduced inactive enzyme. The low frequency components in the echo envelope modulation pattern are also not observed for the reduced enzyme. Furthermore, only Cu is found by chemical analysis, the enzyme is inactivated, and no EPR signal is observed after Cu is removed from the enzyme.

Another possibility is that the echo envelope spectrum does not arise from an endogenous ligand but rather from the interaction with nitrogen atoms in the TRIS buffer. Interaction with nitrogen from the TRIS buffer was checked by repeating the ESE experiments on protein which was dialyzed against phosphate buffer. The spectra for these samples gave identical spectra to the samples run in TRIS buffer, ruling out the possibility that the low frequency modulation on the echo envelope waveform arises from interaction with a nitrogen in the buffer.

II. Numerical Simulation of ESE Frequency Spectra

Numerical simulations were used to aid in identifying the possible nitrogen containing ligands giving rise to the modulation spectrum observed for N_2O reductase. As discussed in Chapter 3, the complexity of the simulation and the number of unknown parameters is greatly reduced by ignoring the anisotropic components of the electron–nuclear dipolar interaction. Neglect of anisotropic components may result in artificially narrow lines and the relative peak intensities will not be correctly represented in the simulated spectrum. Despite these obvious limitations, the hyperfine contact coupling and principal values of the quadrupole interaction can be accurately assigned using this simplified Hamiltonian. It is these interactions that determine the number of lines and the line positions in the ESE

envelope spectrum. Furthermore, the extremely shallow modulation depth observed in the experimental results suggests that the anisotropic contribution to the hyperfine interaction is small so that neglecting the hyperfine anisotropy provides a good first order approximation to the experimental frequency spectrum.

A further simplification can be achieved if a frequency histogram is calculated by sampling orientations uniformly over the hemisphere. It is possible that a more accurate treatment of the orientational averaging process could be achieved by utilizing the "orientation selection" scheme described in Chapter 3. However, spherical averaging provides a good approximation at $g_{\perp}$. In their ESE studies of the copper binding site in phenylalanine hydroxylase, McCracken *et al.*[18] compared the simulations of ^{14}N modulation using spherical averaging to those using "orientation selection" averaging. With identical parameters, the differences between the two are minor and would be difficult to distinguish experimentally. The reason for the validity of the spherical averaging in this instance probably stems from the ESEEM being dominated primarily by the NQI, which is independent of magnetic field direction. Another example is the nitrogenase MoFe protein from *Clostridium pasterianum.* As discussed in Chapter 7, the spherical averaging method was used to simulate the ESEEM spectra taken at $T \sim 5$ K. The coupling parameters obtained from the method are close to what were obtained from simulations with "orientation selection" considerations. It should be noted, however, that this approximation will not be valid in all cases, and the uncertainty in the parameters derived from such simulations is difficult to estimate.

Reasonable starting values for the quadrupole terms can be obtained from zero field quadrupole frequency measurements.[21] Spectra are computed for the appropriate magnetic field value and for a range of quadrupole and hyperfine contact interactions. The ESE envelope spectrum can be simulated using three sets of ^{14}N quadrupole coupling parameters. The corresponding spectra are shown in A

and C of Figures 10.2.1.

The computed spectrum shown in A of Figure 10.2.1 is obtained for an ^{14}N with $e^2qQ/h = 1.44 \pm 0.2$ Mhz, $\eta = 0.7 \pm 0.3$, and a hyperfine contact coupling, $A_{iso} = 0.6 \pm 0.1$ MHz. These quadrupole parameters are characteristic of a protonated distal nitrogen, N1, but with an unusually small A_{iso}, on an imidazole ligand bound to Cu(II). The broad absorption centered at 1.2 MHz is comprised of the ν_0 and ν_- nitrogen quadrupole transitions in the upper and lower electron manifolds. This broad absorption is not readily observed in the experimental spectrum because of the finite spectrometer dead time. Hyperfine anisotropy will further broaden these lines making them even more difficult to detect experimentally. The two main narrow peaks at 1.9 and 2.9 MHz are the two $\Delta M_I = 2$ double quantum nitrogen nuclear transitions, arising from the upper and lower electron manifolds. When $A_{iso}/2 < \omega_N$, these double quantum transitions are narrow compared to the single quantum quadrupole transitions so that they are the only lines detected in the experimental spectrum. Unfortunately, the double quantum lines are less sensitive to the quadrupole asymmetry resulting in the relatively large uncertainty in η.

The spectrum computed for the second ^{14}N, shown in B of Figure 10.2.1, is obtained for $e^2qQ/h = 1.53 \pm 0.2$ MHz, $\eta = 0.87 \pm 0.05$, and $A_{iso} = 1.65 \pm 0.05$ MHz. In model copper–imidazole complexes, hydrogen bonding of the N1 nitrogen has been observed to increase e^2qQ/h by 0.1 MHz but has little effect on the quadrupole asymmetry.[22] The quadrupole parameters for the second nitrogen are therefore assigned to the distal nitrogen on an imidazole ligand bound to Cu(II). The hyperfine contact coupling of 1.65 MHz is closer to the value of 1.8 to 2.0 MHz typically observed for protonated imidazole ligands in type 1 and type 2 copper proteins and copper imidazole complexes. This value is close to the value which

Figure 10.2.1 Simulated spin echo envelope spectra for various nitrogenous ligands. The quadrupole coupling, e^2qQ/h (MHz); quadrupole asymmetry, η; and hyperfine contact couplings, A_{iso} (MHz), are: (A) 1.44, 0.7, 0.6; (B) 1.53, 0.87, 1.65; (C) 2.3, 0.76, 0.65. Other conditions: $g = 2.03$, $H = 3280$ gauss. The weighted intensities for spectrum D are: 1.0 × A + 0.8 × B + 0.2 × C.

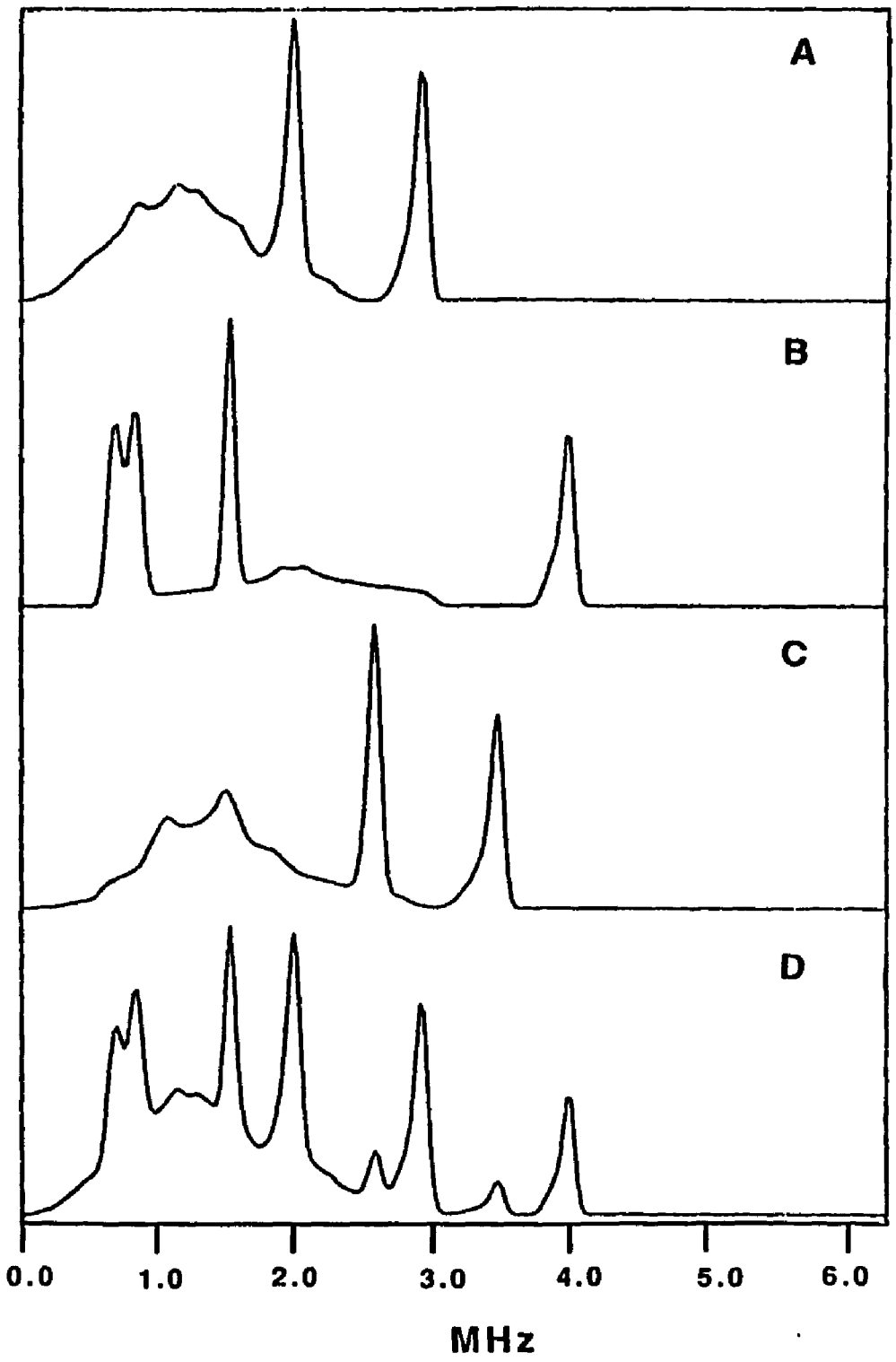

Figure 10.2.1

cancels the ^{14}N nuclear Zeeman splitting and gives rise to the narrow pure nuclear quadrupole resonance lines shown in B of Figure 10.2.1.[13] The doublet centered at 0.8 MHz corresponds to the ν_0 and ν_- transitions while the narrow line at 1.5 MHz corresponds to the ν_+ transition in one of the electron manifolds. The line at 3.8 MHz corresponds to the $\Delta M_I = 2$ transition in the other electron manifold and occurs at approximately $2\omega_N + A_{iso}$. The broad absorption centered at 2 MHz arises from the ν_0 and ν_- transitions in this electron manifold. This broad absorption is not readily observed in the experimental spectrum because of the spectrometer dead time.

The spectrum computed for the third ^{14}N, shown in C of Figure 10.2.1, is obtained for $e^2qQ/h = 2.3 \pm 0.2$ MHz, $\eta = 0.76 \pm 0.15$, and $A_{iso} = 0.65 \pm 0.1$ MHz. The comments made for the spectrum obtained for the first nitrogen, A of Figure 10.2.1, apply equally well to the spectrum obtained from the third nitrogen. Only the double quantum nitrogen quadrupole transitions in the two electron manifolds are observed in the experimental spectrum. The quadrupole interaction of 2.3 MHz is close to that derived from NQR measurements on amide nitrogens[21] and also to that deduced from ESE measurements on substituted imidazole copper complexes.[22] However, for both the amide and the substituted imidazole nitrogens, the quadrupole asymmetry observed is much smaller than that derived from the present experimental results. But, as mentioned above, the double quantum transitions are sufficiently insensitive to the value of the quadrupole asymmetry that either of these could be possible ligands.

The composite spectrum, shown in D of Figure 10.2.1, is obtained by summing A, B and C in Figure 10.2.1, using the weighted intensities of 1.0, 0.8, and 0.2, respectively. This spectrum reproduces the correct number of lines and the correct line positions of the experimental spectrum. As mentioned above, the broad absorption centered at 1.2 MHz is not expected to be observed in the experimental

spectrum because of the finite spectrometer dead time. Hyperfine anisotropy will further broaden the lines observed in the experimental spectrum compared to those in the computed spectrum.

Modulation from directly coordinated nitrogen ligands is not observed on the echo envelope in tetrahedral or square planar copper complexes.[13] However, modulation from directly coordinated axial nitrogen ligands can be observed in five or six coordinate copper complexes.[23] In ESE studies of copper complexes with directly coordinated axial nitrogens, the quadrupole couplings were observed to be larger than those typically obtained for the distal nitrogen on imidazole ligands bound to Cu(II). It is therefore possible that the quadrupole interaction of 2.3 MHz could arise from an axially coordinated nitrogen on a five or six coordinate copper complex. This would most likely be on a copper in the mixed valence half–met site since this possibility is consistent with the g–values and Cu hyperfine splittings observed in the EPR spectrum.

III. Presence of Copper A Sites

Unusual EPR and ESE results have previously been reported for the Cu_A site in cytochrome c oxidase.[24] The EPR spectrum has poorly resolved copper nuclear hyperfine splittings and unusual g–values.[24b] The spin echo envelope modulation spectrum for the Cu_A also does not resemble the spectra typically observed for either type 1 or type 2 sites in copper proteins.[24c] An uncharacteristically shallow modulation depth was observed with modulation frequencies at 0.9, 1.5, 1.9, 3.2, and 4.3 MHz. The ESE results observed for cytochrome c oxidase, while highly anomalous compared to other copper proteins, are very similar to the results for N_2O reductase. In addition to the similarity in modulation depth, a matched set of lines for cytochrome c oxidase are observed in the ESE envelope spectrum of N_2O

reductase. The lines at 0.9, 1.5, and 4.3 MHz in the spectrum of cytochrome c oxidase correspond to the lines at 0.8, 1.5, and 3.8 MHz in the spectrum of N_2O reductase. The double quantum line at 4.3 MHz occurs at a slightly higher frequency because of a slightly larger hyperfine contact coupling compared to N_2O reductase.[25] The lines at 1.9 and 3.2 MHz observed for cytochrome c oxidase correspond to the lines at 1.9 and 2.9 MHz observed for N_2O reductase. The slightly larger frequency splitting between these lines in cytochrome c oxidase can again be accounted for by a slightly larger hyperfine contact coupling.[25] By analogy to the ESE envelope spectra for the Cu_A site in cytochrome c oxidase, we conclude that the two imidazole ligands assigned to the lines at 0.8, 1.5, 3.8 MHz and 1.9, 2.9 MHz in the spectrum of N_2O reductase are coordinated to the Cu_A site. This is consistent with the conclusion derived above, that the nitrogenous ligand giving rise to the pair of lines at 2.5 and 3.4 MHz is coordinated to the half–met site.

The smaller hyperfine contact coupling observed for the two distal nitrogens on the imidazole ligands of the Cu_A site implies a reduced unpaired spin density on these N1 nitrogens. This in turn suggests a reduced unpaired spin density on the directly coordinated (N3) nitrogen of the imidazole ligand. In recent Q–band ENDOR studies on the Cu_A site in cytochrome c oxidase, Werst *et al.*[26] observed two ^{14}N ENDOR resonances corresponding to hyperfine contact couplings of 8.7 and 17.6 MHz which are substantially smaller than the more typical values of 16 – 23 and 32 – 49 MHz for the two directly coordinated N3 nitrogens in other copper proteins[27] and copper tetraimidazole model compounds.[28] Based on the similarities between the ESE results on the Cu_A sites, it is anticipated that the contact hyperfine couplings on the N3 imidazole nitrogens in N_2O reductase will also be substantially reduced compared to type 1 and type 2 copper centers, analogous to the results for cytochrome c oxidase. In a recent Q–band ENDOR experiment, Nakagawa *et al.*[29] observed one type of nitrogen resonance with hyperfine coupling

of 16 MHz on a new form of N_2O reductase. This enzyme was obtained from a mutant strain, with defective Cu chromophore biosynthesis. It has ~ 2 Cu per protein, out of which 50 % are EPR–detectable. It is thought that these EPR–detectable Cu sites are also present in the purple form, corresponding to the Cu_A sites. Since the number of nitrogen ligands can not be determined by the ENDOR experiment, it is possible that both of the direct coordinated nitrogens from the two inequivalent imidazole ligands are responsible for the observed resonance frequencies. The indistinguishability of ENDOR frequencies between two direct coordinated nitrogens can be explained, if these two nitrogens are in a similar environment, while the two distal ones are in slightly different environment. The absence of signals from distal nitrogen in ENDOR experiment may have the same origin as in the case of the MoFe protein. Frequencies due to nitrogen ligated to FeMoco is fairly pronounced in the ESEEM experiment, but were not detected by previous CW–ENDOR experiment.[32] This again shows the complementary nature of two spectroscopies.

The smaller hyperfine contact coupling on the N3 nitrogen would also be expected to result in a reduced hyperfine anisotropy. Since the anisotropic components of the hyperfine interaction determines the depth of the modulation on the echo envelope waveform,[13,19] a reduced anisotropy is consistent with the unusually shallow modulation depth observed. However, we can not exclude the possibility that other copper centers are present in the oxidized enzymes (such as those observed after dithionite reduction) which contribute to the echo intensity but do not contribute to the echo envelope modulation.

Finally, the identification of the Cu_A site in N_2O is further supported by conclusions from other spectroscopic studies[10,16] and from recent genetic sequencing studies[30]. Both the EXAFS and magnetic circular dichroism (MCD)[16] data on N_2O reductase appear to be remarkably similar to the data obtained for cytochrome c

oxidase and different from those obtained for type 1 or type 2 copper protein. In the genetic sequencing studies, the amino acid residues Cys–618, His–622, His–626 and Met–629 show a matched spacing and conserved serin, resembling the proposed Cu_A site of cytochrome c oxidase subunit II.

VI. The Spectroscopic Model

The spectroscopic model for the Cu sites in N_2O reductase that emerges from the present EPR and ESE study is that in the oxidized enzyme, between 70 and 85 % of the copper ions are in the form of EPR silent binuclear type 3 dimers. Between 15 and 30% of the copper ions are EPR active and are comprised of mixed valent half–met sites and isolated cupric sites. The ESE data are also consistent with the presence of multiple chemically inequivalent Cu(II) sites with imidazole coordination. Based on the strong similarity of their ESE results, we conclude that the cupric sites are unusual Cu(II) sites, very similar to the Cu_A sites in cytochrome c oxidase. This is the first time that the Cu_A site has been observed in an enzyme other than cytochrome c oxidase. The additional frequencies in the ESE envelope spectra of N_2O reductase which are not observed in the spectra of cytochrome c oxidase most likely arise from an amide or substituted imidazole ligand coordinated to the EPR active half–met site. Further evidence for the presence of a Cu_A site has been obtained from the results of recent genetic sequencing studies on N_2O reductase[30] where resemblance to the proposed Cu_A site of cytochrome c oxidase subunit II has been found.

Resonance Raman[12] and EXAFS[16] data are consistent with the proposed model. Dooley et al. have reported a resonance Raman study of N_2O reductase and suggested that the activity correlates with the presence of a Cu(II)S2(Cys)N(His) site.[12] EXAFS data suggest the presence of multiple copper sites with greater

covalency than that usually observed for copper proteins.[16] In addition, both the EXAFS and MCD data on N_2O reductase appear to be remarkably similar to the data obtained for cytochrome c oxidase and different from that obtained for type 1 or type 2 copper proteins. Finally, the Q–band CW–ENDOR results on N_2O reductase are similar to those for cytochrome c oxidase, substantiating the expected presence of greatly reduced hyperfine coupling for the directly coordinated nitrogens.

Deeper deuteron modulation is observed for the oxidized enzyme at pH 9.8, indicating that there are more deuterons associated with the EPR active sites at higher pH. The ESE data indicates the presence of a coordinated deuterated ligand, most likely water or hydroxide. It is possible that this deuteron coupling is a consequence of either a pH–induced conformational change or a base–catalyzed proton exchange allowing enhanced access to the copper sites and accounting for the ten fold increase in enzyme activity. It is more likely, however, that at pH 9.8 a new copper site becomes EPR active which has more exchangeable protons than the EPR active copper sites present at pH 7.5. This is consistent with the observed increase in the EPR susceptibility and broader linewidth for the enzyme at pH 9.8.

REFERENCES FOR PART III:

1. Zumft, W. G.; Matsubara, T. *FEBS Lett.* **1982**, *148*, 107–112.

2. Zumft, W. G.; Coyle, C. L.; Frunzke, K. *FEBS Lett.* **1985**, *183*, 240–244.

3. Coyle, C. L.; Zumft, W. G.; Kroneck, P. M. H.; Korner, H.; Jakob, W. *Eur. J. Biochem.* **1985**, *153*, 459–467.

4. (a) Malkin, R.; Malmström, B. G., *Advances in Enzymology and Related Areas of Molecular Biology* **1970**, *33*, 177–244.

   (b) Vanngard, T. in *Biological Application of Electron Spin Resonance*; Swarta, H.M.; Bolton, J.R.; Borg, D.C., Eds.; Academic Press: New York, **1972**, 411–448.

   (c) Boas, F.; Pilbrow, J.R.; Smith, D. in *Biological Magnetic Resonance*; Berliner, L.J.; Reuben, J., Eds.; Plunum Press: New York; **1977**; *1*, 277–342.

   (d) Fee, J.A., *Struct. Bonding* **1975**, *23*, 1–60.

5. (a) Peisach, J. in *Mechanism of Oxidizing Enzymes*; Singer, T. P.; Ondarza, R. W. eds.; Elseveir: New York; **1977**, 285–306.

   (b) Solomon, E. I. in *Copper Proteins*; Spiro, T. ed. Wiley & Sons: New York, **1981**.

   (c) Penfield, K. W.; Fewirth, A. A.; Solomon, E. I. *J. Am. Chem. Soc.* **1985**, *107*, 4519–2529

6. Tainer, J.A.; Getzoff, E.D.; Richardson, J.S.; Richardson, D.A., *Nature* **1983**, *306*, 285–287.

7. Peisach, J.; Blumberg, W.E., *Arch. Biochem. Biophys.* **1974**, *165*, 691–708.

8. Solomon, E. I.; Penfield, K. W.; Wilcox, D. E. *Structure and Bonding* **1983**, *53*, 1–57, and references therein.

9. Lowry, O. H.; Rosebrough, N. J.; Farr, A. L.; Randall, R. J. *J. Biol. Chem.* **1951**, *193*, 265–275.

10. Mehring, M.; Freysoldt, F. *J. Phys.* **1980**, *13*, 894–896.

11. Snyder, S.W.; Hollocher, T. C. *J. Biol. Chem.* **1987**, *262*, 6515–6525.

12. Dooley, D. M.; Moog, R. S.; Zumft, W. G. *J. Am. Chem. Soc.* **1987**, *109*, 6730–6735.

13. (a) Mims, W. B.; Peisach, J. In *Biological Magnetic Resonance*; Berliner, L. J., Reuben, J. Eds.; Plenum Press: New York, **1981**; *3*, 213–263.

   (b) Mims, W. B.; Peisach, J. In *Biological Applications of Magnetic*

Resonance; Shulman, R. G., Ed.; Academic Press: New York, 1979; 221–269.

(c) Mims, W. B.; Peisach, J. *J. Chem. Phys.* **1978**, *69*, 4921–4930.

14. McCracken, J.; Peisach, J.; Dooley, D. M. *J. Am. Chem. Soc.* **1987**, *109*, 4064–4072.

15. (a) Mims, W. B.; Peisach, J.; Davis, J. L. *J. Chem. Phys.* **1977**, *66*, 5536–5550.

(b) Suryanarayana, D.; Narayana, P. A.; Kevan, L. *Inorg. Chem.* **1983**, *22*, 474–478.

(c) Anderson, M. W.; Kevan, L. *J. Phys. Chem.* **1986**, *90*, 6452–6459.

16. Scott, R. A., Zumft, W., G.; Coyle, C. L.; Dooley, D. M. *Proc. Natl. Acad. Sci. USA* **1989**, *86*, 4082–4086.

17. Riester, J.; Kroneck, P. M. H.; Zumft, W. G. *Eur. J. Biochem.* **1989**, *178*, 751–762.

18. McCracken, J.; Pember, S.; Benkovic, S.; Villafrance, J. J.; Miller, R. J.; Peisach, J. *J. Am. Chem. Soc.* **1988**, *110*, 1069–1074.

19. Mims, W. B.; *Phys. Rev.* **1972**, *B5*, 2409–2419.

20. Hurst, G. C.; Henderson, T. A.; Kreilick, R. W. *J. Am. Chem. Soc.* **1985** *107*, 7294–7299.

21. Edmonds, D. T. *Physics Reports* **1977**, *29*, 233–290.

22. Jiang, F.; McCracken, J.; Peisach, J. *XIII International Conference on Magnetic Resonance in Biological Systems*, **1988**, 17–19.

23. Cornelius, J.; Peisach, J. Personal communication.

24. (a) Beinert, H.; Griffiths, D. E.; Wharton, D. C.; Sands, R. H. *J. Biol. Chem.* **1962**, *237*, 2337–2346.

(b) Stevens, T. H.; Martin, C. T.; Wang, H.; Brudvig, G. W.; Scholes, C. P.; Chan, S. I. *J. Biol. Chem.* **1982**, *257*, 12106–12113.

(c)Mims, W. B.; Peisach, J.; Shaw, R. W.; Beinert, H. *J. Biol. Chem.* **1980**, *255*, 6843–6846.

25. Thomann, H.; Bernardo, M.; George, G. N.; Prince, R., to be published.

26. Werst, M.; Zimmerman, B.; Fee, J. A.; Hoffman, B. M., to be published.

27. Roberts, J. E.; Cline, J. F.; Lum, V.; Freeman, H.; Gray, H. B.; Peisach, J.; Reinhammer, B.; Hoffman, B. M. *J. Am. Chem. Soc.* **1984**, *106*, 5324–5330.

28. Van Camp, H.L.; Sands, R. H.; Fee, J. A. *J. Chem. Phys.* **1981**, *75*,

2098–2107.

29 Nakagawa, K.; Hoffman, B. M.; Zumft, W. G., to be published.

30. Viebrock, A. and Zumft, W. G.; *J. Bacteriology* 1988, *170*, 4658–4668.

31. Holm, L.; Saraste, M.; and Wikstrom, M. *EMBO J.* 1987, *6*, 2819–2823.

32. Venters, R. A.; Nelson, M. J.; McLean, P. A.; True, A. E.; Levy, M. A.; Hoffman, B. M.; Orme–Johnson, W. H. *J. Am. Chem. Soc.* 1986, *108*, 3487–3498.

APPENDIX 1 THE TRANSFORMATION OF ANGULAR MOMENTUM EIGENVECTORS UNDER FINITE ROTATIONS

In the following discussions the term rotation will be interpreted as a rotation of the reference frame about the origin, the physical system being supposed fixed. Each point of three–dimensional space is thus given new coordinates, which are functions of the old coordinates and of the parameters which describe the rotation, namely the Euler angles.

As illustrated in Fig. A1, the rotations are to be performed successively in the order:

1) A rotation α $(0 \leq \alpha < 2\pi)$ about the z–axis, bringing the frame of axes from the initial position S into the position S′. The axis of this rotation is commonly called the *vertical*.

2) A rotation β $(0 \leq \beta < \pi)$ about the y–axis of the frame S′, called the *line of nodes*. Note that its position is in general different from the initial position of the y–axis of the frame S. The resulting position of the frame axes is symbolized by S″.

3) A rotation γ $(0 \leq \gamma < 2\pi)$ about the z–axis of the frame of axes S″, called the *figure axis*; the position of this axis depends on the previous rotations. The final position of the frame is symbolized by S‴. Although the position values of α, β and γ are restricted, we do not have an one to one correspondence between rotations and parameters for all possible rotations; for example a rotation symbolized by $(\alpha 0 \gamma)$ is identical with that symbolized by $(\alpha' 0 \gamma')$ if $\alpha + \gamma = \alpha' + \gamma'$.

In 3–D Cartesian space, they corresponds to successive applications to the coordinates column vector of the following three matrices:

$$\text{(A1.1)} \qquad \begin{bmatrix} x' \\ y' \\ z' \end{bmatrix} = \begin{bmatrix} \cos\gamma \sin\gamma & & \\ -\sin\gamma \cos\gamma & & \\ & & 1 \end{bmatrix} \begin{bmatrix} \cos\beta & & -\sin\beta \\ & 1 & \\ \sin\beta & & \cos\beta \end{bmatrix} \begin{bmatrix} \cos\alpha \sin\alpha & & \\ -\sin\alpha \cos\alpha & & \\ & & 1 \end{bmatrix} \begin{bmatrix} x \\ y \\ z \end{bmatrix}$$

or

$$\text{(A1.2)} \qquad \mathrm{R}(00\gamma)\,\mathrm{R}(0\beta0)\,\mathrm{R}(\alpha00)\,\vec{\mathrm{r}} = \mathrm{R}(\alpha\beta\gamma)\,\vec{\mathrm{r}}$$

According to quantum mechanics, when there is a non–zero angular momentum present, this rotation is expressed in terms of unitary operators in an operator form as:

$$\text{(A1.3)} \qquad D(\alpha\beta\gamma) = exp\,\frac{i\gamma}{h} J_z\, exp\,\frac{i\beta}{h} J_y\, exp\,\frac{i\alpha}{h} J_z$$

Note that $D(\alpha\beta\gamma)$ is used for the rotation operator in order to distinguish it from the rotation matrix in the Cartesian space, $R(\alpha\beta\gamma)$. It is defined as $\psi' = D(\alpha\beta\gamma)\ \psi$, where ψ' and ψ are the wave vector after and before the rotation respectively. In particular, $|jM> = \sum_m D(\alpha\beta\gamma)\ |jm>$, or $<jm'|jM> = \sum_m <jm'|\ D(\alpha\beta\gamma)\ |jm>$, where m, M are the indices of the magnetic quantum number of a spin j system before and after the rotation, and they run from $-j$ to j.

It is convenient to write the matrix elements of $D(\alpha\beta\gamma)$ in a more compact from. If we put $<jm'|\ D(\alpha\beta\gamma)\ |jm> \equiv D^{(j)}_{m'm}(\alpha\beta\gamma)$, let ω stand for the three Euler angles, and write $D^{(j)}_{m'm}(0\beta0) \equiv d^{(j)}_{m'm}(\beta)$, it can be shown that

$$\text{(A1.4)} \qquad D^{(j)}_{m'm}(\omega) = exp\ im'\gamma\ d^{(j)}_{m'm}(\beta)\ exp\ im\alpha$$

and

$$(A1.5)\qquad d^{(j)}_{m'm}(\beta) = \left[\frac{(j+m')!(j-m')!}{(j+m)!(j-m)!}\right]^{1/2} \cdot \sum_{\sigma} \binom{j+m}{j-m'-\sigma}\binom{j-m}{\sigma}$$

$$\cdot (-1)^{j-m'-\sigma}\left(\cos\frac{\beta}{2}\right)^{2\sigma+m'+m}\left(\sin\frac{\beta}{2}\right)^{2j-2\sigma-m'-m}$$

For the case of $j = 1$,

$$(A1.6)\qquad D^{(1)}(\alpha\beta\gamma) = \begin{pmatrix} e^{\alpha}\left(\cos\frac{\beta}{2}\right)^2 e^{i\gamma} & \frac{1}{\sqrt{2}}e^{ia}\sin\beta & e^{i\alpha}\left(\sin\frac{\beta}{2}\right)^2 e^{-i\gamma} \\ \frac{1}{2}\sin\beta\, e^{i\gamma} & \cos\beta & \frac{1}{\sqrt{2}}\sin\beta\, e^{-i\gamma} \\ e^{-i\alpha}\left(\sin\frac{\beta}{2}\right)^2 e^{i\gamma} & \frac{-1}{\sqrt{2}}e^{-i\alpha}\sin\beta & e^{-ia}\left(\sin\frac{\beta}{2}\right)^2 e^{-i\gamma} \end{pmatrix}$$

REFERENCES:

A1.1 Brink,D. M.; and Satchler, G. R. *Angular Momentum*, Second Edition; Clarendon Press: Oxford, 1971.

A1.2 Edmonds, A. R. *Angular Momentum in Quantum Mechanics*; Princeton University Press: Princeton; 1974.

A1.3 Rose, M. E. *Elementary Theory of Angular Momentum*; John Wiley & Sons: New York; 1967.

A1.4 Tinkham, M. *Group Theory and Quantum Mechanics*; McCraw–Hill: New York; 1964.

A1.5 Messiah, A. *Quantum Mechanics*; North–Holland: New York; 1961.

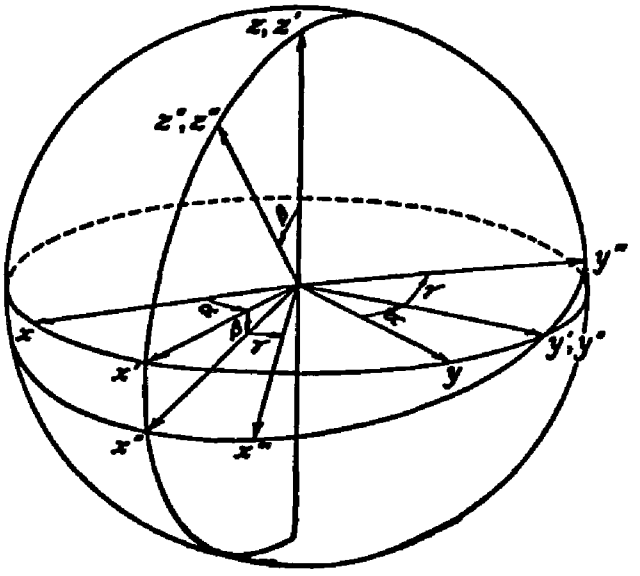

Figure A1 Euler angles and corresponding rotations. (From Edmonds, A. R. *Angular Momentum in Quantum Mechanics*; Princeton University Press, Princeton; 1974)

APPENDIX 2 EXPRESSION OF THE NUCLEAR QUADRUPOLE INTERACTION IN NON–PRINCIPAL AXIS COORDINATES SYSTEM

The nuclear quadrupole interaction, which describes the interaction of the nuclear quadrupole moment of a nucleus with the electric field gradient, can be most easily expressed in its principal axis coordinates system (PAS) as

$$H_Q = \frac{e^2qQ}{4I(2I-1)}\left[3I_z^2 - I(I+1) - \eta(I_x^2 - I_y^2)\right] \tag{A2.1}$$

For example, with $I = 1$, $\langle IM_1|\ H_Q\ |IM_2\rangle$ $(M_1, M_2 = -1,0,1)$ are

$$\frac{e^2qQ}{4I(2I-1)}\begin{bmatrix} 1 & 0 & \eta \\ 0 & -2 & 0 \\ \eta & 0 & 1 \end{bmatrix} \tag{A2.2}$$

To specify the interaction, it is customary to use e^2qQ, η, and a set of Euler angles (see Appendix 1) of the PAS with respect to the chosen reference frame. But it may be required to express this interaction in a non–PAS spin coordinate system. Let us denote the spin wave functions in the PAS as $|IM\rangle$, and in the other, $|Im\rangle$. $\langle Im_1|\ H_Q\ |Im_2\rangle$ can be found in terms of $\langle IM_1|\ H_Q\ |IM_2\rangle$ and $D^{(I)}(\alpha\beta\gamma)$, as discussed in Appendix 1.

According to quantum mechanics,

$$\begin{aligned}&\langle Im_1|\ H_Q\ |Im_2\rangle \\ &= \sum_{M_1}\sum_{M_2} \langle Im_1|IM_1\rangle \langle IM_1|\ H_Q\ |IM_2\rangle \langle IM_2|Im_2\rangle\end{aligned} \tag{A2.3}$$

where $\sum_M |IM\rangle \langle IM| = 1$ (The normalization condition for the projection operator). But $\langle IM|Im\rangle$ is $D^{(I)}_{Mm}(\alpha\beta\gamma)$, and its property of being unitary gives

(A2.4) $$\langle Im|IM\rangle = \langle IM|Im\rangle\dagger = (D^{(I)}_{Mm}(\alpha\beta\gamma))\dagger = D^{(I)}_{mM}(\alpha\beta\gamma)$$

Therefore,

(A2.5) $$\langle Im_1|\, H_Q\, |Im_2\rangle = \sum_{M_1}\sum_{M_2} D^{(I)}_{m_1 M_1}(\alpha\beta\gamma)\, \langle IM_1|\, H_Q\, |IM_2\rangle\, D^{(I)}_{M_2 m_2}(\alpha\beta\gamma)$$

The discussion is not limited to the nuclear quadrupole interaction alone. Similar considerations may have to be taken for the hyperfine interaction.

REFERENCES:

A2.1 Messiah, A. *Quantum Mechanics*; North–Holland: New York; 1961.

A2.2 Schiff, L. *Quantum Mechanics*; John Wiley & Sons: New York; 1975.

APPENDIX 3 Preparation of the MoFe protein***

Cells of *Clostridium pasteurianum W5* were grown as previously described by Mortenson (1972) in a 400 l fermentor (New Brunswick Scientific, Edison, N.J), frozen in liquid nitrogen and stored at –75°C. Crude extracts from 1 kg of cells were made as before (Mortenson, 1972; Zumft and Mortenson, 1973), however, the purification protocol, with strict anaerobic conditions being maintained throughout all steps, has been substantially modified to warrant a more detailed account. The crude extract is loaded onto a DEAE Cellulose–52 (Whatman, Clifton, N.J.) column, 10.0 x 20.0 cm with a flow rate of 1000 ml/hr equilibrated with 50 mM $_{p}$H 7.5 Tris–HCl, 1mM $Na_2S_2O_4$ (buffer A). The column is developed with a linear gradient of 0.08 M to 0.80 M NaCl, 2 l each in buffer A. The MoFe protein eluting at *ca.* 0.25 M Cl^- and the Fe protein eluting at *ca.* 0.35 M Cl^- are monitored by their brown color, collected separately and diluted 2x with water.

The MoFe protein is then loaded onto a 7.5 x 30 cm DEAE Sepharose CL–6B (Pharmacia, Piscataway, N.J.) column, 600 ml/hr previously equilibrated with buffer A. Using the FPLC system of Pharmacia, a linear gradient is developed over 360 min from 0.2 M to 0.45 M KCl in buffer A. The protein is collected and diluted as above and is then applied to a 5.0 x 32 cm DEAE Sephacel (Pharmacia) column, 300 ml/hr in buffer A. Again using the FPLC system, a linear gradient from 0.15 M to 0.35 M KCl in buffer A is developed over 360 min. Fractions are assayed for acetylene reduction activity (Zumft and Mortenson, 1973; Mortenson *et al.* 1976), concentrated by ultrafiltration (Amicon, Danvers, MA) and stored in liquid nitrogen. Typically, yields of 2–3 g of MoFe with a specific activity of

*** Courtesy of Richard E. Bare.

1500–1800 nmol/min/mg can be expected.

^{95}Mo and ^{96}Mo (94.9% and 95.9% enriched, respectively) were obtained from Isotec Inc. (Miamisburg, OH) They were converted from the metal to sodium molybdate as in George *et al.* (1989). Inoculum for the 400 l fermentor was obtained from a 500 ml chemostat (100 ml/hr) which was washed for at least 72 hours to exchange the Mo isotopes. Isotopic enrichments were estimated to be at least 95% (see George *et al.*, 1989).

References:

A3.1. Mortenson, L.E. *Methods Enzymol.*; 1972, *24*, 446–456.

A3.2. Zumft, W.G. and Mortenson, L.E. *Eur. J. Biochem.*; 1973, *95*, 401–409.

A3.3. Mortenson, L.E., Walker, M.N. and Walker, G.A., *Proc. Int. Symp. Nitrogen Fixation, 1st*; Newton, W. E.; Nyman, C. J. eds.; Wash. State Univ. Press; 1976, *1*, 117–149.

A3.4. George, G. N.; Bare, R. E., Jin, H.; Stiefel, E. I.; Prince, R.C. *Biochem. J.*; 1989; *261*, 349.

Abbreviations:

DEAE: Diethylaminoethyl

Tris: Tris(hydroxymethyl)aminoethane

APPENDIX 4 Program Listings

The program PSU_OS2 and subroutines are listed below. They were programed on VAX 8350. Not listed are the routines from EISPACK.

```
      Program PSU_OS2
c
c     FILE:              PSU_OS2
c
c     PURPOSE:  Electron Spin Echo Envelope Modulation simulation
c               for an S=1/2 electron coupled to 1 I=1 nucleus.
c               g-anisotropy is considered instead of effective g.
c               Hamiltonian includes Zeeman(including pseudo effect,
c                pseudo-dipolar, contact term and NQ term
c               (with arbitrary angle).
c               Direct diagonalization method is used. Batch.
c               Automation option. Matchs to the input spectrum
c               are sorted.
c
c     REFERENCES:     W.B.Mims, Phys.Rev.B5, 2409 (1972)
c                                Phys.Rev.B6, 3543 (1972)
c
c     SUBPROGRAMS:
c (MAIN)      ------|- NQ_EULER  adding NQ elements
c                   |- ZEEMAN    nuclear zeeman term
c                   |- SZTERM    terms grouped with Sz
c                   |- SPTERM    terms grouped with S+
c                   |- SMTERM    terms grouped with S-
c                   |- MAT_DIA   diagonalize matrices
c                   |- TEST      confirm eigenvectors correct
c                   |- CAL_ENV   calculate ESE-EM waveform
c                   |- HIST_2P   calculate ESE-EM spectra
c                   |- HIST_3P   calculate ESE-EM spectra
c                   |- IN_BAT4   BATCH input
c                   |- LIS_INF   list information
c                   additional subprograms are
c                         MAT_DIA   diagonalize hermitian matrix
c                         CMATMUL   complex version of MATMUL
c                         MATADD    matrices addition
c                         MAT_EXT   matrices multiplication
c                         MAT_GEN   generate spin matrices
c                         HERMIT    hermitian of matrices
c
c     HAIYONG JIN       Feb. 1989 for Cray/Unicos
c                     Compilation: CFT77 -dp
c-------------------------------------------------------------------------
      implicit double precision(a-h,o-z)
      parameter(idim=4,max=32,io=22,nco=20)
      logical       dipol,xtal,no_dc,smooth,noherm
      byte  header(72)
      integer             pulse,option
```

```
      integer*2          lopcnt(40000)
      real    rmsq(40000),sigma,ydata(2048),delx
      dimension    Qzz(idim),eta(idim),acntct(idim)
      dimension    alpha(idim),gamma(idim),beta(idim)
      dimension    reff(idim),phi_n(idim),the_n(idim)
      dimension     e(2048),ep(max),en(max),amr(max,max)
      dimension     ami(max,max),tempr(max,max),tempi(max,max)
      dimension     hpr(max,max),hhi(max,max),hhr(max,max)
      dimension     hpi(max,max),hnr(max,max),hni(max,max)
      dimension     znr(max,max),zni(max,max)
      common        /mmat/amr,ami
      common              /envlop/e
      common       /gtnsor/g1,g2,g3,geff,h0,the0,phi0
      common       /in_n/acntct,Qzz,eta,alpha,beta,gamma,reff,the_n,phi_n
      be=9.274026d-21
      bn=5.050824d-24
      h=6.626093d-27
      pi=4.0d0*datan(1.0d0)
c ---- input information
      open(9,file='mah.bat',form='formatted',status='old')
      call in_bat4(io,option,tau0,t0,delf,nthe,mout,ispin,gnu,dipol,
     +     no_dc,smooth,sigma,nbest,gep,two_D)
c     if(g1.eq.g2.and.g2.eq.g3) stop
      pulse=2
      if(tau0.ne.0.d0) pulse=3
      v0=bn*h0/h/1.0d6          ! in MHz
      ve0=be*h0/h/1.0d6         ! in MHz
      delx=sngl(delf)
      index=0
c ---- preparation of automation
      if(Qzz(3).ne.0.d0) then
        nQzz=1+idint((Qzz(2)-Qzz(1))/Qzz(3))
      else
        nQzz=1
      endif
      if(eta(3).ne.0.d0) then
        neta=1+idint((eta(2)-eta(1))/eta(3))
      else
        neta=1
      endif
      if(beta(3).ne.0.d0) then
        nbeta=1+idint((beta(2)-beta(1))/beta(3))
      else
        nbeta=1
      endif
      if(alpha(3).ne.0.d0) then
        nalp=1+idint((alpha(2)-alpha(1))/alpha(3))
      else
        nalp=1
      endif
      if(reff(3).ne.0.d0) then
        nreff=1+idint((reff(2)-reff(1))/reff(3))
      else
        nreff=1
```

```
            endif
            if(the_n(3).ne.0.d0) then
              ntn=1+idint((the_n(2)-the_n(1))/the_n(3))
            else
              ntn=1
            endif
            if(phi_n(3).ne.0.d0) then
              npn=1+idint((phi_n(2)-phi_n(1))/phi_n(3))
            else
              npn=1
            endif
            if(Acntct(3).ne.0.d0) then
              nA=1+idint((Acntct(2)-Acntct(1))/Acntct(3))
            else
              nA=1
            endif
            if((na*npn*ntn*nreff*nalp*nbeta*neta*nqzz).gt.40000) stop
c ------ loop over parameters
            do 8000 iQzz=1,nQzz
             Qzz(4)=Qzz(1)+dfloat(iQzz-1)*Qzz(3)
             do 8100 ieta=1,neta
              eta(4)=eta(1)+dfloat(ieta-1)*eta(3)
              do 8200 ibeta=1,nbeta
               beta(4)=beta(1)+dfloat(ibeta-1)*beta(3)
               beta(4)=beta(4)*pi/1.8d2  ! deg. to grad.
               do 8300 ialp=1,nalp
                alpha(4)=alpha(1)+dfloat(ialp-1)*alpha(3)
                alpha(4)=alpha(4)*pi/1.8d2  ! deg. to grad.
                do 8400 ireff=1,nreff
                 reff(4)=reff(1)+dfloat(ireff-1)*reff(3)
                 do 8500 itn=1,ntn
                  the_n(4)=the_n(1)+dfloat(itn-1)*the_n(3)
                  the_n(4)=the_n(4)*pi/1.8d2  ! deg. to grad.
                  do 8600 ipn=1,npn
                   phi_n(4)=phi_n(1)+dfloat(ipn-1)*phi_n(3)
                   phi_n(4)=phi_n(4)*pi/1.8d2  ! deg. to grad.
                   do 8700 ia=1,na
                    acntct(4)=acntct(1)+dfloat(ia-1)*acntct(3)
c ------ initialization
            in=2*ispin
            do 7000 i=1,mout
              e(i)=0.0d0
7000        continue
c ------- nested for # of nuclei
            do 7005 i=1,in
              do 7005 j=1,in
                hpr(i,j)=0.d0
                hpi(i,j)=0.d0
7005        continue
            if(in.eq.6.and.Qzz(4).ne.0.d0) then
              Qxxyy=Qzz(4)*eta(4)
              call nq_euler(Qzz(4),Qxxyy,hpr,hpi,alpha(4),
     +                beta(4),gamma(4))
              call mat_gen(1,2,tempr,imag,coeff,.false.)  ! unit matrix
```

```
            call mat_ext(tempr,hpr,hpr,2,in/2,in)
            call mat_ext(tempr,hpi,hpi,2,in/2,in)
           endif
c ——— terms grouped with Sz matrix
           if(dipol) then
            f=(be/h)*gnu*bn/(reff(4)**3)
           endif
           call szterm(in/2,acntct(4),the_n(4),
     +                phi_n(4),f,hnr,hni,dipol)
           call mat_gen(2,2,tempr,imag,coeff,.false.)
           call mat_ext(tempr,hnr,hnr,2,in/2,in)
           call matadd(hnr,hpr,hpr,in,in,1)
           call mat_ext(tempr,hni,hni,2,in/2,in)
           call matadd(hni,hpi,hpi,in,in,1)
c ——— terms grouped with S+ matrix
           call spterm(in/2,acntct(4),the_n(4),
     +                phi_n(4),f,hnr,hni,dipol)
           call mat_gen(3,2,tempr,imag,coeff,.false.)  ! S+ matrix
           call mat_ext(tempr,hnr,hnr,2,in/2,in)
           call matadd(hnr,hpr,hpr,in,in,1)
           call mat_ext(tempr,hni,hni,2,in/2,in)
           call matadd(hni,hpi,hpi,in,in,1)
c ——— terms grouped with S– matrix
           call smterm(in/2,acntct(4),the_n(4),
     +                phi_n(4),f,hnr,hni,dipol)
           call mat_gen(4,2,tempr,imag,coeff,.false.)  ! S– matrix
           call mat_ext(tempr,hnr,hnr,2,in/2,in)
           call matadd(hnr,hpr,hhr,in,in,1)
           call mat_ext(tempr,hni,hni,2,in/2,in)
           call matadd(hni,hpi,hhi,in,in,1)
c ——— loop for sin(theta)
           do 80 isthe=1,nthe
            xtal=.false.
            theta=pi*dfloat(2*isthe–1)/dfloat(4*nthe) !theta 0–> pi/2
            stheta=dsin(theta)
            if(g1.eq.g2) then
             stheta=dsqrt((geff**2–g3**2)/(g2**2–g3**2))
             theta=dasin(stheta)
             if(geff.eq.g3) xtal=.true.
             phi=dfloat(2*isthe–1)*pi/2.d0/dfloat(nthe)
            else
             if(g2.eq.g3) then
              if(geff.eq.g1) then
               stheta=1.d0
               theta=pi/2.d0
                   phi=0.d0
                   xtal=.true.
               else
                if(stheta.eq.0.d0) then
                          goto 80
               else
                    phi=(geff**2–g2**2)/(g2**2–g1**2)/stheta**2
                 if(phi.gt.1.d0.or.phi.lt.0.d0) then
                  goto 80
```

```
                  else
                    phi=dacos(dsqrt(phi))
                  endif
                endif
              endif
            else
              if(geff.eq.g3) then
                xtal=.true.
                  stheta=0.d0
                  theta=0.d0
                phi=0.d0
              else
                if(geff.eq.g1) then
                  xtal=.true.
                  stheta=1.d0
                  theta=pi/2.d0
                  phi=0.d0
                else
                  if(stheta.eq.0.d0) then
                    goto 80
                  else
                    phi=(geff*2-g3**2)/stheta**2+g2**2-g3**2
                    phi=phi/(g1**2-g2**2)
                    if(phi.gt.1.d0.or.phi.lt.0.d0) then
                      goto 80
                    else
                      phi=dacos(dsqrt(phi))
                    endif
                  endif
                endif
              endif
            endif
c ------ nested for +-sin(theta),and +-cos(phi) on left sphere
            the0=theta
            phi0=phi
            weight=stheta/dfloat(ispin)
c ------ terms grouped with Unit matrix (with H0)
7020        in=2*ispin
            call psu_zmn(gnu,in/2,v0,the0,phi0,hnr,hni,g3,gep,two_D,
     +           Acntct(4),f,the_n(4),phi_n(4))
c           call zeeman(gnu,gnu,gnu,in/2,v0,
c    +                  the0,phi0,hnr,hni)
            call mat_gen(1,2,tempr,imag,coeff,.false.)  ! unit matrix
            call mat_ext(tempr,hnr,hnr,2,in/2,in)
            call matadd(hnr,hhr,hpr,in,in,1)
            call mat_ext(tempr,hni,hni,2,in/2,in)
            call matadd(hni,hhi,hpi,in,in,1)
c ------ add in electronic Zeeman term
            call zeeman(g1,g2,g3,2,ve0,the0,phi0,hnr,hni)  ! electron zeeman
            call mat_gen(1,in/2,tempr,imag,coeff,.false.) ! unit matrix
            call mat_ext(hnr,tempr,hnr,2,in/2,in)
            call mat_ext(hni,tempr,hni,2,in/2,in)
            call matadd(hnr,hpr,hpr,in,in,1)
```

```
            call matadd(hni,hpi,hpi,in,in,1)
c ——— diagonalization and testing
            call mat_dia(in,hpr,hpi,ep,znr,zni) ! diagonalize the whole H
c ——— find M matrix defined in the paper
            in=ispin
            do 7025 i=1,in
              en(i)=ep(i+in)
              do 7025 j=1,in
                  amr(i,j)=znr(i+in,j+in)
                  ami(i,j)=zni(i+in,j+in)
7025        continue
            call hermit(in,znr,zni,hnr,hni)
            call cmatmul(hnr,hni,amr,ami,amr,ami,in,in,in)
c ——— compute histograms
            if(option.eq.2.or.option.eq.4) then
              call cal_env(mout,t0,tau0,delf,weight,in,ep,en,pulse)
            elseif(option.eq.1.or.option.eq.3) then
              if(pulse.eq.3) then
                 call hist_3p(mout,tau0,delf,weight,in,ep,en,no_dc)
              else
                 call hist_2p(mout,delf,weight,in,ep,en,no_dc)
              endif
            endif
c ——— combination of theta and phi
            if(xtal) goto 85
            if(the0.lt.(pi/2.d0)) then
              if(phi0.lt.(pi/2.d0)) then
                 phi0=pi-phi
              else
                 the0=pi-theta
                phi0=phi
              endif
            else
              if(phi0.lt.(pi/2.d0)) then
                phi0=pi-phi
              else
                 phi0=phi0+2.d0*pi          ! exit the loop
              endif
            endif
            if (the0.lt.pi .and. phi0.lt.pi) goto 7020
80          continue
c ——— output to disk
85          do 7030 i=1,mout
             ydata(i)=sngl(e(i))
7030        continue
           if(smooth) call lorentz(mout,ydata,delx,sigma)
            index=index+1
            lopcnt(index)=index
            call match(mout,ydata,rmsq(index))
8700          continue
8600         continue
8500        continue
8400        continue
8300       continue
```

```
8200      continue
8100     continue
8000    continue
        if(index.lt.2) then
         delx=delx*float(mout-1)
         call ftkout(13,mout,delx,ydata)
c        open(13,form='unformatted',status='new')
c        write(13) header
c        do i=1,mout
c         write(13) delx*(i-1),ydata(i)
c        end do
c        close(13)
         close(io,dispose='delete')
         print*,'Root-Mean-Squared error: ',rmsq(1)
         goto 9999
        endif
        call sort2(index,rmsq,lopcnt)
        write(io,2199)
2199    format('1',//,' OUTPUT FROM PROGRAM PSU_OS2:'/)
        write(io,2200)
2200    format(/,3x,'eeqQ(MHz)',6x,'eta',6x,'alpha(deg)',4x,
   +    'beta(deg)',4x,'Aiso(MHz)',4x,'reff(A)',4x,'theta(deg)',4x,
   +    'phi(deg)',/)
        if(nbest.eq.0) nbest=index
        do 7035 i=1,nbest
         itemp=neta*nbeta*nalp*nreff*ntn*npn*na
         ireman=lopcnt(i)
         call cntlop(iQzz,itemp,ireman)
         itemp=itemp/neta
         call cntlop(ieta,itemp,ireman)
         itemp=itemp/nbeta
         call cntlop(ibeta,itemp,ireman)
         itemp=itemp/nalp
         call cntlop(ialp,itemp,ireman)
         itemp=itemp/nreff
         call cntlop(ireff,itemp,ireman)
         itemp=itemp/ntn
         call cntlop(itn,itemp,ireman)
         itemp=itemp/npn
         call cntlop(ipn,itemp,ireman)
         itemp=itemp/na
         call cntlop(ia,itemp,ireman)
         write(io,2600) rmsq(i)
2600     format(/,' Root-Mean-Squared error = ',g12.6,' for:')
         write(io,2300) (Qzz(1)+(iQzz-1)*Qzz(3)),
   +    (eta(1)+(ieta-1)*eta(3)),(alpha(1)+(ialp-1)*alpha(3)),
   +    (beta(1)+(ibeta-1)*beta(3)),(Acntct(1)+(ia-1)*Acntct(3)),
   +    (reff(1)+(ireff-1)*reff(3)),
   +    (the_n(1)+(itn-1)*the_n(3)),(phi_n(1)+(ipn-1)*phi_n(3))
7035    continue
        close(io)
2300    format(8(g12.5,1x))
9999    stop
        end
```

```
c
c
      subroutine cal_env (m,t0,tau,delt,weight,in,wp,wn,kflag)
c
c     PURPOSE:  calculate ESE-EM, for 2- or 3-pulse
c
c     DEFINITION:       m, # of data points
c                       in, dimension of the Hamiltonian
c                       kflag: 2, 2-pulse; 3, 3-pulse
c                       t0,tau: starting time and tau0
c                       wp,wn: ESE freq. for Sz=1/2 and -1/2
c
c-----------------------------------------------------------------------
-----------------

      implicit double precision (a-h,o-z)
      parameter (max=2048,idim=32)
      dimension e(max),wp(idim),wn(idim),amr(idim,idim),ami(idim,idim)
      dimension chi(3,3),chichi(3,2,3,2)
      common      /mmat/amr,ami
      common            /envlop/e
c
c ---- e(k)=emod(tau,t) of W.B.Mims, B6, 3543 (1972)
c
c ---- diagonal (1,1): chi0 in Mims' paper
      chi(1,1)=0.d0
      do 70 i=1,in
       do 70 j=1,in
        chi(1,1)=chi(1,1)+(amr(i,j)**2+ami(i,j)**2)**2
70    continue
c ---- offdiagonal: (i,j) for alpha, (j,i) for beta
      do 75 i=2,in
       do 75 j=1,i-1
        chi(i,j)=0.d0
        chi(j,i)=0.d0
        do 71 k=1,in
          temp=(amr(i,k))**2+(ami(i,k))**2
          temp1=(amr(j,k))**2+(ami(j,k))**2
          chi(i,j)=chi(i,j)+temp*temp1
          temp=(amr(k,i))**2+(ami(k,i))**2
          temp1=(amr(k,j))**2+(ami(k,j))**2
          chi(j,i)=chi(j,i)+temp*temp1
71      continue
75    continue
c ---- chichi: Chi ijkn
       do 73 i=2,in
        do 73 j=1,i-1
         do 73 k=2,in
          do 73 n=1,k-1
           chi1=amr(i,k)*amr(i,n)+ami(i,k)*ami(i,n)
           chi2=amr(j,n)*amr(j,k)+ami(j,n)*ami(j,k)
           temp=amr(i,k)*ami(i,n)-ami(i,k)*amr(i,n)
           temp1=amr(j,n)*ami(j,k)-ami(j,n)*amr(j,k)
           temp2=2.0d0*(chi1*chi2-temp*temp1)
```

```
            chichi(i-1,j,k-1,n)=temp2
73        continue
c
c ------ scan over t
c
          do 74 icon=1,m
           dblt=t0+delt*dfloat(icon-1)
           if (kflag.eq.2) tau=dblt
           e(icon)=e(icon)+chi(1,1)
           do 72 i=2,in
            do 72 j=1,i-1
             temp=wp(i)-wp(j)
             temp1=dcos(temp*tau)
             temp=dcos(temp*dblt)
             e(icon)=e(icon)+chi(i,j)*(temp+temp1)
             temp=(wn(i)-wn(j))
             temp1=dcos(temp*tau)
             temp=dcos(temp*dblt)
             e(icon)=e(icon)+chi(j,i)*(temp+temp1)
             do 72 k=2,in
              do 72 n=1,k-1
               temp=wp(i)-wp(j)
               temp1=(wn(k)-wn(n))
               chi1=dcos(temp*dblt)
               chi2=dcos(temp1*tau)
               temp=dcos(temp*tau)
               temp1=dcos(temp1*dblt)
               e(icon)=e(icon)+chichi(i-1,j,k-1,n)*(chi1*chi2+temp*temp1)
72           continue
74        continue
          return
          end
c
c
          subroutine cntlop(i,inner,reman)
          integer         reman
          if(inner.eq.1) then
           i=reman
           reman=1
          elseif(reman.eq.1) then
           i=reman
          elseif(mod(reman,inner).ne.0) then
           i=reman/inner+1
           reman=mod(reman,inner)
          elseif(mod(reman,inner).eq.0) then
           i=reman/inner
           reman=inner
          endif
          return
          end
c
c
          subroutine cmatmul (a,b,c,d,e,f,m1,m2,m3)
c
```

```
c          PURPOSE:  complex matrices multiplication
c                    (a,b)*(c,d) = (e,f)
c                    when calling, (e,f) could be either input
c
c-------------------------------------------------------------------------
-----------------------
          parameter(max=32)
          double precision a(max,max),b(max,max),c(max,max),d(max,max)
          double precision g(max,max),e(max,max),f(max,max),h(max,max)
c
c    (a,b) is m1 by m2 matrix, (c,d) is m2 by m3 matrix, (e,f) is the product
c
          do 1 i=1,m1
           do 1 j=1,m3
            g(i,j)=0.0d0
            h(i,j)=0.0d0
            do 1 k=1,m2
              g(i,j)=g(i,j)+a(i,k)*c(k,j)-b(i,k)*d(k,j)
              h(i,j)=h(i,j)+a(i,k)*d(k,j)+b(i,k)*c(k,j)
    1     continue
          do 2 i=1,m1
            do 2j=1,m3
              e(i,j)=g(i,j)
              f(i,j)=h(i,j)
2         continue
          return
          end


          SUBROUTINE dlinbro(nfdiv,delf,sigma)
C
C             To use gaussian function to smooth the data
C
C*************************************************************
          implicit double precision(a-h,o-z)
          dimension     ampli(2048),orig(2048)
          common        /finale/ampli
          common        /envlop/orig
c
          do 100 i=1,nfdiv
            orig(i)  = ampli(i)
            ampli(i)=0.0d0
100       continue
          if (sigma .eq. 0.d0) sigma = delf/9.d0
          x = delf/sigma
          nsum = int(0.4d0/x)
          if (nsum .eq. 0) return
          do 110 i=nsum+1,nfdiv-nsum
            do 110 j=(i-nsum),(i+nsum),1
              weight = dexp(-(dfloat(i-j)*x)**2)
              ampli(j) = ampli(j) + orig(i)*weight/dfloat(nsum)
110       continue
          return
          end
```

```
      subroutine ftkout(lunfile,isiz,swidth,yarr)
c      Modified from MB version
c ---- output subroutine
      parameter maxpt=256
      real yarr(2048),swidth
      integer isiz
      real*4 xmx(maxpt)
      integer*4 ints(maxpt)
      equivalence (ints,xmx)
c
c*** Now get output file name and write it out
      open(unit=lunfile,status='new',form='unformatted')
      do 10 i=1,maxpt
       xmx(i)=0.
10    continue
      ints(1)=isiz
      ints(2)=1
      xmx(17)=swidth
      xmx(18)=1.                    !spectrometer frequency
      write(lunfile) -128,(ints(i),i=1,256)
      write(lunfile) isiz,((yarr(i),0.0),i=1,isiz)
      close(lunfile)
      return
      end


      subroutine hermit(idim,a,b,c,d)
c
c     take hermittian of a complex matrix
c
      implicit double precision(a-h,o-z)
      parameter(max=32)
      dimension a(max,max),b(max,max),c(max,max),d(max,max)
      do 1 i=1,idim
        do 1 j=1,idim
          c(i,j)=a(j,i)
          d(i,j)=-b(j,i)
1     continue
      return
      end


      subroutine hist_2p (m,delf,weight,in,wp,wn,no_dc)
c
c     PURPOSE:  compute freq. histogram according to Mims' method
c
c     DEFINITION:       m, # of data points
c                       in, dimension of the Hamiltonian
c                       delf: spectral resolution
c
c-----------------------------------------------------------------------
      implicit double precision (a-h,o-z)
      logical           no_dc
      dimension f(2048),wp(32),wn(32),amr(32,32),ami(32,32)
```

```
      common        /mmat/amr,ami
      common              /envlop/f
c ---- chi zero term
      if(.not.no_dc) then
       chi0 = 0.d0
       do 76 i=1,in
        do 76 j=1,in
         chi0=chi0+(amr(i,j)**2+ami(i,j)**2)**2
 76     continue
       chi0=chi0*weight
       f(1)=f(1)+chi0
      endif
c ---- compute chi1(CHIij) and chi2(CHIkn)
      do 75 i=2,in
       do 75 j=1,i-1
        chi1=0.0d0
        chi2=0.0d0
        do 74 k=1,in
         temp=(amr(i,k))**2+(ami(i,k))**2
         temp1=(amr(j,k))**2+(ami(j,k))**2
        chi1=chi1+temp*temp1
c ---   temp=(amr(k,i))**2+(ami(k,i))**2
c       temp1=(amr(k,j))**2+(ami(k,i))**2
c    CHIijkn term
c        do 73 j=i-1,1,-1
c         do 73 k=in,2,-1
c          do 73 n=k-1,1,-1
      do 73 i=2,in
       do 73 j=1,i-1
        do 73 k=2,in
         do 73 n=1,k-1
          chi1=amr(i,k)*amr(i,n)+ami(i,k)*ami(i,n)
          chi2=amr(j,n)*amr(j,k)+ami(j,n)*ami(j,k)
          temp=amr(i,k)*ami(i,n)-ami(i,k)*amr(i,n)
          temp1=amr(j,n)*ami(j,k)-ami(j,n)*amr(j,k)
          temp2=weight*(chi1*chi2-temp*temp1)
          temp=wp(i)-wp(j)
          temp1=wn(k)-wn(n)
          icon=idnint(dabs(temp+temp1)/delf) ! Wij+Wkn
          if(icon.gt.m) goto 999
          f(icon)=f(icon)+2.0d0*temp2
          icon=idnint(dabs(temp-temp1)/delf) ! Wij-Wkn
          if(icon.gt.m) goto 999
          f(icon)=f(icon)+2.0d0*temp2
 73     continue
      return
999   type *,'*** FATAL *** input freq. range too small'
      stop
      end
c
c
      subroutine hist_3p (m,tau0,delf,WEIGHT,in,wp,wn,no_dc)
```

```
c
c          PURPOSE:   compute freq. histogram according to Mims' method
c
c          DEFINITION:        m, # of data points
c                             in, dimension of the Hamiltonian
c                             delf spectral resolution
c
c-------------------------------------------------------------------------
           implicit double precision (a-h,o-z)
           dimension f(2048),wp(32),wn(32),amr(32,32),ami(32,32)
           logical no_dc
           common          /mmat/amr,ami
           common                  /envlop/f
           twopi=8.d0*datan(1.0d0)
c ------ chi zero term
           if(no_dc.eq..false.) then
             chi0 = 0.d0
             do 76 i=1,in
               do 76 j=1,in
                chi0=chi0+(amr(i,j)**2+ami(i,j)**2)**2
 76          continue
             f(1)=f(1)+chi0*weight
           endif
c ------ compute chi1(CHIij) and chi2(CHIkn)
           do 75 i=2,in
             do 75 j=1,i-1
              chi1=0.0d0
              chi2=0.0d0
              do 74 k=1,in
               temp=(amr(i,k))**2+(ami(i,k))**2
               temp1=(amr(j,k))**2+(ami(j,k))**2
               chi1=chi1+temp*temp1
               temp=(amr(k,i))**2+(ami(k,i))**2
               temp1=(amr(k,j))**2+(ami(k,j))**2
               chi2=chi2+temp*temp1
 74           continue
              icon=idnint(dabs(wp(i)-wp(j))/delf) ! up manifold
              if(icon.gt.m) goto 999
              f(icon)=f(icon)+chi1*weight
              icon=idnint(dabs(wn(i)-wn(j))/delf) ! low manifold
              if(icon.gt.m) goto 999
              f(icon)=f(icon)+chi2*weight
              if(no_dc.eq..false.) then
                f(1)=f(1)+weight*chi1*dcos(twopi*temp*tau0)  ! dc term
                f(1)=f(1)+weight*chi2*dcos(twopi*temp1*tau0) ! dc term
              endif
 75         continue
c
c ------ CHIijkn term
c
           do 73 i=2,in
             do 73 j=1,i-1
              do 73 k=2,in
               do 73 n=1,k-1
```

```
            chi1=amr(i,k)*amr(i,n)+ami(i,k)*ami(i,n)
            chi2=amr(j,n)*amr(j,k)+ami(j,n)*ami(j,k)
            temp=amr(i,k)*ami(i,n)-ami(i,k)*amr(i,n)
            temp1=amr(j,n)*ami(j,k)-ami(j,n)*amr(j,k)
            temp2=weight*(chi1*chi2-temp*temp1)
            temp=wp(i)-wp(j)
            temp1=wn(k)-wn(n)
            icon=idnint(dabs(temp)/delf)
            if(icon.gt.m) goto 999
            f(icon)=f(icon)+2.0d0*temp2*dcos(twopi*temp1*tau0)
            icon=idnint(dabs(temp1)/delf)
            if(icon.gt.m) goto 999
            f(icon)=f(icon)+2.0d0*temp2*dcos(twopi*temp*tau0)
 73        continue
           return
999        type *,'*** FATAL *** input freq. range too small'
           stop
           end


           subroutine in_bat4(iout,option,tau0,t0,delf,nthe,mout,ispin,gnu,
     +     dipol,no_dc,smooth,sigma,nbest,gep,two_D)
c
c          batch input for B_MAH_OS#
c
           implicit double precision(a-h,o-z)
           parameter(idim=4,max=32,nco=20)
           logical          dipol,no_dc,smooth
           integer                  option
           real             w(nco),amp(nco),phase(nco),rdec(nco),sigma,temp
           real             orig(2048),dt,tstart,peak,ymin,ymax,rtemp,tpi
           dimension        Qzz(idim),eta(idim),acntct(idim)
           dimension        alpha(idim),gamma(idim),beta(idim)
           dimension        reff(idim),phi(idim),theta(idim)
           byte   header(72)
           character        string
           common                   /finale/orig
           common           /gtnsor/g1,g2,g3,geff,h0,the0,phi0
           common           /in_n/acntct,Qzz,eta,alpha,beta,gamma,reff,theta,phi
c          equivalence              (tstart,record(403))
c          equivalence              (dt,record(407))
           external         peak
           bn=5.050824d-24
           h=6.626093d-27
           tpi=atan(1.0)*8.0
           io=9
           do 7000 i=1,2048
            orig(i)=0.
7000       continue
           read(io,110) option
           read (io,100) H0
           if(h0.lt.0.d0) stop
           read (io,100) geff
           if(geff.lt.0.d0) stop
```

```
100       format(d16.8)
          read (io,100) g1
          if(g1.le.0.d0) stop
          read (io,100) g2
          if(g2.le.0.d0) stop
          read (io,100) g3
          if(g3.le.0.d0) stop
          read(io,110) nthe
c ------- enter information for the nucleus
          read (io,105) string
105       format(a)
          dipol=.false.
          if(string.eq.'y'.or.string.eq.'Y') dipol=.true.
          read (io,110) ispin
          read (io,100) gnu
c ------- automate Acntct
          read(io,*) acntct(1),Acntct(2),acntct(3)
c ------- automate Qzz
          read(io,*) Qzz(1),Qzz(2),Qzz(3)
c ------- automate eta
          read(io,*) eta(1),eta(2),eta(3)
c ------- automate beta
          read(io,*) beta(1),beta(2),beta(3)
c ------- automate alpha
          read(io,*) alpha(1),alpha(2),alpha(3)
          read(io,100) gamma(4)
          if(dipol) then
c ------- automate reff
            read(io,*) reff(1),reff(2),reff(3)
c ------- automate theta
            read(io,*) theta(1),theta(2),theta(3)
c ------- automate phi
            read(io,*) phi(1),phi(2),phi(3)
          endif
150       format(3d15.8)
c ------- fitting information
          ymax=-10000.
          ymin=10000.
          if(option.eq.2) then
            read (io,100) tau0
            if(tau0.lt.0.d0) stop
c           read (io,120) nch,(filnam(i),i=1,nch)
c120        format(q,40a1)
            open(10,form='formatted',status='old')
c           read(10) record
            read(10,120) tstart,orig(1)
            read(10,120) dt,orig(2)
            dt=dt-tstart
            mout=2
9000        read(10,120,end=9001) temp,orig(mout+1)
120         format(2e20.10)
            mout=mout+1
            if(ymax.lt.orig(i)) ymax=orig(i)
            if(ymin.gt.orig(i)) ymin=orig(i)
```

```
          goto 9000
9001      close(10)
          read(io,110) nbase                    ! baseline
          mout=mout-nbase
         elseif(option.eq.1) then
          read(io,110) mout
110       format(i8)
          if(mout.eq.0) mout=1024
          read (io,100) delf
          read (io,100) tau0
          if(tau0.lt.0.d0) stop
          read(io,105) string
          if(string.eq.'y'.or.string.eq.'Y') then
            no_dc=.false.
          else
            no_dc=.true.
          endif
          read(io,105) string
          if(string.eq.'n'.or.string.eq.'N') then
            smooth=.false.
          else
            smooth=.true.
            read(io,1090) sigma
1090        format(e20.10)
            if(sigma.eq.0.0) sigma=0.1
          endif
          read(io,110) ico
          if(ico.gt.nco.or.ico.le.0) stop
          do 7100 i=1,ico
           read(io,1190) ijunk,rdec(i),w(i),amp(i),phase(i),rtemp
7100      continue
          do 7300 i=1,mout
           do 7200 j=1,ico
            orig(i)=orig(i)+peak(sngl(delf),i,mout,
     +     (w(j)/sngl(delf)),(rdec(j)/sngl(delf)),amp(j),phase(j))
7200       continue
           if(ymax.lt.orig(i)) ymax=orig(i)
           if(ymin.gt.orig(i)) ymin=orig(i)
7300      continue
         elseif(option.eq.4) then
          read(io,110) mout                     ! # of pts
          if(mout.eq.0) mout=1024
          read (io,100) delf                    ! time increment
          if(delf.lt.0.d0) stop
          read (io,100) t0                      ! starting time
          if(t0.lt.0.d0) stop
          read (io,100) tau0
          if(tau0.lt.0.d0) stop
          read(io,110) ico
          if(ico.gt.nco.or.ico.le.0) stop
          do 7400 i=1,ico
           read(io,1190) ijunk,rdec(i),w(i),amp(i),phase(i),rtemp
7400      continue
1190      format(i4,5(3x,e12.5))
```

```
            do 7600 i=1,mout
             rtemp=t0+sngl(delf)*(i-1)
             do 7500 j=1,ico
              orig(i)=amp(j)*exp(-rtemp*rdec(j))*cos(w(j)+phase(j))
     +              + orig(i)
7500         continue
             if(ymax.lt.orig(i)) ymax=orig(i)
             if(ymin.gt.orig(i)) ymin=orig(i)
7600        continue
           elseif(option.eq.3) then
            read (io,100) tau0
            if(tau0.lt.0.d0) stop
            read(io,105) string
            if(string.eq.'y'.or.string.eq.'Y') then
              no_dc=.false.
            else
              no_dc=.true.
            endif
            read(io,105) string
            if(string.eq.'n'.or.string.eq.'N') then
              smooth=.false.
            else
              smooth=.true.
              read(io,1090) sigma
              if(sigma.eq.0.0) sigma=0.1
             endif
c            read (io,120) nch,(filnam(i),i=1,nch)
             open(10,form='formatted',status='old')
c            read(10) record
             read(10,120) tstart,orig(1)
             read(10,120) dt,orig(2)
             dt=dt-tstart
             mout=2
9500         read(10,120,end=9501) temp,orig(mout+1)
             mout=mout+1
             if(ymax.lt.orig(i)) ymax=orig(i)
             if(ymin.gt.orig(i)) ymin=orig(i)
             goto 9500
9501         close(10)
           endif
           read(io,110) nbest
           read(io,100) gep
           read(io,100) two_D
           close(io)
c ------ output to disk
           if(option.eq.2) then
             delf=dble(dt)
             t0=dble(tstart)
           elseif(option.eq.3) then
             delf=dble(dt)
           endif
           open(iout,file='simah.inf',form='formatted',status='new')
           if(option.eq.1.or.option.eq.4) then
             write(iout,2000)
```

```
2000      format(/,1x,'For comparison with following input:',
     +    //,1x,'w(MHzRad)',2x,'R(MHzRad)',2x,'Amplitude',2x,
     +    'Phase(Radian)',3x,'v(MHz)',/)
          do 7700 i=1,ico
           write(iout,2110) w(i),rdec(i),
     +     amp(i),phase(i),(w(i)/tpi)
7700      continue
2110      format(5g12.5)
         elseif(option.eq.2.or.option.eq.3) then
c         write(iout,2800) (filnam(i),i=1,nch)
c2800     format(/,1x,'For comparison with ',40a1)
         endif
         write(iout,2100) H0,geff
2100     format(/' Static magnetic field =',g10.5,' G',
     +   /,5X,'with geff =',g12.7)
         write(iout,2105) g1,g2,g3
2105     format(/,' g1 =',g12.7,5x,'g2 =',g12.7,5x,'g3 =',g12.7)
         fi=gnu*bn*h0/h/1.d6
         write(iout,2200) fi,ispin,gnu
2200     format(/,' Nuclear Zeeman freq. at geff =',
     +   d10.5,' MHz',/,5X,'with 2I + 1 =',i3,',  gn =',d12.7)
         write(iout,2250) gep,two_D
2250     format(/,' Pseudo nuclear Zeeman effect correction parameters:',
     +   /,5x,'g perp =',g12.7,', and 2D=',g12.7,'MHz')
         write(iout,2450) nthe
2450     format(/,' Divisions of sin(theta) wrt g coordinates =',i6)
         write(iout,2205)
2205     format(//,1x,'Starting parameters are:',
     +   //,3x,'eeqQ(MHz)',6x,'eta',6x,'alpha(deg)',4x,'beta(deg)',4x,
     +   'Aiso(MHz)',4x,'reff(A)',4x,'theta(deg)',4x,'phi(deg)',/)
         i=1
         write(iout,2300) Qzz(i),eta(i),alpha(i),beta(i),Acntct(i),
     +   reff(i),theta(i),phi(i)
         write(iout,2400)
2400     format(//,1x,'Ending parameters are:',/)
         i=2
         write(iout,2300) Qzz(i),eta(i),alpha(i),beta(i),Acntct(i),
     +   reff(i),theta(i),phi(i)
         write(iout,2500)
2500     format(//,1x,'Increaments are:',/)
         i=3
         write(iout,2300) Qzz(i),eta(i),alpha(i),beta(i),Acntct(i),
     +   reff(i),theta(i),phi(i)
2300     format(8(g12.5,1x))
         if(option.eq.1.or.option.eq.3) then
          if (tau0.gt.0.d0) then
           write(iout,2710) tau0,(delf*mout),delf
2710       format(/,' 3-pulse at tau= ',g10.5,' us spanning ',g10.5,
     +     ' MHz with resolution= ',g10.5,' MHz'/)
          else
           write(iout,2715) (delf*mout),delf
2715       format(/,' 2-pulse Simulation spanning ',g10.5,
     +     ' MHz with resolution= ',g10.5,' MHz'/)
          endif
```

```
            if(no_dc) write(iout,2735)
2735        format(/,' DC component will be artificially supressed'/)
            if(smooth) write(iout,2740) sigma
2740        format(/,' Simulated Spectrum will be broadened with',
     +      /,8x,'Lorentzian line, where Gamma=',g10.5,' MHz',/)
           elseif(option.eq.2.or.option.eq.4) then
            if (tau0.gt.0.d0) then
             write(iout,2700) t0,delf,mout,tau0
2700        format(/,' 3-pulse Simulation from',g10.5,' us at',g10.5,
     +      ' us for',i5,' points',
     +      /8x,'with tau= ',g10.5/)
            else
             write(iout,2705) t0,delf,mout
2705        format(/,' 2-pulse Simulation from',g10.5,' us at',g10.5,
     +      ' us for',i5,' points'/)
            endif
           endif
           ymax=ymax-ymin
           do 7800 i=1,mout
            orig(i)=(orig(i)-ymin)/ymax
7800       continue
           if(Qzz(3).eq.0.d0.and.eta(3).eq.0.d0.and.Acntct(3).eq.0.d0
     +     .and.alpha(3).eq.0.d0.and.beta(3).eq.0.d0.and.reff(3).eq.0.d0
     +     .and.theta(3).eq.0.d0.and.phi(3).eq.0.d0) then
            ymax=sngl(delf)*mout
            call ftkout(12,mout,ymax,orig)
c           open(unit=12,form='unformatted',status='new')
c           write(12) header
c           do i=1,mout
c             write(12) sngl(delf)*(i-1),orig(i)
c           end do
c           close(12)
           endif
           return
           end


           subroutine lis_inf(option,tau0,t0,delt,nthe,mout,nucl,ispin,dipol,
     +     no_dc,smooth,sigma,io)
c
c ------- output to a file
c
           implicit double precision(a-h,o-z)
           parameter(nuclei=10)
           logical         dipol,smooth,no_dc
           integer                 option
           dimension       ispin(nuclei)
           dimension       gnu(nuclei),Qzz(nuclei),Qxxyy(nuclei)
           dimension       alpha(nuclei),gamma(nuclei),beta(nuclei)
           dimension       reff(nuclei),phi(nuclei),theta(nuclei)
           dimension       acntct(nuclei)
           common          /gtnsor/g1,g2,g3,geff,h0,the0,phi0
           common /in_n/gnu,acntct,Qzz,Qxxyy,alpha,beta,gamma,reff,theta,phi
           be=9.274026d-21
```

```
      bn=5.050824d-24
      h=6.626093d-27
C
C ——— OUTPUT FILE FORMATS
C
      write(io,2100) H0,geff
2100  format(/5x,' Static magnetic field =',g10.5,' G',
     +  /,8X,'with geff =',g12.7,/)
      write(io,2105) g1,g2,g3
2105  format(/5x,' g1 =',g12.7,5x,'g2 =',g12.7,5x,'g3 =',g12.7/)
      write(io,2450) nthe
2450  format(/5x,' Divisions of sin(theta) wrt g coordinates =',i6/)
      write(io,2110) nucl
2110  format(/5x,' The elctron is coupled to',i3,' nuclei.'/)
      do i=1,nucl
      write(io,2115) i,ispin(i)
2115  format(/5x,' For nucleus',i3,' 2I+1 = ',i3/)
      fi=gnu(i)*bn*h0/h/1.d6
      write(io,2200) fi,gnu(i)
2200  format(/8x,' Nuclear Zeeman freq. at geff =',g10.5,' MHz',
     +  /,8X,'with gn =',g12.7)
      write(io,2400) Acntct(i)
2400  format(/8x,' Isotropic contact =',g9.4,' MHz')
      vplus=3.d0*Qzz(i)+Qxxyy(i)
      vminus=3.d0*Qzz(i)-Qxxyy(i)
      write (io,2550) Qzz(i),Qxxyy(i),vplus,vminus
2550  format(/8x,' Nuclear Quadrupole term: Qzz=',g10.5,' MHz',
     +  ' Qxxyy=',g10.5,' MHz',
     +  /,5x,'where v+ = ',g10.5,' MHz, v- = ',g10.5,' MHz.')
      write(io,2730) alpha(i),beta(i),gamma(i)
2730  format(/8x,'wrt g coordinates, alpha= ',g8.3,5x,
     +       ' beta= ',g8.3,5x,' gamma= ',g8.3)
      if(dipol) then
       fdipol=gnu(i)*geff*(be/h)*(bn*1.d+18)/(reff(i)**3)
       write(io,2500) reff(i),theta(i),phi(i),fdipol
2500   format(/8x,' Reff =',g10.5,' Angs.',5x,' theta= ',g8.3,5x,
     +   ' phi= ',g8.3,/11x,'with F at geff is about ',g12.7,' MHz'/)
      endif
      end do
      if(option.eq.2) then
       if (tau0.gt.0.d0) then
        write(io,2700) t0,delt,mout,tau0
2700    format(/5x,' 3-pulse Simulation from',g10.5,' us at',g10.5,
     +   ' us for',i5,' points',
     +   /8x,'with tau= ',g10.5/)
       else
        write(io,2705) t0,delt,mout
2705    format(/5x,' 2-pulse Simulation from',g10.5,' us at',g10.5,
     +   ' us for',i5,' points'/)
       endif
      else
       if(option.eq.1) then
        ftotal=delt*dfloat(mout)
        if (tau0.gt.0.d0) then
```

```
          write(io,2710) tau0,ftotal,delt
2710      format(/5x,' 3–pulse at tau= ',g10.5,' us spanning ',g10.5,
     +     ' MHz with resolution= ',g10.5,' MHz'/)
          else
          write(io,2715) ftotal,delt
2715      format(/5x,' 2–pulse Simulation spanning ',g10.5,
     +     ' MHz with resolution= ',g10.5,' MHz'/)
          endif
          if(no_dc) write(io,2735)
2735      format(/5x,' DC component is artificially supressed'/)
          if(smooth) write(io,2740) sigma
2740      format(/,5x,' Spectrum is smoothed, with Gaussian function:',
     +  /,8x,' e(–{(f–f0)/sigma}**2), where sigma =',g10.5,' MHz',/)
          else
          ftotal=delt*dfloat(mout)
          write(io,2725) h0,ftotal,delt
2725      format(/5x,' EI–ESR Simulation centered at',g12.7,' Gauss,'
     +     ' spanning ',g12.7,' Gauss with resolution= ',g8.3,' Gauss'/)
          endif
          endif
          write (io,2600)
2600      format(//,30x,'**********',/)
          close(unit=io)
          return
          end


          subroutine matadd (a,b,c,m1,m2,jflag)
c
c         PURPOSE:   matrix addition; +: add; –: substract
c
c–––––––––––––––––––––––––––––––––––––––––––––––––––––––––––––––––––––––––––––––
          double precision a(32,32),b(32,32),c(32,32)
          double precision t1
          t1=dfloat(jflag)
          do 1 i=1,m1
           do 1 j=1,m2
            c(i,j)=a(i,j)+b(i,j)*t1
    1     continue
          return
          end


          subroutine match(mout,ydata,rmsq)
          implicit real(a–h,o–z)
          real*4              orig(2048),rmsq,ydata(2048)
          common              /finale/orig
          byte   header(72)
          ymax=ydata(1)
          ymin=ymax
          do i=2,mout
           if(ydata(i).gt.ymax) ymax=ydata(i)
           if(ydata(i).lt.ymin) ymin=ydata(i)
```

```
      end do
      rmsq=0.
      ymax=ymax-ymin
      if(ymax.ne.0.) then
       do i=1,mout
        ydata(i)=(ydata(i)-ymin)/ymax
        rmsq=rmsq+(ydata(i)-orig(i))**2
       end do
      else
       rmsq=float(mout)
      endif
      rmsq=sqrt(rmsq/float(mout))
      return
      end


      subroutine mat_dia(in,a,b,w,c,d)
c
c     PURPOSE:  diagonalize Hermitian matrix, finding
c               eigenvalues and eigenvectors
c
c     CALLING:  CH of EISPACK

c-----------------------------------------------------------------------
      double precision a(32,32),b(32,32),c(32,32)
      double precision d(32,32),w(32)
      double precision fv1(32),fv2(32),fm1(2,32),ww(32)
c     external ch
      call ch(32,in,a,b,w,1,c,d,fv1,fv2,fm1,ieer)
      if (ieer.ne.0) print *,'*** DIAGONIZATION ERROR ***'
      return
      end
c
c
      subroutine mat_ext (a,b,c,m1,m2,m3)
c
c     PURPOSE:  matrix direct product extension
c               restricting to square matrices only

c     PARAMETERS:   a is m1 by m1, b, m2 by m2 and
c               c, m3 by m3 matrices;
c               m1 times m2 equal m3

c-----------------------------------------------------------------------
      double precision  a(32,32),b(32,32),c(32,32)
      m3=m1*m2
      if (m1.eq.1) then
       do 2 i=1,m2
        do 2 j=1,m2
         c(i,j)=a(1,1)*b(i,j)
2      continue
       goto 4
```

```
      endif
      if (m2.eq.1) then
       do 3 i=1,m1
        do 3 j=1,m1
         c(i,j)=a(i,j)*b(1,1)
3     continue
       goto 4
      endif
      do 1 i=m1,1,-1
       do 1 j=m1,1,-1
        do 1 k=m2,1,-1
         do 1 n=m2,1,-1
          n1=(i-1)*m2+k
          n2=(j-1)*m2+n
          c(n1,n2)=a(i,j)*b(k,n)
1     continue
4     return
      end


      subroutine mat_gen(iflag,ispin,a,imag,coeff,add)
c
c     generate matrix according to iflag and isipn, with constant
c     factor and real (imaginery) taken care.
c
c     iflag = 1     unit
c             2     Sz(Iz)
c             3     S+(I+)
c             4     S-(I-)
c             5     Sx(Ix)
c             6     Sy(Iy)
c     ispin = 2     S(I)=1/2
c             3     S(I)=1
c     imag  = 1     matrix is imaginery
c     imag  = 0     matrix is not imaginery
c
      implicit double precision(a-h,o-z)
      logical       add
      dimension     a(32,32)
      imag = 0
      if (.not.add) then
      coeff=1.d0
      do 5 i=1,ispin
       do 5 j=1,ispin
        a(i,j)=0.d0
5     continue
      endif
      go to (10,20,30,40,50,60), iflag
      if(iflag.gt.6.or.iflag.lt.1) stop' *** no such option in MAT_GEN *** '
10    do 15 i=1,ispin
       a(i,i)=a(i,i)+coeff
15    continue
      return
20    a(1,1)=a(1,1)+coeff*dfloat(ispin-1)/2.d0
```

```
      a(ispin,ispin)=a(ispin,ispin)-coeff*dfloat(ispin-1)/2.d0
      return
30    do 25 i=2,ispin
        a(i-1,i)=a(i-1,i)+dsqrt(dfloat(ispin-1))*coeff
25    continue
      return
40    do 35 i=2,ispin
        a(i,i-1)=a(i,i-1)+coeff*dsqrt(dfloat(ispin-1))
35    continue
      return
50    if(ispin.eq.2) then
        a(1,2)=a(1,2)+0.5d0*coeff
        a(2,1)=a(2,1)+0.5d0*coeff
      else
        a(1,2)=a(1,2)+coeff*dsqrt(0.5d0)
        a(2,3)=a(2,3)+coeff*dsqrt(0.5d0)
        a(2,1)=a(2,1)+coeff*dsqrt(0.5d0)
        a(3,2)=a(3,2)+coeff*dsqrt(0.5d0)
      endif
      return
60    imag=1
      if(ispin.eq.2) then
        a(1,2)=a(1,2)-0.5d0*coeff
        a(2,1)=a(2,1)+0.5d0*coeff
      else
        a(1,2)=a(1,2)-coeff*dsqrt(0.5d0)
        a(2,3)=a(2,3)-coeff*dsqrt(0.5d0)
        a(2,1)=a(2,1)+coeff*dsqrt(0.5d0)
        a(3,2)=a(3,2)+coeff*dsqrt(0.5d0)
      endif
      return
      end
c
c
c     subroutine matmul (a,b,c,m1,m2,m3)
c
c     PURPOSE:   matrix multiplication
c
c-----------------------------------------------------------------------
      double precision a(32,32),b(32,32),c(32,32)
c
c   a is m1 by m2 matrix, b is m2 by m3 matrix, c is their product
c
      do 1 i=1,m1
       do 1 j=1,m3
        c(i,j)=0.0d0
        do 1 k=1,m2
         c(i,j)=c(i,j)+a(i,k)*b(k,j)
  1   continue
      return
      end
```

```
      subroutine nq_euler(a,b,hr,hi,alpha,beta,gamma)
c
c     PURPOSE:  adding to Hermitian matrix the NQ term in a
c               coordinate system which is (alpha,beta,gamma)
c               relative to (x,y,z), in the (I,Iz)
c               representation
c               only valid for I=1
c
c     DEFINITION:     a=Qzz; B=Qxxyy
c               alpha, beta and gamma are all in radians
c
c     H. Jin            Feb. 1, 1989
c-----------------------------------------------------------------------
      implicit double precision(a-h,o-z)
      parameter(max=32)
      dimension   hr(max,max),hi(max,max)
      dimension   tran1r(max,max),tran1i(max,max)
      dimension   tran2r(max,max),tran2i(max,max)
c
      chbeta=dcos(beta/2.d0)
      chbeta=chbeta*chbeta
      shbeta=dsin(beta/2.d0)
      shbeta=shbeta*shbeta
      sbeta=dsin(beta)/dsqrt(2.0d0)
      do 10 i=1,3
        do 10 j=1,3
          hr(i,j)=0.d0
          hi(i,j)=0.d0
          tran1r(i,j)=0.d0
          tran1i(i,j)=0.d0
10    continue
c ---- NQI in the PAS
      hr(1,1)=a
      hr(2,2)=-2.0d0*a
      hr(3,3)=a
      hr(1,3)=b
      hr(3,1)=b
c ---- now the transformation matrix
      tran1r(1,1)=chbeta*dcos(alpha-gamma)
      tran1r(3,3)=tran1r(1,1)
      tran1i(1,1)=chbeta*dsin(alpha-gamma)
      tran1i(3,3)=-tran1i(1,1)
      tran1r(2,2)=dcos(beta)
      tran1r(1,2)=sbeta*dcos(alpha)
      tran1i(1,2)=sbeta*dsin(alpha)
      tran1r(3,2)=tran1r(1,2)
      tran1i(3,2)=-tran1i(1,2)
      tran1r(2,1)=-sbeta*dcos(gamma)
      tran1i(2,1)=-sbeta*dsin(gamma)
      tran1r(2,3)=tran1r(2,1)
      tran1i(2,3)=-tran1i(2,1)
c     tran1r(1,2)=-sbeta*dsin(alpha)
c     tran1i(1,2)=sbeta*dcos(alpha)
```

```
c          tran1r(3,2)=-tran1r(1,2)
c          tran1i(3,2)=tran1i(1,2)
c          tran1r(2,1)=-sbeta*dsin(gamma)
c          tran1i(2,1)=sbeta*dcos(gamma)
c          tran1r(2,3)=-tran1r(2,1)
c          tran1i(2,3)=tran1i(2,1)
           tran1r(1,3)=-shbeta*dcos(gamma+alpha)
           tran1r(3,1)=tran1r(1,3)
           tran1i(1,3)=shbeta*dsin(gamma+alpha)
           tran1i(3,1)=-tran1i(1,3)
c ------ now the inverse of transformation maxtrix
           call hermit(3,tran1r,tran1i,tran2r,tran2i)
c ------ T+*H'*T=H
           call cmatmul(tran2r,tran2i,hr,hi,hr,hi,3,3,3)
           call cmatmul(hr,hi,tran1r,tran1i,hr,hi,3,3,3)
           return
           end


           subroutine psu_zmn(gnu,idim,v0,theta,phi,hr,hi,gz,gep,
     +     two_D,Aiso,fdip,the_n,phi_n)
c
c          zeeman energy including pseudo nuclear zeeman effect
c                v0=bn*h0/h
c                gyrat=be/bn
c                two_d=2D for the energy seperation
c                Aiso,fdipol,the_n,phi_n hyperfine parameter
c            pseudo Nuclear zeeman effect:
c
c                V0 * (gn+gn) * I
c
           implicit double precision(a-h,o-z)
           parameter(max=32)
           dimension     hr(max,max),hi(max,max),c(max,max),a(max,max)
           do 10 i=1,idim
             do 10 j=1,idim
               hr(i,j)=0.d0
               hi(i,j)=0.d0
               c(i,j)=0.d0
10         continue
c ------ set up field vetor
           v0x=v0*dsin(theta)*dcos(phi)
           v0y=v0*dsin(theta)*dsin(phi)
           v0z=v0*dcos(theta)
c ------ constant factor
           factor=-1.5d0*1.836141d3*gep/gnu/two_D  ! 1.836141e3=be/bn
c ------ set up gnu matrix
           temp=3.0d0*dsin(the_n)**2
           A(1,1)=factor*(Aiso+fdip*(temp*dcos(phi_n)**2-1.0d0))+gnu
           A(1,2)=factor*fdip*temp*dsin(phi_n)*dcos(phi_n)
           A(2,1)=a(1,2)
           A(2,2)=factor*(Aiso+fdip*(temp*dsin(phi_n)**2-1.0d0))+gnu
           A(3,1)=fdip*dsin(the_n)*dcos(the_n)*dcos(phi_n)factor
           A(3,2)=fdip*dsin(the_n)*dcos(the_n)*dsin(phi_n)*factor
```

```
      A(1,3)=0.d0
      A(2,3)=0.d0
      A(3,3)=gnu
c ----- V0*g*I
      coeff=v0x*A(1,1)+v0y*A(2,1)+v0z*A(3,1)
      call any_i(5,idim,hr,imag,coeff,.true.)
      coeff=v0y*A(1,2)+v0y*A(2,2)+v0z*A(3,2)
      call any_i(6,idim,hi,imag,coeff,.true.)
      coeff=v0z*A(1,3)+v0y*A(2,3)+v0z*A(3,3)
      call any_i(2,idim,c,imag,coeff,.true.)
      call matadd(hr,c,hr,idim,idim,1)
      return
      end


      subroutine smterm(idim,aiso,the_n,phi_n,f,hr,hi,dipol)
c
c     terms grouped with S+
c
      implicit double precision(a-h,o-z)
      logical        dipol
      parameter(max=32)
      common      /gtnsor/g1,g2,g3,geff,h0,the0,phi0
      dimension   hr(max,max),hi(max,max)
      do i=1,idim
        do j=1,idim
          hr(i,j)=0.d0
          hi(i,j)=0.d0
        end do
      end do
      if(.not.dipol) then
        coeff=aiso*g1/2.d0
        call mat_gen(5,idim,hr,imag,coeff,.true.) ! Ix term
        coeff=-aiso*g2/2.d0
        call mat_gen(6,idim,hr,imag,coeff,.true.) ! Iy term
        return
      else
        coeff=(aiso-f)*g1/2.d0
        call mat_gen(5,idim,hr,imag,coeff,.true.) ! Ix term
        coeff=-(aiso-f)*g2/2.d0
        call mat_gen(6,idim,hr,imag,coeff,.true.) ! Iy term
      endif
      cthe=dcos(the_n)
      sthe=dsin(the_n)
      cphi=dcos(phi_n)
      sphi=dsin(phi_n)
      coeff=1.5d0*f*g1*sthe**2*cthe*cphi
      call mat_gen(2,idim,hr,imag,coeff,.true.) ! Iz term
      coeff=1.5d0*f*g2*sthe*cthe*sphi
      call mat_gen(2,idim,hi,imag,coeff,.true.) ! Iz term
      coeff=1.5d0*g1*f*sthe**2*sphi**2
      call mat_gen(5,idim,hr,imag,coeff,.true.) ! Ix term
      coeff=1.5d0*g2*f*sthe**2*cphi*sphi
      call mat_gen(5,idim,hi,imag,coeff,.true.) ! Ix term
```

```
          coeff=-1.5d0*g2*f*sthe**2*cphi**2
          call mat_gen(6,idim,hr,imag,coeff,.true.) ! Iy terrm
          coeff=1.5d0*g1*f*sthe**2*cphi*sphi
        coeff=-1.5d0*g2*f*sthe**2*cphi**2                    rrm
        call mat_gen(6,idim,hr,imag,coeff,.true.) ! Iy terrm
        coeff=1.5d0*g1*f*sthe**2*cphi*sphi


          subroutine sort2(n,ra,rb)
          implicit real*4 (a-h,o-z)
          implicit integer*2 (i-n)
          dimension     ra(n)
          integer*2     rb(n)
c
c   subroutine modified from P.231 "Numerical Recipe"
c
          L=n/2+1
          ir=N
10        continue
           if(L.gt.1) then
             L=L-1
             rra=ra(L)
             irb=rb(L)
           else
             rra=ra(ir)
             irb=rb(ir)
             ra(ir)=ra(1)
             rb(ir)=rb(1)
             ir=ir-1
             if(ir.eq.1) then
               ra(1)=rra
               rb(1)=irb
               return
             endif
           endif
           i=L
           j=L+L
20         if(j.le.ir) then
             if(j.lt.ir) then
               if(ra(j).lt.ra(j+1)) j=j+1
             endif
             if(rra.lt.ra(j)) then
               ra(i)=ra(j)
               rb(i)=rb(j)
               i=j
               j=j+1
             else
               j=ir+1
             endif
             goto 20
           endif
           ra(i)=rra
           rb(i)=irb
          goto 10
```

```
      end


      subroutine spterm(idim,aiso,the_n,phi_n,f,hr,hi,dipol)
c
c     terms grouped with S+
c
      implicit double precision(a-h,o-z)
      logical       dipol
      parameter(max=32)
      common        /gtnsor/g1,g2,g3,geff,h0,the0,phi0
      dimension     hr(max,max),hi(max,max)
      do i=1,idim
        do j=1,idim
          hr(i,j)=0.d0
          hi(i,j)=0.d0
        end do
      end do
      if(.not.dipol) then
        coeff=aiso*g1/2.d0
        call mat_gen(5,idim,hr,imag,coeff,.true.) ! Ix term
        coeff=aiso*g2/2.d0
        call mat_gen(6,idim,hr,imag,coeff,.true.) ! Iy term
        return
      else
        coeff=(aiso-f)*g1/2.d0
        call mat_gen(5,idim,hr,imag,coeff,.true.) ! Ix term
        coeff=(aiso-f)*g2/2.d0
        call mat_gen(6,idim,hr,imag,coeff,.true.) ! Iy term
      endif
      cthe=dcos(the_n)
      sthe=dsin(the_n)
      cphi=dcos(phi_n)
      sphi=dsin(phi_n)
      coeff=1.5d0*f*g1*sthe**2*cthe*cphi
      call mat_gen(2,idim,hr,imag,coeff,.true.) ! Iz term
      coeff=-1.5d0*f*g2*sthe**2*cthe*sphi
      call mat_gen(2,idim,hi,imag,coeff,.true.) ! Iz term
      coeff=1.5d0*g1*f*sthe**2*sphi**2
      call mat_gen(5,idim,hr,imag,coeff,.true.) ! Ix term
      coeff=-1.5d0*g2*f*sthe**2*cphi*sphi
      call mat_gen(5,idim,hi,imag,coeff,.true.) ! Ix term
      coeff=1.5d0*g2*f*sthe**2*cphi**2
      call mat_gen(6,idim,hr,imag,coeff,.true.) ! Iy terrm
      coeff=1.5d0*g1*f*sthe**2*cphi*sphi
      call mat_gen(6,idim,hi,imag,coeff,.true.) ! Iy terrm
      return
      end


      subroutine szterm(idim,aiso,the_n,phi_n,f,hr,hi,dipol)
c
c     terms grouped with Sz
c
```

```
      implicit double precision(a-h,o-z)
      logical          dipol
      parameter(max=32)
      common           /gtnsor/g1,g2,g3,geff,h0,the0,phi0
      dimension        hr(max,max),hi(max,max)
      do i=1,idim
       do j=1,idim
        hr(i,j)=0.d0
        hi(i,j)=0.d0
       end do
      end do
      coeff=g3*aiso
      if(.not.dipol) then
       call mat_gen(2,idim,hr,imag,coeff,.true.) ! Iz term
       return
      endif
      cthe=dcos(the_n)
      sthe=dsin(the_n)
      cphi=dcos(phi_n)
      sphi=dsin(phi_n)
      coeff=coeff-g3*f*(1.d0-3.d0*cthe**2)
      call mat_gen(2,idim,hr,imag,coeff,.true.) ! Iz term
      coeff=3.d0*g3*f*sthe*cthe*cphi
      call mat_gen(5,idim,hr,imag,coeff,.true.) ! Ix term
      coeff=3.d0*g3*f*sthe*cthe*sphi
      call mat_gen(6,idim,hi,imag,coeff,.true.) ! Iy terrm
      return
      end


      subroutine TEST(in,w,hamr,hami,eigr,eigi)
c
c     PURPOSE:   confirm diagonalization
c
c     CALLED BY:        DIRECT (MAIN)
c
c-----------------------------------------------------------------------
      double precision       hamr(32,32),hami(32,32),w(32),b(32,32)
      double precision       eigr(32,32),eigi(32,32),a(32,32)
      external               matadd,matmul
      call matmul (hamr,eigr,a,in,in,in)
      call matmul (hami,eigi,b,in,in,in)
      call matadd (a,b,a,in,in,-1)
      do 1 i=1,in
       do 1 j=1,in
        b(i,j)=eigr(i,j)*w(j)
        if (dabs(b(i,j)-a(i,j)).gt.1.0d-10) print *,'wrong at Re',i,j
1     continue
      call matmul (hamr,eigi,b,in,in,in)
      call matmul (hami,eigr,a,in,in,in)
      call matadd (b,a,b,in,in,1)
      do 2 i=1,in
       do 2 j=1,in
```

```
        eigi(i,j)=eigi(i,j)*w(j)
        if (dabs(eigi(i,j)-b(i,j)).gt.1.0d-10) print *,'wrong at Im',i,j
2       continue
        return
        end


        subroutine zeeman(g1,g2,g3,idim,v0,theta,phi,hr,hi)
c
c       zeeman energy including anisotropic g or chemical shifts tensor
c       for electron v0=b*h0/h
c
        implicit double precision(a-h,o-z)
        parameter(max=32)
        dimension     hr(max,max),hi(max,max)
        do i=1,idim
          do j=1,idim
            hr(i,j)=0.d0
            hi(i,j)=0.d0
          end do
        end do
        gzx=v0*g1*dsin(theta)*dcos(phi)
        gzy=v0*g2*dsin(theta)*dsin(phi)
        gzz=v0*g3*dcos(theta)
        if (idim.eq.2) then
          hr(1,1)=hr(1,1)+0.5d0*gzz
          hr(2,2)=hr(2,2)-0.5d0*gzz
          hr(1,2)=hr(1,2)+0.5d0*gzx
          hr(2,1)=hr(2,1)+0.5d0*gzx
          hi(1,2)=hi(1,2)-0.5d0*gzy
          hi(2,1)=hi(2,1)+0.5d0*gzy
        elseif(idim.eq.3) then
          hr(1,1)=hr(1,1)+gzz
          hr(1,2)=hr(1,2)+dsqrt(0.5d0)*gzx
          hi(1,2)=hi(1,2)-dsqrt(0.5d0)*gzy
          hr(2,1)=hr(2,1)+dsqrt(0.5d0)*gzx
          hi(2,1)=hi(2,1)+dsqrt(0.5d0)*gzy
          hr(2,3)=hr(2,3)+dsqrt(0.5d0)*gzx
          hi(2,3)=hi(2,3)-dsqrt(0.5d0)*gzy
          hr(3,2)=hr(3,2)+dsqrt(0.5d0)*gzx
          hi(3,2)=hi(3,2)+dsqrt(0.5d0)*gzy
          hr(3,3)=hr(3,3)-gzz
        endif
        return
        end
```

BIBLIOGRAPHY

Abragam, A.; Bleaney, B. *Electron Paramagnetic Resonance of Transition Ions*, Clarendon, Oxford, 1970.

Anderson, M. W.; Kevan, L. *J. Phys. Chem.* 1986, *90*, 6452–6459.

Antonio, M. R.; Teo, B. –K.; Orme–Johnson, W. H.; Nelson, M. J.; Groh, S. E.; Lundahl, P. A.; Kauzlarich, S. M.; Averill, B. A. *J. Am. Chem. Soc.* 1982, *104*, 4703.

Ashby, C. I. H.; Cheng, C. P.; Brown, T. L. *J. Am. Chem. Soc.* 1978, *100*, 6057–6063.

Ashby, C. I. H.; Cheng, C. P.; Duesler, E. N.; Brown, T. L. *J. Am. Chem. Soc.* 1978, *100*, 6063.

Astashkin, A. V.; Dikanov, S. A.; Tsvetkov, Y. D. *Chem. Phys. Lett.* 1987, *136*, 204.

Barendswaard, W.; Disselhorst, J. A. J. M.; Schmidt, J. *J. Magn. Reson.* 1984, *58*, 477.

Barkhuijsen, H.; de Beer, J.; Bovee, W. M. M. J.; Van Ormondt, D. *J. Magn. Reson.* 1985, *61*, 465.

Beinert, H.; Griffiths, D. E.; Wharton, D. C.; Sands, R. H. *J. Biol. Chem.* 1962, *237*, 2337–2346.

Biehl, R.; Schmalbein, D. *United States Patent* 1982, 4312204.

Bishop, P. E.; Jarlenski, D. M. L.; Hetherington, D. R. *Proc.* Natl. *Acad. Sci. USA*, 1980, *77*, 7342.

Bishop, P. E. *Trends Biochem. Sci.* 1986, *11*, 225–227.

Blackburn, T. H. in *Microbial Geochemistry*; Krumbein, W. E. ed.; Blackwell Scientific, Oxford, 1983.

Bloembergen, N.; Rowland, T. J. *Phys. Rev.* 1955, *97*, 1679.

Blumberg, W. E.; Mims, W. B.; Zuckerman, D. *Rev. Sci. Instrum.* 1973, *44*, 546.

Boas, F.; Pilbrow, J.R.; Smith, D. in *Biological Magnetic Resonance*; Berliner, L.J.; Reuben, J., Eds.; Plunum Press: New York; 1977; *1*, 277–342.

Brigle, K. E.; Newton, W. E.; Dean, D. R. *Gene* 1985, *37*, 37–44.

Burgmayer, S. J. N.; Stiefel, E. I. *J. Chem. Edu.* 1985, *62*, 943.

Cammack, R.; Chapman, A.; McCracken, J.; Cornelius, J. B.; Peisach, J.; Weiner,

J. H. *Biochim. Biophys. Acta.* **1988**, *956*, 307–312.

Canters, G. W.; de Boer, E. *Mol. Phys.* **1967**, *13*, 395.

Cho, H.; Pfenninger, S.; Gemperle, C.; Schweiger, A.; Ernst, R. R. *Chem. Phys. Lett.* **1989**, *160*, 391.

Cohen, M. H.; Reif, F. *Solid State Physics*; Academic, New York, **1957**; Vol. 5, 321.

Cole, T.; Heller, C.; McCornell, H. M. *Proc. Natl. Acad. Sci. USA* **1959**, *45*, 525.

Conradson, S. D.; Burgess, B. K.; Newton, W. E.; Mortenson, L. E.; Hodgson, K. O. *J. Am. Chem. Soc.* **1987**, *109*, 7507.

Cowen, J. A.; Kaplan, D. A. *ibid.* **1961**, *124*, 1098.

Coyle, C. L.; Zumft, W. G.; Kroneck, P. M. H.; Korner, H.; Jakob, W. *Eur. J. Biochem.* **1985**, *153*, 459–467.

Cramer, S. P.; Hodgson, K. O.; Gillum, W. O.; Mortensen, L. E. *J. Am. Chem. Soc.* **1978**, *100*, 3398.

Cramer, S. P. *Adv. in Inorg. & Bioinorg. Meth.* , **1983**, *2*, 259–316.

Das, T. P.; Hahn, E. L. *Solid State Physics*; Academic, New York, **1958**; Suppl. 1.

Deisenhofer, J.; Epp., O.; Miki, K.; Huber, R.; Michel, H. *Nature* **1985**, *318*, 618.

Dikanov, S. A.; Shubin, A. A.; Parmon, V. N. *J. Magn. Reson.* **1981**, *42*, 474–487.

Dikanov, S. A.; Evelo, R. G.; Hoff, A. J.; Tyryshkin, A. M. *Chem. Phys. Lett.* **1989**, *154*, 34.

Dixon, R. A. *J. Gen. Micro.* **1984**, *130*, 2745.

Doi, K.; McCracken, J.; Peisach, J.; Aisen, P. *J. Biol. Chem.* **1988**, *263*, 5757–5763.

Dooley, D. M.; Moog, R. S.; Zumft, W. G. *J. Am. Chem. Soc.* **1987**, *109*, 6730–6735.

Edmonds, D. T.; Summers, C. P. *J. Magn. Reson.* **1973**, *12*, 134–142.

Edmonds, D. T. *Physics Report* **1977**, *29*, 233–290.

Fauth, J. –M.; Schweiger, A.; Braunschwieler, L.; Forrer, J.; Ernst, R. R. *J. Magn. Reson.* **1986**, *66*, 74–85.

Fee, J.A., *Struct. Bonding* **1975**, *23*, 1–60.

Fee, J. A.;Peisach, J.; Mims, W. B. *J. Biol. Phys.* **1981**, *256*, 1910–1914.

Fermi, E. *Z. Physik* 1930, *60*, 320.

Flanagan, H. L.; Single, D. J. *J. Chem. Phys.* 1987, *88*, 5606.

Flanagan, H. L.; Gerfen, G. L.; Lai, A.; Single, D. J. *J. Chem. Phys.* 1988, *88*, 2162.

George, G. N.; Bare, R. E.; Jin, H.; Stiefel, E. I.; Prince, R. C. *Biochem. J.* 1989, *262*, 349–352.

Griffith, J. S. *The Theory of Transition–Metal Ions*, Cambridge University Press, 1961.

Hahn, E. L. *Phys. Rev.* 1950, *80*, 580.

Hardy, R. W. F. *Treatise on Dinitrogen fixation*, Wiley and Sons, New York, 1979.

Hase, T.; Wakabayashi, S.; Nakano, T.; Zumft, W. G.; Matsubara, H. *FEBS* 1984, *166*, 39–43

Huisjen, M.; Hyde, J. S. *Rev. Sci. Instrum.* 1974, *45*, 669.

Hausinger, R. P.; Howard, J. B. *J. Biol. Chem.* 1983, *258*, 13486.

Hawkes, T. R.; McLean, P. A.; Smith, B. E. *Biochem. J.* 1984 *217*, 317.

Hoffman, B. M.; Martisen, J.; Venters, R. A. *J. Magn. Reson.* 1984, *59*, 110.

Hoffman, B. M.; Venters, R. A.; Martisen, J. *ibid*, 1985, *62*, 537.

Holm, L.; Saraste, M.; and Wikstrom, M. *EMBO J.* 1987, *6*, 2819–2823.

Hoover, T. R.; Imperial, J.; Ludden, P. W.; Shah, V. K. *Biochemistry* 1989, *28*, 2768–2771.

Hsieh, Y. –N.; Rubebacker, G. V.; Cheng, C. P.; Brown, T. L. *J. Am. Chem. Soc.* 1977, *99*, 1394–1389.

Hunt, M. J.; Mackay, A. L. *J. Magn. Reson.* 1974, *15*, 402–414.

Hunt, M. J.; Mackay, A. L.; Edmonds, D. T. *Chem. Phys. Lett.* 1975, *34*, 473–475.

Hunt, M. J.; Mackay, A. L. *J. Magn. Reson.* 1976, *22*, 295–301.

Hurst, G. C.;Henderson, T. A.; Kreilick, R. W. *J. Am. Chem. Soc.* 1985, *107*,7294.

Hurst, G. C.; Henderson, T. A.; Kreilick, R. W. *ibid*, 1985, *107*, 7299.

Jiang, F.; McCracken, J.; Peisach, J. *XIII International Conference on Magnetic Resonance in Biological Systems*, 1988 pp 17–19.

Jin, H.; Thomann, H.; Coyle, C. L.; Zumft, W. G. *J. Am. Chem. Soc.* 1989, *111*, 4262.

Kamaresan, R.; Tufts, D. W. *IEEE Trans.* 1982, *ASSP–30*, 833,Kay, S. M.; Marple, S. L. *Proc. IEEE* 1981, *69*, 1380.

Kevan, L. in *Time Domain Electron Spin Resonance*, Kevan, L.; Schwartz, R. N. eds.; Wiley, New York, 1979, 279.

Kosman, D. J.; Peisach, J.; Mims, W. B. *Biochemistry.* 1980, *19*, 1304–1308.

Lowry, O. H.; Rosebrough, N. J.; Farr, A. L.; Randall, R. J. *J. Biol. Chem.* 1951, *193*, 265–275.

Lucken, E. A. C. *Nuclear Quadrupole Coupling Constants*; Academic, New York, 1969.

Makhoul, J. In *Modern Spectral Analysis*, Childers, D. G. ed.; IEEE Press, Wiley, New York, 1978, 99–118.

Malkin, R.; Malmström, B. G., *Advances in Enzymology and Related Areas of Molecular Biology* 1970, *33*, 177–244.

Marshall, A. G. ed. *Fourier, Hadamad, and Hilbert Transforms in Chemistry*; Plunum, New York, 1982.

McCornell, H. M.; Chestnut, D. B. *J. Chem. Phys.* 1958, *28*, 107.

McCracken, J.; Peisach, J.; Dooley, D. M. *J. Am. Chem. Soc.* 1987, *109*, 4064–4072.

McCracken, J.; Pember, S.; Benkovic, S.; Villafrance, J. J.; Miller, R. J.; Peisach, J. *J. Am. Chem. Soc.* 1988, *110*, 1069–1074.

McGarvey, B., R. in "*Transition Metal Chemistry*"; Carlin, R. L. ed.; Marcel Dekker, New York, 1966; Vol. 3, 89–201.

Mehring, M.; Freysoldt, F. *J. Phys.* 1980, *13*, 894–896.

Merzbacher, E. *Quantum Mechanics*; John Wiley, New York, 1970.

Messiah, A. *Quantum Mechanics*; Interscience, John Wiley, New York, 1972.

Mims, W. B.; Nassau, K.; McGee, J. D. *Phys. Rev.* 1961, *123*, 2059.

Mims, W. B. *Phys. Rev.* 1972, *B5* 2409 (1972).

Mims, W. B. *ibid* 1972, *B6*, 3543.

Mims, W. B. *Electron Paramagnetic Resonance*, S. Geschwind ed.; Plenum, New York, 1972.

Mims, W. B.; Davis, J. L. *J. Chem. Phys.* **1976**, *64*, 4836–4846.

Mims, W. B.; Peisach, J.; Davis, J. L. *J. Chem. Phys.* **1977**, *66*, 5536–5550.

Mims, W. B.; Peisach, J. *J. Chem. Phys.* **1978**, *69*, 4921.

Mims, W. B.; Peisach, J. *J. Biol. Phys.* **1979**, *254*, 4321–4323.

Mims, W. B.; Peisach, J. *Biological Application of Magnetic Resonance*, Shulman, R. G. ed.; Academic Press, New York; **1979**, 221.

Mims, W. B.; Peisach, J.; Shaw, R. W.; Beinert, H. *J. Biol. Chem.* **1980**, *255*, 6843–6846.

W. B. Mims, W. B.; Peisach, J. *Biological Magnetic Resonance*, Berliner L. J. ; Reuben, J. eds.; Plenum, New York, **1981**; Vol.3, 213.

Mims, W. B. in *Fourier, Hadamad, and Hilbert Transforms in Chemistry*, Marshall, A. G. ed.; Plunum, New York, **1982**.

Mims, W. B. *J. Magn. Reson.* **1984**, *59*, 291–306.

Mims, W. B.; Peisach, J. Preprint.

Mortensen, L. E.; Thorneley, R. N. F. *Ann. Rev. Biochem.* **1979**, *48*, 387–418.

Münck, E.; Rhodes, H.; Orme–Johnson, W. H.; Davis, L. C.; Brill, W. J.; Shah, V. K. *Biochim. Biophys. Acta.* **1975**, *400*, 32.

Nakagawa, K.; Hoffman, B. M.; Zumft, W. G., to be published.

Nakos, G.; Mortenson, L. E. *Biochim. Biophys. Acta.* **1971**, *229*, 431–436.

Orme–Johnson, W. H.; Hamilton, W. D.; Ljones, T.; Tso, M.– Y.; Burris, R. H.; Shah, V. K.; Brill, W. J. *Proc. Natl. Acad. Sci. USA* **1972**, *69*, 3142–3145.

Orme–Johnson, W. H.; Davis, L. C.; Henzl, M. T.; Averill, B. A.; Orme–Hohnson, N. R.; Münck, E.; Zimmerman, R. *Recent Developments in Nitrogen Fixation*; Newton, W. E.; Postage, J. R.; Barrueco, C. R. eds.; Academic press, New York, **1977**, 131.

Orton, J. W. *Electron Paramagnetic Resonance*; Iliffe, London, **1968**.

Palmer, G.; Multani, J. S.; Zumft, W. G.; Mortenson, L. E. *Arch Biochem. Biophys.* **1972**, *153*, 325.

Pau, R. N. *TIBS* **1989**, *14*, 5.Peisach, J.; Blumberg, W.E., *Arch. Biochem. Biophys.* **1974**, *165*, 691–708.

Peisach, J. in *Mechanism of Oxidizing Enzymes*; Singer, T. P.; Ondarza, R. W. eds.; Elseveir: New York; **1977**, 285–306.

Peisach, J.; Mims, W. B.; Davis, J. L. *J. Biol. Chem.* **1979**, *254*, 12379–12389.

Penfield, K. W.; Fewirth, A. A.; Solomon, E. I. *J. Am. Chem. Soc.* **1985**, *107*, 4519–2529

Postage, J. R. *Fundamentals of Nitrogen Fixation*; Cambridge University Press, Cambridge, New York, 1982.

Que, L. ed. *Metal Clusters in Proteins*; ACS Symposium Series 372, Washington, D. C., 1988.

Reinhammer, B.; Hoffman, B. M. *J. Am. Chem. Soc.* **1984**, *106*, 5324–5330.

Riester, J.; Kroneck, P. M. H.; Zumft, W. G. *Eur. J. Biochem.* **1989**, *178*, 751–762.

Rist, G. H.; Hyde, J. S. *J. Chem. Phys.* **1968**, *49*, 2449.

Rist, G. H.; Hyde, J. S. *J. Chem. Phys.* **1970**, *52*, 4532.

Rist, G. H.; Hyde, J. S. *J. Chem. Phys.* **1970**, *52*, 4633.

Roberts, J. E.; Cline, J. F.; Lum, V.; Freeman, H.; Gray, H. B.; Peisach, J.; Rowan, L. G.; Hahn, E. L.; Mims, W. B. *Phys. Rev.* **1965**, *137*, A61.

Robinson, B. *et al.* in *Electron Magnetic Resonance in Solid States*, Weil, J. ed.; Canadian Chemical Society; **1988**.

Scott, D. J.; May, H. D.; Newton, W. E.; Brigle, K. E.; Dean, D. R. Submitted to *Nature*.

Scott, R. A., Zumft, W., G.; Coyle, C. L.; Dooley, D. M. *Proc. Natl. Acad. Sci. USA* **1989**, *86*, 4082–4086.

Schiff, L. E. *Quantum Mechanics*; McGraw–Hill, New York, **1968**.

Schweiger, A.; Ernst, R. R. *J. Magn. Reson.* **1988**, *77*, 512–523.

Semin, G. K.; Babnshkina, T. A.; Yakobson, G. G. *Nuclear Quadrupole Resonance in Chemistry*; Isreal Program for Scientific Translation, John Wiley; **1972**.

Shah, V. K.; Davis, L. C.; Brill, W. J. *Biochim. Biophys. Acta.* **1971**, *256*, 498–511.

Shah, V. K.; Brill, W. J. *Proc. Natl. Acad. Sci. USA* **1977**, *74*, 3249.

Shimizu, T.; Mims, W. B.; Peisach, J.; Davis, J. L. *J. Chem. Phys.* **1979**, *70*, 2249.

Slichter, C. P. *Principle of Magnetic Resonance*; Springer–Verlag, New York, **1980**.

Smith, B. E.; Lowe, D. J.; Bray, R. C. *Biochem. J.* **1972**, *130*, 641–643.

Smith, B. E.; Lowe, D. J.; Bray, R. C. *Biochem. J.* **1973**, *135*, 331–341.

Smith, B. T. *et al. Matrix Eigensystem Routines – EISPACK Guide*, 2nd ed.; Leture Notes in Computer Science, Springer–Verlag, New York; 1981.

Snyder, S.W.; Hollocher, T. C. *J. Biol. Chem.* 1987, *262*, 6515–6525.

Solomon, E. I. in *Copper Proteins*; Spiro, T. ed. Wiley & Sons: New York, 1981.

Solomon, E. I.; Penfield, K. W.; Wilcox, D. E. *Structure and Bonding* 1983, *53*, 1–57, and references therein.

Stephens, P. J. in *Molybdenum Enzymes*; Spiro, T. G. ed.; Wiley and Sons, New York, 1985, 117.

Stevens, T. H.; Martin, C. T.; Wang, H.; Brudvig, G. W.; Scholes, C. P.; Chan, S. I. *J. Biol. Chem.* 1982, *257*, 12106–12113.

Stiefel, E. I.; Cramer, S. P. in *Molybdenum Enzymes*; Spiro, T. G. ed.; Wiley and Sons, New York, 1985, P88.

Stiefel, E. I.; Thomann, H.; Jin, H.; Bare, R. E.; Morgan, T. V.; Burgmayer, S. J. N.; Coyle, C. L. *Metal Clusters in Proteins*; Que, L. ed., ACS Symposium Series 372, Washington, D. C., 1988.

Sundaresan, V.; Ausubel, F. M. *J. Biol. Chem.* 1981, *256*, 2808.

Suryanarayana, D.; Narayana, P. A.; Kevan, L. *Inorg. Chem.* 1983, *22*, 474–478.

Tainer, J.A.; Getzoff, E.D.; Richardson, J.S.; Richardson, D.A., *Nature* 1983, *906*, 285–287.

Tang, J.; Lin, C. P.; Bowman, M. K.; Norris, J. R. *J. Magn. Reson.* 1985, *62*, 167–171.

Tang, J.; Norris, J. R. *J. Magn. Reson.* 1988, *78*, 23–30.

Tang, J.; Norris, J. R. *J. Magn. Reson.* 1988, *79*, 190–196.

Thomann, H.; Dalton, L. R.; Pancake, C. *Rev. Sci. Instrum.* 1984, *55*, 389–398.

Thomann, H.; Morgan, T. V.; Jin, H.; Bergmayer, S. J. N.; Bare, R. E.; Stiefel, E. I. *J. Am. Chem. Soc.* 1987, *109*, 7913.

Thomann, H. *et al.* in *Electron Magnetic Resonance in Solid States*, Weil, J. ed.; Canadian Chemical Society; 1988.

Townes, C. H.; Dailey, B. P. *J. Chem. Phys.* 1949, *17*, 782–796.

True., A. E.; Nelson, M. J.; Venters, R. A.; Orme–Johnson, W. H.; Hoffman, B. M. *J. Am. Chem. Soc.* 1988, *110*, 1935–1943.

Van Camp, H. L.; Sands, R. H.; Fee, J. A. *J. Chem. Phys.* 1981, *75*, 2098–2107.

Vanngard, T. in *Biological Application of Electron Spin Resonance*; Swarta, H.M.; Bolton, J.R.; Borg, D.C., Eds.; Academic Press: New York, 1972, 411–448.

Venter, R. A.; Nelson, M.; McLean, P. A.; True, A. E.; Levy, M. A.; Hoffman, B. M.; Orme–Johnson, W. H. *J. Am. Chem. Soc.* 1986, *108*, 3487.

Viebrock, A. and Zumft, W. G.; *J. Bacteriology* 1988, *170*, 4658–4668.

Walters, M. A.; Chapman, S. K.; Orme–Johnson, W. H. Polyhedron 1986, *5*, 561.

Wang, S. –Z.; Chen, J. –S.; Johnson, J. L. *Biochemistry* 1988, *27*, 2800–2810.

Wertz, J. E.; Bolton, J. R. *Electron Spin Resonance*; Chapman and Hall, New York, 1986.

Wilkinson, J. H.; Reinsch, C. *Linear Algebra*, Vol. 11 of *Automatic Computations*; Springer–Verlag, New York, 1971.

Yang, S. S.; Pan, W. H.; Friesen, G. D.; Burgess, B. K.; Corbin, J. L.; Stiefel, E. I.; Newton, W. E. *J. Biol. Chem.* 1982, *257*, 8042.

Zaviosky, E. *J. Phys. U. S. S. R.* 1945, *9*, 211.

Zumft, W. G.; Hase, T.; Matsubara, H. in *Molybdenum Chemistry of Biological Significance*; Newtow, W. E.; Otsuka, S., Eds.; Plunum, New York, 1980; 59–72.

Zumft, W. G.; Matsubara, T. *FEBS Lett.* 1982, *148*, 107–112.

Zumft, W. G.; Coyle, C. L.; Frunzke, K. *FEBS Lett.* 1985, *183*, 240–244.

Zweier, J. J.; Peisach, J.; Mims, W. B. *J. Biol. Phys.* 1982, *257*, 10314–10316.